Regulation of low repeat spike timing-dependent LTP in CA1 of mouse hippocampal slices by GABAergic inhibition and Dopamine signaling

Thesis

For the degree of

doctor rerum naturalium (Dr. rer. nat.)

approved by the Faculty of Natural Sciences of Otto von Guericke University Magdeburg

by   **Babak Khodaie, Doctorate of veterinary medicine**

born in 05 May 1989 in Tehran, Iran

Examiner: **Prof. Dr. rer. nat. Volkmar Leßmann**

Prof. Dr med. Jochen Roeper

submitted on: **16 December 2022**

defended on: **03 July 2023**

Table of contents

Abbreviations

Δt	spike timing in ms
AACs	axo-axonic cells
A/C loop	associative/commissural loop
AC	adenylyl cyclase
ACSF	artificial cerebrospinal fluid
ADP	afterdepolarization
AMPAR	α-amino-3-hydroxy-5-methylisoxazole-4-propionic acid receptor
ANOVA	analysis of variance
AP	action potential
Arc	activity-regulated cytoskeleton
BAPTA	1,2-bis(o-aminophenoxy)ethane-N, N,N′,N′-tetraacetic acid
β-Receptor	β-Adrenergic receptor
BLA	basolateral amygdala
CC	current clamp
C_m	membrane capacitance
CA1	cornu ammonis 1
CA2	cornu ammonis 2
CA3	cornu ammonis 3
CaMKII	calcium/calmodulin-dependent protein kinase II
cAMP	cyclic adenosine monophosphate
CB1R	cannabinoid type 1 receptor
CC	current clamp
Chr	channelrhodopsin
CP-AMPAR	calcium-permeable AMPA receptor
CREB	cAMP response element-binding protein
DA	dopamine
DG	dentate gyrus
DH	dorsal hippocampus
DL-APV	DL-2-amino-5-phosphonopentanoic acid
DMSO	dimethyl sulfoxide
EC	entorhinal cortex
eCB	endocannabinoid
E-LTP	early long-term potentiation
ER	endoplasmic reticulum
EPSC	excitatory postsynaptic current
EPSP	excitatory postsynaptic potential
EYFP	enhanced yellow florescent protein
GABA	gamma-aminobutyric acid
GAD	glutamic acid decarboxylase
GAT	GABA transporter
GIRK	gated inward-rectifying K^+
GPCRs	G protein-coupled receptors
HCN	hyperpolarization-activated cyclic nucleotide–gated
HFS	high frequency stimulation

IH	intermediate hippocampus
IP3	inositol-tris-phosphate
IPSCs	inhibitory postsynaptic currents
ISI	interstimulus intervals
ISIs	interneuron selective interneurons
IVCs	ivy cells
LC	locus coeruleus
LFS	low frequency stimulation
LJP	liquid junction potential
LTD	long-term depression
LTP	long-term potentiation
L-LTP	late long-term potentiation
mPFC	medial prefrontal cortex
mGluR	metabotropic glutamate receptor
MF	mossy fiber
NA	noradrenaline
NAc	nucleus accumbens
NaCl	sodium chloride
NGCs	neuroglia form cells
NMDA	N-methyl-D-aspartate
NMDAR	N-methyl-D-aspartate receptor
NO	nitric oxide
O-LM	oriens-lacunosum moleculare
PCs	pyramidal cells
PKA	protein kinase A
PKC	protein kinase C
PLC	phospholipase C
PPD	paired pulse depression
PPF	paired-pulse facilitation
PPI	prepulse inhibition
PPR	paired-pulse ratio
PSD	postsynaptic density
PV	parvalbumin
PVBCs	parvalbumin expressing basket cells
R_{in}	input resistance
R_m	membrane resistance
RI	recurrent inhibition
RMP	resting membrane potential
SC	schaffer collateral
SCACs	schaffer collateral-associated cells
SC-CA1	schaffer collateral - Cornu Ammonis 1 synapse
SCH23390	R-(+)-7-Chloro-8-hydroxy-3-methyl-1-phenyl-2,3,4,5-tetrahydro-1H-3-benzazepine hydrochloride
S.r.	stratum radiatum
S.o.	stratum oriens
S.p.	stratum pyramidale
S.l.m	stratum lacunosum moleculare
SEM	standard error of the mean
STDP	spike timing-dependent plasticity

TAP	temporoammonic path
TH	tyrosine hydroxylase
t-LTP	timing-dependent long-term potentiation
VC	voltage clamp
VH	ventral hippocampus
VGCC	voltage-gated Ca^{2+} Channel
VMAT	vesicular monoamine transporter
VTA	ventral tegmental area
WT	wild type
YFP	yellow florescent protein

List of figures

Abstract

The hippocampus and its associated medial temporal lobe structures evolved as a complex micro-network of excitatory and inhibitory synapses to process learning and memory relevant information. The longitudinal axis of the hippocampus is divided into dorsal (DH), intermediate (IH), and ventral (VH) parts. Each of these longitudinal axis heterogeneous expression of GABAergic, glutamatergic, and neuromodulatory receptors, creating diverse and partially exclusive synaptic regulatory mechanisms. Consequently, synaptic plasticity could be differentially modulated by various excitatory, inhibitory, and neuromodulatory interactions along this longitudinal axis of the hippocampus. Whereas conventional long-term potentiation (LTP) induced by high-frequency stimulation and long-term depression (LTD) induced by low-frequency stimulation are considered cell population models of memory formation, spike timing-dependent plasticity (STDP) allows investigation of timing-dependent t-LTP and t-LTD at the single cell level. While the systematic investigation of physiologically relevant low repeat STDP paradigms is of utmost importance to explain learning mechanisms *in vivo*, very few previous studies have investigated the contribution of the distinct GABAergic, glutamatergic, and neuromodulatory mechanisms on activity-dependent plasticity measured at single Schaffer-collateral (SC)-CA1 synapses along the longitudinal axis of the hippocampus. Using low repeat (6x) STDP at SC-CA1 synapses by pairing one presynaptic action potential (AP) with either one postsynaptic AP (canonical 1:1 t-LTP) or with a burst of 4 APs (burst 1:4 t-LTP) this dissertation investigated how these low repeat STDP protocols are mediated by distinct presynaptic (6x 1:1) and postsynaptic (6x 1:4) expression mechanisms. We then explain the role of distinct sources of postsynaptic Ca^{2+} elevation during induction of the two forms of t-LTP. Whereas NMDA receptors and L-type Ca^{2+} channels are crucial for 6x 1:1 t-LTP induction in the intermediate (IH) region, the 6x 1:4 paradigm depends mainly on the activation of metabotropic glutamate receptors (mGluR1 and mGluR5). Moreover, this dissertation shows that postsynaptic insertion of GluA2-lacking AMPARs into the cell membrane is the main step for both paradigms to induce synaptic changes. In addition, the release of Ca^{2+} from internal stores mediated by mGluR1/5-dependent activation of IP3 and ryanodine receptors are triggering the induction of both 6x 1:1 and 6x 1:4 t-LTP. On the other hand, both dorsal (DH), and ventral hippocampus (VH) depend mainly on L-type Ca^{2+} channels to provide an external Ca^{2+} source during 6x 1:4 t-LTP induction. Blockade of dopamine (DA) receptor (DR) signaling revealed that t-LTP induction by the 6x 1:1 protocol required co-application of D1- and D2R antagonists in DH and VH, whereas in IH, t-LTP induced by both

protocols depended on D1 and/or D2R signaling. In contrast, the 6x 1:4 protocol in VH was blocked by either D1 or D2R antagonism but remained unaffected in DH. These results revealed a gradient of dopaminergic regulation of STDP that depended on the paradigm used to induce t-LTP (i.e. 6x 1:1 vs. 6x 1:4) along the longitudinal axis of the hippocampus, and was possibly determined by the gradient in D1 and D2R expression levels (VH>IH>DH).

Optogenetic silencing of DAergic inputs was ideally suited to address the role of endogenously released DA for low repeat t-LTP. Our results suggest that a sufficiently elevated ambient DA levels are crucial shortly before and during the induction of 6x 1:1 and 6x 1:4 t-LTP paradigms, whereas inhibition of DA release at later time points did not interfere with 6x 1:1 t-LTP.

GABAergic regulation of t-LTP induction under either intact GABAergic inhibition (physiological condition) or under fully blocked inhibition using co-applied GABA$_A$R and GABA$_B$R blockers showed that t-LTP is modulated differently along the longitudinal axis of the hippocampus and depends on the t-LTP stimulation pattern. We found a complex association of excitatory and inhibitory responses depending on stimulation protocols (canonical or burst) and studied regions (DH or VH). While the 6x 1:1 protocol lost its dependency on GABAergic signaling to induce robust t-LTP from DH to VH, the 6x 1:4 protocol mainly depended on active GABA$_B$R signaling during t-LTP induction. Furthermore, both neuronal excitability and synaptic transmission of SC-CA1 synapses depended on GABAergic inhibition and were diversely regulated along the longitudinal axis of the hippocampus (DH>IH>VH).

These results enable a better understanding of the complex hippocampal micro-networks and shed light on the association and interaction of excitatory, inhibitory, and modulatory mechanisms in t-LTP induction along the longitudinal axis of the hippocampus.

Zusammenfassung

Der Hippocampus und die damit verbundenen medialen Temporallappenstrukturen haben sich als komplexes Mikronetzwerk aus erregenden und hemmenden Synapsen entwickelt, um lern- und gedächtnisrelevante Informationen zu verarbeiten. Die Längsachse des Hippocampus ist in dorsale (DH), intermediäre (IH) und ventrale (VH) Teile unterteilt. Jeder dieser Unterabschnitte zeigt eine heterogene Expression von GABAergen, glutamatergen und neuromodulatorischen Rezeptoren, wodurch vielfältige und teilweise exklusive synaptische Regulationsmechanismen geschaffen werden. Folglich könnte die synaptische Plastizität durch verschiedene exzitatorische, inhibitorische und neuromodulatorische Wechselwirkungen entlang dieser Längsachse des Hippocampus unterschiedlich moduliert werden. Während die konventionelle Langzeitpotenzierung (LTP), die durch Hochfrequenzstimulation induziert wird, und die Langzeitdepression (LTD), die durch Niederfrequenzstimulation induziert wird, als Zellpopulationsmodelle der Gedächtnisbildung angesehen werden, ermöglicht die Spike-*Timing*-abhängige Plastizität (STDP) die Untersuchung der *Timing*-abhängigen t-LTP und t-LTD auf Einzelzellebene. Während die systematische Untersuchung physiologisch relevanter *Low-Repeat*-STDP-Paradigmen von größter Bedeutung ist, um Lernmechanismen *in vivo* zu erklären, haben nur sehr wenige frühere Studien den Beitrag der unterschiedlichen GABAergen, glutamatergen und neuromodulatorischen Mechanismen zur aktivitätsabhängigen Plastizität an einzelnen Schafferkollateral (SC)-CA1-Synapsen entlang der Längsachse des Hippocampus untersucht. Unter Verwendung von STDP mit geringer Wiederholung (6x) an SC-CA1-Synapsen durch Paarung eines präsynaptischen Aktionspotentials (AP) mit entweder einem postsynaptischen AP (kanonisches 1:1 t-LTP) oder mit einem Burst von 4 APs (*Burst* 1:4 t-LTP) untersuchte diese Dissertation, wie diese *Low-Repeat*-STDP-Protokolle durch unterschiedliche präsynaptische (6x 1:1) und postsynaptische (6x 1:4) Expressionsmechanismen vermittelt werden. Weiter wird die Rolle unterschiedlicher Quellen für die postsynaptische Ca^{2+}-Erhöhung während der Induktion der beiden Formen von t-LTP erklärt. Während NMDA-Rezeptoren und L-Typ-Ca^{2+}-Kanäle entscheidend für die 6x 1:1-t-LTP-Induktion in der intermediären (IH)-Region sind, hängt das 6x 1:4-Paradigma hauptsächlich von der Aktivierung von metabotropen Glutamatrezeptoren (mGluR1 und mGluR5) ab. Darüber hinaus zeigt diese Dissertation, dass die postsynaptische Insertion von GluA2-defizienten AMPARs in die Zellmembran der Hauptschritt für beide Paradigmen ist, um synaptische Veränderungen zu induzieren. Außerdem löst die Freisetzung von Ca^{2+} aus internen Speichern, vermittelt durch mGluR1/5-abhängige Aktivierung von IP3- und Ryanodinrezeptoren, die Induktion von sowohl 6x 1:1 als auch 6x 1:4 t-LTP aus. Andererseits hängen sowohl der dorsale (DH) als auch

der ventrale Hippocampus (VH) hauptsächlich von L-Typ-Ca^{2+}-Kanälen ab, um eine externe Ca^{2+}-Quelle während einer 6x 1:4 t-LTP-Induktion bereitzustellen.

Die Blockade der Dopamin (DA)-Rezeptor (DR)-Signalgebung zeigte, dass die t-LTP-Induktion durch das 6x 1:1-Protokoll die gleichzeitige Anwendung von D1- und D2R-Antagonisten in der DH- und VH-Region erforderte, während in der IH-Region t-LTP durch beide Protokolle induziert wurde aber von D1- und/oder D2R-Signalwegen abhing. Im Gegensatz dazu wurde das 6x 1:4-Protokoll in der VH-Region entweder durch D1- oder D2R-Antagonismus blockiert, blieb aber in der DH-Region unbeeinflusst. Diese Ergebnisse zeigten einen Gradienten der dopaminergen Regulation der STDP, der von dem zur Induktion von t-LTP verwendeten Paradigma (d.h. 6 x 1:1 vs. 6 x 1:4) entlang der Längsachse des Hippocampus abhing und möglicherweise durch den Gradienten der D1- und D2R-Expression (VH > IH > DH) bestimmt wurde.

Die optogenetische Stummschaltung von DAergen Eingängen war ideal geeignet, um die Rolle von endogen freigesetztem DA für *Low-Repeat*-t-LTP zu adressieren. Unsere Ergebnisse deuten darauf hin, dass ein ausreichend hoher ambienter DA-Spiegel kurz vor und während der Induktion von 6x 1:1- und 6x 1:4-t-LTP-Paradigmen entscheidend ist, während die Hemmung der DA-Freisetzung zu späteren Zeitpunkten nicht ausreichte, um die 6x 1:1 t-LTP zu stören.

Die GABAerge Regulation der t-LTP-Induktion unter entweder intakter GABAerger Hemmung (physiologischer Zustand) oder unter vollständig blockierter Hemmung unter Verwendung von gleichzeitig angewendeten GABA$_A$R- und GABA$_B$R-Blockern zeigte, dass t-LTP entlang der Längsachse des Hippocampus unterschiedlich moduliert wird und von dem t-LTP-Stimulationsmuster abhing. Wir fanden eine komplexe Assoziation von exzitatorischen und inhibitorischen Reaktionen in Abhängigkeit von Stimulationsprotokollen (kanonisch oder *Burst*) und von der untersuchten Region (DH oder VH). Während das 6x 1:1-Protokoll seine Abhängigkeit von der GABAergen Signalübertragung zur Auslösung robuster t-LTP von DH zu VH verlor, hing das 6x 1:4-Protokoll hauptsächlich von der aktiven GABA$_B$R-Signalübertragung während der t-LTP-Induktion ab. Darüber hinaus hingen sowohl die neuronale Erregbarkeit als auch die basale synaptische Übertragung an SC-CA1-Synapsen von der GABAergen Hemmung ab und wurden unterschiedlich entlang der Längsachse des Hippocampus(DH > IH > VH) reguliert.

Diese Ergebnisse ermöglichen ein besseres Verständnis der komplexen Hippocampus-Mikronetzwerke und beleuchten die Assoziation und Interaktion von exzitatorischen, inhibitorischen und modulatorischen Mechanismen bei der t-LTP-Induktion entlang der longitudinalen Achse des Hippocampus.

1. Introduction

1.1 History of neurophysiological studies in the hippocampus

In 1880, three scientists during proposed the initial idea of an association between the hippocampal system and memory function, named as Korsakoff psychosis (Wernicke 1881, Korsakoff 1889). Few years later, Hungarian anatomist Karl Schaffer named the axons from CA3 cells, terminating into CA1 cells as Schaffer collaterals (Schaffer 1892). At the beginning of the 19th century, Ramon y Cajal's drew hippocampus structure (Cajal 1911), which later on, in 1934, Rafael Lorente de Nó significantly extended his picture of the hippocampus and described a complex network of interconnected neurons and clearly defined CA1 to CA4 division of the hippocampus. Yet, until the early 1930s, the hippocampal formation was thought to be part of the olfactory system (Rose 1935). A few years later, James W. Papez 1937 suggested that the hippocampus could be a part of a circuit that interconnects cortical and subcortical structures (Papez 1937). This view was further confirmed by later studies by Brodal suggesting that fibers arising from the olfactory bulb did not directly innervate any part of the hippocampus. He proposed that the entorhinal cortex might play an intermediate role in transmitting olfactory impulses and other cortical signals to the hippocampus (Brodal 1947). In its more comprehensive form, this idea today is known as the Papez circuit, and the hippocampus is nominated as the collector of sensory information, developing an emotional state and transferring it to the subcortical nucleus. However, more direct evidence for hippocampal involvement in memory formation was proposed by William Scoville and Brenda Milner in 1957 (Scoville and Milner 1957). Later studies on different memory deficits (sensory discrimination, spontaneous alternation, response inhibition) following hippocampal damage, however, failed to provide a convincing conclusion (Kaada, Rasmussen et al. 1961, Kimble 1963, Douglas and Isaacson 1964, Kveim, Setekleiv et al. 1964), until around 1970, when developments such as new memory testing paradigms and single-cell recording techniques lead to the development of new concepts about memory and confirmed substantial roles of the hippocampus in processing different kinds of memory.

1.2 Features of the hippocampus

Several properties attracted scientists to study the neurobiological and anatomical features of the hippocampus.

- Hippocampal cells can be grown in culture
- Acute hippocampal slices can survive for a rather long time for in-vitro studies
- Hippocampal synapses are highly plastic
- It is synaptically connected to a series of cortical and subcortical regions
- It consists of a single layer of principal neuronal cells with laminated inputs
- Intrinsic fibers make an active connection to the central dendritic axis

1.3 Intrinsic properties of CA1 pyramidal neurons

CA1 pyramidal cells (PCs) have a resting membrane potential (RMP) in the range of -60 to -70 mV recorded in slice preparation and need to be depolarized by about 20 mV to trigger action potentials (APs), which could have amplitudes of 100 mV. In CA1 PCs, each AP is usually followed by an afterdepolarization (ADP). Current-clamp recording in hippocampal slices indicated that ADP is mediated by a Ni^{2+}-sensitive calcium tail current, consistent with R-type voltage gated calcium channels' pharmacological and biophysical profile (Metz, Jarsky et al. 2005). R-type calcium channel activation happens during AP and remains active long after the AP, correlates directly with burst firing in CA1 neurons, provides a critical neuronal function during the encoding of place fields, and enhances synaptic plasticity. The half-width of APs in CA1 PCs is typically about 1 ms (Staff, Jung et al. 2000). Step current injection in CA1 PCs is usually followed by a gradual reduction in spike frequency, called spike-frequency accommodation, mediated by accumulative activation of K^+ conductance. This train of action potentials generates then a prolong after hyperpolarization (AHP), which is thought to be mediated by calcium-activated K^+ currents (Sah and Clements 1999), since calcium-activated K^+ channels are deactivated when intracellular calcium is strongly buffered (Sah and Bekkers 1996).

Several aspects of CA1 PCs are also under neuromodulatory control. For instance, dopamine (DA) induces long-lasting membrane depolarization of CA1 PCs (Gribkoff and Ashe 1984). Depleting endogenous DA in sucrose-containing ACSF significantly affects spike rise times, firing latencies, and

accommodation properties during repetitive spiking (Edelmann and Lessmann 2013). Noradrenaline (NA) reduces spike-frequency accommodation, facilitates depolarization of interneurons in all strata, and increases inhibitory postsynaptic potential in CA1 PCs (Madison and Nicoll 1988, Bergles, Doze et al. 1996). Understanding neuronal responses to a given synaptic input depends on three main factors: **1)** location of the synapse along the dendritic tree, known as dendritic geometry, which led Wilfrid Rall to propose the "cable theory" (Rall 1959, Rall 1964), later discussed by Segev and colleagues (Segev, Rinzel et al. 2003). Based on Rall's theory, neurons are considered as long, leaky cables, where synaptic current propagation only depends on membrane resistance (R_m), membrane capacitance (C_m), and internal resistance (R_i). Therefore, geometry is an essential factor (dendrites compare to somata have higher membrane resistance, smaller capacitance, and higher axial resistance). His cable theory (Rall 1959, Rall 1964) provides the foundation for modern computational analysis of neurons. **2)** Passive membrane properties are defined by steady-state amplitude and the time course of the voltage change, determined by the neuron's input resistance (R_{in}). Accordingly, R_{in} depends on R_m and geometry, where more giant neurons with many dendrites and low R_m have the lowest R_{in}. **3)** Active membrane properties largely depend on membrane potential (e.g., voltage-gated Na^+ and K^+ channels). Therefore, it might be more accurate to refer to the RMP of the CA1 cells to be affected mainly by passive membrane properties. Non-uniform membrane properties and high R_{in} lead to attenuation of synaptic inputs as they propagate toward the soma (Golding, Mickus et al. 2005).

1.4   Hippocampal excitatory synaptic circuits

The hippocampal formation comprises several functionally related brain regions: the hippocampus, dentate gyrus (DG), entorhinal cortex (EC), subiculum, presubiculum, and parasubiculum (Amaral, Andersen et al. 2007). The hippocampus region consists of CA4, CA3, CA2, and CA1 (CA comes from cornu ammonis). Most of the neocortical inputs to the hippocampus pass through the EC. The EC is a critical gateway to relay cortical inputs to the hippocampus and receives encoded information back (Buzsáki 1989). Cortical polymodal sensory information mainly targets EC's deep layer (V), PCs in the deep layer then project to superficial layers II and III of the EC. Primary hippocampal synaptic input originates from the layer II of EC. It provides glutamatergic fibers to apical dendrites of granule cells of the DG, reaching the PCs of the CA3 region and called the perforant path (Treves and Rolls 1992, Rolls 1996). However, neurons in layer III of EC project to the CA1 region of the hippocampus,

innervating distal apical dendrites of CA1 PCs and forms the so-called temporoammonic path; TAP (Amaral and Witter 1989, Witter, Groenewegen et al. 1989, Scharfman and Chao 2013). CA3 PCs receive excitatory fibers from three different sources. The most critical innervation arises from granule cells of the DG, known as the mossy fiber (MF) pathway (Nicoll and Schmitz 2005), which provides powerful excitatory synapses onto CA3 pyramidal cells and also interneurons. As shown earlier, CA3 also receives extensive monosynaptic input from EC through the perforant path (Andersen, Blackstad et al. 1966, Henze, Urban et al. 2000). There is also an excitatory interconnection between CA3 PCs of both brain hemispheres that mediates initial memory storage, known as the associative/commissural (A/C) loop (Rebola, Carta et al. 2017). Each CA3 PC gives rise to heavily collateralized axonal fibers (Ishizuka, Weber et al. 1990), which highly innervate the CA1 region through both stratum radiatum (via Schaffer collaterals) and also stratum oriens. CA1 PCs project to the adjacent subiculum and deep layers of the EC, thereby completing this circular synaptic pathway (EC → DG → CA3 → CA1 → EC, **Fig.1.1**). New studies extended our knowledge of CA PCs connections to another hippocampal area, the CA2 area. CA2 PCs lack direct input from EC layer III but receive a solid input from DG via MFs. Furthermore, ChR2-YFP-positive CA2 fibers and patch-clamp recordings from CA3 PCs revealed an inhibitory loop of the connections between CA2 and CA3 (Kohara, Pignatelli et al. 2014).
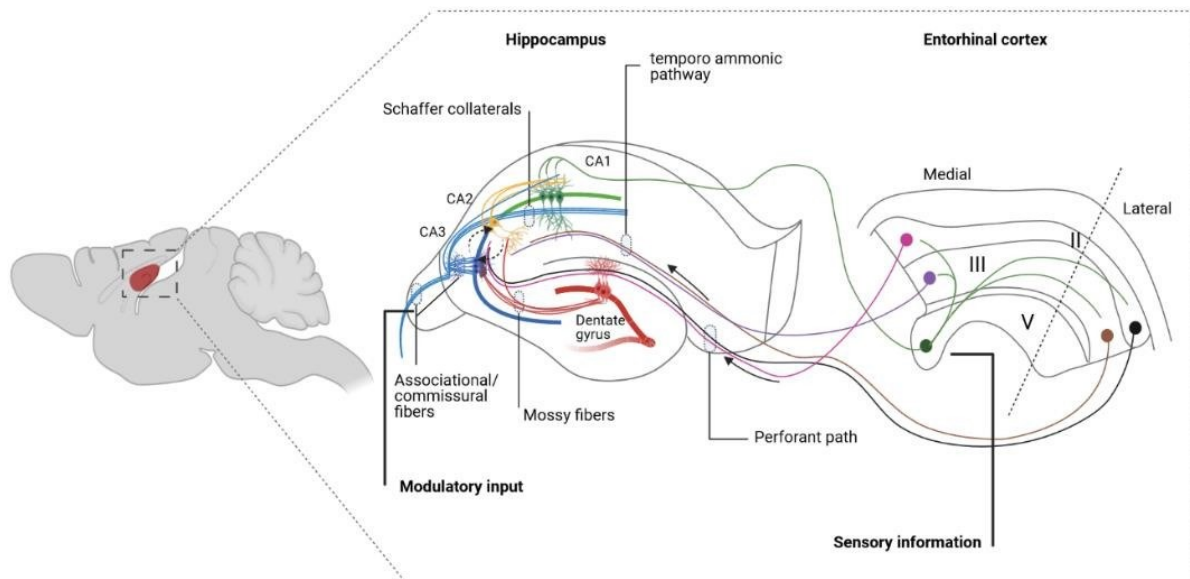
Figure 1.1: The neuronal connection diagram of the hippocampus is classically known as a trisynaptic loop. The perforant path gives rise to the significant axonal wiring, which transfers sensory information from layer II neurons of the entorhinal cortex to the dentate gyrus. Axonal fibers

of the perforant path make excitatory synaptic contact with the dendrites of granule cells. DG cells send their axons as MFs to the apical dendrites of CA3 PCs. Then CA3 PCs project to CA1 PCs through Schaffer collaterals fibers. Layer II cells of the entorhinal cortex also directly innervate CA3 PCs. In addition to the classical trisynaptic circuit, a monosynaptic connection originates from layer III of EC and innervates CA1 pyramidal cells directly through the temporoammonic pathway. CA2 PCs receive fiber projections via MFs and build reciprocal inhibitory connections with CA3 and excitatory connections with CA1 through striatum orients. In turn, CA1 PCs project back to layer V of EC to complete the informational loop. The hippocampus is also interconnected by distinct subgroups of inhibitory neurons not shown in the modified diagram version (adapted from (Neves, Cooke et al. 2008)).

Long-term potentiation (LTP) was initially described in the DG. However, most recent studies have focused on the CA1 region during the last decades. Field potential and intracellular recordings to study synaptic transmission and plasticity are much more accessible in the CA1 region of the hippocampus. Due to CA1's homogeneous SC-fibers arising from the CA3 region, it is easier to keep synaptic inputs alive during preparation. Furthermore, two extensively branched dendritic trees emerge from CA1 PC somata in the pyramidal layer, occupying stratum oriens (basal dendrites) and stratum radiatum (S.r. apical dendrites). This clearly structured CA1 connectivity has provided a tremendous advance in studying synaptic transmission, integration, and plasticity in neuronal cells, using electron microscopic, immunocytochemical, and neurophysiological analyses. Experiments revealed that synaptic spines are mainly found in the distal part of apical dendrites in the S.r. and basal dendrites in the stratum oriens (S.o.), while inhibitory inputs target mainly somata and proximal dendrites (Andersen, Blackstad et al. 1966, Megías, Emri et al. 2001).

1.4.1   Local circuit inhibitory interneurons

In contrast to glutamatergic cell bodies, which are highly organized in laminal structures (e.g., CA3/CA1 stratum pyramidale), the somata of local circuit GABAergic inhibitory interneurons are scattered throughout the hippocampus. While interneurons represent only 10% of all hippocampal cell populations, they show a vast diversity of structural and functional properties. Interneurons have a short-range projection to their targets and release the inhibitory neurotransmitter gamma-Aminobutyric acid (GABA, reviewed in (Chebib and Johnston 1999).

Studies showed that each interneuron population has specific dendritic domains of pyramidal neurons, which provides absolute control over the generation of Na^+ and Ca^{2+} mediated action potentials and regulates synaptic plasticity (Kepecs and Fishell 2014). GABA is synthesized by the

decarboxylation of glutamate by glutamic acid decarboxylase (GAD) and acts as a central inhibitory transmitter. GAD67 is mainly present in the soma, while GAD65 expresses in the presynaptic terminals of GABAergic cells (Soghomonian and Martin 1998). GABA release from GABAergic terminals affects postsynaptic ionotropic (GABA$_A$) and metabotropic (GABA$_B$) receptors. Furthermore, synaptically released GABA appears to also exert extrasynaptic actions (Isaacson, Solis et al. 1993). GABA reuptake from the synaptic cleft is mediated by the GABA transporter (GAT) family (Schousboe 2000). GABA induces fast inhibitory postsynaptic currents (IPSCs) through GABA$_A$ receptor activation. Benzodiazepines can potentiate GABAergic transmission by enhancing GABA$_A$ receptor affinity (Hájos, Katona et al. 2000) or increasing single-channel conductance (Eghbali, Curmi et al. 1997), while barbiturates keep GABA-liganded channels open for a more extended period to prolong the IPSC (Study and Barker 1981) and provide sedative, anxiolytic, and antiepileptic effects. Cl$^-$ ions are the main charge carriers of IPSCs through GABA$_A$ receptors and mediate synaptic inhibition either through direct hyperpolarization or shunting of EPSCs. However, while GABA$_A$ receptors are predominant at the synaptic site, a great number of GABA$_A$ receptors exist at peri- and extrasynaptic locations. Although fast phasic inhibition is exerted through large transients mediated by synaptic GABA$_A$ receptors, still low ambient GABA can persistently activate extrasynaptic receptors to induce tonic inhibition (Peng, Hauer et al. 2002, Glykys and Mody 2007). Tonic inhibition can be experimentally tested as changes in RMP changes upon applying bicuculline, gabazine, or picrotoxin to block GABA$_A$ receptors (Lee and Maguire 2014). Tonic inhibition, on the other hand, is essential in controlling neuronal excitability and action potential output in PCs (Semyanov, Walker et al. 2003, Farrant and Nusser 2005). GABA$_B$ receptors are coupled to G proteins, which interact with inwardly-rectifying potassium channels (GIRK or Kir$_3$), resulting in membrane hyperpolarization of postsynaptic cells.

However, presynaptic activation of GABA$_B$ receptors on various interneurons negatively modulates GABA release through activation of GIRK channels and inhibition of Voltage-gated calcium channels (VGCCs) coupled to vesicular release (Hefft, Kraushaar et al. 2002, Booker, Gross et al. 2013), a process which is suggested to be mediated by GABA$_B$ autoreceptors that facilitates synaptic plasticity (Davies, Starkey et al. 1991, Mott and Lewis 1991, Remondes and Schuman 2003). This process emphasizes the importance of disinhibition in gating synaptic plasticity during physiological conditions.

Therefore, GABA release from interneurons regulates cell excitability and provides a temporal window for synaptic excitation, affecting the timing of afferent and efferent information flow.

Furthermore, interneurons are responsible for synchronizing oscillatory activity across the hippocampal network (reviewed in (Roth and Draguhn 2012)). Axo-axonic cells (AACs, chandelier cells) are located in stratum pyramidale (S.p.) and have their dendrites expanded to S.r. and stratum lacunosum moleculare (S.l.m.) where they receive excitatory input from SC fibers (Buhl, Halasy et al. 1994, Klausberger, Magill et al. 2003). The Calcium-binding protein parvalbumin (PV) is used as a molecular marker for mature AACs that are important for feed-forward inhibition of CA1 PCs (Soriano, Nitsch et al. 1990, Somogyi and Klausberger 2005, Baude, Bleasdale et al. 2007).

Another major group of interneurons in the CA1 region of the hippocampus are parvalbumin-expressing Basket Cells (PVBCs), which are also located close to S.p. with projections to S.r. to receive excitatory input from SC fibers (Buhl, Halasy et al. 1994, Sik, Penttonen et al. 1995). Bistratified cells are another group of interneurons with somata in S.p. but shorter dendrites limited to S.r. layer (compare **Figs. 1. 2**). The largest group of CA1 interneurons are Ivy cells (IvCs), mainly placed in S.p. They have dense dendritic arborization targeting more basal CA1 PCs dendrites (Fuentealba, Begum et al. 2008). Ivy cells extend beyond their axonal span to provide feed-forward recruitment by CA3 SC inputs and feedback recruitment by CA1 PCs collaterals (Somogyi, Szabo et al. 2012); (**Fig. 1. 2**). Moreover, recent studies using transgenic animals and circuit mapping tools (e.g., two-photon Dodt ISGC) detect a group of interneuron called interneuron selective interneurons (ISIs), which comprise almost 20% of all CA1 interneurons and mediate circuit disinhibition by selectively targeting other interneurons over PCs (Freund and Buzsaki 1996, Freund and Gulyás 1997, Chamberland, Salesse et al. 2010, Chamberland and Topolnik 2012, Bezaire and Soltesz 2013).

Feed-forward and feedback inhibition in CA1 PCs constitute a significant function of interneurons for controlling the temporal summation of excitatory inputs (Pouille and Scanziani 2001). Feedback inhibition is represented by interneurons positioned in S.o, layer, a class of these interneurons called oriens-lacunosum moleculare (O-LM) cell, receives excitatory inputs from CA1 PC axon collateral branches in S.o. (Ali and Thomson 1998, Pouille and Scanziani 2004, Leão, Mikulovic et al. 2012). They evoke IPSPs in distal apical dendrites of CA1 PCs to control the gating of excitatory inputs to CA1 PCs (Maccaferri, David et al. 2000, Elfant, Pál et al. 2008). In the CA1 region of the hippocampus, feedback inhibition is mainly provided by O-LM cells with dendrites in the S.o. and axonal projections to the S.l.m. layer (Blasco-Ibanez and Freund 1995, Kullmann 2011). In addition, Axo-axonic cells (AACs) located in S.o. also participate in feedback inhibition with its short projection to the perisomatic region of CA1 PCs. Most interneurons in the CA1 region that contribute to feed-forward inhibition receive excitatory innervation from SC fibers (**Fig. 1.2**). The kinetics of elicited IPSPs

can inhibit excitation or mediate push-pull effects of CA1 PCs (Jang, Chung et al. 2020). Three primary excitatory fibers activate feed-forward inhibition: perforant path fibers activate neuroglia form cells (NGCs) in S.l.m, Schaffer collateral-associated cells (SCACs) in S.r., and NGCs in S.l.m. activated by SC-fibers. IVCs receive excitatory innervation from SC-fibers, and local PCs and participate in both feedback and feed-forward inhibition (Klausberger 2009, Kullmann 2011), (**Figs. 1.2**).
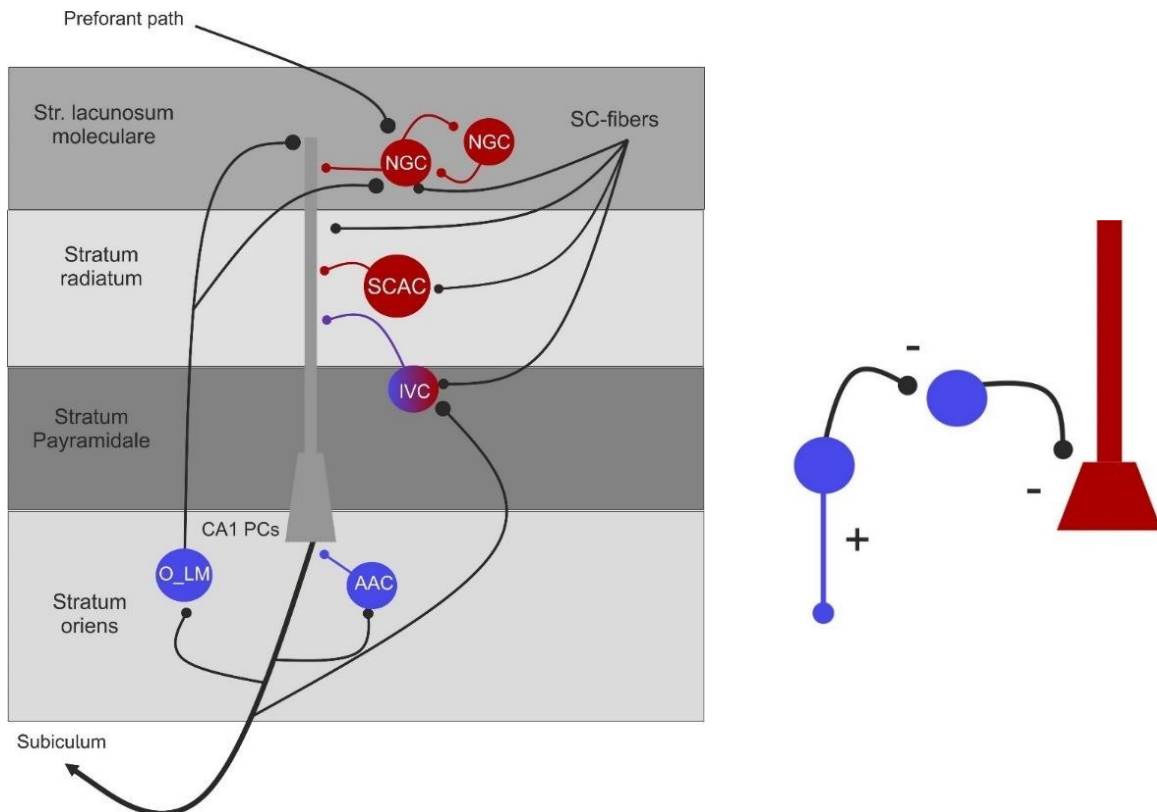
Figure 1.2: Interneuron network of hippocampus. **Left**: A simplified schematic illustration of the interneuron networks that mediate feedback (blue) and feed-forward (red), and both feedback and feed-forward (combined) inhibition in the CA1 PCs. Excitatory input reaches through SC fibers, leading to the activation of PC dendrites, which then activates feed-back inhibition through axonal projections to stratum oriens-lacunosum moleculare (S. o-LM), axo-axonic cells (AACs), and Ivy (IVC) interneurons participating in feedback inhibition. Both SC fibers and perforant path together with excitation of apical PC dendrites also activate feed-forward inhibition by exciting neuroglia form cells (NGC), thereby creating a reactivation loop. SC-fibers also excite Schaffer collateral-associated cells (SCACs) and Ivy cells, which regulate dendritic excitation in S.l.m. and s.r. layers. Ivy cells have a dual role (as shown by their double color) in inhibition circuits through both feedback and feed-forward inhibition. Other interneurons not discussed in this dissertation are not included in the scheme. **Inset on the right** represents how interneuron selective interneurons (ISIs) form a disinhibition circuit that could then alternate neuronal excitation of PCs.

1.5   Longitudinal hippocampal axis

For many years the hippocampus has been considered a curved homogenous structure present across all mammalian orders and elongated along a dorsal (septal)-to ventral (temporal) axis in rodents. However, recent reports have shown that regional differences in the hippocampus' genetic, morphological, and functional properties suggest that PCs are heterogeneous along the longitudinal axis of the hippocampus (Moser and Moser 1998, Fanselow and Dong 2010, Strange, Witter et al. 2014). The longitudinal (also called dorso-ventral) axis of the hippocampus contains dorsal (DH), intermediate (IH), and ventral (VH) parts. A gradual functional change towards the ventral pole of the hippocampus has been reported earlier (McDonald, Jones et al. 2006, Pandis, Sotiriou et al. 2006, Papatheodoropoulos and Kouvaros 2016, Dubovyk and Manahan-Vaughan 2018, Levone, Codagnone et al. 2021).

1.5.1   Connectivity

Cortical and subcortical areas distinctly innervate the dorsal and ventral regions of the hippocampus. The DH mainly revives visual and spatial information from sensory cortices via dorsolateral EC and caudal medial EC (MEC), connected to perirhinal and postrhinal cortices. In contrast, VH mainly receives input from ventromedial EC that is connected to piriform, infralimbic, and periamygdaloid cortices (Burwell and Amaral 1998, Dolorfo and Amaral 1998). The DH's output primarily reaches the dorsolateral septum and leads the mammillary body to process spatial navigation memory (Risold and Swanson 1996). The output of the VH projects primarily to the medial amygdala (Kishi, Tsumori et al. 2006) and also to the ventral lateral septum and subthalamic nucleus associated with hypothalamic–pituitary–adrenal axis (Risold and Swanson 1996) to process emotional, fear, olfactory and learning (Fanselow and Dong 2010).

1.5.2   Electrophysiological properties of CA1 PCs

Many studies used whole-cell patch-clamp recordings from CA1 neurons in slices prepared along the longitudinal axis of the hippocampus to explore their electrophysiological properties. RMP and neuronal firing properties indicate differences in excitability. RMP of PCs in the VH showed to be more depolarized than those recorded from DH (Milior, Di Castro et al. 2016). Smaller values for Rheobase were observed in VH neurons in response to step current injections. Several authors

concluded that hyperexcitability in VH PCs is probably controlled by a network-level phenomenon, where an imbalance of excitatory and inhibitory synaptic inputs exists (Papatheodoropoulos, Asprodini et al. 2002, Derchansky, Shahar et al. 2004). This explanation could be considered, knowing that diverse expression patterns of ligand-gated ion channels are already reported along the dorso-ventral axis of the hippocampus (Papatheodoropoulos, Moschovos et al. 2005, Pandis, Sotiriou et al. 2006). Although neuronal morphology is considered to be important for determining somatic R_{in} but is less likely to affect RMP, significant differences in the expression of voltage-gated ion channels along the dorso-ventral axis must be assumed (Marcelin, Lugo et al. 2012). Hönigsperger et al. reported that the expression of M-type (Kv7) potassium channels is higher in DH than VH and could affect somatic excitability and spike frequency adaptation (Hönigsperger, Marosi et al. 2015). Further, differences in ion channels are not limited to the soma, and distal dendrites of VH CA1 neurons show a lower level of A-type K^+ channels than DH (Marcelin, Lugo et al. 2012). The same study found increased back-propagation of action potentials (APs) in VH CA1 PC dendrites due to lower A-type potassium currents. Another key factor in regulating membrane excitability along the longitudinal axis of the hippocampus is the Hyperpolarization-activated cyclic nucleotide–gated (HCN) channel-mediated I_h (Zemankovics, Káli et al. 2010), which was found to be differentially expressed along the dorso-ventral axis of the hippocampus (Marcelin, Lugo et al. 2012, Dougherty, Nicholson et al. 2013). Membrane properties and excitability in CA1 neurons are also regulated by GIRKs, however, its expression along the dorso-ventral axis is not fully explained (Kim and Johnston 2015). Similar to neuronal excitability, synaptic transmission is also affected along the longitudinal axis of the hippocampus. Chemical transmission between neurons is divided into glutamate release mediated fast excitatory synaptic transmission employing ionotropic (AMAPRs, NMDARs) as well as slow metabotropic glutamate receptors (mGluRs), and fast inhibitory transmission mediated by GABA or Glycine release and postsynaptic activation of ionotropic $GABA_A$ and slow metabotropic $GABA_B$ receptors. Moreover, slow synaptic transmission is conducted by less specialized postsynaptic sites and volume transmission as well as some neuromodulators like dopamine (Greengard 2001). At most excitatory hippocampal synapses, postsynaptic currents (EPSCs) are mediated by AMPA and NMDA receptors together with Kainate receptors. Most of the AMPARs in the hippocampus are constituted of GluR1 or GluR2-3 subunits. Upon exposure to glutamate release (1mM), Na^+ influx will generate a rapid excitation current with a rise-time about (100–600 µs). Rise-time indicates the ability of a circuit to respond to fast input signals (Valley and Wallman 1948), and its fast binding kinetics and high opening probability (Jonas, Major et al. 1993), as well as the location of the synaptic

input on the dendritic tree (Magee and Cook 2000). On the other hand, NMDA receptors have slower kinetics and rise-times of approximately 7 ms and deactivate in 200 ms (Lester, Clements et al. 1990). The Ca^{2+} permeability and Mg^{2+} blockade of NMDARs explain their role as synaptic coincidence detectors (Bender, Bender et al. 2006). Using autoradiographic and saturation experiments demonstrate lower expression density of both NMDAR and AMPAR in the VH region compared to DH (Martens, Capito et al. 1998, Pandis, Sotiriou et al. 2006), confirmed by in situ hybridization experiments. Moreover, several studies showed diverse NMDAR composition along the longitudinal axis of the hippocampus, which may reflect different functional characteristics of NMDAR mediated responses. It was suggested that the lower NR2A/NR2B ratio detected in VH probably leads to a less efficient magnesium block of the NMDAR channel (Monyer, Burnashev et al. 1994), explaining greater involvement of VH in the formation of epileptiform discharges (Papatheodoropoulos, Moschovos et al. 2005). Moreover, a higher NR2A/NR2B ratio contributes to a faster decay of EPSPs (Liu, Wong et al. 2004, Massey, Johnson et al. 2004). Higher levels of NR2A containing NMDARs might facilitate LTP induction in the hippocampus, whereas NR2B subunits seem to be implicated especially in long-term depression (Liu, Wong et al. 2004). Larger NMDAR-mediated components lead to a longer decaying phase of evoked synaptic response in VH CA1 neurons (Papatheodoropoulos, Moschovos et al. 2005). GABAergic transmission is also modulated through $GABA_A$ and $GABA_B$ receptor properties. $GABA_A$ receptor-mediated IPSCs have a fast onset but a slower decay time than AMPAR-mediated EPSCs. In contrast, $GABA_B$ receptors activation triggers signaling cascades that lead to activation of G protein-gated inward-rectifying K^+ (GIRK) channels and causes a slow IPSP. While $GABA_B$ receptors show the lowest expression in DH, $GABA_A$ receptor were shown to exhibit the opposite expression (DH > IH > VH) pattern (Dubovyk and Manahan-Vaughan 2018). The frequency of miniature GABAergic events was higher in the VH compared to the DH (Milior, Di Castro et al. 2016). Later they noticed that $GABA_A$ receptor mediated recurrent inhibition (RI) less efficiently controls CA1 excitatory output in VH than DH. Also, the slicing procedure influenced the strength of RI (Petrides, Georgopoulos et al. 2007). Furthermore, diversity in the distribution of interneurons subclasses is reported along the dorso-ventral axis (Caballero, Diah et al. 2013, Czéh, Varga et al. 2015). It is proposed that $GABA_B$Rs control NMDAR-dependent excitation less efficiently in VH, leading to diverse local network dynamics when comparing DH to VH (Papatheodoropoulos 2015). Importantly, both GABA and glutamate release are also affected by neuromodulator fiber projections to the hippocampus, which are much stronger in VH than DH (Strange, Witter et al. 2014). Neuromodulator release could positively modulate the basal level of GABA and glutamate release in the hippocampal CA1 region. While VH was reported to

receive purely DAergic fibers originating from VTA, DH receives neuromodulatory innervation from LC, most likely enabling DA and noradrenaline release (Kempadoo, Mosharov et al. 2016). DAergic D1- and D2- like receptors (D1Rs and D2Rs) also show variable expression pattern along the longitudinal axis of the hippocampus. D1R and D2R have the highest expression in VH of rats (Dubovyk and Manahan-Vaughan 2018, Dubovyk and Manahan-Vaughan 2019), but it's not well described in mouse hippocampus. It should also be considered that LC catecholaminergic fibers innervating the DH are more prominently releasing NA (Nullmeier, Panther et al. 2014) while this mechanism is more restricted in VH (Hsu 1996).

1.5.3   Functional properties

The DH region mainly receives visual and somatosensory information via dorsolateral fibers from EC and is important in processing spatial navigation (Moser, Moser et al. 1993, Dolorfo and Amaral 1998, Furtak, Wei et al. 2007). This was confirmed by studies showing that DH lesion led to spatial learning impairment and reduced memory span for novel object discrimination (Moser, Moser et al. 1995, Lee and Kesner 2003, Sannino, Russo et al. 2012). Further studies revealed that CA1 PCs in the DH region also process temporal order during visual object recognition (Hoge and Kesner 2007). A study by Kempadoo and colleagues on mice provided direct evidence that neuromodulatory regulation in DH could affect selective attention and spatial learning and memory (Kempadoo, Mosharov et al. 2016). Interestingly, input from medial and lateral EC to DH is highly specified, meaning that spatial information is represented by the medial and non-spatial information by the lateral EC (Hargreaves, Rao et al. 2005). Retrieval and encoding of multimodal associative memory are processed in the IH region (Small, Nava et al. 2001). Lesion of IH also revealed that hippocampal input to the medial prefrontal cortex (mPFC) is critical for the temporal organization of prefrontal activity (Burton, Hok et al. 2009). It is well known that both IH and VH are anatomically connected to the amygdala, which plays a crucial role in the processing of valence information (Beyeler, Namburi et al. 2016). Anatomical studies revealed that PCs in CA3 of the DH send their projections to IH, while VH shows heavy intrinsic instead of extrinsic connections (Swanson, Wyss et al. 1978, Laurberg 1979). It is a well-known concept that IH has relatively overlapping characteristics with its neighbors separated into DH and VH poles of the hippocampus, suggesting a gradient-like function (Cenquizca and Swanson 2007, Fanselow and Dong 2010, Levone, Codagnone et al. 2021). VH is believed to be more important for processing emotional and body state information (Fanselow and Dong 2010). There

are still some reports that VH could contribute to both spatial and non-spatial tasks (de Hoz, Knox et al. 2003, McDonald, Jones et al. 2006). Further studies also indicate that VH is involved in the processing of working memory (Kesner, Hunsaker et al. 2011), stress responses (Levone, Codagnone et al. 2021), fear conditioning (Rogers, Hunsaker et al. 2006), and unconditioned fear (Kjelstrup, Tuvnes et al. 2002). Furthermore CA1 neurons in the DH seem to be involved in encoding and retrieving contextual fear, while VH is recruited during the retention of contextual fear (Burman, Starr et al. 2006, Hunsaker and Kesner 2008). The activity of VH also regulates synaptic plasticity by control DA levels in the nucleus accumbens (Legault, Rompré et al. 2000). Numerous studies investigated different contribution of behavioral regulation, including learning and memory formation, by the different hippocampus sub-regions from DH to VH. Thus, it seems plausible that this comes with distinct efficacy and regulation of synaptic transmission underlying the control of DH, IH, and VH, which is certainly influenced by differences in their receptor, ion channel, and synaptic circuit settings, as well as by their distinct electrophysiological properties (Strange, Witter et al. 2014).

1.5.4   Synaptic plasticity

One of the fascinating properties of hippocampal synapses is their ability to respond and change depending on neuronal activation patterns they receive, a phenomenon named synaptic plasticity. Also, today, it is known that plasticity is a property of most excitatory synapses in the brain, leading to either long-term potentiation (LTP) or long-term depression (LTD). Nevertheless, no other type of synaptic plasticity still attracts more interest than LTP in the CA1 region of the hippocampus. Since it is known that the hippocampus is a critical component of various forms of long-term memory (Zola-Morgan and Squire 1993), it highly represents the cellular mechanisms of information storage (Bliss and Collingridge 1993). Moreover, LTP and LTD can be readily generated in ex-vivo hippocampal slices. When two stimuli arrive at a short interval in the presynaptic terminals, it could either enhance or depress the release of neurotransmitters from the presynaptic site. Two major types of use-dependent, short-term synaptic plasticity regulate neurotransmitter release, it could be either depression or facilitation. Paired pulse depression (PPD) is a common form of short-term synaptic plasticity usually observed when two presynaptic APs are generated at intervals <20 ms, probably leading to the inactivation of voltage-dependent sodium or calcium channels or transient depletion of synaptic vesicles. In contrast, Paired-pulse facilitation (PPF) is observed at longer interstimulus

intervals (20-500 milliseconds), which is explained by residual calcium in presynaptic boutons due to the first action potential (Malenka 2001). Commonly, at a fixed stimulation interval reduction in paired-pulse ratio (PPR; 2[end] pulse divided by 1st pulse) after stimulation is interpreted as an increase in transmitter release probability and would be expected to be mainly mediate presynaptically. However, repetitive stimulation of SC synapses onto CA1 PCs by tetanic stimulation, like high-frequency stimulation protocols including delivery of one or several trains of pulses at 50–100 Hz for 1 sec (Lüscher and Malenka 2012). Another variant of these LTP induction protocols called pairing protocol, where synaptic changes elicited by presynaptic stimulation followed by postsynaptic spike "pre-post" firing, reversing the order will lead to LTD. Furthermore, the direction of synaptic changes relies on the timing between the pre- and postsynaptic spikes, this phenomenon is called spike timing-dependent plasticity; STDP (Abbott and Nelson 2000, Malenka 2003, Dan and Poo 2006). Triggering of LTP in the postsynaptic cell initially needs AMPA receptor activation to provide inward current to trigger N-methyl-d-aspartate (NMDA) receptor activation by the release of Mg^{2+} block of NMDA receptors. At SC-CA1 excitatory synapses NMDAR is the primary source of intracellular calcium elevation, therefore blockade of calcium influx through specific NMDAR antagonists or loading a postsynaptic neuron with calcium chelators (e.g., 1,2-bis (o-aminophenoxy) ethane-N, N,N′,N′-tetraacetic acid; BAPTA) inhibits LTP induction (Cepeda-Prado*, Khodaie* et al. 2021).

In theory, LTP expression (increase in synaptic strength) happens either by more transmitter release from presynaptic axons being activated or the same amount of transmitter, which has a greater effect due to an increased sensitivity of the postsynaptic cell. Many types of LTP have also been shown to recruit new postsynaptic AMPA receptor expression, known as GluR2 lacking AMPA receptors or Ca^{2+}-permeable AMPA receptors (AMPAR). This type of AMPAR is transiently inserted into the postsynaptic site following LTP induction and is critical for LTP maintenance (Kauer and Malenka 2006). Metabotropic glutamate receptors (mGluRs) are also activated upon glutamate release from the presynaptic site. Group I family consists of mGluR1 and mGluR5, which have been described to contribute to different types of hippocampal LTP (Wang, Ardiles et al. 2016). Group I mGluR family work through G protein activation (Tigaret, Olivo et al. 2016) leads to subsequent inositol-tris-phosphate (IP3) receptors activation. mGluR1 was found to be involved in the induction of LTP, and it seems that mGluR5 plays an important role in the protein synthesis-dependent phase of LTP in the perforant path–dentate gyrus granule cell synapses in vivo (Balschun and Wetzel 2002, Naie and Manahan-Vaughan 2005) and in SC-CA1 synapses in vitro (Cepeda-Prado*, Khodaie* et al. 2021). Postsynaptic depolarization can also activate voltage-gated calcium channels (VGCCs), leading to

more Ca²⁺ influx into the postsynaptic cell. A second wave of intracellular calcium elevation can at some synapses also be provided by the group I family of mGluRs, triggered intracellular signaling cascades by stimulating phospholipase C (PLC) and, thereby, formation of IP3 (Berridge 2005, Taylor and Tovey 2010). Decisive evidence from previous studies indicates that IP3 is the prime candidate linking events at the plasma membrane to Ca²⁺ release from intracellular stores (Takechi, Eilers et al. 1998, Wang, Ardiles et al. 2016). This second wave of Ca²⁺ together with the initial Ca²⁺ elevation, can trigger Ca²⁺ induced Ca²⁺ release via Ryanodine receptors (RYR) from the endoplasmic reticulum (ER), which will amplify Ca²⁺ release from intracellular stores (Karagas and Venkatachalam 2019). The large increase in postsynaptic Ca²⁺ levels can activate calcium/calmodulin-dependent protein kinase II (CaMKII), which is known as a key component of the molecular machinery for LTP reviewed by (Sanes and Lichtman 1999). CaMKII can boost several other signaling proteins such as adenylyl cyclase (AC) and cyclic adenosine monophosphate–dependent protein kinase A (PKA) (Blitzer, Connor et al. 1998, Makhinson, Chotiner et al. 1999). Moreover, protein kinase C (PKC) possibly also underlies the potentiation of neurotransmitter release in the presynaptic site (Brager, Capogna et al. 2002). LTP consequently causes changes in the number of AMPARs expressed in the postsynaptic cell membrane, which is known to be phosphorylated by CaMKII or partially by PKC (Barria, Derkach et al. 1997).

1.6   Spike timing dependent plasticity

Regardless of the specific synaptic connection investigated, synaptic transmission is intensely regulated by synaptic stimulation patterns, whereby co-activated groups of neurons can form cell assemblies that are electrically active at the same time, do to activity-dependent changes in synaptic strengths at shared connections. Consequently, repeated neuronal co-activation strengthens newly formed assemblies. The basic idea of this process proposed by the Canadian neuropsychologist Hebb is that "*cells that fire together, wire together*" (Hebb 1949).

"When an axon of cell A is near enough to excite a cell B and repeatedly or persistently takes part in firing it, some growth process or metabolic change takes place in one or both cells such that A's efficiency, as one of the cells firing B, is increased" reviewed later in (Hebb 2005). Repetitive activation of excitatory synapses in the hippocampus can increase synaptic strength, which may last up to days (Bliss and Collingridge 1993). Such long-lasting changes in synaptic activity, known as long-term potentiation (LTP), are the subject of intensive studies (Bliss and Collingridge 1993, Lisman 2017, Nicoll 2017). It is believed to be a critical phenomenon in understanding molecular mechanisms of memory formation and modification (Bliss and Collingridge 1993).

To study synaptic function on inputs to CA1 PCs, we used Spike-timing-dependent plasticity (STDP) as a physiological relevant pattern of synaptic activity and an in-vitro model for memory studies (Abbott and Nelson 2000, Masquelier, Guyonneau et al. 2009, Edelmann, Cepeda-Prado et al. 2015). STDP consists of precise timing between pre- and postsynaptic activity within a few milliseconds, when a presynaptic spike is followed by postsynaptic AP then it will enhance synaptic strength also referred as timing-dependent LTP (t-LTP). If the temporal order of spikes is anti-causal (i.e. postsynaptic AP precedes presynaptic AP) long-term depression (t-LTD) will occur (Markram, Gerstner et al. 2012, Edelmann, Cepeda-Prado et al. 2015). On the second step, new AMPAR expression on the postsynaptic site, will interact with several proteins of the postsynaptic density; PSD (Elias and Nicoll 2007). PKA, CaMKIV, protein kinases and different signaling molecules as well as extracellular signal–regulated kinase (ERK) recruit protein synthesis locally in the dendrites through newly produced mRNA or by nuclear transcription (Sacktor 2008, Lüscher and Malenka 2012). However, in reality, the process of expression and maintenance do not occur sequentially, but structural changes like spine growth or increase of the PSD size initiate rapidly after induction.

Two STDP stimulation protocols, which were recently tested and established in our lab are represented in **Fig 1.3** (Edelmann, Cepeda-Prado et al. 2015).

Using different pharmacological and optical tools, the current thesis experiments tried to shed light on the mechanisms of induction, maintenance, and expression of t-LTP that determine the t-LTP magnitude at SC-CA1 synapses along the longitudinal axis of the hippocampus.
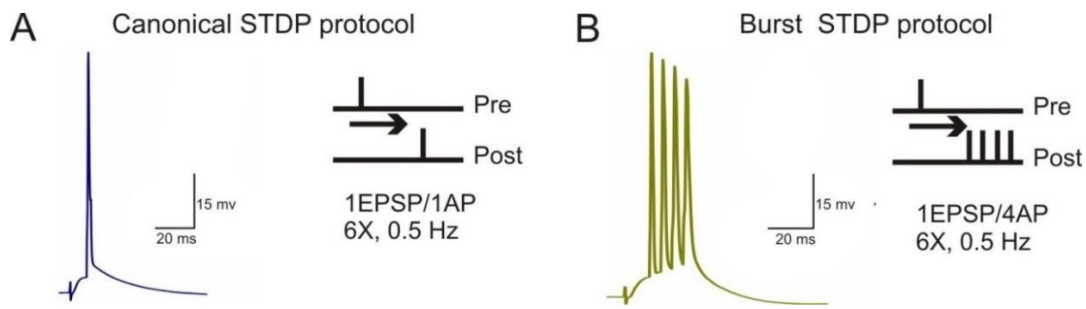
Figure 1.3: Two STDP protocols previously established in our lab and used in this thesis to express t-LTP along the longitudinal axis of the hippocampus. A) Canonical STDP protocol consisting of the coincident firing of 1 pre- and 1 postsynaptic action potential, repeated 6x at 0,5 Hz, and **B)** a burst STDP protocol consisting of 1 pre- and 4 postsynaptic action potential, repeated 6x at a frequency of 0,5 HZ.

1.7 Neuromodulation of t-LTP at hippocampal SC-CA1 synapses

Compared to the classical neurotransmitters glutamate and GABA, other neuromodulatory transmitters are present only at a few synapses or at extrasynaptic locations and mainly play a role in determining the overall excitability and biochemical signaling states at a given synapse within the hippocampal circuitry. Noradrenaline (NA), DA, and serotonin (5-HT) are three main neuromodulators in the brain (Brzosko, Mierau et al. 2019).

1.7.1 Catecholamines

Dopamine (DA) is one of the most critical neuromodulators in the brain that controls basal synaptic transmission and works as a part of the brain reward circuitry (Russo and Nestler 2013). The source of DAergic innervation to the hippocampus is not well defined. The ventral tegmental area (VTA) is a prominent source of DA fibers projecting to the hippocampus (Gasbarri, Packard et al. 1994, Ghanbarian and Motamedi 2013). Several other studies proposed that the Locus coeruleus ;LC (Smith and Greene 2012, Kempadoo, Mosharov et al. 2016) and the nucleus accumbens (NAc) also provide DAergic innervation to different parts of the hippocampus (Baulac, Verney et al. 1986). Last but not least, also the substantia nigra pars compacta (Somayaji and Sulzer , Rosen, Cheung et al. 2015) is another source of DA projections to the hippocampus. **Figure 1.4A** provides further details regarding DAergic innervation of the hippocampal region. The extent of (additional) NA release from these DAergic fibers is not well known and thus a matter of ongoing debate (see e.g. Edelmann and

Lessmann, 2014). Furthermore, pattern of dopaminergic innervation along the dorso-ventral hippocampal axis reviewed by (Edelmann and Lessmann 2018), suggesting an equal dopaminergic innervation along the dorso-ventral axis as well as gradient of dopaminergic innervation (Fig. 1.4B)
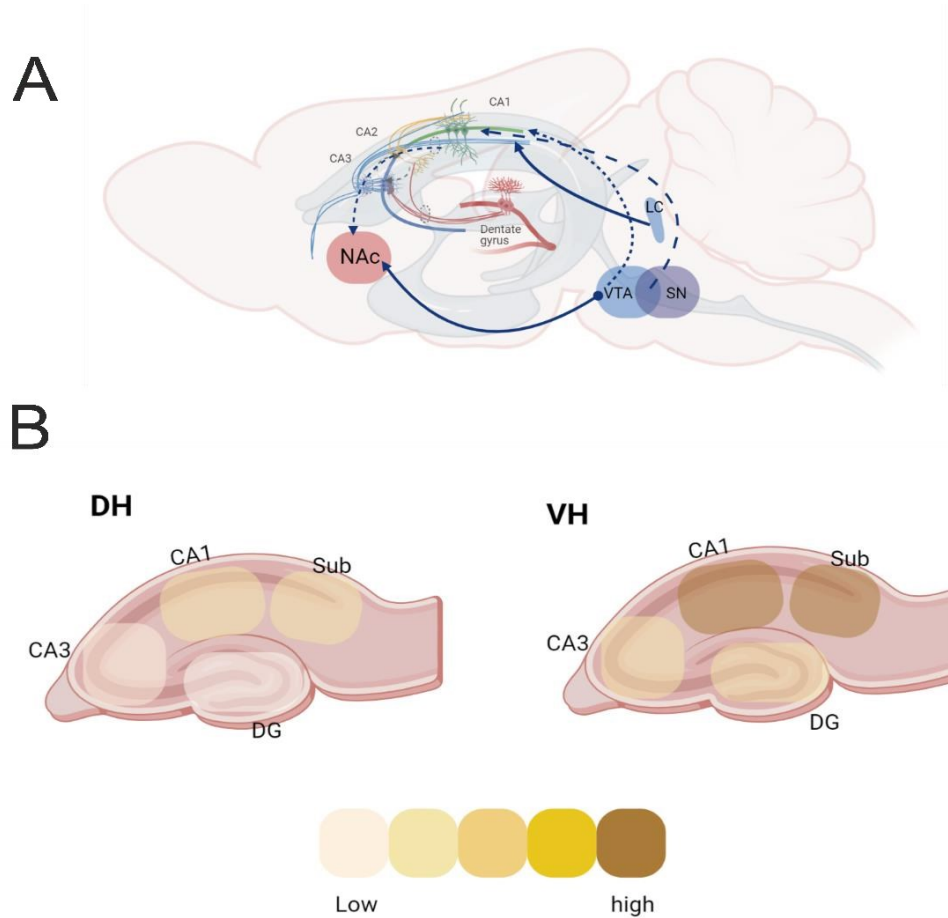
Figure 1.4: DAergic projections to the hippocampus and its subregions along the dorso-ventral axis. **A)** Primary connections come from the ventral tegmental area (VTA) and substantia nigra (SN) to the CA1 pyramidal layer. Although, the primary reward circuit includes DAergic innervation from VTA to the nucleus accumbens (nAc). This connection is responsible for DA release in nAc in response to reward-related stimuli and that nAc also receives glutamatergic neurons from the hippocampus. Studies also revealed that DAergic fibers originated from Locus coeruleus (LC) innervating to the hippocampal CA1 subregion. **B)** Dorso-ventral gradient of dopaminergic innervation, with an intermediate level of innervation density restricted in CA1 and subiculum region in DH and low level of innervation in the CA3 and DG, and higher density of dopaminergic input fibers in the VH pole of the hippocampus in CA1 and subiculum and intermediate level in CA3 and DG. Discussed in detail in (Edelmann and Lessmann 2018). The figure was prepared using Biorender.com.

L-tyrosine is the primary amino acid for DA production. In the process of DA release from catecholaminergic synapses, tyrosine hydroxylase (TH) as a catecholamine synthesis enzyme activates hydroxylation tyrosine to L-DOPA (Molinoff and Axelrod 1971). After decarboxylation to DA, L-DOPA is transferred into the synaptic vesicle by the vesicular monoamine transporter (VMAT) and will be prepared to be released upon an influx of calcium (Daubner, Le et al. 2011). Depending on the type of neurons, catecholamine synthesis continues inside the vesicle in noradrenergic terminals by dopamine-β-hydroxylase to produce NA and even further by phenylethanolamine-N-methyltransferase to build adrenaline (Drinkwater, Gee et al. 2009, Daubner, Le et al. 2011), (**Fig. 1.5**). Once released from presynaptic terminals, DA binds to two main types of metabotropic receptors, which based on their structural, pharmacological, and signaling properties divided into two subfamilies, D1 and D5 receptors belong to D1-like receptors, while D2, D3, and D4 receptors are grouped into the D2-like receptor class (RANKIN, Hazelwood et al. 2010, Tritsch and Sabatini 2012). The affinity of D2-like receptors to DA was reported to be 10 to 100-fold higher than D1-like receptors (Beaulieu and Gainetdinov 2011). Both DAergic receptor families activate heterotrimeric G proteins and then activated intracellular proteins, which are immensely varied and primarily mediate opposite effects, this complex signaling cascade described by several other studies, reviewed in **Figure 1.5** (Neve, Seamans et al. 2004, FISONE 2010, Beaulieu and Gainetdinov 2011). While D1-like receptors activation leads to positive modulation of AC, and then production of cyclic adenosine monophosphate (cAMP) followed by activation of PKA, activation of D2-like receptors inhibit AC and limit PKA activation (Tritsch and Sabatini 2012). PKA activation by D1-like receptors leads to the regulation of several intracellular mechanisms as well as voltage-gated K^+, Na^+, and Ca^{2+}channels, ionotropic glutamate, and GABA receptors activity. Independent of the cAMP/PKA signaling cascade, DA receptors (both D1 and D2-like receptors) can also regulate ligand- and voltage-gated ion channels to modulate intracellular Ca^{2+} levels (Tritsch and Sabatini 2012). D2- like receptor-activated G proteins can contribute directly or indirectly via activation of PLC to decrease CaV2.2 (N-type) and CaV1 (L-type) Ca^{2+}currents. D1-like receptor activation in cells expressing D1/D2 heterodimers can also lead to activation of PLC (Lee, So et al. 2004). In addition, activation of D1 and D2 like receptors will alter the membrane trafficking of NMDA, $GABA_A$ receptors and CaV2.2 channels by direct protein-protein interactions or by downstream action of tyrosine kinase activation (Tritsch and Sabatini 2012).

Available evidence indicates that DAergic neurotransmission within the hippocampus during a specific time point seems necessary to consolidate long-term memory (Rossato, Bevilaqua et al.

2009). DA modulation is also critical for inducing hippocampus-dependent synaptic plasticity and memory (Jay 2003, Lisman, Grace et al. 2011). The DA D1-like receptor family regulates persistent synaptic plasticity and contributes to encoding and retaining novel and salient information within the hippocampus (Adcock, Thangavel et al. 2006, Lemon and Manahan-Vaughan 2006). Furthermore, activation of the D1 receptor family was shown to alter excitability in the hippocampus (Ito and Schuman 2007), therefore reducing the threshold for synaptic plasticity induction and memory encoding (Otmakhova and Lisman 1996, Roggenhofer, Fidzinski et al. 2010). At the same time, the D2-like receptor family seems less critical for hippocampus-dependent information processing (Manahan-Vaughan and Kulla 2003). In vitro studies on SC-CA1 synapses indicated that both early LTP (Otmakhova and Lisman 1996) and late LTP are affected by inhibiting the D1-like receptor family (Huang and Kandel 1995, Granado, Ortiz et al. 2008). Existing in-vivo studies in freely behaving rats partially supported these cellular findings on a systemic level (Lemon and Manahan-Vaughan 2006). Immunohistochemical studies localized DA receptors on both excitatory glutamatergic projection neurons and multiple types of inhibitory GABAergic interneurons in the mouse hippocampus (Gangarossa, Longueville et al. 2012). In addition, both D1 and D5 receptors are shown to be pre- and postsynaptically localized, indicating high efficiency of DA-mediated mechanisms of synaptic changes (Bergson, Mrzljak et al. 1995). Tight DA-dependent regulation of the excitability of glutamatergic neurons and of GABAergic inhibition provides a critical starting point for DAergic modulation of synaptic plasticity (Wagner and Alger 1995, Kullmann, Asztely et al. 2000). D1 receptor signaling is mediated via positive coupling to AC (Undieh 2010), leading to the phosphorylation of different cell membrane receptors. Activation of AC initiates an intracellular cascade that targets PKA through cAMP, potentiates NMDA receptor function (Cepeda and Levine 2006), and regulates T-type Ca^{2+} currents (Drolet, Bilodeau et al. 1997). On the other hand, D5 receptors activate PLC, which induces hydrolysis PI to produce diacylglycerol and inositol-1,4,5-trisphosphate (IP3) as second messengers (Berridge and Irvine 1984). The formation of IP3 can induce calcium release from internal calcium sources, which is a critical step in enabling synaptic plasticity (Dudman, Tsay et al. 2007, Wiera, Nowak et al. 2017). Enhancing intracellular calcium levels can activate calcium–calmodulin-dependent protein kinase and lead to CREB protein expression (Undieh 2010, Hansen and Manahan-Vaughan 2014). In contrast, D2-like receptor activation will possibly decrease NMDAR mediated currents by internalizing NMDARs induced by inhibition of CaMKII and PKA production (Wang, Zhong et al. 2003).

The primary source of noradrenergic innervation to the hippocampus originates from neurons in the LC (Loy, Koziell et al. 1980). It is considered to be the sole provider of NA to the hippocampus and

neocortex. Recent studies indicated that NA neuronal circuits are involved in alert waking and state-dependent cognitive processes (Berridge and Waterhouse 2003). NA acts on three main G-protein coupled receptors, known as β-, α-1, and α-2 NA receptors. While β-receptors are more broadly expressed at postsynaptic sites, α2-receptors exist pre- and postsynaptically (Dohlman, Thorner et al. 1991). Depending on interaction sites and concentration of NA, each of these receptors might exert complex effects on neuronal excitability and synaptic transmission (Arnsten, Wang et al. 2012, Waterhouse and Navarra 2019).
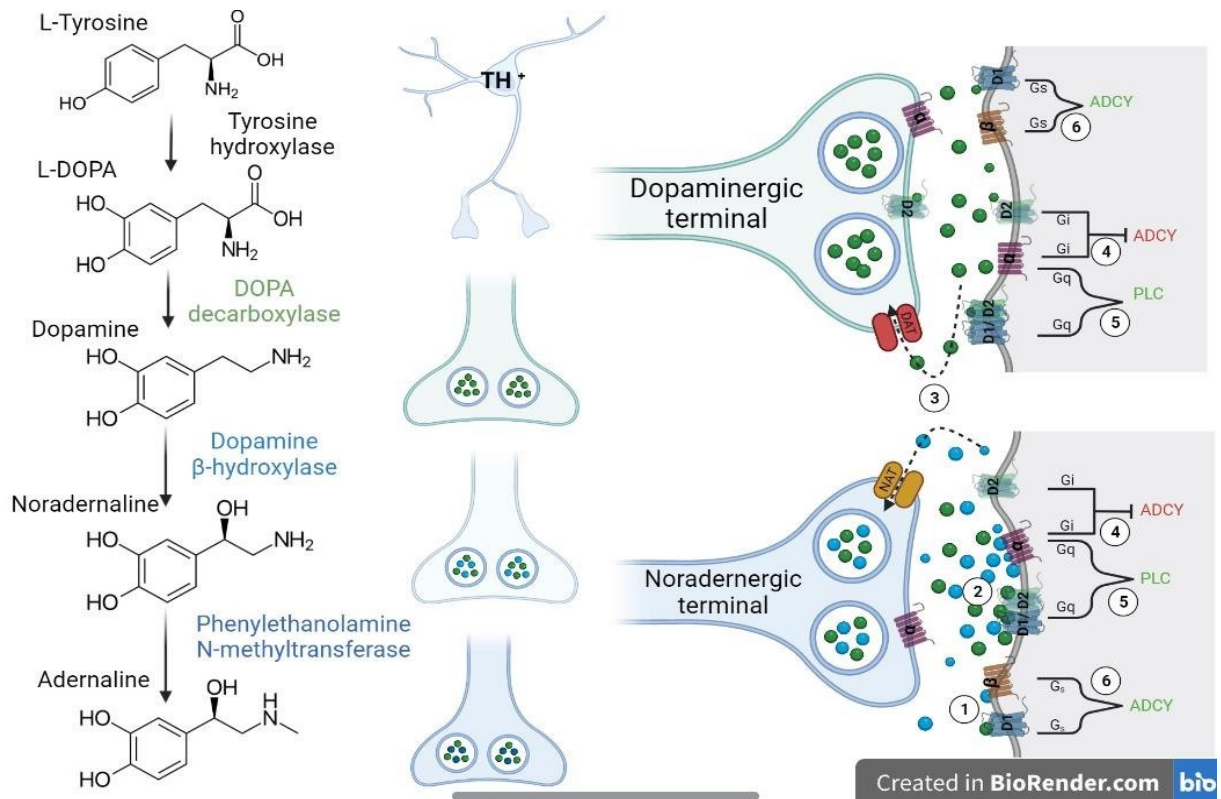
Figure 1.5: Catecholamines biosynthesis from L-tyrosine under the effects of different enzymes, producing L-Dopa. Then DA stores inside the vesicle of DAergic terminals or can further synthesize NA or adrenaline inside the vesicle to shape noradrenergic terminals. The middle panel shows how tyrosine hydroxylase-expressing neurons could shape DAergic or noradrenergic terminals. On the right side: **(1)** NAergic and DAergic terminals release or co-release DA (green) and NA (blue) and bind to specific receptors on target neurons. **(2)** At high concentrations, it might include non-specific binding to other catecholamine receptors. **(3)** Reuptake by NA transporters (NAT) or by DA transporters (DAT). The intracellular signaling cascade shared between both NA and DA receptors leads to either activation or blockade **(4-6)** of PLC, phospholipase C; AC, adenylyl cyclase.

Activation of β-receptors, which are coupled to Gs protein, will enhance cAMP signaling, while, α2-adrenoceptors coupled with Gi leads to suppression of AC and reduction of cAMP. Meanwhile, α2-receptor activation in the presynaptic site suppresses the synaptic release of neurotransmitters in several brain regions. α1- receptor activation will positively modulate the PLC signaling pathway through Gq protein (Yavich, Lappalainen et al. 1997, Nasse and Travers 2014), thus leading to Ca^{2+} release from internal stores and PKC activation.

NA release from LC neurons is regulated by two different modes; tonic and phasic activity. Tonic activity mode is characterized by sustained low-frequency AP discharges, accordingly observed at the highest rate during waking, but lower rate discharge during slow-wave sleep, and paradoxical silence sleep (Foote, Aston-Jones et al. 1980). The release rate of NA is also prognostic for animal behavior (Aston-Jones and Bloom 1981). Phasic discharge, however, is closely associated with sustained attention or vigilance induced by conditioned stimuli (Aston-Jones, Rajkowski et al. 1994). This NA release may then activate β-receptors affecting synaptic transmission and contributing to memory acquisition and maintenance. It is now accepted that emotionally-charged events usually lead to the creation of vivid, long-lasting memories (Cahill and McGaugh 1998, McGaugh 2004). Improvement in memory consolidation happens partially due to NA release and adrenergic receptors stimulation in the nervous system (Izquierdo and Medina 1997, McGaugh 2004). Released NA also affects β-receptors in the basolateral amygdala, modulating the expression of activity-regulated cytoskeleton-associated (Arc) protein in the hippocampus (McIntyre, Miyashita et al. 2005). Several studies also showed the noradrenergic system to be important in the consolidation of memory for emotionally significant experiences (reviewed by e.g., (McGaugh 2000, Tully and Bolshakov 2010)). The noradrenergic system is also shown to be affected by GABA receptor activity, supporting the view that drugs affecting GABAergic receptor activity are capable of modulating emotional memory by controlling the level of NA (McGaugh, Cahill et al. 1996). Generally, numerous studies confirmed that infusing NA into various sites in the brain could improve memory performance (McGaugh, Introini-Collison et al. 1993, Van Stegeren 2008), while blockade of β-adrenergic receptors can negatively affect memory acquisition (Cahill and McGaugh 1996, McGaugh 2004). NA can also affect basal EPSP responses of neurons in different ways, as α2-adrenoreceptor activation reduced EPSP amplitude, whereas β-adrenoreceptors activation led to the strengthening of glutamatergic neurotransmission (Ferry, Magistretti et al. 1997). Hiroshi Katsuki and colleagues observed that NAplays a modulatory role in inducing hippocampal synaptic plasticity (Katsuki, Izumi et al. 1997). While, 10 μM, NA had little effect on LTP induced with theta-burst-patterned stimulation, LTD triggered by 900 pulses of 1-Hz was inhibited. Moreover, NA was shown to facilitate LTP induction

through phosphorylation of the GluR1 AMPAR subunit and enhances AMPA receptor trafficking to synaptic sites (Hu, Real et al. 2007). In genetically modified animals, where NA release was inhibited, CA1 synapses could be induced to show LTD, whereas induction of LTP was blocked (Yang, Lin et al. 2002). Downstream signaling pathways following activation of β-adrenoreceptors by NA in soma and dendrites of CA1 PCs include MAP kinase/ ERK activation in a PKA-dependent fashion (Winder, Martin et al. 1999), which can mediate LTP induction at SC-CA1 synapses.

1.8 Objective of the study

It has been discussed previously how distinct spike timing-dependent plasticity (STDP) protocols can lead to distinguishable pre- or postsynaptic expression of t-LTP at SC-CA1 synapses in acute mouse hippocampal slices (Edelmann, Cepeda-Prado et al. 2015, Edelmann, Cepeda-Prado et al. 2017). Still, new experiments were required to elucidate how two distinct low repeat (6 times at 0.5 Hz) STDP paradigms (i.e., 1:1 or 1:4) that employ physiological relevant numbers of coincident pre- and postsynaptic action potentials recruit distinct sources for postsynaptic Ca^{2+} elevation during induction of t-LTP. So, the first objective of the present dissertation was:

1.) To elucidate how both external and internal sources of Ca^{2+} contribute to t-LTP induction using two distinct low repeat STDP paradigms (6x 1:1 and 6x 1:4 protocols).

Previous studies pointed to distinctly different expression patterns of neurotransmitters and their receptors as well as neuromodulatory signaling and voltage gated ion channels along the longitudinal axis of hippocampus, comprising dorsal (DH), intermediate (IH), and ventral (VH) sections. Likewise, DH, IH, and VH are differentially connected with cortical and other subcortical brain areas. These differences were shown previously to affect CA1 PC electrophysiological properties that might be important for t-LTP mechanism (Milior, Di Castro et al. 2016, Dubovyk and Manahan-Vaughan 2018). We therefore, argued that these differences would most probably also lead to corresponding differences in the magnitude and in the induction and expression mechanisms of low repeat t-LTP in DH, IH, and VH. While the magnitude of classical LTP along the dorso-ventral axis had been investigated before at selected synapse, very few studies addressed to the best of our knowledge, differences in t-LTP at the single-cell level along the longitudinal axis of the hippocampus. Thus, while distinct expression of NMDARs (Bear and Malenka 1994, Fox, Russell et al. 2006, Dubovyk and Manahan-Vaughan 2018), group I and II mGluRs (Mukherjee and Manahan-Vaughan 2013), GABA receptors (Paulsen and Moser 1998) and DA receptors (Hansen and Manahan-Vaughan 2014) were

reported along the DH-VH axis (Papatheodoropoulos, Moschovos et al. 2005, Pandis, Sotiriou et al. 2006, Dubovyk and Manahan-Vaughan 2018), corresponding effects of this variation on t-LTP magnitude along the dorso-ventral axis of CA1 PCs and interaction of GABAergic inhibition and neuromodulatory systems on excitatory synapses at SC-CA1 connection have not been previously investigated and would be extremely interesting to know. We reasoned that such study would provide novel insights into the complex interaction of excitatory synaptic transmission plasticity (t-LTP) with GABAergic inhibition, and neuromodulation at the single cell level. The corresponding experiments in the current thesis therefore aimed at:

2.) Determining differences in excitability of CA1 PCs, and of basal synaptic transmission at SC-CA1 synapses between DH, IH, and VH.

3.) Revealing possible differences in the efficiency to induce t-LTP and in induction and expression mechanisms of low repeat t-LTP (6x 1:1 and 6y 1:4 protocols) along the longitudinal axis of the hippocampus

4.) Deciphering the role of $GABA_A$ and $GABA_B$ receptor-mediated synaptic inhibition in regulating the efficacy of low repeat STDP protocols (i.e. 6x 1:1 and 6x 1:4 protocols) to elicit t-LTP at SC-CA1 synapses in DH, IH, and VH.

5.) Pinpointing the neuromodulatory role of DA and NA signaling in regulating low repeat t-LTP at SC-CA1 synapses along the longitudinal axis of the hippocampus (i.e. in DH, IH, VH).

6.) Finally, we wanted to explore with optogenetic stimulation the required timing of endogenous DA release for successful induction of t-LTP for the DA sensitive 6x 1:1 t-LTP paradigm at S-CA synapses. This task should be accomplished by taking advantage of combining optogenetic tools with electrophysiological recording, using genetically modified mouse lines with the targeting expression of halorhodopsin to dopaminergic neurons.

2 Material and Methods

2.1 Animals

In the present study, juvenile male C57BL/6J mice (Charles River, Sulzfeld, Germany, P28-P35 days old) were used. All experiments were conducted following the European Committee Council Directive (2010/63/EU) on experimental animal methods, protection and ethical guidelines, and were also approved by the local animal care committee (Landesverwaltungsamt Sachsen-Anhalt).

2.2 Hippocampal slice preparation and maintenance

All experiments were performed in the CA1 region of acute mouse hippocampal slices. We used two different cutting angles, including sagittal cuts, to get dorsal hippocampal (DH) slices and transversal cuts for both the intermediate (IH) and ventral (VH) regions. Briefly, animals were deeply anesthetized using forene (Isofluran CP, cp-pharma, Germany) before decapitation. The brain was rapidly dissected and transferred into the ice-cold artificial cerebrospinal fluid (ACSF) cutting solution containing (in mM): 125 NaCl, 2.5 KCl, 25 $NaHCO_3$, 0.8 NaH_2PO_4, 25 glucose, 6 $MgCl_2$, 1 $CaCl_2$, saturated with 95% O_2 and 5% CO_2 (pH 7.2-7.4; 303-305 mOsmol/kg). Sagittal cuts: after chilling the brain an in ice-cold solution, the hemispheres were separated by a sagittal cut along the midline. Each hemisphere was then mounted onto the stage and sliced starting from the lateral surface parallel to the sagittal plane to obtain sagittal slices for the DH (Tidball, Burn et al. 2017) using a vibratome (VT 1200 S, Leica, Germany). Transversal cuts: to obtain IH and VH slices, the complete brain with both hemispheres containing the hippocampus and the entorhinal cortex were sectioned transversally. The CA1 region was isolated from excessive CA3 inputs by a single cut between CA3 and CA2 to reduce spontaneous EPSPs and bursting when inhibition was blocked with picrotoxin and when measurements were performed at higher temperatures (Fink and O'Dell 2009, Edelmann and Lessmann 2011). Next, we transferred slices to a hydrophilic membrane (0.4 μm Millicell culture insert, PICMORG50, Millipore, Germany) placed in a handmade interface chamber submerged in pre-warmed carboxygenated ACSF cutting buffer to rest for 25 min at 32°C for recovery. Following 25 min of incubation, slices were kept for at least 1 hour at room temperature (22-25°C) to improve slice viability before being used for recording (Cepeda-Prado*, Khodaie* et al. 2021). Electrophysiological

recordings in acutely isolated hippocampal slices: After more than 1 hr of incubation at room temperature, a slice was transferred to a submerged recording chamber of a patch clamp setup. A ring with parallel nylon threads was used to restrict the movement of hippocampal slices during the whole recording procedure. Carboxygenated ACSF buffer containing (in mM): 125 NaCl, 2.5 KCl, 0.8 NaH_2PO_4, 25 $NaHCO_3$, 25 Glucose, 1 $MgCl_2$, 2 $CaCl_2$; pH 7.4; ~301-303 mOsmol/kg, saturated with 95% O_2 and 5% CO_2, was used as recording solution (1-2 ml per min). ACSF temperatures were kept at 30 ± 0.2°C using an inline heater (Model SH-27B Inline heater, Warner Instrument Corporation, USA) and continuously monitored using a heat controller (Model TC-324 Heat Controller, Warner Instrument Corporation, USA). In most STDP experiments, the $GABA_A$ mediated synaptic inhibition was blocked by adding 100 μM picrotoxin (Sigma, Germany). In some experiments $GABA_B$ receptor inhibitor CGP 55845 hydrochloride (10 μM; Tocris, Germany) was added to the picrotoxin containing ACSF to provide complete blockade of GABAergic inhibition. For whole-cell recording, slices were visualized using a fixed stage Zeiss microscope (Carl Zeiss, Jena, Germany) coupled to a charge-coupled device (CCD)-infrared (IR) camera (PCO AG, Kelheim, Germany) shown in **Figure 2.2**. A glass pipette was used as a recording pipette (resistance 4-6 MΩ) was filled with a freshly prepared internal solution containing (in mM): 10 HEPES, 20 KCl, 115 potassium gluconate, 10 Na^+ phosphocreatine, 0.3 Na-GTP, and 4 Mg-ATP; pH 7.4, 285-290 mOsmol/kg used to patch the cells. Cells were held at -70 mV in the current clamp or voltage clamp (liquid junction potential of +10 mV of the internal solution was corrected manually) with an EPC-8 patch-clamp amplifier (HEKA, Lamprecht, Germany). A glass stimulation electrode (resistance 0.7 – 0.9 MΩ) containing recording solution was placed in the S.r. of the CA1 subfield used to generate an excitatory postsynaptic potential (EPSP, at 0.05Hz) at SC-CA1 synapses (**Fig. 2.3A**). The stimulus intensity was adjusted to evoke EPSP amplitudes of 4-5 mV corresponding to 30%–50% of maximal EPSP amplitudes (stimulus duration 0.7 ms, intensity 90 to 700 μA).

2.3 Experimental scheme

After visualization of the hippocampal region (CA3 curve) in the slices using 5x objective, a glass electrode (resistance 0.7- 0.9 MΩ) filled with intracellular ACSF solution was positioned in S.r. in CA1 over SC axonal bundles to stimulate SC-CA1 fibers (**Fig. 2.1**). Recording pipette filled with internal solution (explained in **section 2.5**) was placed in the patch pipette holder. Two electromotor-
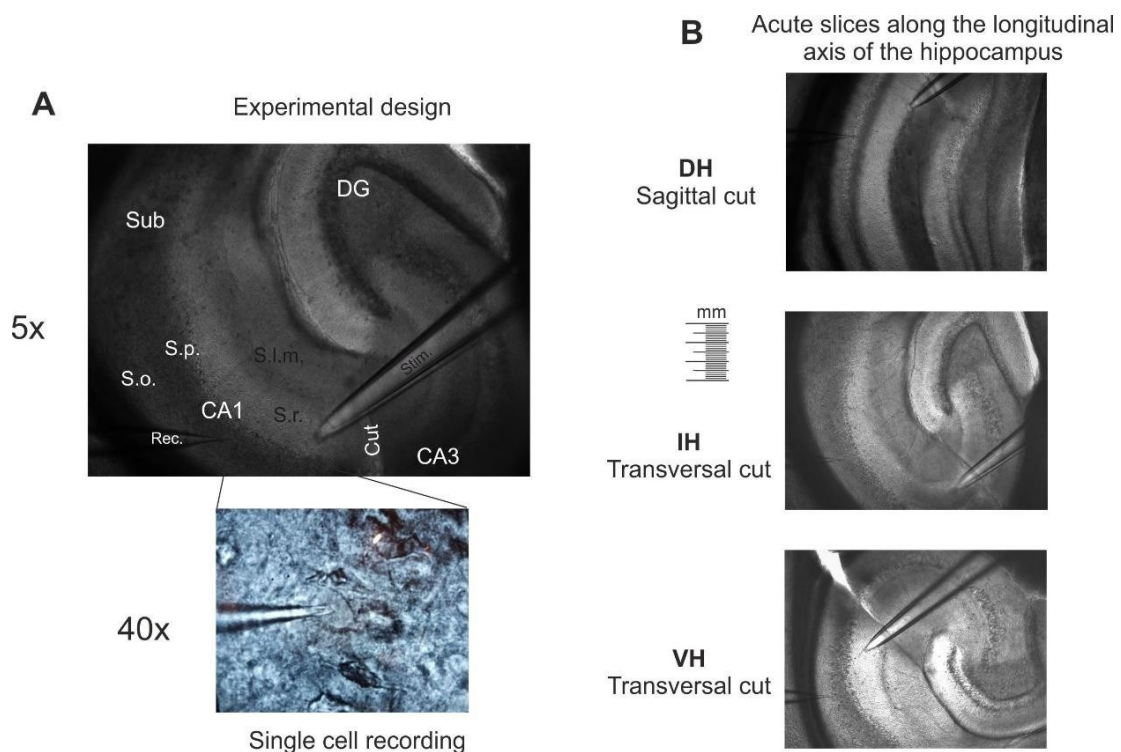
Figure 2.1: Experimental design. **A)** Acute hippocampal slices from 1-month-old C57BL/6J mice. A focal (glass pipette) stimulation (stim.) electrode is positioned in the S.r. to stimulate the SC fibers as presynaptic input to induce EPSP in recorded CA1 neurons in striatum pyramidale (S.p.) under a 5x objective lens. The lower panel shows a recorded cell at higher magnification (40x). The patch clamp recording electrode (Rec.) was also used to stimulate CA1 PCs through depolarizing current injections during t-LTP experiments. **B)** Slices were taken along the longitudinal axis of the hippocampus using two different cutting planes, including sagittal (for DH), and transversal (IH and VH) cutting angles.

controlled micromanipulators (Luigs & Neumann GmbH, Ratingen, Germany) micromanipulators (Luigs & Neumann GmbH, Ratingen, Germany) were used for control of recording and stimulation electrodes. Both electrodes were made from borosilicate glass with filaments (outside 1.5 mm, inside 1.05 mm diameter; Science products, Hofheim, Germany), prepared by a two-step puller device (Narishige Scientific Instrument Lab, Tokyo, Japan). The pipette's tip followed down under the microscope's focus until it got close to the cell surface. Then slight positive pressure was applied using a 1 ml syringe coupled to a three-way valve connector (**Fig. 2.2**). The pipette moved slowly until the shadow over the cell soma appeared. Immediately, the positive pressure was released, andnegative pressure was rapidly applied until it reached 200 Mega-Ohm (MΩ); at this point, negative pressure was removed to increase the resistance to one

gigaohm (GΩ) to form the gigaseal configuration. One last negative pressure was used to break into the cell and reach the whole-cell patch-clamp configuration (compare **Fig. 2.2)**. For certain experiments, either current clamp (CC) or voltage clamp (VC) modes were used. At the beginning and the end of recording under CC recordingmode, action potential parameters were tested to check cell viability using steps of steady depolarizing current (20 pA increment per step for 1 sec; **Fig. 2.3A**). AP firing differences and other basal and intrinsic excitability properties were all recorded in different CA1 PCs along the longitudinal axis of the hippocampus. During the EPSP test period, each EPSP was evoked by SC fiber depolarization for 0.7 ms with different intensities ranging from 90 to 700 µA and delivered every 20 sec (0.05 Hz; **Fig. 2.3B)**. The stimulus intensity was adjusted to evoke responses with amplitudes of 4–7 mV corresponding to 30–50% of maximal EPSP amplitudes and kept constant during the whole experiment. Paired pulse ratio facilitation was recorded with two electrical pulses at an inter- stimulus interval of 50 ms in VC recording mode, inducing two consecutive SC fiber depolarization, resulting in two evoked EPSCs in the postsynaptic neuron (**Fig. 2.3C)**. The PPR ratio was calculated by dividing the peak amplitude in the 2nd EPSC response to the peak amplitude of the 1st evoked EPSCs response. We also evaluated plasticity-related incorporation of new AMPA receptors into the postsynaptic membrane by calculating the ratio between AMPAR and NMDAR currents (I_{AMPAR}/ I_{NMDAR}) at the end of the experiments (Cepeda-Prado*, Khodaie* et al. 2021). The AMPAR/NMDAR current ratio was measured at the end of the EPSP recording after t-LTP induction along thelongitudinal axis of the hippocampus as a read-out of AMPA receptor insertion after inducing t-LTP. AMPA receptor-mediated components were determined as EPSC peak currents recorded at a holding potential of −70 mV. NMDAR-mediated slow current components were determined from EPSCs recorded at -20 mV holding potential at different time points after EPSC start (DH: 45 ms, IH and VH: 50 ms; compare **Fig. 2.3D**), due to distinct kinetics of NMDAR mediated EPSP components along thelongitudinal axis (Pandis, Sotiriou et al. 2006). The AMPAR/NMDAR current ratio was calculated from these two amplitudes of the EPSCs (Wyllie, Livesey et al. 2013). GABA$_B$R mediate response was also read-out during the hyperpolarization phase of EPSP (150 ms following EPSP depolarization).
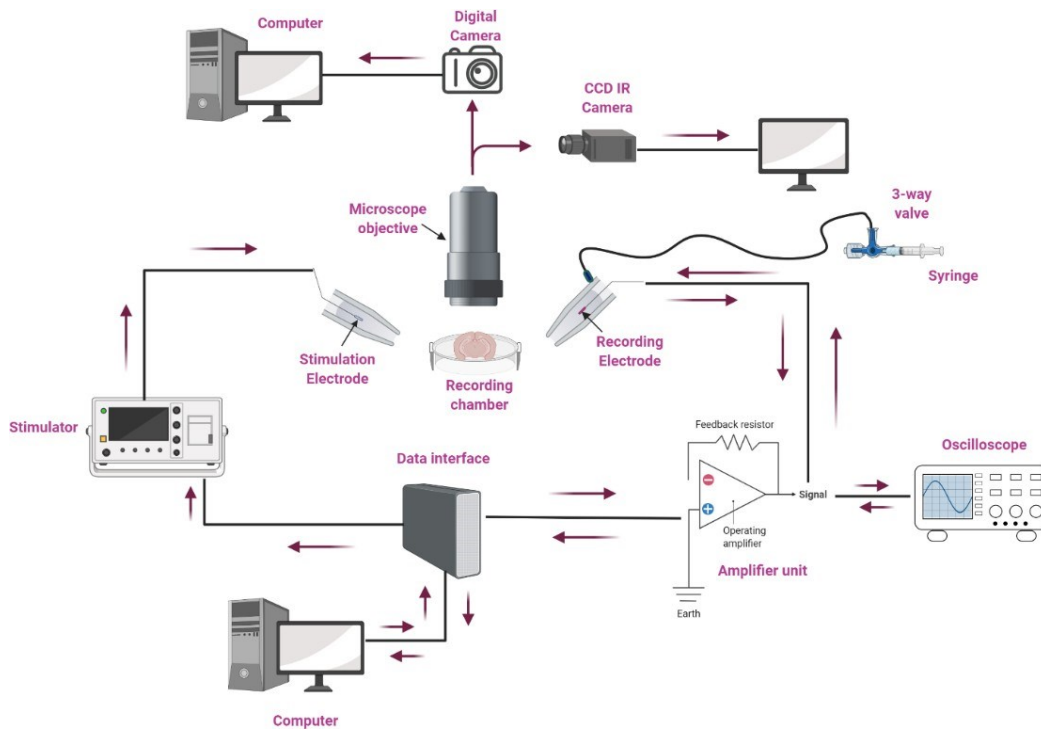
Figure 2.2: Patch clamp setup. Schematic representation of the electrophysiological setup used for this project, showing the connections between the different parts and devices that build the electrophysiological setup. The purple arrows indicate how the electrical signals flow through the system. Created in BioRender.com
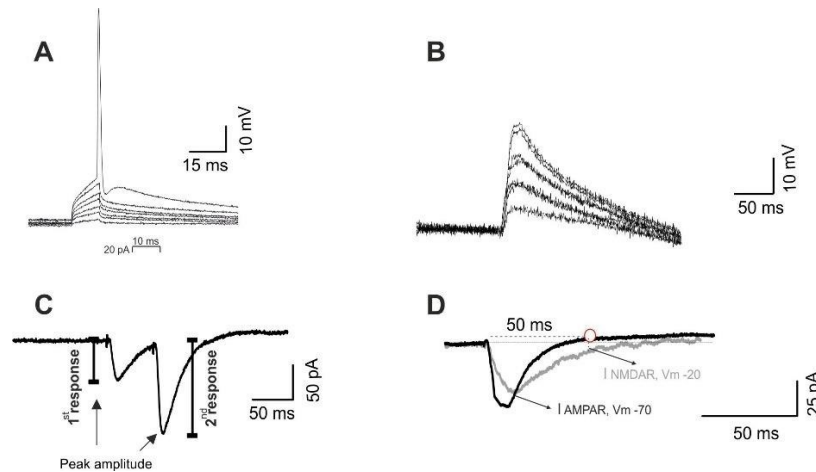
Figure 2.3: Basal intrinsic properties of CA1 PCs measure by running different protocols. **A)** AP firing in response to increasing current injection. **B)** EPSP test by stimulation of SC fibers using different stimulation intensities, 50 % of stimulation intensity inducing maximum response were used throughout an STDP experiment. **C)** Original traces of two evoked EPSCs elicited within a time interval of 50 ms. Black lines indicate the points from which the peak amplitude was calculated. **D)** NMDAR/AMPAR current ratio analysis of evoked EPSC components at the holding potential of -70mV

for AMPAR responses and at -20 mV holding potential for NMDAR receptor-mediated components, which is determined 50 ms after the onset of the EPSC.

2.4 Induction of spike timing-dependent plasticity

Spike timing-dependent plasticity (STDP) was induced by the pairing of a single EPSP generated by extracellular stimulation of SC, with a single action potential (AP) in our 1:1 protocol, or with a burst of 4 postsynaptic APs, which is named 1:4 protocol (spike frequency 200 Hz) induced by somatic current injection (2 ms; 1 nA) through the recording electrode. Pairings of postsynaptic EPSP and APs were performed with a time interval of +10 ms (Δt) and were repeated for 1:1 (6x, 25x, 50x, and 70x), and for 1:4 (2x, 3x, 6x, and 35x) at a frequency of 0.5 Hz to elicit t-LTP. Changes in the synaptic strength were monitored every 20 sec (0.05 Hz; **Fig. 2.1B**). The first 10 min of an EPSP experiment before induction of t-LTP protocols (i.e., 6x 1:1 or 6x 1:4) were recorded as the baseline strength of synaptic transmission (time point: -10 to 0 min). EPSPs were elicited every 20 s (i.e., 0.05 Hz) for 10 minutes baseline and then 30 minutes after STDP induction. The paradigm and repeat number dependent t-LTP magnitude was calculated by comparing the 10min baseline to the last 10min of recording and expressed as change from baseline (in %). A separate group of cells was used to assess possible spontaneous changes in synaptic transmission (stimulation at 0.05 Hz for 40 min) without any STDP stimulation and served as negative controls (designated as 0:0 controls).

2.5 Light dependent manipulation of DA release in acute hippocampal slices

Previous studies showed that DA modulation can regulate the excitability of CA1 pyramidal neurons (Henze, González-Burgos et al. 2000, Edelmann and Lessmann 2011, Edelmann and Lessmann 2013). Furthermore, under DA receptor blockade, both 6x 1:1 and 6x 1:4 protocols failed to induce robust t-LTP (Cepeda-Prado*, Khodaie* et al. 2021). Therefore in another set of experiments we combine optogenetic tools with electrophysiological recording in acute slices from transgenic eNpHR3.0-EYFP (MGI:5014747) mice which express halorhodopsin from the halophilic bacterium Natronomas pharaonis (NpHR) fused in-frame with an enhanced yellow fluorescent protein (EYFP) known as B6;129S-Gt(ROSA)26Sortm39(CAG-hop/EYFP) Hze/J mice, was crossed to tyrosine hydroxylase driver line 7630403G23Rik Tg(Th-cre)1Tmd, result in Th-Cre Halorhodopsin (eNpHR) mice lines available in the institute and previously tested by (Stuber, Stamatakis et al. 2015, Bui, Nguyen et al. 2018) to restrict expression of halorhodopsin to TH positive dopaminergic neurons. In the offspring,

mutation 1 (eNpHR3.0-EYFP; Halorhodopsin) and mutation 2 (Th-IRES-Cre; Th-Cre) were determined by PCR from ear punches taken by the animal caretaker. In our experiments, we employed heterozygous mice for both mutations (Halo: +/-, and Th-Cre: +/-; referred as +eNpHR) as experimental groups and their WT littermates (Halo: +/-, and Th-Cre: WT; referred as -eNpHR) as control animals. To confirm the co-expression of the EYFP fused with the NpHR gene in TH-positive dopaminergic neurons, we decapitated 2 to 3 months old animals (+eNpHR: n=6 / N=3) and prepared coronal (350 μm thick) sections to harvest hippocampal slices. Coronal cuts enabled us also to include the VTA known to harbor large quantities of DA cell somata and the highest expression of the EYFP signal was expected to serve as a positive control. Slices were visualized using confocal microscopy under a GFP filter (excitation with argon laser line at 488 nm, emission filter: 519-621 nm, **Fig. 3.26**). EYFP signals were detected in the VTA, and the catecholaminergic fiber tracts could be followed to various brain areas (e.g., the S.r. of the CA1 hippocampal region). To screen for changes in synaptic transmission due to light-induced inactivation of DAergic inputs, we electrically stimulated SC fibers and recorded EPSPs from CA1 PCs before and after inhibition of DAergic fibers by light stimulation (Nominal wavelength; 561 nm, Laserglow LRS-0561, Laserglow Technologies, Ontario, Canada) running constantly all along with the experiment and/or started at different time-points as explained in respective Results section (**3.14**). AP firing frequency and EPSP changes in response to 50% of maximum stimulation intensity of extracellular SC stimulation were tested in +eNpHR animals in the absence and presence of constant light illumination (light: +eNpHR$_{ON}$) and compared to -eNpHR as well as wild type animals. We then measured changes in resting membrane potential (RMP) before light, during light, and 10 minutes after light illumination in slices taken from +eNpHR animals. In the next step, we tested STDP paradigms in the presence of light in +eNpHR and in -eNpHR animals, and compared results to STDP recorded in the absence of laser illumination (+eNpHR$_{OFF}$: see **Fig. 3.29**). Furthermore, to confirm the laser light induced inhibitory effect on DA release we added 20 μM exogenous DA (40 μM Vitamin C was added as an antioxidant to DA containing ACSF; running from the beginning of recording at the same time when light illumination started at -10 min) to the recordingACSF, which completely rescued t-LTP induction (**Fig. 3.30**).

Following these control experiments, we used the optogenetic tool to silence DA release during different time intervals of the t-LTP experiments, i.e., before (-10 to 0 min), during (0 to +10 min), and starting at +10 min after t-LTP induction (referred as early expression) or starting at +20 min. after t-LTP induction (referred as late expression) in +eNpHR animals.

2.6 Pharmacological tools

To investigate the requirement of NMDARs activation during t-LTP induction, we bath applied an NMDAR antagonist (50 µM DL-APV, DL-2-Amino-5-phosphonopentanoic acid; Tocris, Bristol, UK). 10 µM NBQX (Tocris, Bristol) was used in some experiments to inhibit AMPAR mediated currents, used to estimate wash-in time of our ACSF. Dependency of t-LTP on L-type voltage gated Ca^{2+} channels (VGCCs) was assessed by adding a selective VGCC inhibitor Nifedipine (25 µM; Sigma, Germany) to our recording ACSF. DAergic modulation of STDP was investigated by bath applications of D1-like (10 µM SCH23390; Sigma, Germany) or D2-like antagonists (10 µM Sulpiride; Sigma, Germany). Furthermore, we tested the role of group I metabotropic glutamate receptors (mGluR1 and mGluR5) in STDP by adding mGlu1R (1 µM YM298198; Tocris, Bristol, UK) and mGluR5R (10 µM MPEP; Tocris, Bristol, UK) antagonists to the recording ACSF solution. In a separate set of experiments, the contribution of Ca^{2+}-permeable (cp-)AMPA receptors (Rs) to t-LTP (Kauer and Malenka 2006) was verified by application of the selective cp-AMPAR inhibitors NASPM trihydrochloride (100 µM 1-Naphthyl acetyl spermine trihydrochloride; Tocris, Bristol, UK) and IEM 1460 (100 µM; Tocris, Bristol, UK) through the recording using a minipump (P720 peristaltic pump, INSTECH), which used for expensive drugs, solvent controls equally with continuous perfusion (1–2 mL per min) of prewarmed (30 ± 0.2 ◦ C) solution. Both NASPM and IEM were applied 15 min before STDP induction. The role of internal Ca^{2+} stores for t-LTP induction was tested by adding the Inositol 1, 4, 5-trisphosphate (IP3) receptors inhibitor 2-APB (100 µM, 2-Aminoethoxydiphenyl Borane; Tocris, Bristol, UK) running by mini-pump. We also intracellularly infused Ryanodine (100 µM, Tocris, Germany) through the patch pipette internal solution for at least 15 min before t-LTP induction to block ryanodine receptors of internal calcium stores. The β-adrenergic non-selective antagonist, propranolol (10 µM 2-propanol hydrochloride, Tocris, Germany) was added to the bath solution to assess the contribution of β-adrenergic receptors to t-LTP. If not stated otherwise, we blocked GABA$_A$ receptor mediated inhibition during our recordings by adding 100 µM picrotoxin in our recording ACSF. However, in experiments addressing the role of GABAergic modulation on hippocampal STDP, different GABA receptors were blocked. In a subset of experiments either GABA$_B$ receptor-mediated components were blocked by the addition of CGP 55845 hydrochloride to the recording solution (10 µM, Tocris, Germany), or GABA$_A$R components were blocked by adding picrotoxin (Sigma, Germany, dissolved in 100% ethanol, final the concentration of ethanol in ACSF was 0.2%) were added to the recording solution. Distilled water was used for all other pharmacological compounds for dilution.

Nitric oxide (NO) synthase inhibitor L-NAME (200 μM, Tocris, UK) was added to recording ACSF to determine the role of NO as a possible retrograde messenger in t-LTP.

2.7   Data acquisition

Whole-cell recordings were obtained using a patch-clamp amplifier (EPC-8, HEKA, Germany) connected to a LiH 8+8 interface. Data were filtered at 3 kHz and digitized at 10 kHz using PATCH MASTER software (HEKA, Germany). Data analysis was performed using FITMASTER (HEKA, Germany). Current clamp mode at a holding potential of -70 mV was used in all experiments, except for the paired-pulse ratio (PPR), miniature EPSCs, as well as AMPAR/NMDAR current ratios which were recorded in the voltage-clamp mode at -60 mV and -10 mV (for NMDA current) holding potential. Of note, the liquid junction potential of +10 mV resulting from the combination of internal and external solutions was corrected. The mean of EPSP slope was calculated from the initial 2 ms after EPSP onset. The baseline of synaptic responses before inducing STDP was set to 100 % (average over 10 min), and all EPSPs after induction of STDP were normalized to this baseline. Input resistance was controlled by hyperpolarizing current steps (250 ms; 20 pA), elicited prior to EPSP responses. The change of EPSP slopes was used to calculate synaptic strength as the average of EPSP slopes 20 to 30 min after t-LTP induction, divided by the mean EPSP slope measured during 10 min before STDP stimulation (baseline). Cells were only included for analysis if the initial resting membrane potential (RMP) was between -55 and -70 mV. Cells were excluded when the input resistance varied more than 30% over the entire experiment. Furthermore, cells showing visible "run-up" or "run-down" of EPSP slopes during baseline recording were excluded. The AMPAR/NMDAR current ratio was measured at the end of the EPSP recording after t-LTP induction as a read-out of AMPA receptor insertion after inducing t-LTP. In voltage clamp recordings, AMPA receptor-mediated components were determined as EPSC peak currents recorded at a holding potential of –60 mV. NMDAR-mediated current components were determined from EPSCs recorded at -10 mV holding potential. Due to distinct kinetics of NMDAR mediated EPSP components along the longitudinal axis of the hippocampus (Pandis, Sotiriou et al. 2006), NMDA components were read out as the remaining current amplitude at different time points after EPSC start (i.e. DH: 45 ms, IH and VH: 50 ms; compare **Fig. 3.20C**). The AMPAR/NMDAR current ratio was calculated from these two amplitudes of the EPSCs (Wyllie, Livesey et al. 2013)

2.8   Statistical analysis

Data are shown as mean ± standard error of the mean (SEM), representing the results of at least three animals per group. The respective number of experiments (n) and the number of animals (N) is reported in the Figure legends. Statistical analysis of data was performed with GraphPad Prism version 8.0 (GraphPad Software, California, USA). The distribution of all data was determined using the Shapiro-Wilk normality test and analyzed with respective statistical tests. Paired and unpaired Student's t-tests were used to compare two groups with a normal distribution; otherwise, a nonparametric Mann-Whitney U-test was applied. Multiple comparisons were assessed with a one-way analysis of variance (ANOVA) followed by a post hoc Tukey test or Kruskal-Wallis test followed by post hoc Dunn's multiple comparisons test for parametric and nonparametric data, respectively. To compare the cumulative distribution of EPSC frequencies and amplitudes before and after t-LTP we used two samples Kolmogorov-Smirnov test. A one-sample t-test was applied in some cases to determine the significance of t-LTP magnitude compared to the baseline of the same cell. The respective statistical tests used for each group is indicated in the result part. P-value of <0.05, <0.01, and <0.001 were set as levels of significance and are indicated by asterisks (*, **, and ***, respectively). Origin 8.1G (Additive GmbH, Germany), and BioRender.com was used in the preparation of graph.

3 Results

3.1 Induction of Spike timing dependent plasticity at Schaffer collateral-CA1 synapses

Using Spike timing-dependent plasticity protocols, we tested timing-dependent (t-) LTP and t-LTD at Schaffer collateral-CA1 (SC-CA1) synapses. Stimulation procedures and different cutting planes to access slices along the longitudinal axis of the hippocampus are explained in detail in Methods **sections 2.2 and 2.4,** and also **3.1**. In the first part of the current dissertation, we focused on the mechanism underlying synaptic changes following 6x 1:1 and 6x 1:4 paradigms. We previously developed these two STDP paradigms in the lab, which induces t-LTP when presynaptic stimulation is paired with a positive spike timing (+Δt) with an AP in the postsynaptic cell, whereas reverse pairing (-Δt) leads to t-LTD (**Fig. 3.1B)**.
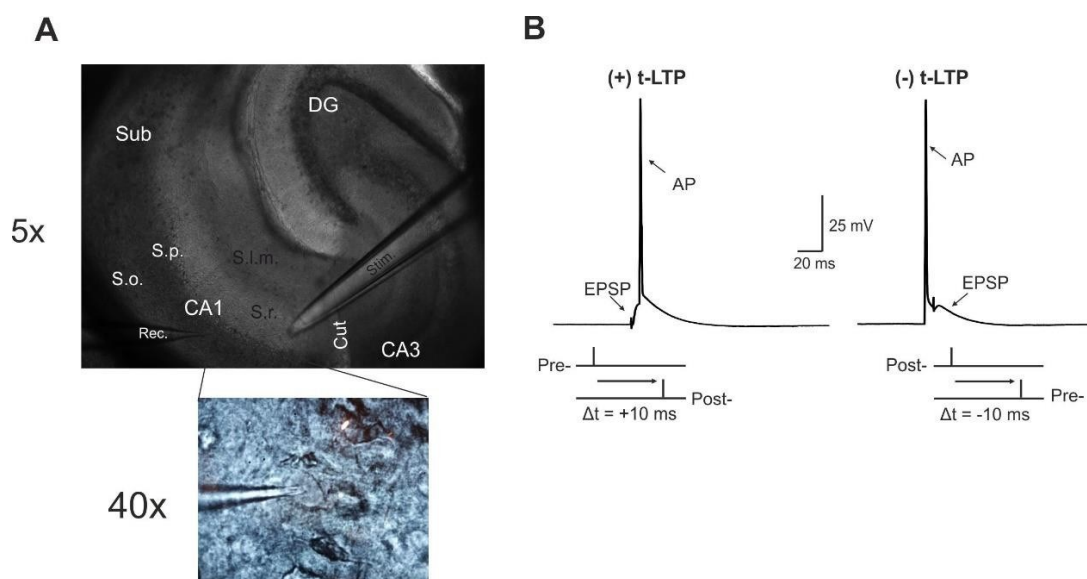
Figure 3.1: **Experimental setting used for STDP experiment**. **A)** STDP experiments were performed in acute hippocampal slices of 1-month-old C57BL/6J mice, a stimulation (stim.) electrode positioned in the S.r. over SC-CA1 fibers used to induce presynaptic stimulation (EPSP), which was paired with one or four action potentials in CA1 PCs stimulated via the recording electrode (Rec.); lower panel shows higher magnification (40x) of recorded CA1 cell. **B)** Original traces of spike pairing (canonical protocol; 1:1) with 10 ms positive (+Δt) settings were used to induce t-LTP and negative pairing (-Δt) settings were used to induce t- LTD.

3.2 STDP stimulation employing different numbers of spike pairings at Schaffer collateral-CA1 synapses induces robust t-LTP

Previous studies suggested that synaptic changes in the hippocampus (Tse, Langston et al. 2007) and the olfactory region (Brennan, Kaba et al. 1990, Lesburguères, Gobbo et al. 2011) can shape long-term memories with only a few presentations of stimuli or even with a single trial (for more details see (Otto, Eichenbaum et al. 1991)). We initially performed a group of experiments to determine how the change of t-LTP magnitude induced by canonical (1:1) and burst (1:4) protocols was affected by different numbers of repeats during STDP induction. We used acute intermediate hippocampal (IH) slices to tackle this question. We tested the t-LTP magnitude using 6, 25, 50, and 70 repeats for 1:1, and 3, 6, 35, and 100 pairing repeats for 1:4 protocols. The intervals between two successive spike pairings were set to 2 s (i.e. 0.5 Hz intervals). Then the magnitude of repeat-number dependent t-LTP was compared with negative controls (0:0), in which no STDP was induced but the synapses were test stimulated every 20 s for 40 min (the same as for all t-LTP experiments). Our 1:1 t-LTP experiments revealed that 6 repeats (6x) of pre-and postsynaptic activation at 0,05Hz is the lowest repeat number to induce robust (significant) t-LTP at SC-CA1 synapses (147.11% ± 6.14%, 60 recorded cells/33 mice) compared to 0:0 (98.31% ± 5.06%, 13/6, Kruskal-Wallis test, $H_{(5)}$ = 18.94; p = 0.0003; **Fig. 3.2B and C**). Similar results were obtained with 25 repeats (141.10% ± 10.36%, 25/8; p = 0.05; **Fig. 3.2B and C**). While the magnitude of t-LTP induced with the 50x 1:1 paradigm showed a non-significant increase compared to 0:0 (146.21% ± 13.82%, 5/3; p = 0.143; **Fig. 3.2B**), probably only due to the relatively low "n", it shows a significant potentiation compared to 100% baseline (Student's t-test p = 0.028, one-sample t-test). A robust t-LTP was again induced with the 70x 1:1 protocol compared to the 0:0 control group (152.83% ± 12.92%, 7/5; p=0.016; **Fig. 3.2B and C**). Typical time courses for single experiments for 0:0, and potentiated groups with 6x 1:1, 25x 1:1 and 70x 1:1 are presented in **Figure 3.2C.** The stability of the recording was determined by resistance input (R_{in}) and is shown for the different single experiments.
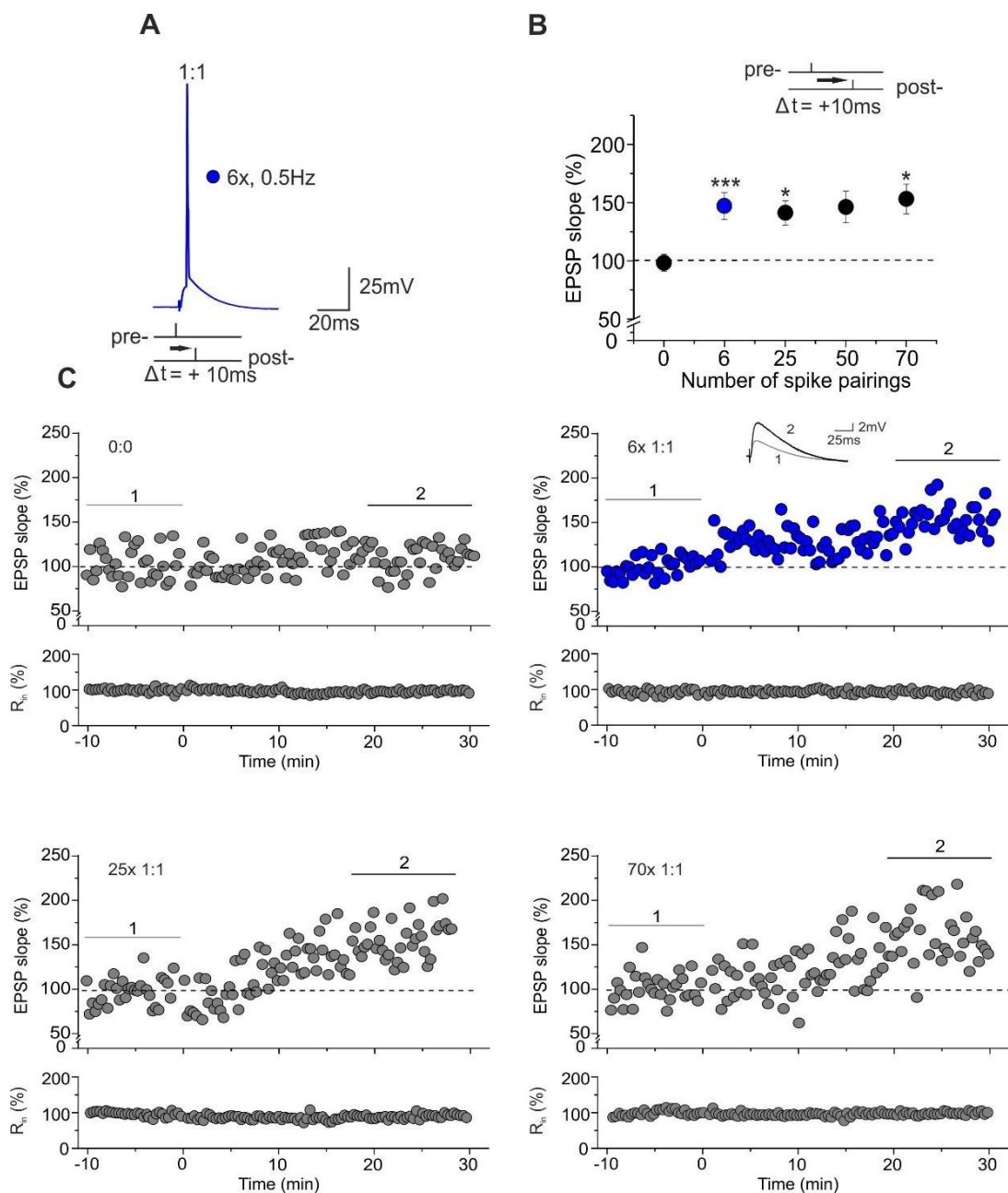
Figure 3.2. Induction threshold for 1:1 t-LTP at SC-CA1 synapses. A) Original trace for the 6x 1:1 t-LTP protocol. **B)** Dependence of t-LTP magnitude in the intermediate hippocampus (IH) on the number of spike pairings. The p-values were obtained using Kruskal-Wallis test $H_{(5)}$ = 18.50; p = 0.001, followed by Dunn's multiple comparison test post hoc analysis. * P < 0.05, and *** p < 0.001. Data shown are mean ± SEM. **C)** Typical time courses of individual cells are shown for negative control (0:0), 6x 1:1, 25x 1:1, and 70x 1:1. At the top of the graphs, the inserts represent the average EPSPs during baseline recording **(1)** and 20 min after stimulation with STDP protocol **(2)**. The number of recorded cells and number of animals for each paradigm were: 0:0 (n=13 / N=6); 6x (n=60 / N=33); 25x (n=25 / N=8); 50x (n=5 / N=3), and for 70x (n=7 / N=5).

52

Pairing presynaptic stimulation with a burst of four postsynaptic APs (at 200 Hz) and a $\Delta t = 10$ ms, was previously established in our lab by (so-called 1:4 t-LTP paradigm, (Edelmann, Cepeda-Prado et al. 2015)). However, the minimum repetition of pre-and postsynaptic activation to induce synaptic changes in the SC-CA1 synapse was a matter of debate. Hence, the 1:4 burst stimulation paradigm was tested with lower repeat number in this dissertation (2, 3, and 6 times; **Fig. 3.3**).

Interestingly, the corresponding results that robust t-LTP could be induced even with only 3 repeats of this 1:4 paradigm (3x 1:4: 159.38% ± 16.86%, 10/4) compared to the negative control (98.31% ± 5.06%, 13/6; Kruskal-Wallis test, $H_{(5)} = 31.92$; p = 0.0095, **Fig. 3.3B**). Similarly, 6 repeats (6x 1:4 paradigm) also induced reliable t-LTP (163.52% ± 6.59%, 53/29; p< 0.0001; **Fig. 3.3B and C**). Further reduction of repeat numbers to 2 times did not induce a reliable potentiation at SC-CA1 synapses (111.99% ± 6.63%, 11/4; p > 0.99, **Fig. 3.3B**), while stimulation with higher repeatnumbers (35x 1:4) led to a non-significant increase of synaptic strength (140.58% ± 11.72%, 9/6; p= 0.14, **Fig. 3.3B**) probably only due to the relatively low "n", it shows a significant potentiation compared to 100% baseline (Student's t-test p = 0.008, one-sample t-test).

The characteristics of the patterned stimulations to induce t-LTP described above are similar to naturally occurring spiking patterns observed in the hippocampus of freely behaving animals during learning *in vivo* discussed by (Otto, Eichenbaum et al. 1991). Given that in our recordings 6 repeats of 1:1 and 1:4 stimulation proved to be sufficient to observe t-LTP with both protocols, we selected these six spike pairings to systematically investigate the properties of t-LTP at hippocampal SC-CA1 synapses. From now on, we call these STDP paradigms 6x 1:1 canonical protocol or stimulation (in blue, **Fig. 3.2**), and 6x 1:4 or burst protocol/stimulation (in red, **Fig. 3.3**).
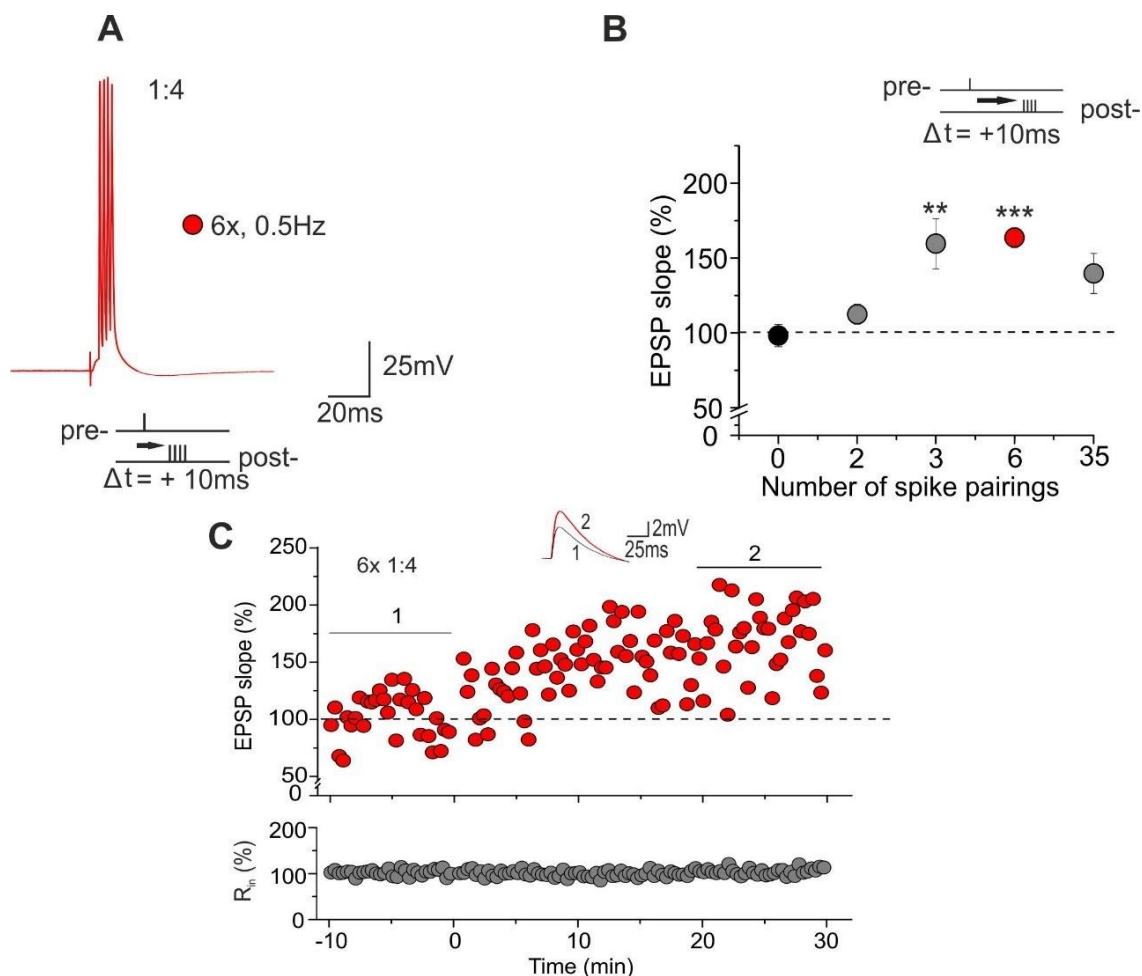
Figure 3.3. Low-repeat STDP paradigms with a 1:4 pattern were tested for the robustness of t-LTP at SC-CA1 synapses. A) Original trace of 6x 1:4 protocol with a 10 ms positive pairing of pre- and postsynaptic spikes. Four APs in the postsynaptic cell were delivered at 200 Hz, pairings were performed every 2s. **B)** Dependence of t-LTP magnitude in the intermediate hippocampus (IH) on the numbers of spike pairings. The p-values were obtained using Kruskal-Wallis test H $_{(5)}$ = 31.92; p = 0.0001, followed by Dunn's multiple comparison test post hoc analysis. ** p < 0.01, *** p < 0.001. Data shown are mean ± SEM. **C)** Typical time course of 6x 1:4 t-LTP in an individual cell indicating how the EPSP slope starts to increase 5 min after the burst protocol execution. At the top of the graph, an insert shows EPSP changes before **(1)** and after **(2)** the STDP induction. The number of recorded cells and number of animals for each paradigm were: 0:0 (n=13 / N=6); 2x (n=11 / N=4); 3x (n=10 / N=4); 6x (n=53/ N=29), and 35x (n=9/ N=6).

3.3 Successful induction of t-LTP at Schaffer collateral-CA1 synapses depends on coincident spiking of pre- and postsynaptic cells

Based on the concepts of Hebbian plasticity, STDP represents an associative form of synaptic plasticity (Hebb 2005), which works by the pairing of pre- and postsynaptic cells. To test the importance of this principle, we also tested two stimulation protocols that either consisted exclusively of presynaptic spiking (6x 1:0, at 0.5 Hz) or of postsynaptic (3x 0:4, 4 spikes at 200 Hz; 3 repeats at 0.5 Hz) AP firing (**Fig. 3.4A**). No significant changes in synaptic strength were observed with only presynaptic spiking (6x 1:0; 103.93% ± 6.89%, 7/4; **Fig. 3.4B**) or postsynaptic burst firing alone (3x 0:4; 110.03% ± 9.59, 9/4; **Fig. 3.4B**) compared to the negative control (0:0. i.e. continuous test stimulation at 0.05 Hz for 40 min: 98.31% ± 5.06%, 13/6; Kruskal-Wallis test, $H_{(3)}$ = 0.759, followed by Dunn's multiple comparison test post hoc analysis, **Fig. 3.4B**).
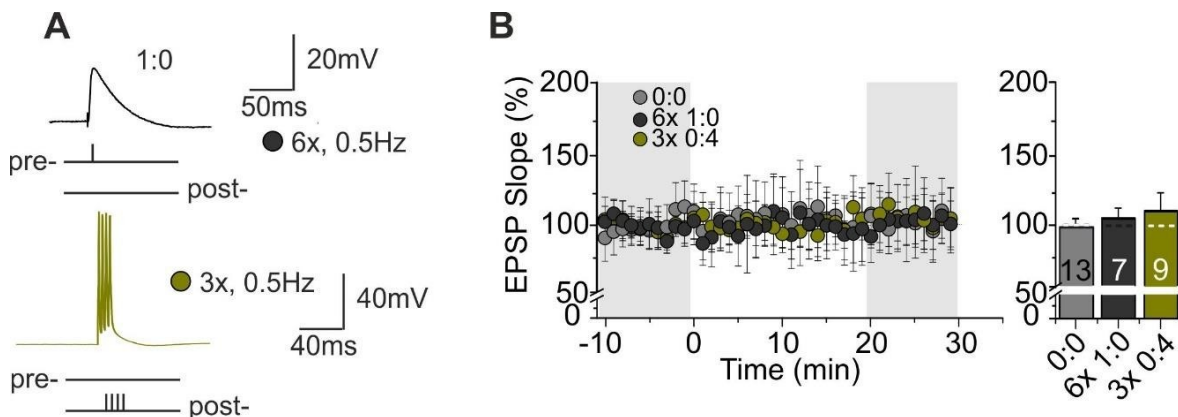
Figure 3.4. Unpaired stimulation of either pre-or postsynapse at SC-CA1 synapses has no effects on synaptic strength. A) Original trace of 6x 1:0 presynaptic stimulation (upper panel; in black) and 3x 0:4 postsynaptic stimulation (lower panel; dark yellow symbol). **B)** No changes in synaptic strength in response to unpaired (6x 1:0 at 0.5 Hz), or (3x 0:4, 4 spikes at 200 Hz; 3 repeats at 0.5 Hz) AP firing. Data are shown as mean ± SEM. The number of recorded cells and number of animals for each paradigm were: 0:0 (n=13 / N=6); 3x 0:4 (n=9 / N=4), and 6x 1:0 (n=7 / N=4).

It is very well described that at glutamatergic synapses, induction of t-LTP and t-LTD depend on the precise timing of the presynaptic AP that elicits the EPSP relative to the postsynaptic AP. If the postsynaptic AP follows the presynaptic AP (positive timing; +Δt) t-LTP is observed, while the reversed order (negative timing; -Δt) will induce t-LTD (Abbott and Nelson 2000). Moreover, the

temporal order of pre- and postsynaptic activation must be restricted to less than +20 ms to induce robust t-LTP (Kampa, Letzkus et al. 2007) reviewed in (Caporale and Dan 2008). We tested the critical time-window for induction of synaptic plasticity for positive and negative pairing at different Δt (i.e., -15, +10 and +20, +30, +40 ms, (Cepeda-Prado*, Khodaie* et al. 2021)). Our results indicated that low repeat STDP protocols (6x 1:1 and 6x 1:4) failed to induce robust t-LTP when paired at intervals longer than +10 ms, (Cepeda-Prado*, Khodaie* et al. 2021). Interestingly, these data narrowed down the temporal window for synaptic changes induced with the 6x 1:1 and 6x 1:4 protocols to 6 spike pairings within just 10 seconds (**Fig. 3.2 and 3.3**). The threshold repeat number for 1:4 t-LTP (3x, **Fig 3.3**) extended this time window further up to 100 millisecond (ms).

Regarding the spike pairing intervals, we found in subsequent experiments that the 3x 1:4 paradigm could induce robust t-LTP not only at Δt= +10 ms, but also at time windows of +40 ms (140.61% ± 8.57%, 11/5) and +100 ms (171.59% ± 11.24%, 13/6) compared to the negative control (0:0; 93.31% ± 5.06%, 13/8 Kruskal-Wallis test, H $_{(4)}$ = 26.37, followed by Dunn's multiple comparison test post hoc analysis, +40 ms vs. 0:0; p = 0.054 and +100 ms vs. 0:0, p < 0.0001; **Fig. 3.5B**).
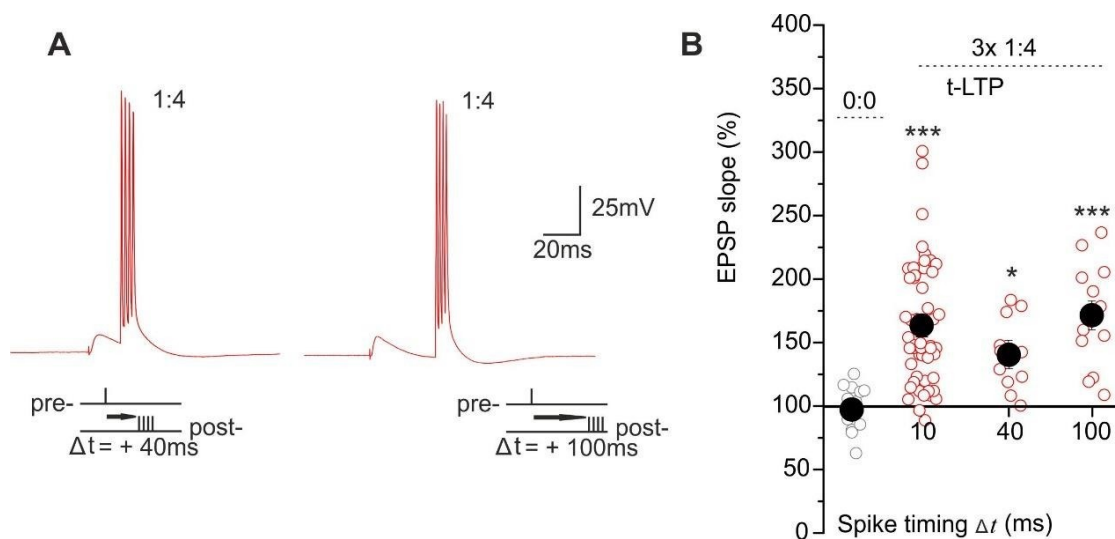
Figure 3.5. 3x 1:4 t-LTP expands the temporal window for t-LTP induction at SC-CA1 synapses. A) Original trace of 3x 1:4 stimulation in the postsynaptic neuron (+40 ms Δt; left and +100 ms Δt; right). **B)** Robust t-LTP in response to the 3x 1:4 paradigm for different spike time intervals (i.e., 10 ms, 40 ms, and 100 ms). The open symbols depict results from individual cells. Data shown are mean ± SEM. The number of recorded cells and number of animals for each paradigm were: 0:0 (n=13 / N=8); 10ms (n=53 / N=29); 40ms (n=11 / N=5), and 100ms (n=13 / N=6).

3.4   Expression of t-LTP depends on the stimulation paradigm

In a previous study performed in our lab (Edelmann, Cepeda-Prado et al. 2015), t-LTP expression of high-repeat 1:1 and 1:4 paradigms was intensively studied (discussed e.g., in Edelmann et al., 2017). We then designed a series of experiments based on those results to investigate if low-repeat STDP protocols use similar molecular and cellular mechanisms to induce synaptic changes and recruit similar sites for expression (Cepeda-Prado*, Khodaie* et al. 2021). We performed a series of experiments to investigate the locus of expression of synaptic plasticity induced by 6x 1:1 and 6x 1:4 protocols. Paired-pulse ratio (PPR; 50 ms inter-stimulus interval, see **methods section 2.3**) was used to monitor how glutamate release probability is affected by 6x 1:1 and 6x 1:4 t-LTP paradigms. (Original traces represented in **Fig. 3.6B**). Analyzing PPR before vs. after t-LTP induction revealed a significant reduction in PPR after 6x 1:1 t-LTP induction (before; 1.87 ± 0.07, after; 1.62 ± 0.07, 57/38, paired Student's t-test, t $_{(57)}$ =4.92; p<0.001). However, 6x 1:4 protocol induced no significant changes in the PPR when comparing pre- to post-t-LTP stimulation (before; 1.73 ± 0.06, after; 1.76 ± 0.05, 53/33, paired Student's t-test, t $_{(53)}$ =0.40; p=0.69; **Fig. 3.6A**). Similarly, non-stimulated negative control measurements (0:0) also revealed no significant changes in the PPR (before; 1.81 ± 0.07, after; 1.89 ± 0.18, 12/6, paired Student's t-test, t $_{(12)}$ =0.51; p=0.62; **Fig. 3.6A**).
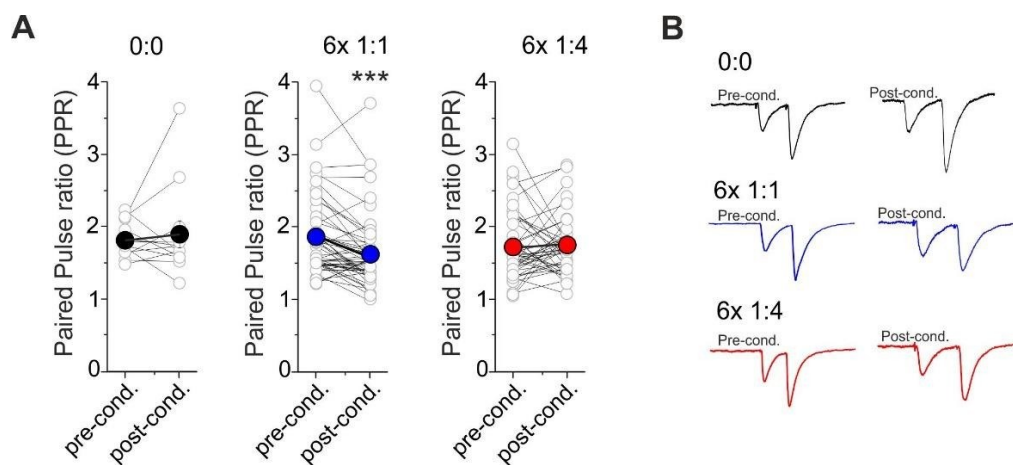
Figure 3.6. According to PPR measurements only 6x 1:1 t-LTP is expressed presynaptically. A) The paired-pulse ratio (PPR) was recorded before and after STDP induction in VC mode at -70mV holding potential and determined with an interval of 50 ms between both pulses. The open symbols depict results from individual cells. Closed symbols show mean ± SEM. ***p<0.001, using paired Student's t-test. **B)** Original traces of PPR in the three experimental groups, comparing pre- to post-t-LTP. The number of animals for each paradigm was: negative control (0:0; n=12 / N=6), 1:1 (n=57 / N=38) and 1:4 (n=53 / N= 33).

Further evidence for a stimulation pattern-dependent expression locus of t-LTP was determined by measurement of the I_{NMDAR}/I_{AMPAR} ratio after t-LTP induction with both 6x 1:1 and 6x 1:4 protocols compared to 0:0 negative controls (**Fig. 3.7A)**. Our results indicate that I_{NMDAR}/I_{AMPAR} ratio calculated in cells post 6x 1:1 t-LTP induction did not show a significant change compared to 0:0 control cells (5.69 ± 0.51, 14/8 vs. 6.16 ± 0.74, 9/6), whereas, a significant increase in the I_{NMDAR}/I_{AMPAR} ratio was observed after inducing 6x 1:4 t-LTP compared to 0:0 control (9.77 ± 1.28, 13/9; Kruskal-Wallis test, $H_{(3)}$ = 10.47, p = 0.054, **Fig. 3.7B**) and to 6x 1:1 stimulation protocol (p = 0.006, **Fig. 3.7B**).
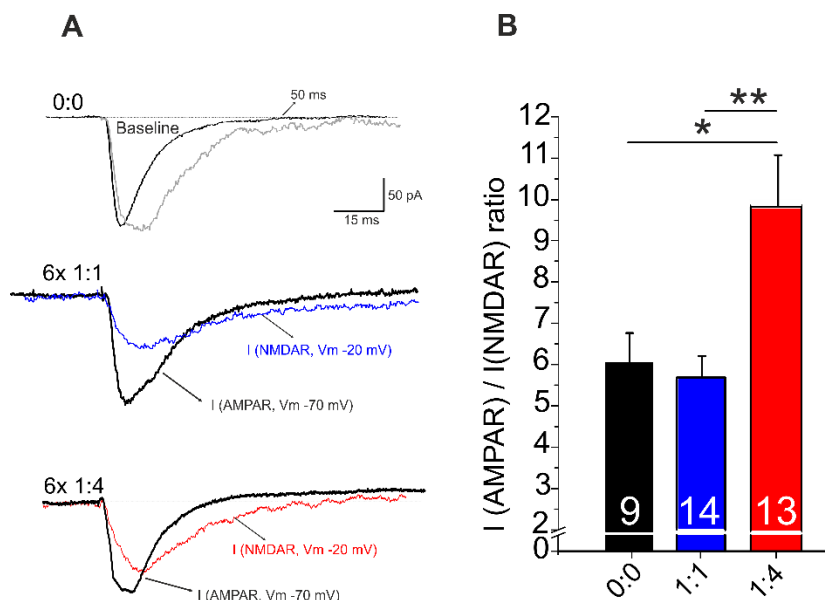
Figure 3.7. I_{AMPAR}/I_{NMDAR} ratio at SC-CA1 synapses following t-LTP induction with 6x repeat STDP paradigms, recorded in VC mode. A) Original traces of AMPAR (at -70 mV holding potential; VC mode) and NMDAR (at -20 mV holding potential; VC mode) evoked EPSCs for each paradigm are shown. The dotted line at 50 ms after the onset of EPSCs indicates where the slow NMDAR-mediated component was determined. **B)** The ratios were calculated at the end of the recording for negative controls (0:0; n=9 / N=10) and both 6x 1:1 (n=14 / N=11) and 6x 1:4 (n=13 / N=10) paradigms after successful t-LTP induction. The p-values were obtained using the Mann-Whitney U test, * p < 0.05, and ** p < 0.01. Data are shown as mean ± SEM. The number of cells is represented in the bar graph.

We next performed an occlusion experiment to further confirm the distinct types of t-LTP elicited by low repeat (6x) 1:1 and 1:4 protocols (**Fig. 3.8A**). To this aim, we subsequently applied the 6x 1:4 stimulation after potentiation induced by the 6x 1:1 protocol in the same cell and observed that both protocols seem to give rise to independent potentiation (Cepeda-Prado*, Khodaie* et al. 2021). However, repeating two consecutive 6x 1:1 stimulation 30 minutes apart did not result in a higher potentiation after the second 6x 1:1 stimulation. Thus, our data indicate that the two different

protocols can lead to additive potentiation by activating different LTP pathways, while repetitive stimulation with the 6x 1:1 protocol results in LTP occlusion (**Fig. 3.8B**).
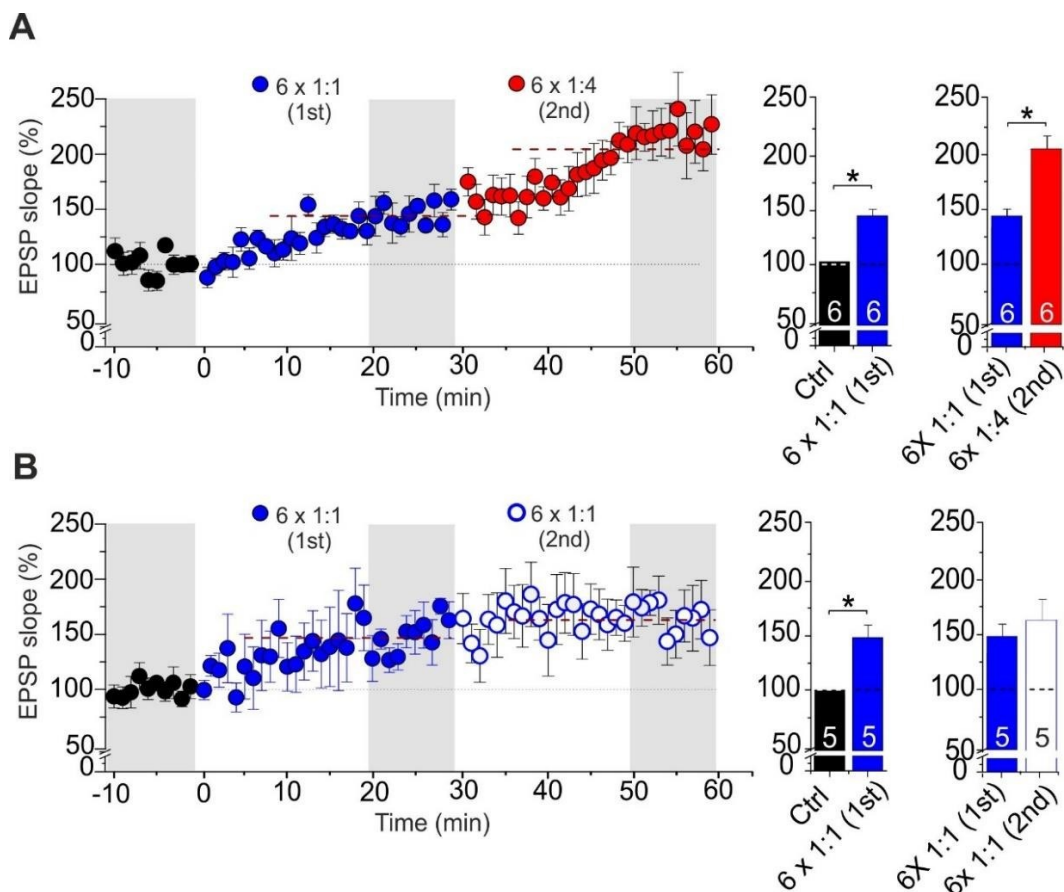
Figure 3.8: Two subsequent stimulations with the 6x 1:1 t-LTP protocol or combination with 6x 1:4 t-LTP. SC-CA1 synapses were recorded in IH at -70 mV and 6x 1:1 t-LTP stimulation was performed at time point 0. There was no sign of occlusion when 6x 1:4 t-LTP was induced after successful induction of 6x 1:1 t-LTP, whereas a second stimulation with the 6x 1:1 protocol did not give rise to additional potentiation. **A)** The second induction in the same cell was performed with the 6x 1:4 protocol and yielded additional and independent second potentiation. **B)** Two consecutive 6x 1:1 stimulations did not show significant additional t-LTP magnitude. The respective experiments show the average time course of potentiation and mean (± SEM) magnitude of t-LTP for different cells as indicated by numbers in bars (Adapted from (Cepeda-Prado*, Khodaie* et al. 2021)).

Previous reports suggested that changes in the presynaptic release probability following t-LTP induction could be regulated by retrograde a messenger, such as endocannabinoids or nitric oxide (Fitzsimonds and Poo 1998, Blundon and Zakharenko 2008). In order to test nitric oxide (NO) for

function as a putative retrograde messenger in our 6x 1:1 t-LTP variant, a new set of experiments was carried out in the presence of the NO synthase inhibitor L-NAME (200 µM; added to the recording ACSF). Our result showed that NO synthase inhibition did not affect 6x 1:1 t-LTP induction (163.92% ± 9.76%, 7/3) compared to ACSF controls (150.73% ± 12.96%, 13/6; unpaired Student's t-test, $t_{(14)}$ = 2.27; p = 0.45; 9/5, **Fig. 3.9**). These data provide evidence that NO does not act as retrograde messenger in 6x 1:1 t-LTP.
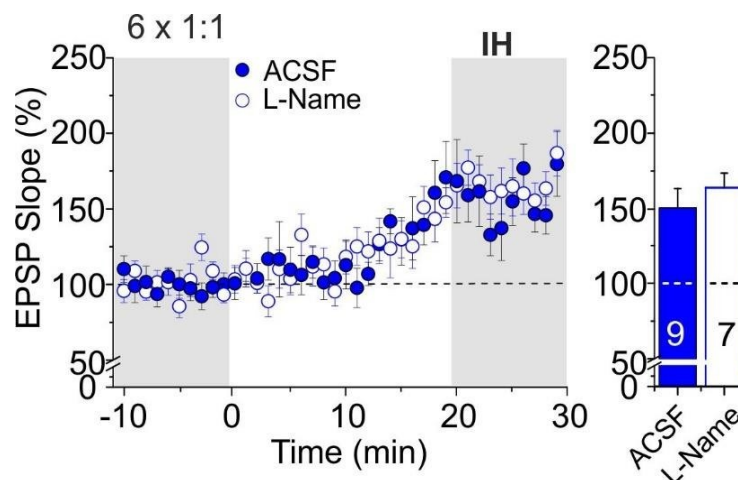
Figure 3.9. Retrograde signaling of nitric oxide has no role in 6x 1:1 t-LTP. Averaged time course of normalized EPSP slopes in the presence of the NO synthase inhibitor L-Name (200 µM L-Name) for 6x 1:1 protocol compared with untreated controls (ACSF). Number of recordings/animals used for the 6x 1:1 protocol in ACSF control was (n=9 / N=5), and for NO synthase inhibitor L-Name n=7 / N=3). Time course of the normalized EPSP slope is shown over 40 min. Data are represented as mean ± SEM.

3.5 Low repeat STDP paradigms recruit distinct calcium sources to induce t-LTP

3.5.1 The role of extracellular calcium sources

There is a general concept that a long-lasting increase in synaptic strength depends on the postsynaptic influx of Ca^{2+} ions through NMDARs (Collingridge 1987). L-type voltage-gated Ca^{2+} channels (VGCC) are another source contributing to intracellular Ca^{2+} elevation following t-LTP induction (Voglis and Tavernarakis 2006).

Using different drugs, we aimed to determine how these two sources of Ca^{2+} influx mediate t-LTP induction by low repeat STDP stimulation. Adding 10 µM DL-APV as a NMDAR antagonist led to the

significant blockade of 6x 1:1 t-LTP compared to ACSF control (unpaired Student's t-test, $t_{(17)}$ = 2.72; 8/6, 11/7, p = 0.014; **Fig. 3.10A**). Similarly, a selective blockade of L-type Ca^{2+} channels by Nifedipine (25 µM) significantly blocks 6x 1:1 t-LTP induction compared to the DMSO control group (Mann-Whitney U test, U = 37; 6/4, 6/5, p = 0.0022; **Fig. 3.10C**). However, neither APV (Mann-Whitney U test, U = 32; 9/7, 6/4, p = 0.128; **Fig. 3.10B**) nor Nifedipine (unpaired Student's t-test, $t_{(13)}$ = 1.64; p = 0.123; **Fig. 3.10D**) did affect 6x 1:4 t-LTP induction (compare (Cepeda-Prado*, Khodaie* et al. 2021)).
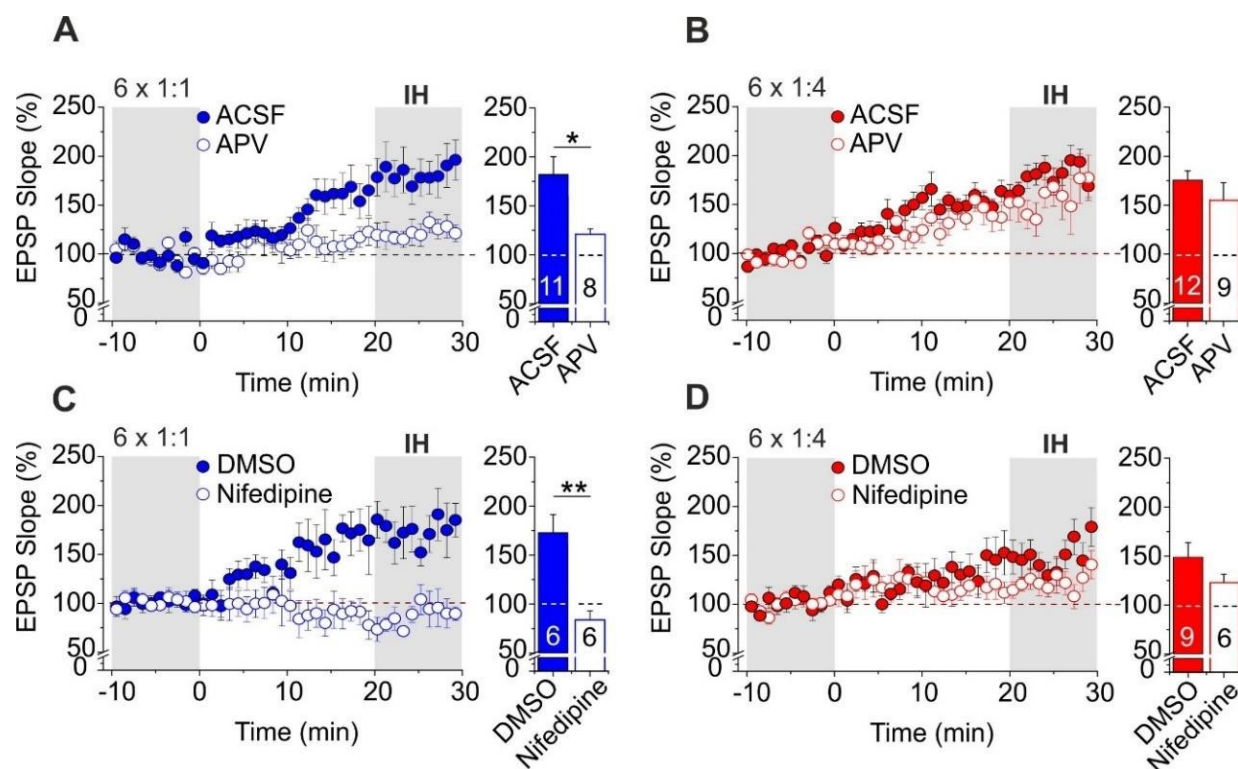
Figure 3.10: Contribution of primary calcium sources to t-LTP induction for low repeat 6x 1:1 and 6x 1:4 t-LTP. **A and B)** Contribution of NMDARs to low repeat 1:1 (in blue; A) and 1:4 (in red; B) t-LTP induction tested in the presence of the NMDAR antagonist DL-APV (10 µM, open symbols) compared to control ACSF (closed symbols). The number of recordings/animals used for 6x 1:1 protocol in ACSF was (n=11 / N=6) and for DL-APV (n=8 / N=6). Number of recordings/animals used for the 6x 1:4 protocol in ACSF was (n=12 / N=7), and for DL-APV n=9 / N=7). **C and D)** Contribution of VGCC was tested with Nifedipine (25 µM; open symbol) in 6x 1:1 (in blue; C), and 6x 1:4 (in red; D) t-LTP compared to 0.05% DMSO control (close symbol). Number of recordings/animals used for the 6x 1:1 protocol in 0.05% DMSO control was (n=6 / N=4), and for Nifedipine n=6 / N=4). Number of recordings/animals used for the 6x 1:4 protocol in 0.05% DMSO control was (n=9 / N=6), and for Nifedipine n=6 / N=4). The time course of normalized EPSP slope is shown over 40 min. Data are represented as mean ± SEM. * p < 0.05, and ** p < 0.01(Adapted from (Cepeda-Prado*, Khodaie* et al. 2021)).

Previous studies revealed the importance of Ca^{2+}-permeable (CP-) AMPA receptor (R) in-cooperation into the cell membrane following LTP protocols (Kauer and Malenka 2006). Plant and colleagues (2006) suggested that this specific type of AMPARs appears in the synaptic membrane shortly after LTP induction and is known to be critical for maintaining the increase in synaptic strength (Plant, Pelkey et al. 2006). This transient change in AMPAR composition happens shortly after LTP induction and remains for 25 minutes (Kauer and Malenka 2006). To investigate the role of CP-AMPARs in our low repeat t-LTP we applied in the next set of experiments selective inhibitors of these receptors during t-LTP induction. We used a mini-pump driven perfusion (used for expensive drugs) to add 100 µM Naspm trihydrochloride (NASPM) to our recording ACSF to block CP-AMPAR during t-LTP induction. Our results revealed that NASPM completely blocked both 6x 1:1 (unpaired Student's t-test, $t_{(14)}$ = 3.3502; P = 0.0048; **Fig. 3.11A**) and 6x 1:4 (unpaired Student's t-test, $t_{(19)}$ = 4.829; P = 0.0002**; Fig. 3.11B**) t-LTP compared to untreated control cells. A second inhibitor (IEM-1460; 100 µM) of CP-AMPARs was used to verify CP-AMPAR contribution in low repeat t-LTP induction. Consistent with our previous results obtained by adding NASPM to recording ACSF, we observed also with IEM-1460 a significant inhibition of t-LTP by both protocols compared to untreated controls (6× 1:1; unpaired Student's t-test, $t_{(12)}$ = 2.762; P = 0.0172, **Fig. 3.11C** and 6× 1:4; unpaired Student's t-test, $t_{(12)}$ = 4.4567; P = 0.0007, **Fig. 3.11D**).
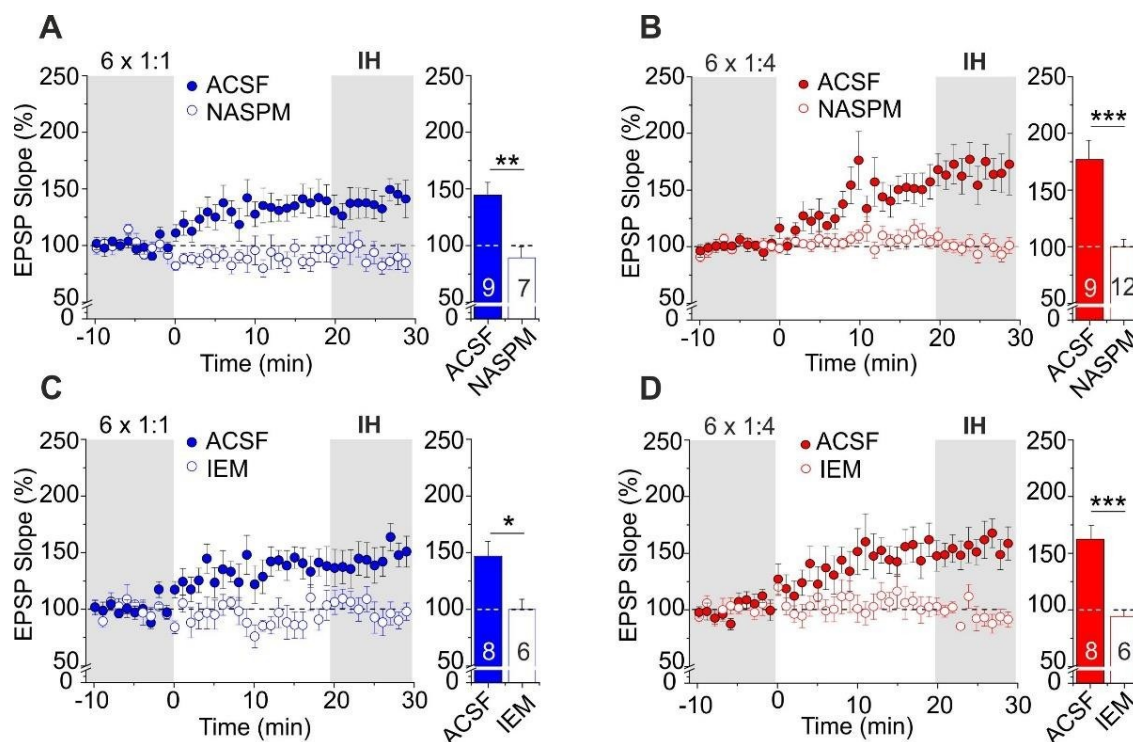
Figure 3.11: Ca^{2+} influx via GluA2-lacking calcium-permeable AMPARs is required for low-repeat t-LTP induction. A and B) Contribution of GluA2-lacking calcium-permeable AMPARs to low repeat 1:1 (in blue; A) and 1:4 (in red; B) t-LTP induction tested a selective inhibitor of Ca^{2+} permeable AMPARs NASPM (100 μM, open symbols) compared to control ACSF (closed symbols). Number of recordings/animals used for 6x 1:1 protocol in ACSF was (n=9 / N=6) and for NASPM (n=7 / N=3). Number of recordings/animals used for the 6x 1:4 protocol in ACSF was (n=9 / N=6), and for NASPM n=12 / N=5). **C and D)** Also IEM-1460 (100 μM), a second specific inhibitor of cp-AMPARs was tested (open symbol) in 6x 1:1 (in blue; C), and 6x 1:4 (in red; D) t-LTP compared to control ACSF (close symbol). Number of recordings/animals used for the 6x 1:1 protocol in ACSF was (n=8 / N=5), and for IEM-1460 n=6 / N=3). Number of recordings/animals used for the 6x 1:4 protocol in ACSF was (n=8 / N=5), and for IEM-1460 n=6 / N=3). The time course of the normalized EPSP slope is shown over 40 min. Data are represented as mean ± SEM. * p < 0.05, ** p < 0.01 and *** p < 0.001 (Adapted from(Cepeda-Prado*, Khodaie* et al. 2021)).

To investigate a possible role of postsynaptic CP-AMPAR insertion also in 35x 1:4 and 70x 1:1 high repeat t-LTP we performed another series of experiments in the presence of NASPM. Our results indicate that adding 100 μM NASPM to ACSF significantly blocked t-LTP induced by the 35x 1:4 protocol (unpaired Student's t-test, t $_{(17)}$ = 2.243; P = 0.038**; Fig. 3.12B**). Interestingly, however, robust t-LTP could still be induced by the 70x 1:1 protocol in the presence of NASPM (**Fig. 3.12A)**.
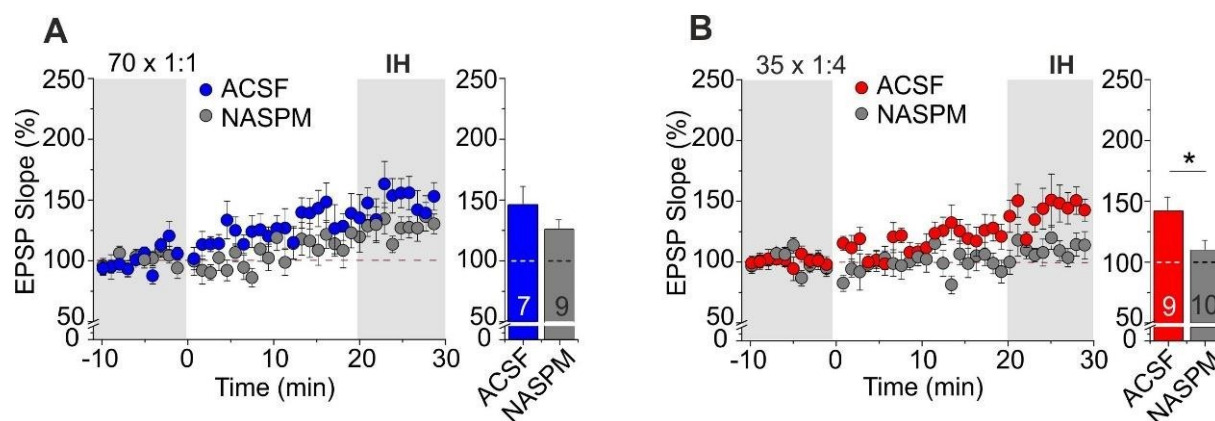
Figure 3.12: CP-AMPAR is required for 1:4 high repeat STDP paradigms. **A)** CP-AMPAR contribution to high repeat 1:1 (in blue) and **(B)** 1:4 (in red) protocols in the presence of the NASPM (100 μM, grey symbols) compared to ACSF control (colored symbols). Number of recordings/animals used for the 70x 1:1 protocol in ACSF was (n=7 / N=4), and for NASPM n=9 / N=7). Number of recordings/animals used for the 35x 1:4 protocol in ACSF was (n=9 / N=5), and for NASPM n=10 / N=6). The time course of normalized EPSP slope is shown over 40 min. Data are represented as mean ± SEM. * p < 0.05.

3.5.2 The role of intracellular calcium stores in low repeat t-LTP at SC-CA1 synapses

It is very well known that postsynaptic Ca^{2+} elevation is the most critical step during LTP induction. We verified this for our low repeat t-LTP protocols by loading postsynaptic neurons with 10 mM of the Ca^{2+} chelator BAPTA via the intracellular recording solution (Cepeda-Prado*, Khodaie* et al. 2021). Together with external Ca^{2+} sources, Ca^{2+} release from internal stores plays a crucial role during t-LTP induction, a process, which is thought to be initiated by activating metabotropic glutamate receptors (mGluRs) and subsequent activation of IP3 receptors (Tigaret, Olivo et al. 2016). To investigate the role of metabotropic glutamate receptors (mGluR1 and mGluR5) in low repeat t-LTP at SC-CA1 synapses we co-applied both mGluR1 (YM-298198, 10 μM) and mGluR5 (MPEP, 10 μM) antagonists in our recording solution. This led to the significant blockade of 6x 1:4 t-LTP induction (unpaired Student's t-test, $t_{(22)}$ = 2.248; P = 0.0093; **Fig. 3.13B**) compared to control ACSF, whereas the magnitude of 6x 1:1 t-LTP was not affected by the blocker (**Fig. 3.13A**).
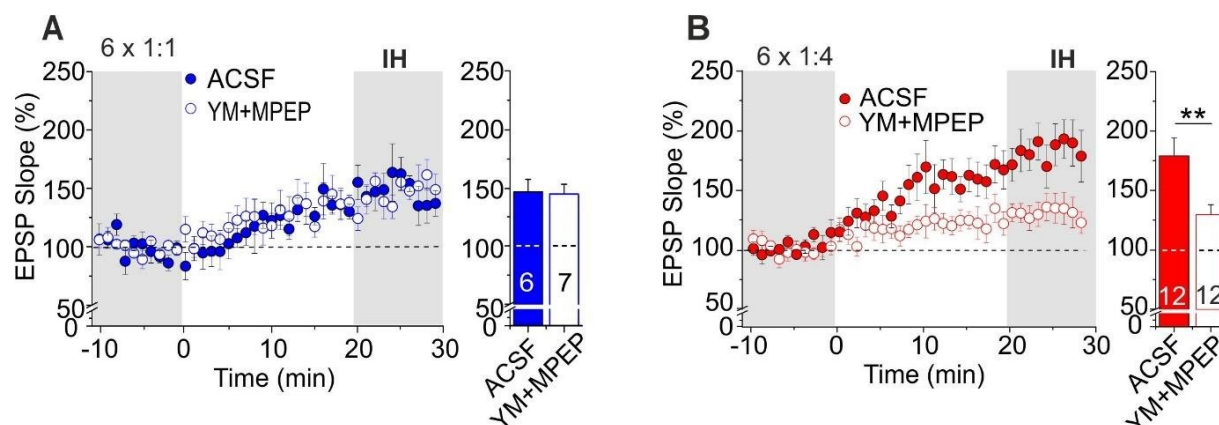
Figure 3.13: Metabotropic glutamate receptors are required for 6x 1:4 STDP paradigms. **A)** Co-application of both mGluR1 and mGluR5 antagonist used to test the importance of mGuRs activation during low repeat 1:1 (in blue) and **B)** 1:4 (in red) protocols t-LTP induction. T-LTP magnitute compared in the presence of the YM-298198 (10 μM) and MPEP (10 μM), open symbols, to control ACSF (closed symbols). Number of recordings/animals used for the 6x 1:1 protocol in ACSF was (n=6 / N=3), and for YM+MPEP n=7 / N=3). Number of recordings/animals used for the 6x 1:4 protocol in ACSF was (n=12 / N=8), and for YM+MPEP n=12 / N=5). The time course of normalized EPSP slope is shown over 40 min. Data are represented as mean ± SEM. ** p < 0.01 (Adapted from (Cepeda-Prado*, Khodaie* et al. 2021)).

To further elucidate downstream signaling mechanisms coupled to mGluR receptors, we investigated a putative dependency of 6x 1:4 t-LTP on mGluR-mediated Ca^{2+} release from internal stores. Therefore, we added 2-APB as an inhibitor of IP3-receptors to our recording ACSF. As expected, 6x 1:4 t-LTP was completely blocked by inhibition of IP3-mediated Ca^{2+} release from internal sources (unpaired Student's t-test, $t_{(15)}$ = 4.0297; P = 0.0019; **Fig. 3.14A**). Furthermore, an initial rise in intracellular Ca^{2+} levels could activate Ca^{2+}-dependent Ca^{2+} release via ryanodine receptors (RyR) resident in the endoplasmic reticulum (ER) membrane. Therefore, we applied 100 μM ryanodine (a concentration known to inhibit RyR irreversibly (Gao, Voss et al. 2005) to our internal solution (i.e., postsynaptic loading) and observed a complete blockade of 6x 1:4 t-LTP induction in presence of this intracellularly applied RyR blocker (Mann–Whitney U test, U = 5.5; P = 0.0003;' **Fig. 3.14B**).
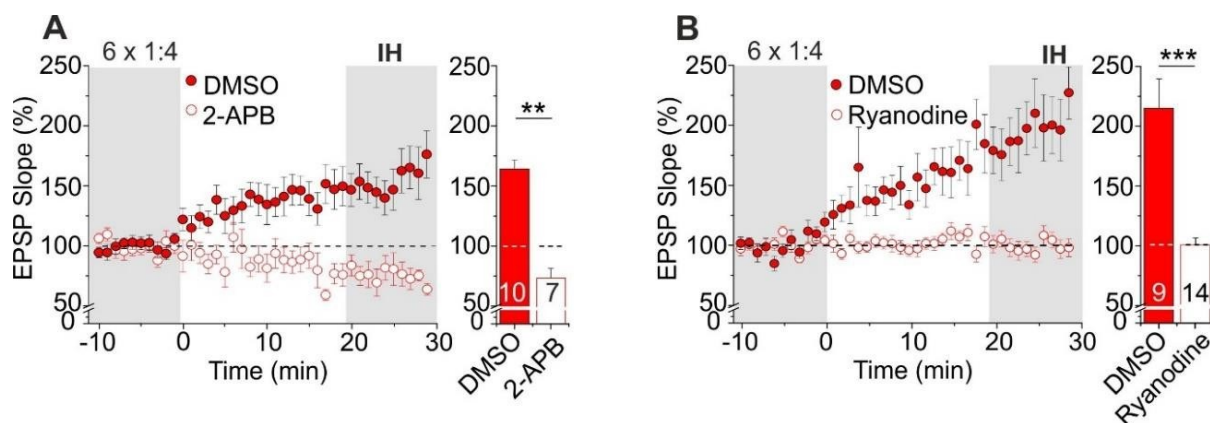
Figure 3.14: Release of Ca²⁺ from internal stores contributes to 6x 1:4 t-LTP induction.
A) Blockade of IP3 receptors by 100 μM 2-APB (in 0.05% DMSO; open symbol)inhibits 6x 1:4 t-LTP induction compared to DMSO solvent control treated slices (closed symbols).
B) Application of the RyR blocker Ryanodine led to significant blockade of 6x 1:4 t-LTP compared to DMSO control cells. Number of recordings/animals used for the 6x 1:4 protocol in 0.05% DMSO was (n=10 / N=5), and for 2-APB n=7 / N=3). Number of recordings/animals used for the 6x 1:4 protocol in 0.05% DMSO was (n=9 / N=5), and for Ryanodine n=14 / N=4). The time course of normalized EPSP slope is shown over 40 min. Data are represented as mean ± SEM. ** p < 0.01, and *** p < 0.001 (Adapted from (Cepeda-Prado*, Khodaie* et al. 2021)).

Next, we tested the contribution of calcium release from internal sources for 6x 1:1 t-LTP. Interestingly, our results indicate that both IP3 receptors (unpaired Student's t-test, $t_{(9)}$ = 3.590; P = 0.0058, **Fig. 3.15A**) and RyR (unpaired Student's t-test, $t_{(17)}$ = 2.816; P = 0.0119; **Fig. 3.15B**) activation are critically important for 6x 1:1 t-LTP induced synaptic changes.
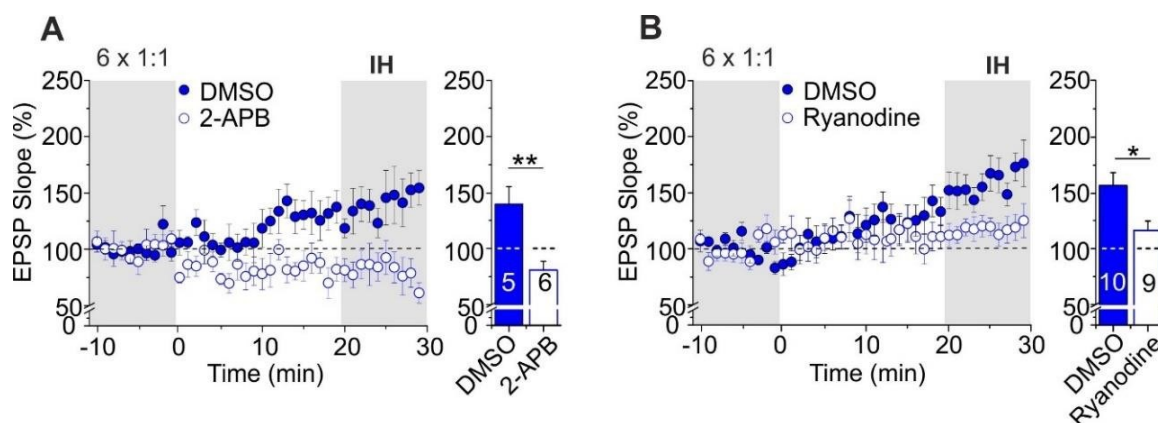
Figure 3.15: Internal Ca²⁺ release are important for 6x 1:1 t-LTP induction. **A)** Inhibition of IP3 receptors by 100 μM 2-APB (in 0.05% DMSO; open symbol) blocked 6x 1:1 t-LTP induction compared to DMSO (solvent control) treated slices (closed symbols). **B)** Similarly, inhibition of

RyRs with 100 µM ryanodine significantly blocked 6x 1:1 t-LTP induction. Number of recordings/animals used for the 6x 1:1 protocol in 0.05% DMSO was (n=5 / N=4), and for 2-APB n=6 / N=4). Number of recordings/animals used for the 6x 1:1 protocol in 0.05% DMSO was (n=10 / N=4), and for Ryanodine n=9 / N=3). The time course of normalized EPSP slope is shown over 40 min. Data are represented as mean ± SEM. * p < 0.05, and ** p < 0.01 (Adapted from (Cepeda-Prado*, Khodaie* et al. 2021)).

In summary, our results so far suggest that different low repeat t-LTP stimulation paradigms trigger distinct signaling mechanisms in pre- and postsynaptic cells to induce synaptic plasticity. While our 6x 1:1 paradigm depends on NMDARs and L-type Ca^{2+} channels to induce plasticity at SC-CA1 synapses, the 6x 1:4 protocol mainly depends on metabotropic glutamate receptors activation. At the same time, the elevation of the postsynaptic Ca^{2+} level is a critical step regardless of the specific t-LTP paradigm. We further noticed the importance of Ca^{2+} release from internal sources for both low repeat t-LTP protocols. Moreover, the insertion of CP-AMPARs (also known as GluR2 lacking AMPARs) into the postsynaptic membrane is crucial to observe low repeat t-LTP.

Most of the data shown up to here have been published in a shared first author publication to which Efrain Cepeda-Prado and I contribute equally (Cepeda-Prado*, Khodaie* et al., 2022). However, the whole set of data shown in this thesis were performed, recorded and analyzed by myself (Babak Khodaie). In the remaining parts of the result sections, I will show yet unpublished data.

Next, we were interested to investigate possible differences of low repeat t-LTP along the longitudinal axis of the hippocampus and how basic neuronal properties, receptors expression, and neuromodulatory responses might affect plasticity in CA1 PCs along this axis (Fanselow and Dong 2010, Schumacher, Vlassov et al. 2016, Dubovyk and Manahan-Vaughan 2018). Therefore, I first investigated the basic neuronal properties of CA1 PCs along the longitudinal axis of the mouse hippocampus.

3.6 CA1 PCs have diverse properties along the longitudinal axis of the hippocampus

While both intermediate (IH) and ventral (VH) hippocampal slices could be easily obtained by transversal cutting plane as we previously used, getting healthy dorsal hippocampal (DH) slices was a bit more challenging. To optimize our cutting plane for DH slices, we tested three different cutting planes to obtain healthy and stable CA1 PCs with intact Schaffer collateral (SC) mediated excitation

in DH slices (methods are described in **section 2.2**). Interestingly, CA1 PCs of DH revealed at SC inputs an t-LTP magnitude that was strongly depend on the cutting plane and t-LTP paradigms. While differences in excitability and basal synaptic properties along the longitudinal axis have been reported previously especially for rat hippocampal slices differences in STDP along this axis have not yet been investigated systematically especially not in mice.

3.7 Basic properties of CA1 pyramidal neurons along the longitudinal axis of the hippocampus

Using whole-cell patch-clamp recording in postsynaptic CA1 PCs located along the longitudinal axis of the hippocampus, we measured the basal electrical and synaptic properties of these CA1 neurons (**Fig. 3.16A**). In the presence of the $GABA_AR$ inhibitor of picrotoxin (100 µM), the resting membrane potential (RMP) of CA1 PCs was significantly more depolarized in intermediate (IH) and ventral hippocampus (VH) compared to dorsal hippocampus (DH) PCs (IH: -70.52 ± 0.57 mV, and VH: -70.62 ± 0.50 mV vs. DH: -75.37 ± 0.57 mV; ANOVA $F_{(2,58)}$ = 24.91 P < 0.0001, post hoc Tukey-test P < 0.0001, **Fig. 3.16B**). In the next set of experiments, we analyzed the action potential (AP) frequencies induced by somatically injected step currents, (represented for three different stimulation intensities (140, 160, and 180 pA) in **Fig. 3.16C**). With 180 pA current injection, the AP frequency was 30.19 ± 1.36 Hz in IH, 26.90 ± 1.46 Hz in VH, and 19.95 ± 1.22 Hz in DH CA1 PCs, showing a significantly higher AP frequency in both IH and VH compared to DH (ANOVA $F_{(2,58)}$ = 14.38 P < 0.0001, post hoc Tukey-test for IH vs. DH P < 0.0001, and VH vs. DH P= 0.002, **Fig. 3.16C**). Intrinsic neuronal excitability can be determined with the rheobase, the minimal current injection needed to elicit a spike (Wei, Liu et al. 2013). The rheobase was 155.24 ± 11.54 pA in IH, and 139.05 ± 10.55 pA in VH, compared to 188.42 ± 13.62 pA in DH CA1 PCs, indicating significantly lower excitability in DH compared to VH PCs (Kruskal–Wallis test $H_{(3)}$ = 8.93; P = 0.011, **Fig. 3.16D**). To determine the strengths of SC synaptic inputs along the longitudinal axis of the hippocampus we determined input-output curves (I/O curve; i.e. strength of SC extracellular stimulation current vs. slope of postsynaptic EPSPs) at different presynaptic stimulation intensities. At 200 µA stimulation intensity, EPSP slope was significantly different in VH compared to DH CA1 PCs (VH: 2.06 ± 0.27 mV/ms, and DH: 0.73 ± 0.13 mV/ms; ANOVA $F_{(2, 22)}$ = 5.96 P = 0.0085, **Fig. 3.16E**). At 250 µA stimulation intensity both VH and IH revealed significantly stronger responses compared to DH (VH: 2.07 ± 0.22 µV/V, IH: 1.86 ± 0.15 µV/V and DH: 1.16 ± 0.06 µV/V; ANOVA $F_{(2, 22)}$ = 9.52 P = 0.0011, post hoc Tukey test for VH vs. DH P = 0.0012, and

IH vs. DH P= 0.011). Likewise, also with 300 µA intensity, VH and IH SC-CA1 synaptic responses were significantly larger than for DH (VH: 2.67 ± 0.29 µV/V, IH: 2.04 ± 0.26 µV/V and DH: 1.10 ± 0.13 µV/V; ANOVA $F_{(2, 21)}$ = 6.54 P = 0.0062, post hoc Tukey test for VH vs. DH P = 0.012, and IH vs. DH P= 0.015, **Fig. 3.16E**). Taken together, we conclude that VH and IH have more depolarized RMP, fire higher frequencies of APs, and show higher efficiency of excitatory synaptic transmission at SC-CA1 synapses than the DH.
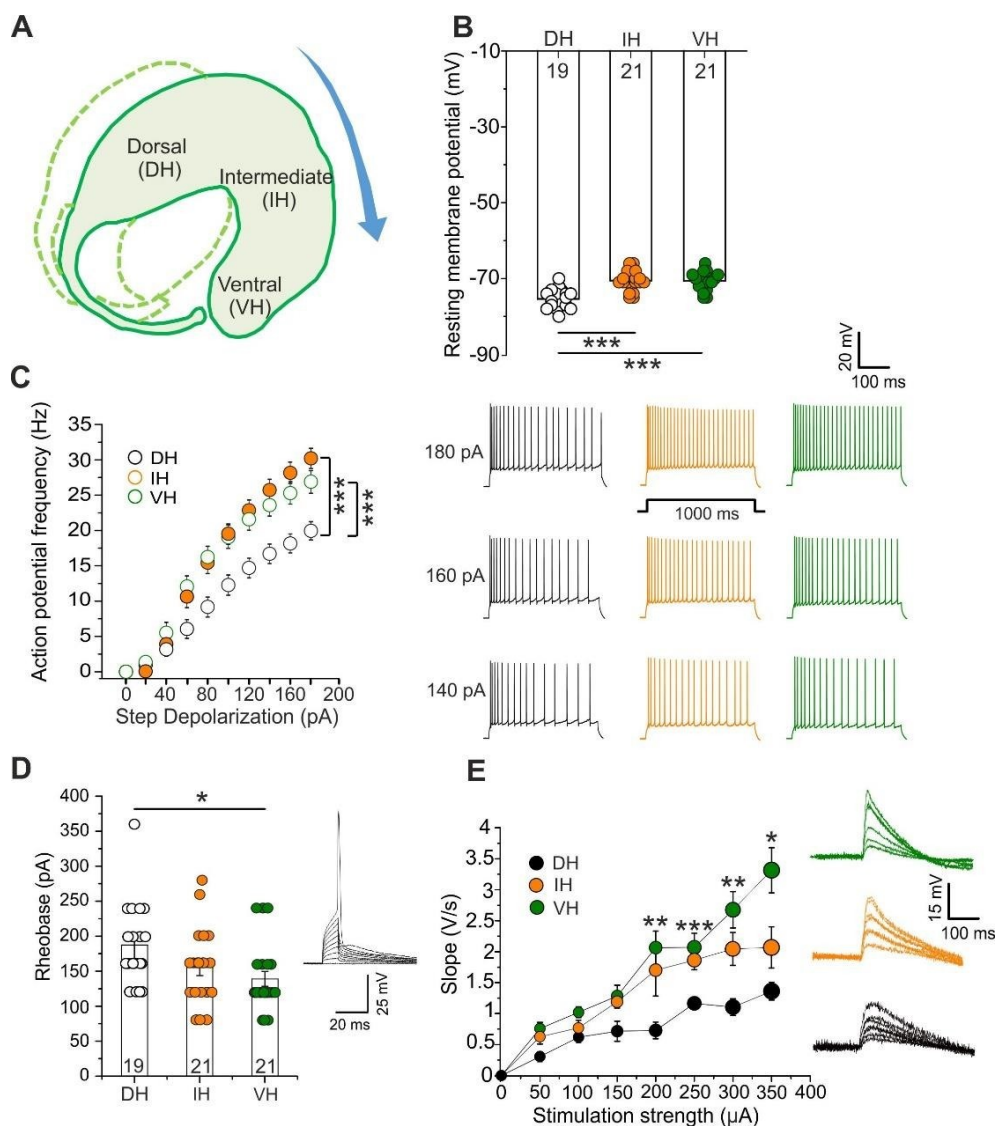
Figure 3.16: Basal intrinsic and synaptic properties of CA1 pyramidal neurons along the

longitudinal axis of the hippocampus. All recordings were performed in the CC mode of whole cell patch clamp recordings. **A)** Schematic graph illustrating the different hippocampal poles along its longitudinal axis. **B)** The resting membrane potential (RMP) of cells in IH (n=21 / N=11) and VH (n=21 / N=10) was more depolarized than in DH (n=19 / N=10). C to E recorded at -70 mV holding potential. **C)** Action potential (AP) frequency measured along the dorso-ventral pole of the hippocampus for different depolarization steps, indicating higher intrinsic excitability of CA1 PCs in both IH and VH compared to DH PCs. Insets: AP firing in CA1 neurons in response to three different depolarization steps (140, 160, and 180 pA somatic current injection (1s duration) in DH (black), IH (orange), and VH (green). **D)** Higher current amplitudes are required to elicit a spike in PCs of DH compared to VH. Digits in the bars represent the number of recorded cells. **E)** Input-output curves for SC-CA1 inputs are steeper in VH and IH than DH, indicating higher synaptic transmission toward the VH pole of the hippocampus. Original traces of cell response to different stimulation intensities are represented on the right side of the figure. Data are shown as mean ± SEM. * $p < 0.05$, ** $p < 0.01$, and *** $p < 0.001$. Scale bars are shown in the figures. Multiple comparisons were performed with ANOVA using post hoc Tukey test.

3.8 Region-specific changes of release probability of SC-CA1 synapses along the longitudinal axis of the hippocampus

Previous studies suggested a large differences in the presynaptic release probability of SC-CA1 synapses along the dorso-ventral axis in rat hippocampus (Papatheodoropoulos and Kostopoulos 2000, Dubovyk and Manahan-Vaughan 2018). Changes in the paired-pulse ratio (PPR) along the dorso-ventral axis are usually used as an easy method to measure release probability (Manita, Suzuki et al. 2007). PPR is a phenomenon that determines how neurons respond to two subsequent stimulations of presynaptic fibers. Using the minimal stimulation protocols Dobrunz and Stevens (1997) provided direct evidence for the inverse relation of changes in PPR to presynaptic release probability (Dobrunz and Stevens 1997). Therefore, a low PPR is interpreted to indicate a high transmitter release probability in response to the first stimulus. In our recordings, the mean PPR of CA1 PCs was 2.11 ± 0.15 in DH, 1.79 ± 0.12 in IH, and 1.68 ± 0.11 in VH PCs, showing a significantly smaller PPR and therefore a high release probability in VH compared to DH (ANOVA $F_{(2, 57)}$ = 3.16 P = 0.05; **Fig. 3.17B**). As an additional measure of glutamate release probability and the quantal size we tested miniature excitatory postsynaptic currents (mEPSCs) in CA1 PCs along longitudinal axis of the hippocampus (**Fig. 3.17C**). Hippocampal CA1 neurons in IH and VH showed significantly higher mean mEPSC amplitudes (IH: 11.91 ± 0.77 pA; VH: 11.65 ± 0.61 pA) than DH PCs (VH: 9.64 ± 0.31 pA; ANOVA $F_{(2, 26)}$ = 6.19 P = 0.0063; post hoc Tukey test for IH vs. DH P = 0.013, and VH vs. DH P= 0.029, **Fig. 3.17D**). Accordingly, we also found a significantly different cumulative mEPSC amplitude distribution between DH compared to VH and IH (Kruskal–Wallis test $H_{(3)}$ = 232; P < 0.0001, **Fig.**

3.17D). We then determined mean mEPSC frequencies along the longitudinal axis, indicating a significant reduction of mEPSC frequencies in DH PCs (0.25 ± 0.03 Hz) compared to IH and VH (IH: 0.85 ± 0.15 Hz, and VH: 0.6 ± 0.14 Hz; ANOVA F $_{(2, 26)}$ = 9.67 P = 0.0007; post hoc Tukey test P= 0.0006, and P= 0.046 respectively, **Fig. 3.17E**). Accordingly, cumulative mEPSC inter-event interval (IEI) distribution indicated a significantly lower presynaptic release probability in DH compared to IH and VH (Kruskal–Wallis test H $_{(3)}$ = 840.9; P < 0.0001, **Fig. 3.17E**).
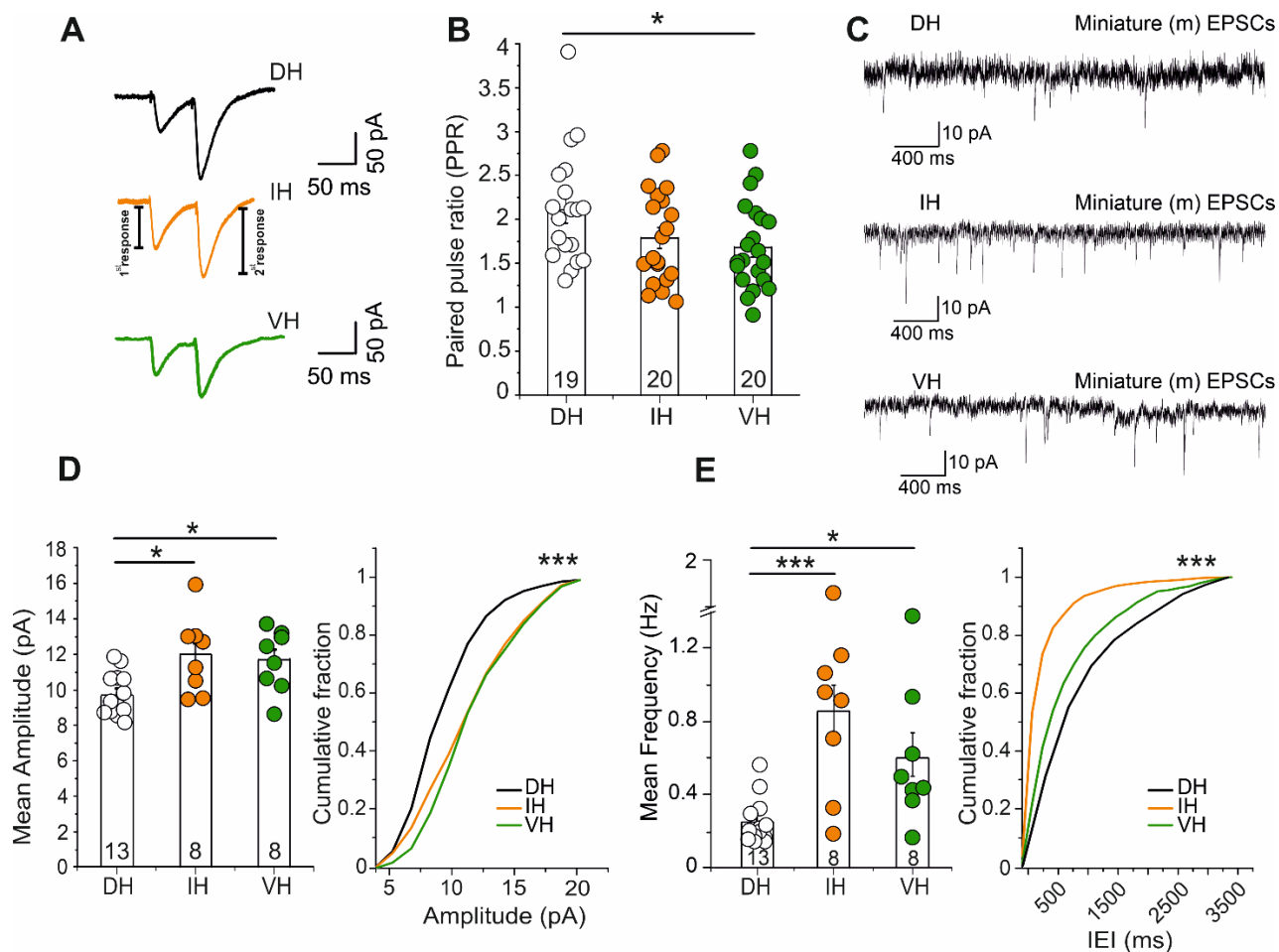
Figure 3.17: Evoked and spontaneous SC-CA1 synaptic transmission along the longitudinal axis of the hippocampus showed regional differences. All recordings were performed in VC mode of the patch clamp technique and at a holding potential of -70 mV. **A)** Original current traces representing the response of the postsynaptic cell to 2 subsequent SC fiber stimulations with an interval of 50 ms. 2nd current amplitude divided by the 1st amplitude was used to calculate the PPR. **B)** PPR is significantly higher in DH PCs (n=19 / N=10) compared to VH PCs (n=20 / N=10), showing higher release probability at the VH pole of the hippocampus, while IH PCs (n=20 / N=9) show intermediate release probability.

C) Original traces of miniature (m) EPSCs recorded in acute hippocampal slices along the longitudinal axis of the hippocampus. **D and E)** Mean amplitudes, frequency, and cumulative fraction of inter event intervals (IEI) of mEPSCs along the longitudinal axis of the hippocampus (DH; n=13 / N=5, IH; n=8 / N=4, and VH; n=8 / N=5), each dot representing an individual cell. The number of recorded cells is indicated in the bars. Data are shown as mean ± SEM. * $p < 0.05$, and *** $p < 0.001$. Scale bars are shown in the figures. Multiple comparisons were performed with ANOVA using the post hoc Tukey test.

3.9 Schaffer collateral-CA1 t-LTP along the longitudinal axis of the hippocampus

For t-LTP induction we used two different recently established more physiologically relevant (Otto, Eichenbaum et al. 1991) low repeat (6 times; 6x) t-LTP protocols consisting of a coincident pairing of a single presynaptic AP with either one (1:1) or four (1:4) postsynaptic APs (Cepeda-Prado*, Khodaie* et al. 2021). Typical original stimulation traces are represented in **Figure 3.18**. Experimental details for t-LTP recordings are described in method **section 2.4**. Both protocols reliably induced successful t-LTP compared to negative controls (0:0) in all studied regions along the longitudinal axis of the hippocampus (**Fig. 3.18**).
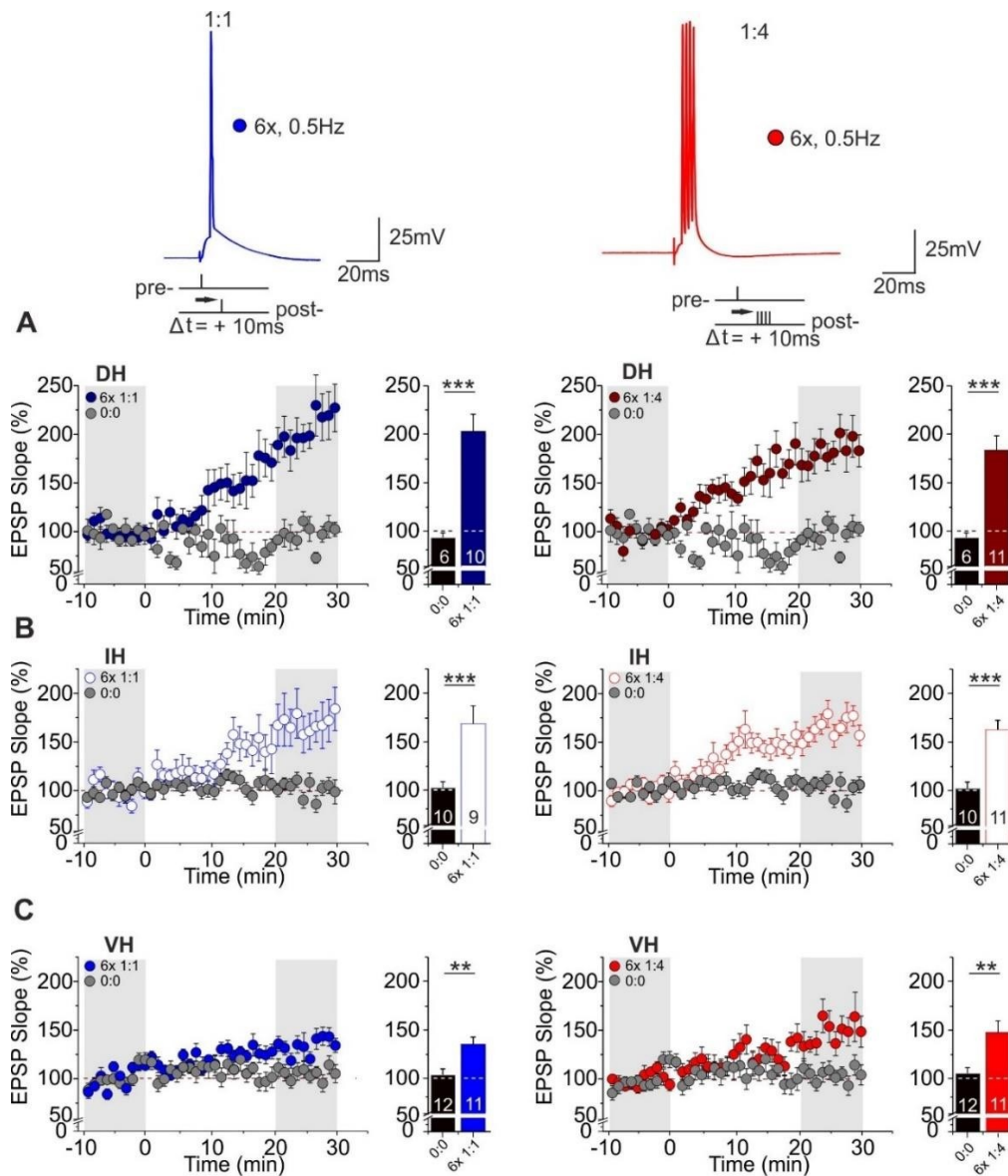
Figure 3.18: Robust t-LTP induction by 6x 1:1 and 6x 1:4 protocols compared to non-paired negative control (0:0) along the longitudinal axis. **A)** STDP induced by both 6x 1:1 and 6x 1:4 protocols in DH region. Significant t-LTP magnitude is observed for 6x 1:1 (blue symbols) and 6x 1:4 t-LTP (dark red symbols) compared to 0:0 negative control (grey symbols). **B)** T-LTP recordings in the IH region revealed robust potentiation induced by 6x 1:1 (open bluesymbols) and 6x 1:4 (open red symbols) compared to 0:0 (grey symbols). **C)** Also in VH, t-LTP was successfully induced with 6x 1:1 and 6x 1:4 stimulation, compared to 0:0 negative control. Number of recordings/animals used for in DH for the 6x 1:1 protocol was (n=10 / N=5), and for 6x 1:4 n=11 / N=6), and negative control (n=6 / N=4). Number of recordings/animals used for in IH for the 6x 1:1 protocol was (n=9 / N=5), and for 6x 1:4 n=11 / N=5), and negative control (n=10 / N=5).). Number of recordings/animals used for in VH for the 6x 1:1 protocol was (n=10

73

/ N=5), and for 6x 1:4 n=11 / N=6), and negative control (n=9 / N=5). Blue symbols indicate the 6x 1:1 paradigm, red symbols the 6x 1:4 paradigm, while negative control is shown in grey and black. The number of recorded cells is indicated in the bars. Data are shown as mean ± SEM. ** p < 0.01, and *** p < 0.001. Scale bars are shown in the figures. Multiple comparisons were performed with ANOVA using the post hoc Tukey test.

Interestingly the magnitude of t-LTP induced by 6x 1:1 stimulation was significantly higher in CA1 PCs of the DH (203.20 ± 17.26%) compared to VH (135.09 ± 7.41%; ANOVA $F_{(2, 27)}$ = 5.59 P = 0.0093; post hoc Tukey-test P= 0.007, **Fig. 3.19A**), whereas in IH the 6x 1:1 paradigm induced an intermediate level of potentiation (168.50 ± 18.92%). As shown in **Figure 3.19B**, the 6x 1:4 paradigm induced t-LTP with similar efficacy in VH, IH, and DH. The t-LTP magnitude was 184.54 ± 14.10% in DH, 162.55 ± 9.70% in IH and 146.77 ± 12.74% in VH, showing a non-significant reduction in t-LTP magnitude from the DH to the VH pole of the hippocampus (Kruskal–Wallis test, H $_{(3)}$ = 3.838; P = 0.147, **Fig. 3.19B**).
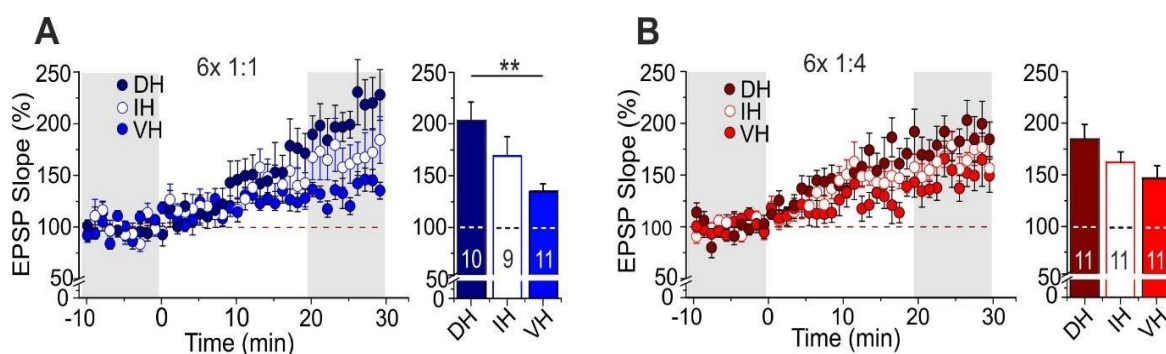
Figure 3.19: Comparison of t-LTP magnitude induced by low-repeat canonical and burst STDP protocols along the longitudinal axis (A, blue) and burst (B, red) STDP protocols along the longitudinal axis. **A)** The time courses of t-LTP expression revealed significantly weaker t-LTP induced with 6× 1:1 paradigm in VH compared to DH, while IH shows an intermediate t-LTP magnitude. **B)** t-LTP magnitude induced by 6x 1:4 protocol along the dorso-ventral axis shows no statistically significant difference comparing DH PCs to IH and VH PCs, although t-LTP magnitude was slightly reduced along the longitudinal axis DH>IH>VH. Number of recordings/animals used for the 6x 1:1 protocol along the longitudinal axis of the hippocampus was (for DH n=10 / N=7), for IH n=9 / N=6), and for VH n=11 / N=7). Number of recordings/animals used for the 6x 1:4 protocol along the longitudinal axis of the hippocampus was (for DH n=11 / N=7), for IH n=11 / N=6), and for VH n=11 / N=6). The time course of the normalized EPSP slope is shown over 40 min. Data are represented as mean ± SEM. ** p < 0.01.

3.10 Expression loci of t-LTP induced by the low repeat 1:1 and 1:4 paradigms along the longitudinal axis of the hippocampus

We previously reported distinct loci of t-LTP expression of low repeat (6x) 1:1 and 1:4 paradigms in the IH (Cepeda-Prado*, Khodaie* et al. 2021). Given the regionally distinct magnitudes of t-LTP from DH to VH (DH>IH>VH, **Fig. 3.19**), we next asked whether the loci of expression of 6x 1:1 and 6x 1:4 t-LTP differ along the dorso-ventral axis of the hippocampus. To this aim, we analyzed the changes in PPR before, and 30 min after t-LTP induction by two successively evoked EPSCs elicited at 50 ms inter stimulus interval (**Fig. 2.20A, and B**). Of note, a reduction in PPR after t-LTP induction is considered to represent presynaptically expressed synaptic plasticity (i.e. increased glutamate release to enhance synaptic strength). Following stimulation with 6x 1:1 paradigm, mean PPR recorded at SC-CA1 synapses of IH showed a significant reduction (before: 2.19 ± 0.24, after: 1.53 ± 0.17; paired Student's t-test, $t_{(8)}$ = 4.338; P = 0.0025). Similarly in VH PCs, we found a significant decrease in PPR after 6x 1:1 t-LTP induction (before: 1.82 ± 0.2, after: 1.30 ± 0.09; paired Student's t-test, $t_{(10)}$ = 3.72; P = 0.004, **Fig. 3.20A**), when Schaffer collateral fibers were activated. However, in DH there were no changes in PPR recorded after 1:1 t-LTP stimulation (before: 2.22 ± 0.24, after: 2.16 ± 0.21, paired Student's t-test, $t_{(9)}$ = 0.22; P = 0.827; **Fig. 3.20A**).

We observed no reduction in PPR for the 6x 1:4 t-LTP in DH PCs (before: 2.18 ± 0.17, after: 2.42 ± 0.16, paired Student's t-test, $t_{(9)}$ = 1.042; P = 0.32), however, we found a tendency toward reduction of PPR after 6x 1:4 t-LTP paradigm in IH (before: 1.83 ± 0.16, after: 1.74 ± 0.15, paired Student's t-test, $t_{(10)}$ = 0.43; P = 0.67), and also in VH (before: 1.97 ± 0.16, after: 1.71 ± 0.12, paired Student's t-test, $t_{(10)}$ = 1.58; P = 0.14, **Fig. 3.20B**). Presynaptic versus postsynaptic expression for 6x 1:1 t-LTP was further investigated by analysis of mEPSCs frequencies and amplitudes before and after successful 6x 1:1 t-LTP induction (Edelmann, Cepeda-Prado et al. 2015, Cepeda-Prado*, Khodaie* et al. 2021). These data confirmed presynaptic expression loci of 6x 1:1 t-LTP in IH and suggest similar mechanisms for 6x 1:1 t-LTP in VH (**Fig. 3.20A)**. To investigate the contribution of postsynaptic mechanisms to both t-LTP paradigms, we then analyzed the changes in AMPA/NMDA receptor (R)-mediated current ratios after t-LTP induction with 6x 1:1 and 6x 1:4 paradigms compared to 0:0 negative control. Of note, due to differences in NMDAR subunit expression (GluN2A vs. GluN2B) along the longitudinal axis of the hippocampus (Dubovyk and Manahan-Vaughan 2018), NMDAR-mediated currents at SC-CA1 synapses in the VH (GluN2A < GluN2B)

decay three times more slowly than in the DH (GluN2A > GluN2B) (Pandis, Sotiriou et al. 2006, Wyllie, Livesey et al. 2013). Thus, while AMPAR-mediated peak EPSCs were measured at a holding potential of −70 mV, NMDAR-mediated current components (measured at -20 mV holding potential) were evaluated at slightly different time points for VH, IH and DH after the onset of EPCSs (see **Methods section 2.3**), to optimize NMDAR-mediated current measurements.

Our analysis of the AMPAR/NMDAR current ratio indicated a statistically significant increase in AMPAR- versus NMDAR-mediated EPSC component after 6x 1:4 t-LTP induction in IH CA1 PCs (0:0; 6.16 ± 0.75, 6x 1:1; 5.69 ± 0.65, and 6x 1:4; 9.77 ± 1.29; ANOVA $F_{(3, 36)}$ = 10.47; P = 0.0053, **Fig. 3.20C**). A similar effect was found in the VH (0:0; 6.77 ± 1.15, 6x 1:1; 5.32 ± 0.7, and 6x 1:4; 9.94 ± 0.83; ANOVA F(3, 30) = 10.26; P = 0.0059, **Fig. 3.20C**). Interestingly, in DH PCs the AMPAR/NMDAR ratio was significantly increased by successful 6x 1:4, and also by successful 6x 1:1 t-LTP induction, compared to non-STDP stimulated control cells (0:0; 4.67 ± 0.73, 6x 1:1; 9.07 ± 0.48, and 6x 1:4; 9.49 ± 1.24; ANOVA $F_{(3, 27)}$ = 5.55; P = 0.009, **Fig. 3.20C**). These results are consistent with postsynaptic change after 6x 1:4 t-LTP in IH, VH and DH, while in DH CA1 PCs postsynaptic changes were seen also after induction of 6x 1:1 t-LTP. Incorporation of new GluA1 containing AMPARs into the postsynaptic plasma membrane following t-LTP stimulation has been shown previously to account for the increased AMPA/NMDA current ratio in response to the 6x 1:4 t-LTP (see (Shi, Hayashi et al. 2001) and (Cepeda-Prado*, Khodaie* et al. 2019).

Taken together, these results indicate a presynaptic expression of 6x 1:1 t-LTP in VH and IH, whereas in DH results are consistent with postsynaptic expression. Regarding 6x 1:4 t-LTP, results in all three regions are consistent with a postsynaptic expression mechanism.
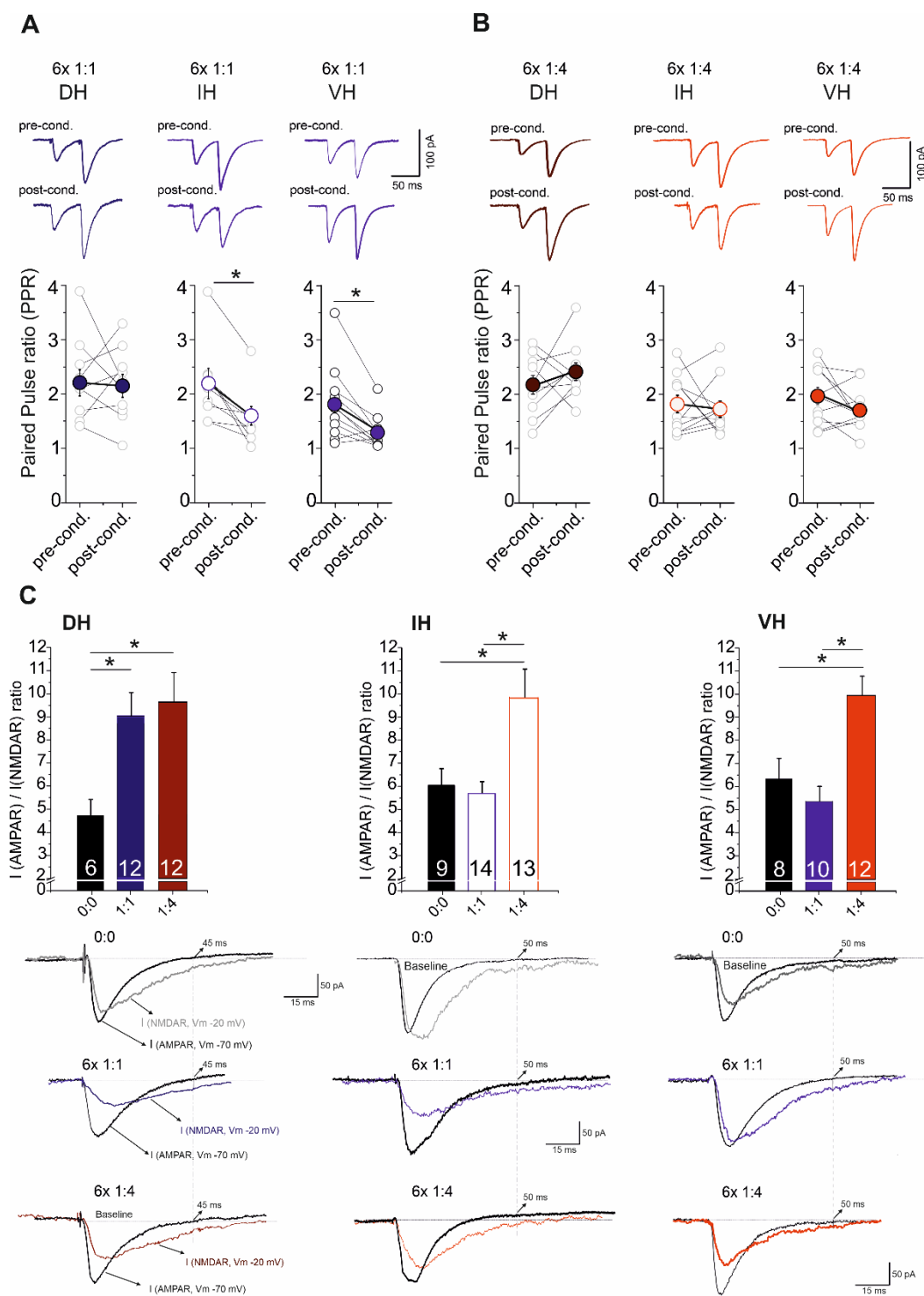
Figure 3.20: Different expression loci of t-LTP induced by the low repeat 1:1 and 1:4 paradigms along the longitudinal axis of the hippocampus. All recordings were

performed in VC mode at -70 mV holding potential (HP; A and B). In C, HP was -70 mV for AMPAR and +20 mV for NMDAR components, respectively. **A)** The paired-pulse ratio (PPR) was calculated before (pre-cond.) and 30 min after (post-cond.) successful 6x 1:1 t-LTP induction in the same cell (DH; n=10 / N=7, IH; n=9 / N=5, and VH; n=11 / N=6, showing significant changes in PPR after 6x 1:1 t-LTP induction in IH and VH. **B)** PPR measurement after successful induction of 6x 1:4 t-LTP revealed no significant changes in presynaptic release probability in none of the studied regions (DH; n=10 / N=7, IH; n=11 / N=6, and VH; n=11 / N=6). Scale bars are shown in the figures*.* **C)** Original traces of AMPA/NMDAR ratio measurements (AMPAR: peak current at -70 mV; NMDAR: current amplitude 50 ms after the start of EPSC (in IH and VH), and 45 ms (in DH), recorded at -20 mV), for DH negative control (0:0; n=6 / N=5) after successful t-LTP induction (6x 1:1; n=12 / N=7; 6x 1:4; n=12 / N=6). Where applicable, increased AMPAR/NMDAR current ratio seen after both 6x 1:1 and 6x 1:4 t-LTP, suggest postsynaptic changes. In IH, the AMPAR/NMDAR current ratio increased only after 6x 1:4 t-LTP (n=13 / N=8), but was not affected after 6x 1:1 t-LTP (n=14 / N=10) or in the non-stimulated control group (n=9 / N=7). In VH, 6x 1:4 t-LTP induced a similar increase in the AMPAR/NMDAR current ratio (n=12 / N=9), and no changes after 6x 1:1 t-LTP (n=10 / N=8) or in negative controls (n=8 / N=6). This indicates a postsynaptic change only after 6x 1:4 t-LTP in IH and VH. Data are shown as mean ± SEM. * $p < 0.05$, and ** $p < 0.01$. Each dot represents an individual cell. The number of recorded cells is indicated (n) in the bars. N= number of animals.

3.11 Distinct modulation of low repeat t-LTP by NMDARs along the longitudinal axis of the hippocampus

In the results **section 3.5.1** and **Figure. 3.10,** we discussed NMDAR contribution to t-LTP induction in IH, but NMDARs are differentially expressed and show a heterogeneous expression of NMDAR subunits (GluN2A and GluN2B) along the longitudinal axis of the hippocampus (Dubovyk and Manahan-Vaughan 2018), thereby affecting NMDAR-mediated current amplitudes and kinetics (Pandis, Sotiriou et al. 2006, Wyllie, Livesey et al. 2013). Nonetheless, we expected a dependence of t-LTP induction by NMDARs in all areas along the longitudinal axis of the hippocampus. When adding 10 µM of the NMDAR antagonist DL-APV in DH recordings, there was no significant blockade of neither 6x 1:1 t-LTP induction (ACSF: 189.98 ± 19.61% vs. APV: 165.79 ± 14.68%; unpaired Student's t-test, $t_{(16)}$ = 0.98; 9/6, 9/6, p = 0.34; **Fig. 3.21A**) nor of 6x 1:4 t-LTP induction (ACSF: 179.77 ± 15.52% vs. APV: 160.91 ± 12.78%; unpaired Student's t-test, $t_{(13)}$ = 0.92; 8/5, 7/5, p = 0.374; **Fig. 3.21B**). In contrast, 6x 1:1 t-LTP induction was significantly blocked in the presence of APV in IH experiments, whereas 6x 1:4 t-LTP induction was not affected by APV (results **section 3.5.1** and **Fig. 3.21C and D**). In VH, both the 6x 1:1 (ACSF: 135.36 ± 7.34% vs. APV: 129.32 ± 11.63%, 12/8, 8/4, **Fig. 3.21E**)

and the 6x 1:4 paradigm induced robust t-LTP in the presence of APV (ACSF: 166.54 ± 14.56% vs. APV: 149.06 ± 13.95%, 12/8, 9/7, **Fig. 3.21F**).
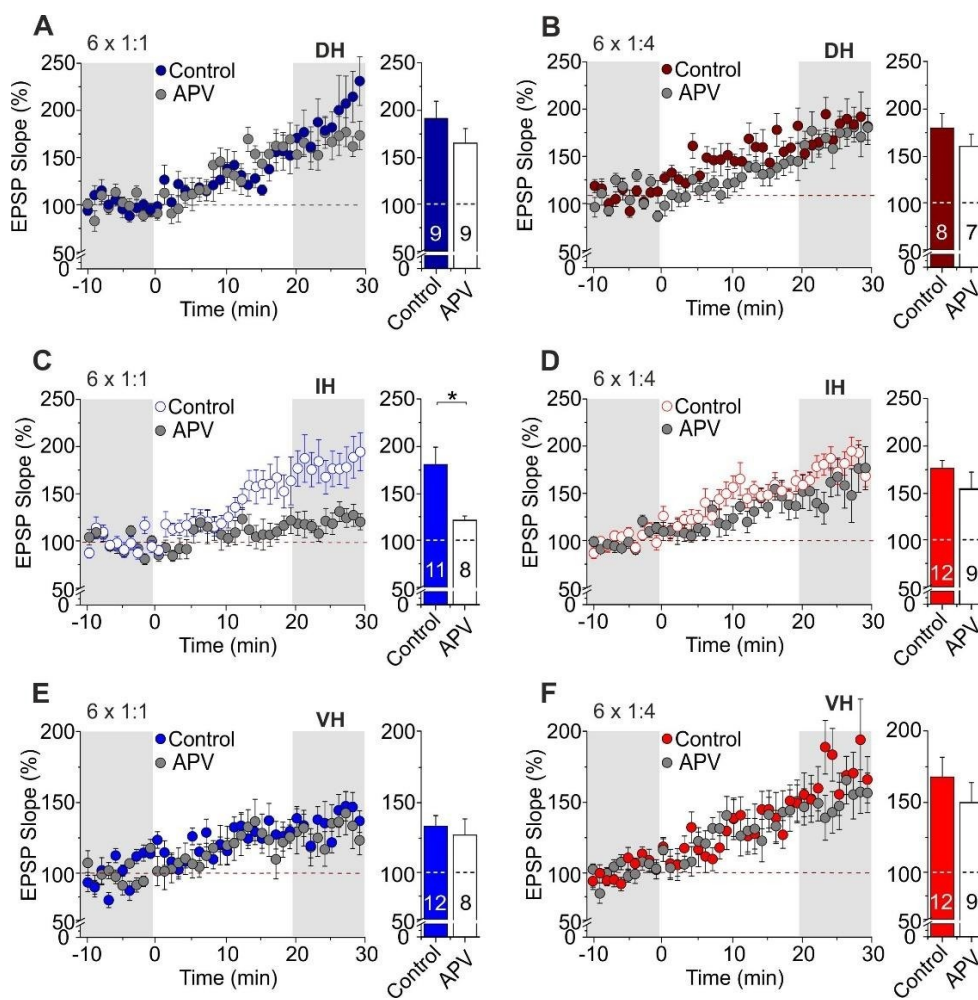
Figure 3.21: Contribution of NMDAR signaling to low repeat 1:1 and 1:4 STDP paradigms along the longitudinal axis. All recordings were performed in the CC mode at -70 mV holding potential. NMDAR contribution to low repeat 1:1 (in blue; A) and 1:4 (in red; B) induced t-LTP in the presence of the NMDAR antagonist (10 µM DL-APV, grey symbols) was compared to ACSF control (colored symbols). **A** and **B)** The number of animals/recordings used for the 6x 1:1 protocol in DH was: ACSF: n=9 / N=6; DL-APV: n=9 / N=6, and for 6x 1:4 t-LTP in ACSF: n=8 / N=5; DL-APV: n=7 / N=5. **C** and **D)** The number of animals/recordings used for the 6x 1:1 protocol in IH was: ACSF: n=11 / N=6; DL-APV: n=8 / N=5, and for 6x 1:4 t-LTP in ACSF: n=12 / N=7; DL-APV: n=9 / N=6. **E** and **F)** The number of animals/recordings used for the 6x 1:1 protocol in VH was: ACSF: n=12 / N=8; DL-APV: n=8 / N=4, and for 6x 1:4 t-LTP in ACSF: n=12 / N=8; DL-APV: n=9 / N=7. The time course of the normalized EPSP slope is shown over 40 min. Data are represented as mean ± SEM. * p < 0.05.

3.12 Distinct modulation of low repeat t-LTP by VGCC along the longitudinal axis of the hippocampus

Region specific modulation of t-LTP by VGCC was tested along the longitudinal axis of the hippocampus for the 6x 1:4 STDP paradigm. Our results revealed that in DH, adding 25 µM Nifedipine to the recording ACSF significantly inhibited t-LTP induction compared to DMSO solvent control (DMSO: 142.22 ± 7.29% vs. Nifedipine: 92.04 ± 3.35%; unpaired Student's t-test, $t_{(22)}$ = 5.493; 14/5, 10/4, p < 0.0001; **Fig. 3.22A**), whereas in IH the t-LTP magnitude was not affected (DMSO: 148.03 ± 14.44% vs. Nifedipine: 121.73 ± 8.89%; 9/5, 6/4, **Fig. 3.22B**). In VH, the 6x 1:4 t-LTP paradigm failed to induce significant potentiation in the presence of Nifedipine in the ACSF compared to the DMSO solvent control (DMSO: 153.56 ± 16.32% vs. Nifedipine: 93.04 ± 8.06%; unpaired Student's t-test, $t_{(10)}$ = 2.294; 7/5, 5/4, p = 0.015; **Fig. 3.22C**).
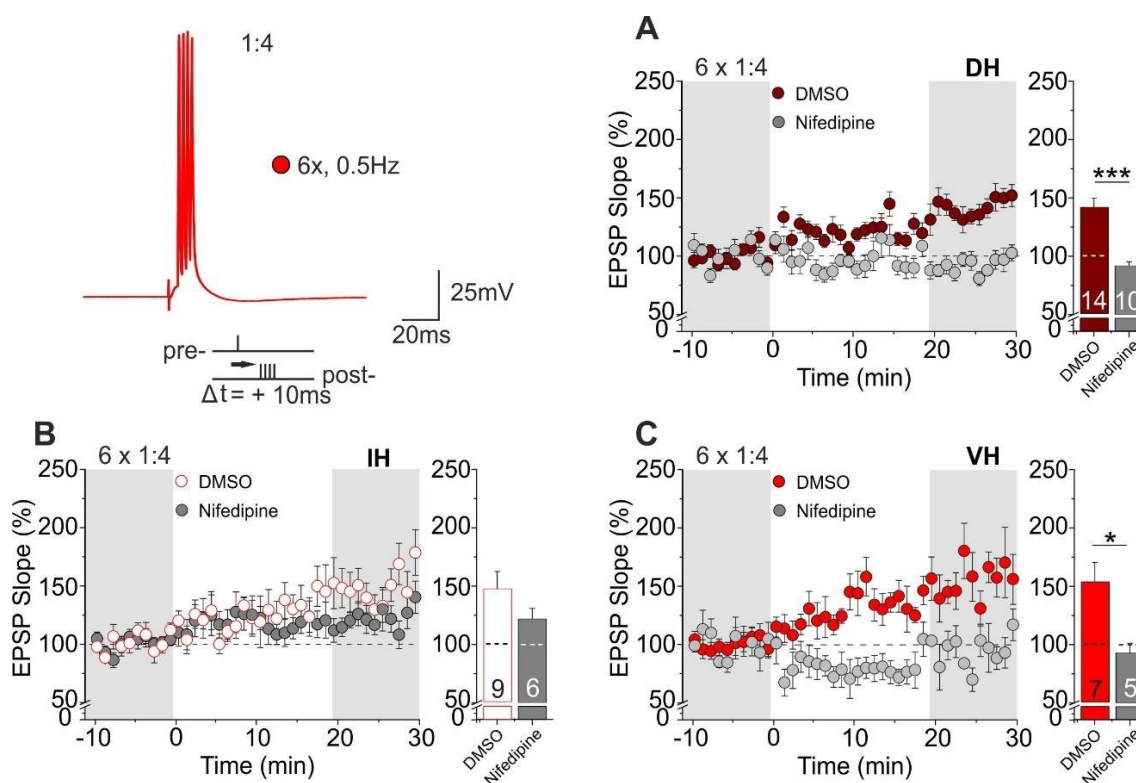
Figure 3.22: Contribution of VGCC signaling to low repeat 1:4 STDP paradigm. All recordings were performed in the CC mode at -70 mV holding potential. 6x 1:4 was tested in the presence of the VGCC antagonist Nifedipine (25 µM, grey symbols) in the recording ACSF, compared to DMSO the VGCC antagonist Nifedipine (25 µM, grey symbols) in the recording ACSF, compared to DMSO solvent control (red symbols). **A)** The number of

animals/recordings used for the 6x 1:4 protocol in DH was in 0.05% DMSO: n=14 / N=5, and for Nifedipine: n=10 / N=4). **B)** The number of animals/recordings used for the 6x 1:4 protocol in IH was in 0.05% DMSO: n=9 / N=5, and for Nifedipine: n=6 / N=4). **C)** The number of animals/recordings used for the 6x 1:4 protocol in VH was in 0.05% DMSO: n=7 / N=5, and for Nifedipine: n=5 / N=4). Normalized EPSP slope represented over 40 min of the time course. The number of recorded cells is indicated in the bars. Data are represented as mean ± SEM. * p < 0.05, and *** p < 0.001.

3.13 Catecholaminergic modulation of low repeat t-LTP along the longitudinal axis of the hippocampus

3.13.1 Region specific modulation of low repeat t-LTP by Adrenergic receptors along the longitudinal axis of the hippocampus

In the next set of experiments, we tested whether β-Adrenergic receptors modulate low repeat t-LTP induction at SC-CA1 synapses along the longitudinal axis of the hippocampus. To do so, we added 10 µM of propranolol (PPN) as β-Adrenergic receptor antagonist to our recording ACSF. Our results indicate a non-significant reduction in 6x 1:1 t-LTP magnitude in DH compared to ACSF control (ACSF: 181.54 ± 18.17% vs. PPN: 135.74 ± 14.66%; unpaired Student's t-test, $t_{(13)}$ = 1.923; 14/7, 6/5, p = 0.07; **Fig. 3.23A**), whereas 6x 1:4 t-LTP was unaffected by β-Adrenergic receptor blockade (ACSF: 173.22 ± 20.93% vs. PPN: 143.30 ± 16.84%; Mann-Whitney U test, $U_{(17)}$ p = 0.383, 7/6, 7/5; **Fig. 3.23A**). Similarly in the IH region, blockade of β-Adrenergic receptors reduced 6x 1:1 t-LTP magnitude compared to ACSF solution, but it did not reach to a statistically significant level (ACSF: 181.09 ± 18.36% vs. PPN: 142.25 ± 15.09%; unpaired Student's t-test, $t_{(16)}$ = 1.488; 11/7, 8/6, p = 0.15; **Fig. 3.23B**). However, the 6x 1:4 paradigm failed to induce t-LTP in the presence of the β-Adrenergic receptor inhibitor, compared to ASCF control (ACSF: 175.94 ± 9.83% vs. PPN: 127.07 ± 13.92%; unpaired Mann-Whitney U test$_{(10)}$; p = 0.005, 12/6, 7/4; **Fig. 3.23B**). In VH, 6x 1:1 t-LTP was induced with similar efficiencies when comparing the β-Adrenergic receptor blocker group and ASCF control (ACSF: 135.36 ± 7.34% vs. PPN: 136.20 ± 20.20%; unpaired Student's t-test, $t_{(17)}$ = 0.049, 12/8, 8/6, p = 0.96; **Fig. 3.23C**). Likewise 6x 1:4 t-LTP was not inhibited by β-Adrenergic receptor signaling compared to ACSF control (ACSF: 166.54 ± 14.55% vs. PPN: 141.07 ± 15.36%; unpaired Student's t-test, $t_{(16)}$ =1.088, 12/7, 7/5, p = 0.292; **Fig. 3.23C**).
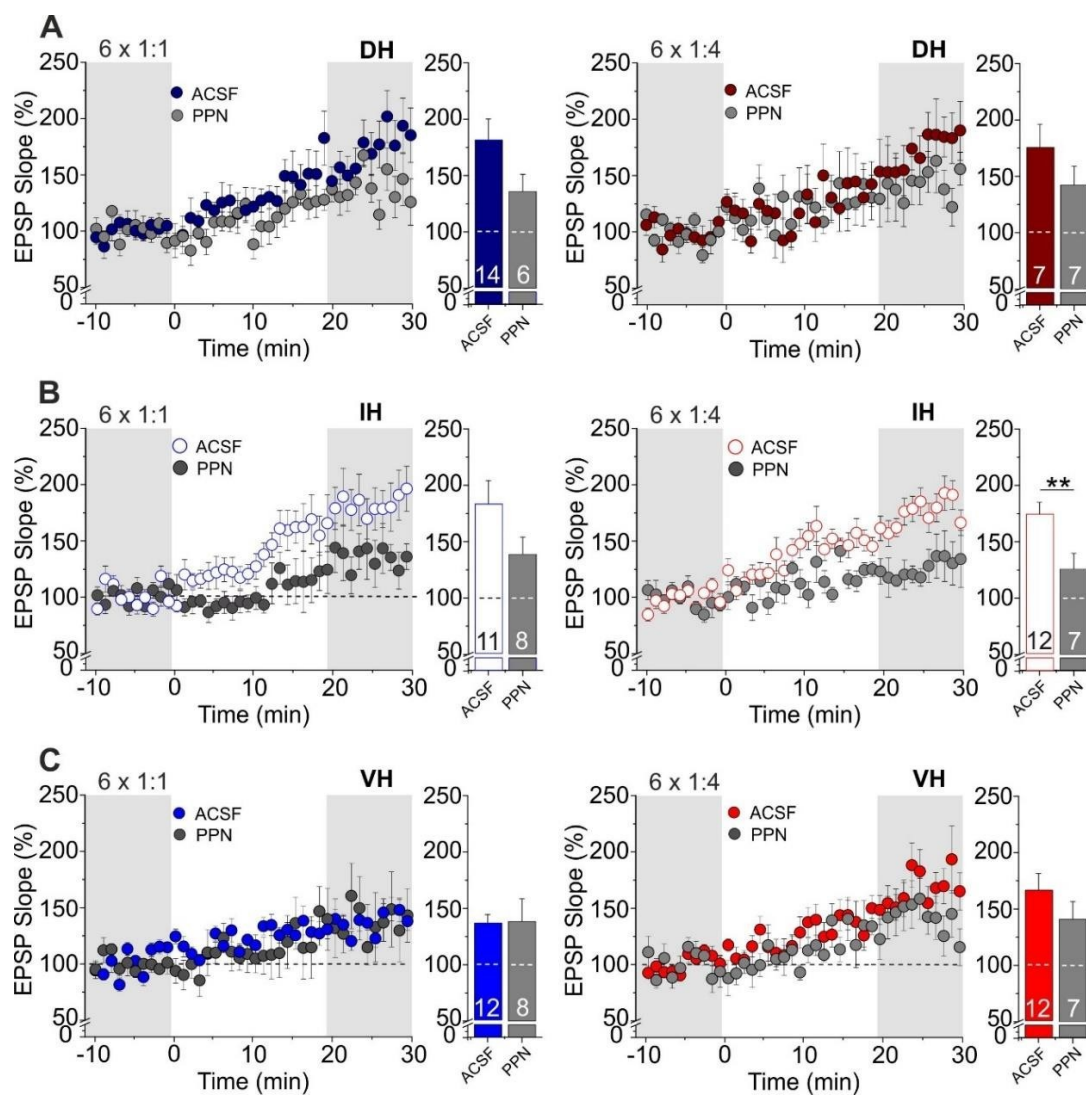
Figure 3.23: Adrenergic signaling in low repeat 1:1 and 1:4 STDP paradigms along the longitudinal hippocampal axis. β-Adrenergic signaling to 6x 1:1 and 6x 1:4 t-LTP paradigm was tested by adding 10 µM of propranolol as a β-Adrenergic blocker (PPN; grey symbols) compared to control ACSF (blue and red symbols). **A)** The number of animals/recordings used for the 6x 1:1 protocol in DH was: ACSF: n=14 / N=7; DL-APV: n=6 / N=5, and for 6x 1:4 t-LTP in ACSF: n=7 / N=6; DL-APV: n=7 / N=5). **B)** The number of animals/recordings used for the 6x 1:1 protocol in IH was: ACSF: n=11 / N=7; DL-APV: n=8 / N=6, and for 6x 1:4 t-LTP in ACSF: n=12 / N=6; DL-APV: n=7 / N=4). **C)** The number of animals/recordings used for the 6x 1:1 protocol in VH was: ACSF: n=12/N=8; DL-APV: n=8 / N=6, and for 6x 1:4 t-LTP in ACSF: n=12 / N=7; DL-APV: n=7 / N=5). Normalized EPSP slope represented over 40 min of the time course. The number of recorded cells is indicated in the bars. Data are represented as mean ± SEM. ** p < 0.01.

3.13.2 Distinct modulation of low repeat t-LTP by dopaminergic signaling along the longitudinal axis of the hippocampus

Dopamine (DA) receptor signaling is well known to modulate conventional LTP (Lisman, Grace et al.) and high repeat t-LTP (Edelmann and Lessmann 2011, Edelmann and Lessmann 2013, Edelmann and Lessmann 2018). Therefore we tested the influence of D1 and D2 receptor signaling also for our recently discovered low repeat t-LTP paradigms along the dorso-ventral hippocampal axis. In DH, we found that inhibition of D2 signaling by Sulpiride had no significant effect on t-LTP magnitude induced by both 6x 1:1 (191.58 ± 24.04%) and 6x 1:4 protocols (172.82 ± 14.53%). Adding 10 μM of the D1 dopamine receptor inhibitor SCH23990 to our recording ACSF led to a non-significant reduction in t-LTP magnitude induced by the 6x 1:1 protocol (ACSF: 197.64 ± 20.37% vs. D1R blocker: 140.12 ± 11.83% $F_{(3, 26)}$ = 7.307, 8/7, 7/5, P = 0.11; **Fig. 3.24A**), whereas no SCH23990 induced changes were observed for 6x 1:4 t-LTP in DH (176.79 ± 25.21%). Additionally, in the next set of experiments we tested the co-application of D1 and D2 receptor antagonists, which significantly inhibited 6x 1:1 t-LTP (ACSF: 197.64 ± 20.37% vs. D1+D2R blockers: 107.01 ± 5.96%; ANOVA $F_{(3, 26)}$ = 7.307, 8/7, 9/8, P = 0.001; post hoc Tukey-test, ACSF vs. SCH+Sul P = 0.002, and Sul vs. SCH+Sul P = 0.005, **Fig. 3.24A**). In contrast, t-LTP induced by the 6x 1:4 protocol was unaffected in DH (ACSF; 177.16 ± 13.83% vs. SCH+Sul; 159.97 ± 21.59%, 8/5, 9/6, **Fig. 3.25A**).

In the IH region, 6x 1:1 t-LTP was neither affected by D1R blockade with SCH23990 (151.20 ± 14.92%), nor by D2R blockade with sulpiride (163.62± 14.66%). However, co-application of D1R and D2R antagonists significantly blocked 6x 1:1 t-LTP induction (ACSF: 168 ± 18.95% vs. D1+D2R blockers: 103.94 ± 6.55%; ANOVA $F_{(4, 35)}$ = 12.73, 9/5, 8/4, P = 0.0053; post hoc Dunn's-test, ACSF vs. SCH+Sul P = 0.013, and Sul vs. SCH+Sul P = 0.014, and SCH vs. SCH+Sul P = 0.046, **Fig. 3.24B**). 6x 1:4 t-LTP in IH was significantly reduced when D2R signaling was inhibited with sulpiride (117.31 ± 15.67%) compared to ASCF control (177.32 ± 16.28%; ANOVA $F_{(3, 29)}$ = 5.303, 7/5, 11/5, P = 0.0049; post hoc Tukey test, P = 0.05, **Fig. 3.24B**). Moreover, 6x 1:4 t-LTP was blocked by co-application of D1R and D2R antagonists (101.82 ± 6.40%; ANOVA $F_{(3, 29)}$ = 5.303, 8/4, P = 0.0049; post hoc Tukey test, P = 0.009, **Fig. 3.25B**), compared to ASCF control, whereas 6x 1:4 t-LTP remained unaffected when only blocking D1R signaling (SCH23990: 169.28 ± 23.72%).

Finally, we performed a similar set of experiments in the VH. Our results revealed that t-LTP could be induced by 6x 1:1 protocol independent from either D1 or D2 receptor inhibition (SCH; 150.33± 15.08%, Sul; 134.83 ± 10.07%, 7/4, 6/6, **Fig. 3.24C**). However, co-application of D1R and D2R

antagonists significantly blocked 6x 1:1 t-LTP (ACSF: 137.44 ± 8.56% vs. D1R+D2R blockers: 95.42 ± 12.94%; ANOVA $F_{(4, 28)}$ = 8.36, 9/8, 6/4, P = 0.039; post hoc Dunn's-test, ACSF vs. SCH+Sul P = 0.045, **Fig. 3.24C**).
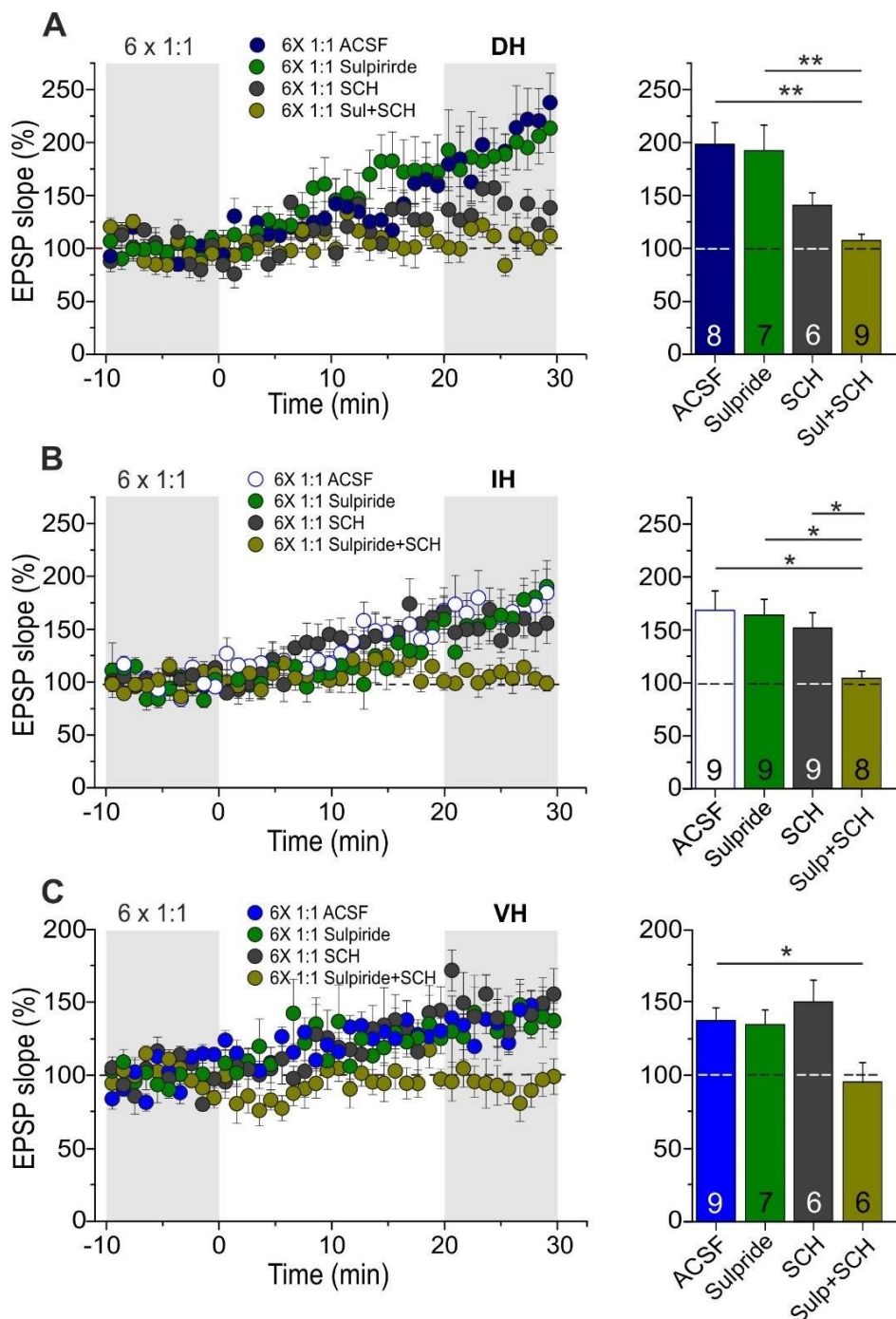
Figure 3.24: Contribution of DA receptor signaling to 6x 1:1 t-LTP induction. Low repeat (6x 1:1) protocol was tested for the contribution of DA receptor signaling to elicit t-LTP in the

presence of the D1R antagonist (SCH23990; 10 μM, grey symbols), the D2R antagonist (Sulpiride; 10 μM, green symbol), or co-application of D1R and D2R antagonist (dark yellow symbols), compared to ACSF control (purple symbols). **A)** The number of animals/recordings used for the 6x 1:1 protocol in DH was in ACSF: n=8 / N=7, D1R blocker n=7 / N=5, D2R blocker n=6 / N=4 and for D1R+D2R blocker: n=9 / N=8). **B)** The number of animals/recordings used for the 6x 1:1 protocol in IH was in ACSF: n=9 / N=5, D1R blocker n=9 / N=4, D2R blocker n=9 / N=5 and for D1R+D2R blocker: n=8 / N=4). **C)** The number of animals/recordings used for the 6x 1:1 protocol in VH was in ACSF: n=9 / N=8, D1R blocker n=7 / N=4, D2R blocker n=6 / N=6 and for D1R+D2R blocker: n=6 / N=4). Normalized EPSP slope represented over 40 min of the time course. The number of recorded cells is indicated in the bars. Data are represented as mean ± SEM. * p < 0.05, and ** p < 0.01.

The most striking result emerges from the data recorded from the VH, suggesting the highest dependency of t-LTP induced by the 6x 1:4 protocol on both D1 and/or D2 receptor activation, because any inhibition of dopaminergic receptors (D1R or D2R) significantly blocked t-LTP. The magnitude of 6x 1:4 t-LTP was 116.22 ± 14.17% in SCH 23390, 109.81 ± 7.81% in Sulpiride, and 89.18 ± 7.46% in SCH 23390 (SCH) + Sulpiride (Sulp), showing significant blockade in t-LTP induction compared to ACSF (169.36 ± 12.74%; ANOVA $F_{(3, 36)}$ = 10.79, 9/5, 8/4, 9/4, and 14/8, P < 0.0001; post hoc Tukey test, P = 0.012, P = 0.0021, and P <0.0001, respectively, **Fig. 3.25C**).

Taken together, these results suggest that there is a correlation between D1 and D2 receptor expression (for both D1 and D2 receptor expression decreases from VH>IH>DH) and dependency of t-LTP magnitude on D1R and D2R inhibition along the longitudinal axis of the hippocampus (higher dependency in VH at least for 6x 1:4 protocol; for the gradient of receptor expression see (Dubovyk and Manahan-Vaughan 2018, Dubovyk and Manahan-Vaughan 2019). To the best of our knowledge, no previous study studies exist regarding the mechanisms involved in t-LTP induction along the longitudinal axis of the hippocampus.

Taken together, the experiments with D1R and D2R antagonists proved the high sensitivity of the two low repeat t-LTP forms to dopaminergic signaling, whereas adrenergic signaling seemed to be involved less. Importantly, our experiments thus far dealt with tonic ambient DA and noradrenaine levels present in the slice or phasic release that is likely co-activated during SC stimulation. Therefore, in the next series of experiments, we set out to more specifically interfere with DA release in our slices by using optogenetic stimulation.
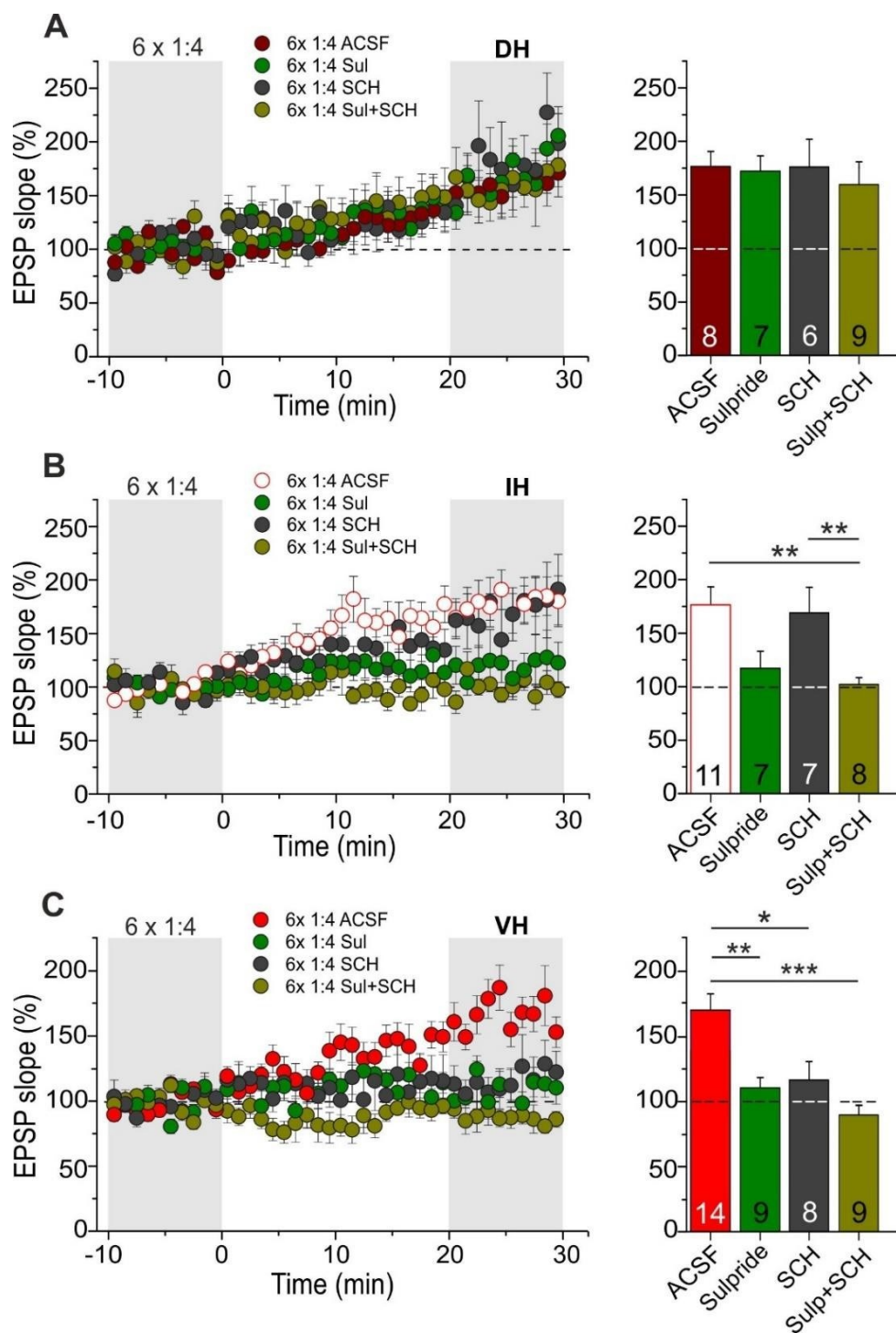
Figure 3.25: Contribution of DA receptor signaling to 6x 1:4 t-LTP induction. Low repeat (6x 1:4) protocol was tested for the contribution of DA receptor signaling to elicit t-LTP in the presence of the D1R antagonist SCH23990 (10 μM, grey symbols), the D2R antagonist Sulpiride (10 μM, green symbol), or co-application of D1R and D2R antagonists (dark yellow

symbols), compared to ACSF control (purple symbols). **A)** The number of animals/recordings used for the 6x 1:4 protocol in DH was in ACSF: n=8 / N=5, D1R blocker n=7 / N=4, D2R blocker n=6 / N=5 and for D1R+D2R blocker: n=9 / N=6). **B)** The number of animals/recordings used for the 6x 1:1 protocol in IH was in ACSF: n=11 / N=5, D1R blocker n=7 / N=5, D2R blocker n=7 / N=4 and for D1R+D2R blocker: n=8 / N=4). **C)** The number of animals/recordings used for the 6x 1:1 protocol in VH was in ACSF: n=14 / N=8, D1R blocker n=9 / N=5, D2R blocker n=8 / N=4 and for D1R+D2R blocker: n=9 / N=4). Normalized EPSP slope represented over 40 min of the time course. The number of recorded cells is indicated in the bars. Data are represented as mean ± SEM. * $p < 0.05$, ** $p < 0.01$, and *** $p < 0.001$.

3.14 Optogenetic control of DA release in mouse hippocampal slices using a Cre-lox mouse model

We inhibited DA release from truncated DAergic fibers by employing transgenic mice that express Cre recombinase from an exogenous mice tyrosine hydroxylase driver line (B6.Cg-7630403G23RikTg (Th-cre) 1Tmd/J) crossed to B6;129S-Gt(ROSA)26Sortm39(CAG-hop/EYFP) Hze/J result in TH-Cre Halorhodopsin mice (eNpHR). Using PCR screening offspring are for EYFP mutation always (+/-) but for Th-cre mutation positive we named as (+eNpHR) which yields an expression of the inhibitory/hyperpolarizing Halorhodopsin only in TH-positive neurons, or negative (-eNpHR; WT for Th-cre mutation) also see (**method section 2.5**). Using continued illumination with yellow laser light (Nominal wavelength: 561 nm) in +eNpHR mice (+eNpHR $_{ON}$) enabled us to silence spontaneous and evoked DA release that might be co-activated during SC electrical stimulation compared to no laser light (+eNpHR $_{OFF}$). This approach enabled us to precisely inhibit DA release in our slices to determine the contribution of DA signaling at different stages of t-LTP (induction/expression) on the efficacy to elicit t-LTP. Expression of the YFP-tagged halorhodopsin in +eNpHR mice was verified with wide field and confocal microscopy. We detected YFP fluorescence in cell clusters (compare **Fig. 3.26**) that were located in the VTA region using mouse brain atlas (Allen Institute for Brain Science (2004)), known to harbor large quantities of DA cell somata (compare **Fig.3.26B**). As expected, YFP-labeled axonal fibers of DAergic neurons were clearly visible in S.r. of our acute hippocampal slices (**Fig. 3.26C**). To manipulate DA release in these hippocampal slices during t-LTP recordings, we used slices from 2-month-old male animals and subjected them to electrophysiological recordings combined with optogenetical silencing of DA release. In the first series of experiments we aimed at proving the efficacy and time course of optogenetic silencing. Since DAergic modulation is known to regulate the excitability of CA1 pyramidal neurons (Henze,

González-Burgos et al. 2000, Tritsch and Sabatini 2012), we tested the effects of DA fiber silencing on AP properties of CA1 PCs.
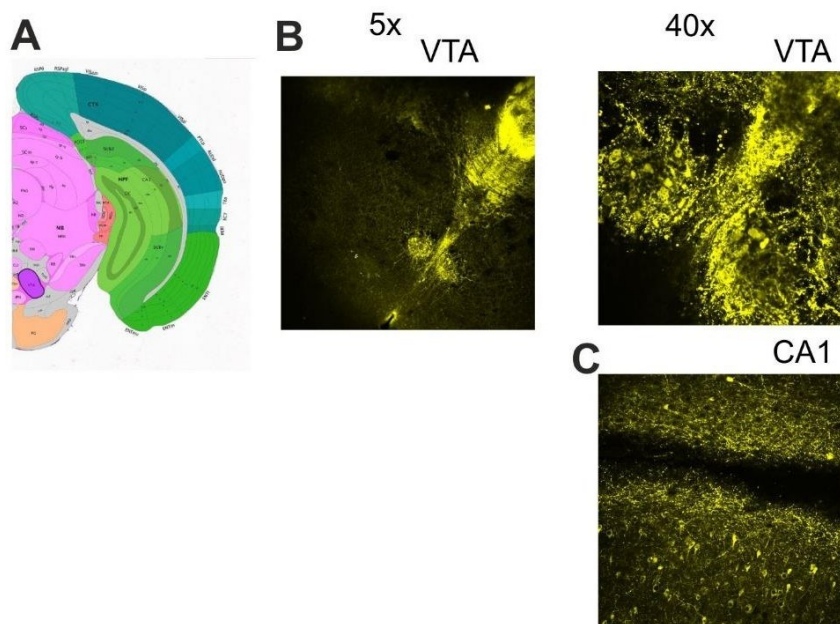
Figure 3.26: EYFP co-expression in +eNpHR mouse in VTA and hippocampal regions. A) VTA location highlighted in the Allen mouse brain atlas. **B)** Using confocal microscopy, EYFP expression indicated in the VTA region of +eNpHR mouse (Th-cre mutation: +/-, EYFP mutation: +/- animals). **C)** Dopaminergic fibers (EYFP positive) are also clearly visible in S.r of our acute +eNpHR mouse hippocampal slices. Coronal slices with different magnifications (5x, and 40x).

In these experiments combining light inactivation with electrophysiology, the blockade of DA receptors (D1R and D2R) in CA1 pyramidal neurons of the IH lead to a significant reduction of action potential (AP) firing frequency (**Fig. 3.27**). At 180 pA current injection, AP frequency was 30.19 ± 1.36 Hz in WT (non-transgenic animals) with ACSF solution, 18.85 ± 0.96 Hz in WT animals under co-application of D1R (SCH23990; 10 μM) and D2R (Sulpiride; 10 μM) antagonists, and 11.77 ± 1.10Hz in +eNpHR animals (15 min after constant light illumination), showing a significant reduction in AP firing frequency (ANOVA $F_{(2,40)}$ = 48.36 P < 0.0001, post hoc Tukey test for WT vs. WT-D1+D2Rs P < 0.0001, WT vs. +eNpHR$_{ON}$, P < 0.0001, and WT-D1+D2Rs vs. +eNpHR$_{ON}$, P = 0.0066, **Fig. 3.27**).
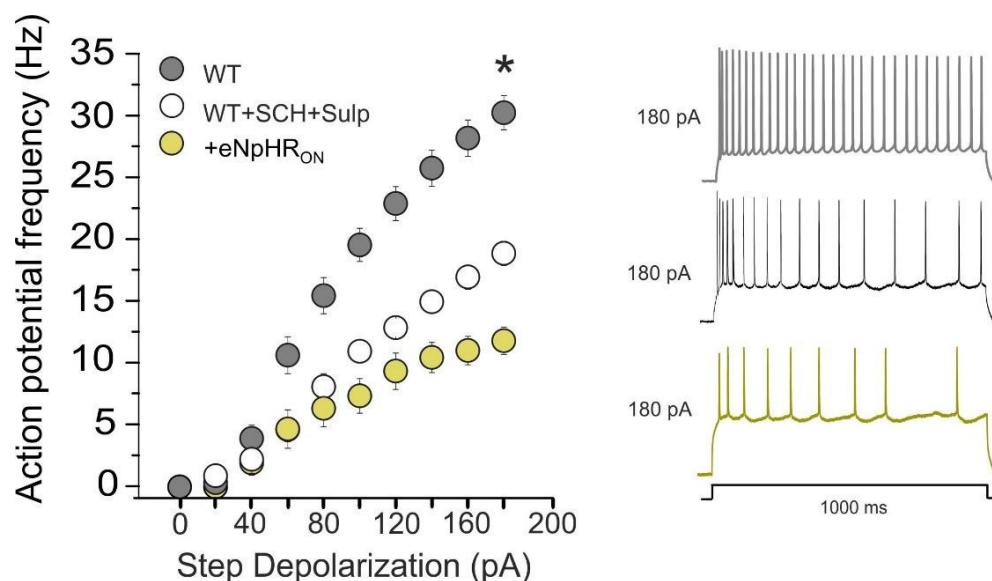
Figure 3.27: Light-dependent modulation of action potential frequencies in CA1 PCs of +eNpHR mice. Patch clamp whole cell recordings were performed in acute hippocampal slices of 2 month-old mice. Cells were recorded in CC mode at -70 mV holding potential and stimulated with increasing depolarizing current pulses. Action potential (AP) frequencies were plotted against step depolarizations (left). Insets (right) show individual voltage traces AP firing in CA1 neurons responding to 180 depolarization steps of somatic current injection. Results are shown for slices **1)** from WT animals in normal ACSF (n=21 / N=13, grey symbols), **2)** from WT animals in the co-presence of the D1R antagonist SCH23990 (10 µM), and the D2R antagonist Sulpiride (10 µM; WT+SCH+Sulp (n=13 / N=9, white symbols), and **3)** from +eNpHR animals after 15 min constant illumination with laser light (561 nm; n=9 / N=3, yellow symbols). The results indicate a significantly higher AP frequency of CA1 PCs in WT animals compared to WT animals under D1R + D2R antagonism, and +eNpHR animals. Data are represented as mean ± SEM.

In another approach, we used the DA-dependent depolarization of the RMP in CA1 PCs to elucidate the on/off kinetics of DA depletion in our hippocampal slices. The mean RMP of +eNpHR cells during the first 5 minutes (15 sweeps) after the start of constant light illumination (561 nm) approached -62.55 ± 0.15 mV. Such a hyperpolarization of the RMP was not observed after identical light stimulation of slices taken from –eNpHR (**method section 2.5** (61.82 ± 0.6 mV)), or of slices from wild-type animals (WT; -61.50 ± 0.05 mV). Our results revealed a significantly higher hyperpolarization in +eNpHR cells during light illumination compared to –eNpHR and Wt slices (ANOVA $F_{(2,42)}$ = 29.40 P < 0.0001, **Fig. 3.28**).

Taken together, both experiments revealed a successful saturating inhibition of DA release in slices of +eNpHR mice following 6-7 min of constant light illumination that was not observed in slices taken from both –eNpHR and WT animals (**Fig. 3.28)**.
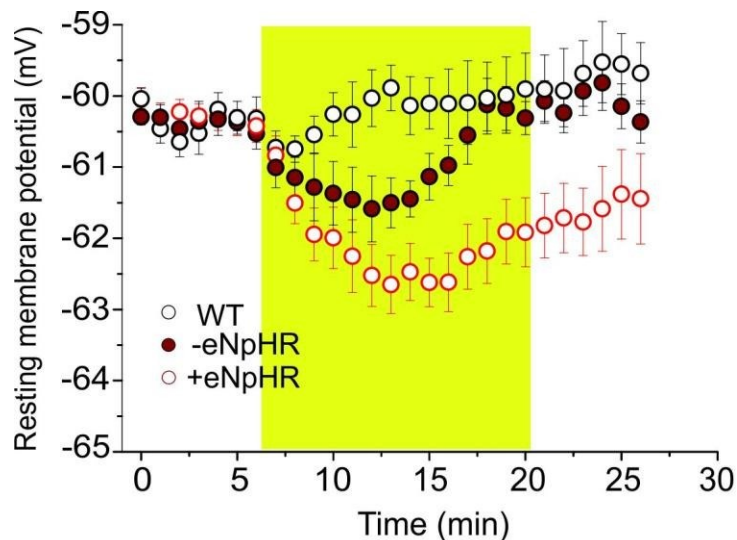
Figure 3.28: Laser light-activated hyperpolarization of membrane potential in +eNpHR slices. Patch clamp whole cell recordings were performed in acute hippocampal slices of 2 month-old mice. Cells were recorded in CC mode at -70 mV holding potential and stimulated with SC fiber stimulation every 20s without further compensation of RMP. Laser light illumination (561 nm, started from minute 6 and was turned off at 20 min. Changes in membrane potential (MP) shortly after light illumination compared to no light illumination (no light = 0-6 min and light = 6-20min) in different slices, including slices taken from WT (n=7 / N=4), -eNpHR (n=10 / N=6), and +eNpHR (n=12 / N=6) animals. We observed stronger hyperpolarization in +eNpHR than -eNpHR and Wt animals. RMP was not compensated during the recording.

In the next step, we tested the effects of light-induced DA release inhibition in acute hippocampal slices of +eNpHR mice using 6x 1:1 t-LTP induction protocol at SC-CA1 synapses. 6x 1:1 t-LTP paradigm failed to induce potentiation in +eNpHR slices under light illumination (+eNpHR$_{ON}$) started at the beginning of baseline recording (light started at -10 min and continued throughout the whole recording period) compared to Wt animals (WT: 157.35 ± 12.61% vs. +eNpHR$_{ON}$ slices, 93.71 ± 6.42%; unpaired Student's t-test, $t_{(20)}$ = 4.72, 10/7, 12/6, p = 0.0001; **Fig. 3.29A**). However, robust t-LTP could be induced in the absence of light illumination in +eNpHR slices (+eNpHR$_{OFF}$; 145.54 ± 11.44%) compared to +eNpHR$_{ON}$ (93.72 ± 6.42%; unpaired Student's t-test, $t_{(17)}$ = 4.29, 7/3, 12/6 p = 0.0005; **Fig. 3.29B**).
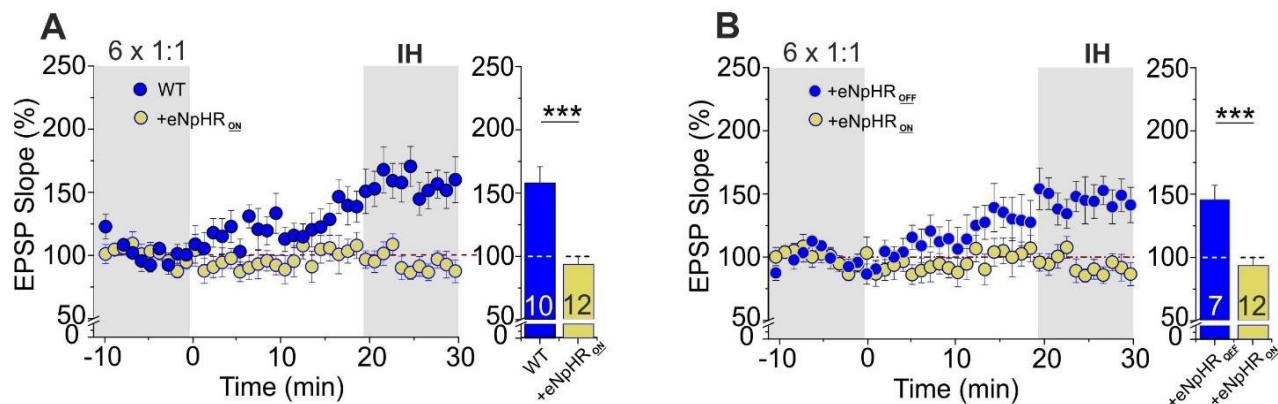
Figure 3.29: Optogenetic inhibition of DA release inhibits 6x 1:1 t-LTP. Whole cell patch clamp recordings were performed in acute hippocampal slices of 2 month-old mice. Cells were recorded in CC mode at -70 mV holding potential, with light illumination (indicated with subscript letter "ON", 561 nm) started at the beginning of recording or with no light (indicated with subscript letter "OFF"). **A)** The number of animals/recordings used for the 6x 1:1 protocol in IH was in +eNpHR$_{ON}$: n=12 / N=6 and for WT: n=10 / N=7). **B)** The number of animals/recordings used for the 6x 1:1 protocol in IH was in +eNpHR$_{ON}$: n=12 / N=6 and for +eNpHR$_{OFF}$: n=7 / N=3). Normalized EPSP slope represented over 40 min of the time course. The number of recorded cells is indicated in the bars. Data are represented as mean ± SEM. *** p < 0.001.

To check whether reduction of DA release during light illumination in +eNpHR slices was responsible for 6x 1:1 t-LTP failure (**Fig.29A**), we added 20 µM exogenous DA (40 µM Vit C was added as an antioxidant to DA containing ACSF; running from the beginning of recording at the same time when light illumination started at -10 min) to the recording ACSF, which completely rescued induction of 6x 1:1 t-LTP (light: 92.28 ± 5.58% vs. light+ DA: 175.25 ± 24.50%; unpaired Student's t-test, t$_{(18)}$ = 4.69, 14/7, 6/3, p = 0.0002; **Fig. 3.30**).
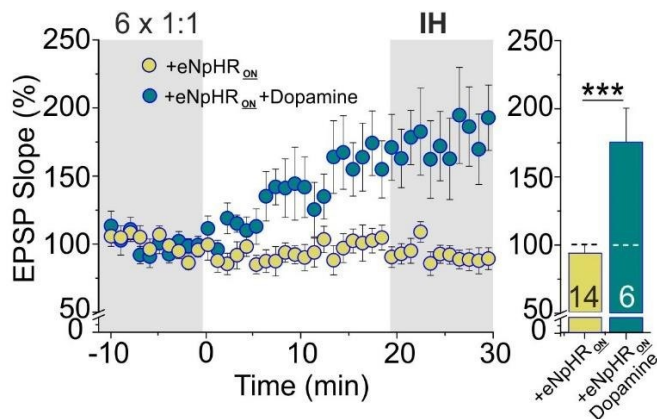
Figure 3.30: Exogenous DA rescued 6x 1:1 t-LTP upon optogenetic inhibition of endogenous DA secretion in slices from +eNpHR mice. Patch clamp whole cell recordings were performed in acute hippocampal slices of 2 month-old mice. Cells were recorded in CC mode at -70 mV holding potential, under light illumination (561 nm) started at the beginning of the recording. The number of animals/recordings used for the 6x 1:1 protocol in IH wasin +eNpHR$_{ON}$: n=14 / N=7 and for +eNpHR$_{ON}$ with DA (20 μM+ Vit C; 40 μM) added to recording ACSF: n=6 / N=3). Normalized EPSP slope represented over 40 min of the time course. The number of recorded cells is indicated in the bars. Data are represented as mean ± SEM. * p < 0.001.

A considerable number of studies tried to divide LTP into diverse temporal phases, with different biochemical mechanisms. Based on these observations LTP can probably be divided into at least two phases: early LTP (E-LTP; dependent on kinase activity) and late LTP (L-LTP; dependent on cAMP and gene transcription, discussed by (Frey, Huang et al. 1993, Huang 1998)). Bolshakov et al proposed that the two LTP phases may work through different mechanisms. While E-LTP is based on presynaptic changes in transmitter release, L-LTP involves both presynaptic and postsynaptic modifications (Bolshakov, Golan et al. 1997). This suggests that LTP should be treated as a dynamic phenomenon and could be modulated by many factors, including time, stimulation etc. DA-induced changes in synaptic plasticity were discussed earlier e.g., by (Otmakhova and Lisman 1996), where D1/D5 receptors induced a synapse-specific enhancement of E-LTP. We also earlier discussed how two distinct STDP protocols are regulated by DAergic modulation (**section 3.13.2 and Fig. 3.24 and 3.25**; compare also (Cepeda-Prado*, Khodaie* et al. 2021)). To test the effect of light inhibited DA release at different time points during t-LTP we used the experimental set-up represented in **Figure 3.31**, indicating light illumination at different time-points (-10 min: beginning, 0: during t-LTP stimulation termed as induction, +10 min; termed as early expression and 20 min; termed as late expression). In all experiments, light illumination continued until the end of recording. Light illumination constantly ran from the starting points indicated by the arrows.
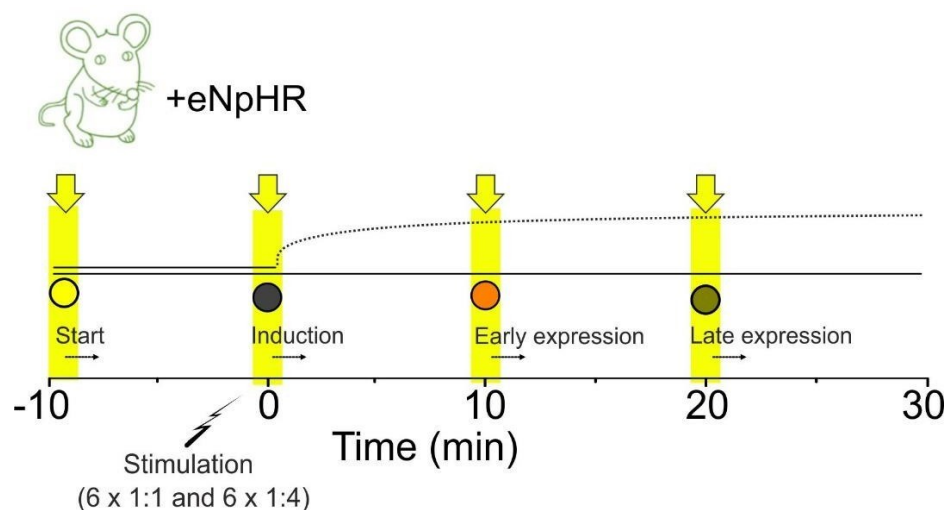
Figure 3.31: Schematic drawing of light inactivation of DAergic inputs towards Schaffer collateral CA1-Synapse in slices form +eNpHR mouse during t-LTP recordings. Light illumination either started at the start of EPSP recording 10 min before STDP paradigm (yellow symbol), or during t-LTP induction (Grey symbols), 10 min after t-LTP induction (early expression, orange), and 20 min after t-LTP induction (late expression, dark yellow symbol). As shown by arrows, light illumination constantly ran after starting at different time points. STDP paradigms were performed at the 0-time point, as shown by the stimulation symbol.

The effect of laser light-induced inhibition of DA release on t-LTP was tested along different time points of recording (e.g., before and after STDP paradigms). Our results showed that in IH, light illumination 10 min before evoking 6x 1:1 t-LTP significantly blocked 6x 1:1 t-LTP induction (**Fig. 3.29 and 3.32A**). Similarly, light illumination during 6x 1:1 t-LTP induction (0 min: induction) significantly reduced the magnitude of t-LTP ($87.25 \pm 9.51\%$) compared to the control condition (No light: $154.09 \pm 13.09\%$; Kruskal-Wallis test, $H_{(5)} = 20.12$, 10/7, 8/6, $p = 0.0014$, **Fig. 3.32A**). While light illumination during the early phase of t-LTP expression led to a non-significant reduction in 6x 1:1 t-LTP magnitude ($117.01 \pm 14.47\%$), 6x 1:1 t-LTP remained unaffected when light illumination started during late phases of t-LTP expression ($137.25 \pm 13.05\%$), showing the significantly higher magnitude of t-LTP compared to light illumination during induction group (Kruskal-Wallis test, $H_{(5)} = 20.12$, $p = 0.025$, **Fig. 3.32A).** Next, we performed a similar set of experiments to test for the effects of optogenetically inhibited DA release in +eNpHR animals on 6x 1:4 t-LTP (**Fig. 3.32B**). Light illumination at the start of recording (-10 min) similarly blocked 6x 1:4 t-LTP compared to no light condition (No light: $154.09 \pm 13.09\%$ vs start: $110.08 \pm 12.37\%$; ANOVA $F_{(4,26)} = 7.08$, 8/6,5/4, $P < 0.0005$, post hoc Tukey-test $P < 0.03$, **Fig. 3.32B).** Moreover, 6x 1:4 t-LTP was blocked when light

illumination started during t-LTP stimulation (0 min; 90.17 ± 6.11%) compared to control (ANOVA $F_{(4,26)}$ = 7.08, 8/6, 8/7, P < 0.0005, post hoc Tukey-test P < 0.0002, **Fig. 3.32B).** In contrast, t-LTP induced by 6x 1:4 protocol was unaffected when light illumination started during early expression (+10 min); 120.15 ± 11.11%) or late expression (+20 min); 130.06 ± 14.33%).
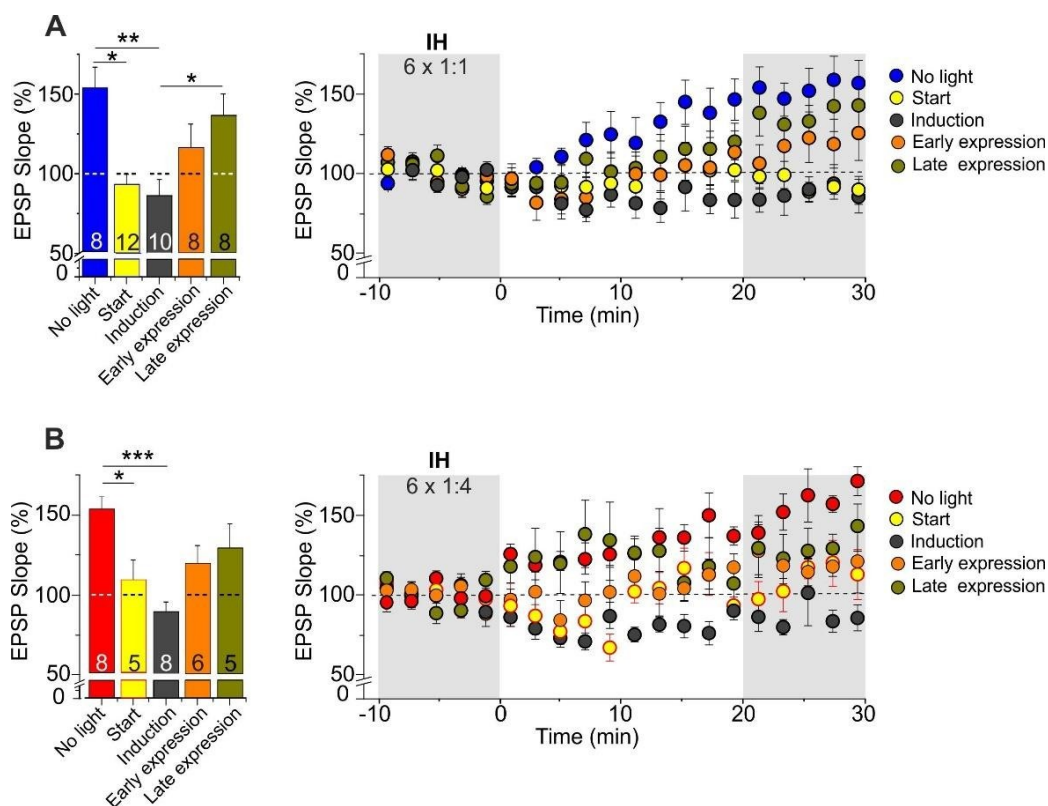
Figure 3.32: Light induce inhibition of DA release in slices from +eNpHR animals at different time points of EPSP recording and 6x 1:1 and 6x 1:4 t-LTP induction. Patch clamp whole cell recordings were performed in acute hippocampal slices of 2 month-old mice. Cells were recorded in CC mode at -70 mV holding potential, under light illumination (561 nm) at different time-point during recording. Including: at the beginning of EPSP recording 10 min before STDP paradigm (yellow symbol), during t-LTP induction (Grey symbols, time point), 10 min after t-LTP induction (early expression, orange), and 20 min after t-LTP induction (late expression, dark yellow symbol). **A)** The number of animals/recordings used for the 6x 1:1 protocol in IH was in +eNpHR animals in no light n=8 / N=6, the start of recording n=12 / N=10, during t-LTP induction n=10 / N=7, early expression n=8 / N=6, and for late expression n=8 / N=5). **B)** The number of animals/recordings used for the 6x 1:4 protocol in IH was in +eNpHR animals in no light n=8/N=6, the start of recording n=5 / N=4, during t-LTP induction n=8 / N=7, early expression n=6 / N=5, and for late expression n=5 / N=4). Time course of t-LTP during 30 minutes of recording after t-LTP induction is represented on the left side of each figure. The number of recorded cells is indicated (n) in the bars and N= animal number. Data are shown as

mean ± SEM. * p < 0.05, ** p < 0.01, and *** p < 0.001. Multiple comparisons were performed with ANOVA using post hoc Tukey test.

3.15 Region specific GABAergic inhibition of SC-CA1 synapses along the longitudinal axis of hippocampus

In the next series of experiments, we wanted to systematically investigate how the two 6x t-LTP paradigms depends on GABA-A and GABA-B receptor mediated inhibition along the longitudinal axis of the hippocampus. GABA mediates fast inhibitory responses through $GABA_A$ receptors and slow inhibitory responses via $GABA_B$ receptor activity in the hippocampus (Isaacson, Solis et al. 1993, Sallard, Letourneur et al. 2021). Distinct gradients of $GABA_A$ receptor (DH>IH>VH) and $GABA_B$ receptor (DH<IH<VH) expression were reported along the longitudinal axis of the rat hippocampus (Dubovyk and Manahan-Vaughan 2018). In the previous t-LTP experiments reported here, we always added picrotoxin (100 µM) to block $GABA_AR$ responses, while the $GABA_BR$ component response that can be inhibited by CGP (10 µM) was intact (+PIC/-CGP condition). To quantify the strength of $GABA_B$ receptor mediated inhibition in our synaptic recordings, we measured the hyperpolarization following the SC stimulation induced EPSPs, which is known to be triggered by SC-dependent activation of GABAergic neurons (Fink, Sarinana et al. 2007, Price, Scott et al. 2008) (**Fig. 3.33A**). Our results obtained in the presence of the $GABA_A$ receptor inhibitor picrotoxin (+PIC/-CGP) revealed stronger $GABA_B$ components in DH compared to VH and IH CA1 neurons, being consistent with previous reports (Papatheodoropoulos, Asprodini et al. 2002, Petrides, Georgopoulos et al. 2007). To confirm that the hyperpolarization was mediated by $GABA_B$ receptors, we added the $GABA_BR$ blocker CGP (10 µM) to our picrotoxin containing recording solution (+PIC/+CGP), which strongly inhibited the hyperpolarization (**Fig. 3.33, A2**), (Lenz, Pitler et al. 1997). As represented in **Figure 3.33B**, the hyperpolarization after the EPSP in DH reached -1.32 ± 0.11 mV in +PIC/-CGP solution and was significantly different from the -0.35 ± 0.04 mV recorded in ACSF containing both inhibitors (+PIC/+CGP) (unpaired Student's t-test, $t_{(25)}$ = 7.37; P <0.0001). While the $GABA_B$ receptor mediated hyperpolarization was smaller in IH and VH CA1 cells compared to DH, they were also significantly reduced in the presence of CGP (IH: -0.80 ± 0.1 mV in +PIC/-CGP, and -0.29 ± 0.03 mV in +PIC/+CGP, unpaired Student's t-test, $t_{(35)}$ = 4.35; P =0.0001; VH: -0.6 ± 0.06 mV in +PIC/-CGP, and -0.26 ± 0.05 mV in +PIC/+CGP, unpaired Student's t-test, $t_{(31)}$ = 3.908; P =0.0005; **Fig. 3.33B**).

Overall, these data suggest that SC stimulation induced GABA$_B$ receptor mediated inhibition reduces excitability of CA1 neurons largely in DH than in IH/VH.
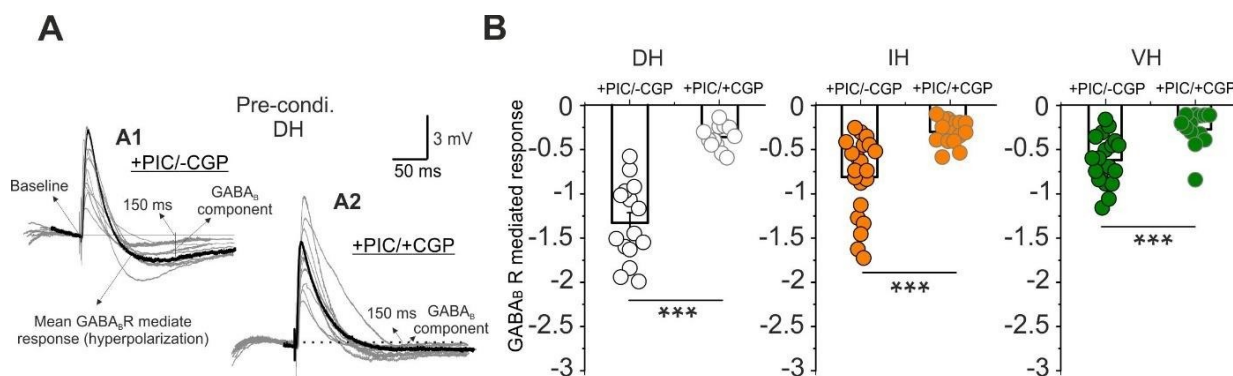
Figure 3.33: GABA$_B$R component at SC-CA1 synapses along the longitudinal axis of the hippocampus. **A)** Original traces of an EPSP response recorded 150 ms after EPSP in DH PCs representing how GABA$_B$R mediated response (hyperpolarization) reduced comparing +PIC/-CGP to +PIC/+CGP, preconditioning (pre-cond.). **B)** GABA$_B$R mediated component response in DH (+PIC/-CGP; n=15 / N=8, and +PIC/+CGP; n=12 / N=6), in IH +PIC/-CGP; n=21 / N=13, and +PIC/+CGP; n=16 / N=9), and in VH (+PIC/-CGP; n=19/ N=9, and +PIC/+CGP; n=14 / N=10) along the longitudinal axis of hippocampus, revealed a significant reduction in hyperpolarization in all studied regions after adding CGP (GABA$_B$R blocker). Each dot represents a single response. The number of recorded cells is indicated (n) in the bars and N= animal number. Data are shown as mean ± SEM. *** p < 0.001.

3.16 Effects of GABAergic inhibition on glutamate release probability at SC-CA1 synapses along the longitudinal axis of the hippocampus

To determine how GABAergic inhibition affects glutamate release at SC-CA1 synapses we kept picrotoxin out from our recording solution, thus providing intact (physiological) GABAergic inhibition (-PIC/-CGP condition), and recorded miniature EPSCs to study effects on spontaneous glutamate release probability. We found that mean mEPSC frequencies in DH and VH CA1 PCs were not changed under conditions of intact GABA$_A$R mediated inhibition (DH: +PIC/-CGP: 0.25 ± 0.03 Hz, vs. -PIC/-CGP: 0.31 ± 0.04 Hz, **Fig. 3.34A;** VH: +PIC/-CGP: 0.57 ± 0.1 Hz, vs. -PIC/-CGP: 0.56 ± 0.06 Hz, **Fig. 3.34E**), while in IH, intact inhibition via GABA$_A$Rs significantly reduced mEPSC frequencies (+PIC/-CGP: 0.81 ± 0.01 Hz, vs. -PIC/-CGP: 0.52 ± 0.03 Hz; unpaired Student's t-test, $t_{(10)}$ = 17.99; P =0.049; **Fig. 3.34C**). Correspondingly, mEPSC inter event intervals (IEI) were not affected in both DH

and VH under conditions of intact $GABA_A$ receptor-mediated inhibition, while in IH IEI intervals were decreased (Kolmogorov–Smirnov two-sample test: Z = 0.386, P < 0.0001, **Fig. 3.34C**).

As a second read-out of glutamate release probability, we also determined the PPR at SC-CA1 synapses. While in DH and VH, PPR was not significantly changed by intact $GABA_A$R mediated inhibition (DH: (+PIC/-CGP: 2.11 ± 0.14, -PIC/-CGP: 1.83 ± 0.08, **Fig. 3.34B;** VH: +PIC/-CGP: 1.68 ± 0.1, -PIC/-CGP: 2.02 ± 0.25, **Fig. 3.34F**), PPR in IH CA1 PCs was significantly reduced under conditions of intact GABAergic conditions compared to $GABA_A$R blockade (+PIC/-CGP: 1.79 ± 0.12, -PIC/-CGP: 1.49 ± 0.06, unpaired Student's t-test, $t_{(34)}$ = 2.07.; P = 0.046, **Fig. 3.34D**).

Together, results for PPR and mEPSC frequencies suggest, that in DH and VH glutamate release probability is not affected by $GABA_A$ receptor blockade, while in IH the results are consistent with changed glutamate release probability in the presence of the $GABA_A$ antagonist.
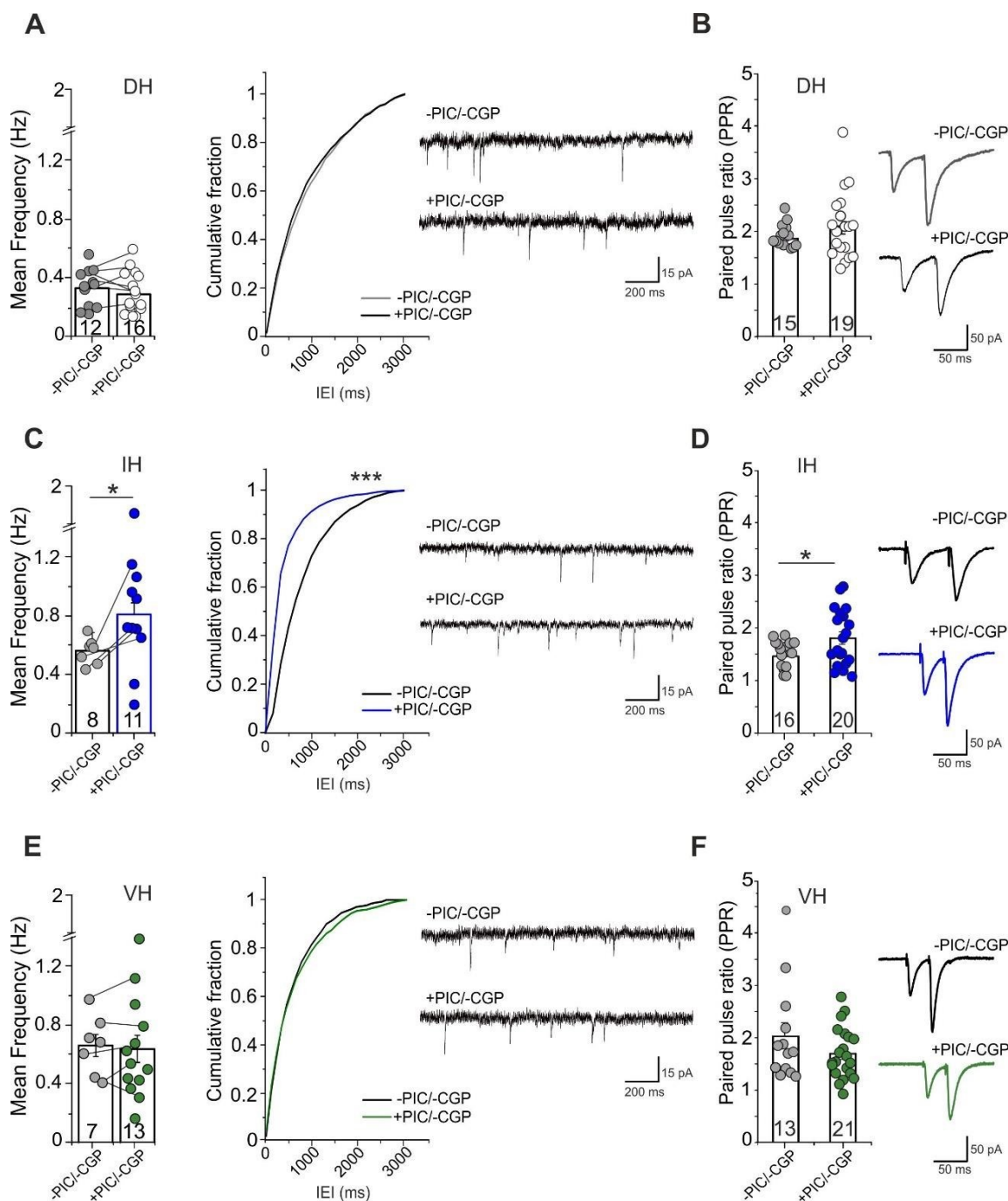
Figure 3.34: GABAergic inhibition regulates presynaptic glutamate release probability at SC-CA1 synapses. **A)** Mean frequency and cumulative distribution of inter-event intervals (IEI) of putative mEPSCs in DH PCs comparing intact GABAergic inhibition (-PIC/-CGP; n=12 / N=8) to GABA$_A$R inhibition (+PIC/-CGP; n=16 / N=11) show no significant changes in IEI under intact GABAergic inhibition, similar to mean frequency. Original traces of miniature (m) EPSCs were recorded in acute hippocampal slices along the longitudinal axis of the hippocampus. **B)** PPR was

also not changed comparing intact GABAergic inhibition (n=15 / N=7) to GABA$_A$R inhibition (n=19 / N=9). Original traces represent postsynaptic cells' response to SC-CA1 fiber stimulations with an interval of 50 ms, the second current response divided by the first response used to calculate PPR. **C)** Mean frequency and cumulative distribution of IEI of putative mEPSCs in IH, however, were significantly affected under intact GABAergic inhibition (n=8/ N=4) compared with GABA$_A$R inhibition (n=11 / N=8). **D)** PPR in IH PCs also revealed a significant increase comparing intact GABAergic inhibition (n=16 / N=9) to GABA$_A$R inhibition (n=20 / N=9). **E)** Mean frequency and cumulative distribution of IEI of putative mEPSCs in VH indicate similar frequency, and IEI under GABA$_A$R inhibition (n=13 / N=9) compared to intact GABAergic inhibition (n=7 / N=5). **F)** PPR measurements indicate similar values comparing intact GABAergic inhibition (n=13 / N=9) to GABA$_A$R inhibition (n=21 / N=11). Each dot indicates one cell's data. The number of recorded cells is indicated (n) in the bars and N= animal number Data are shown as mean ± SEM. * p < 0.05, and *** p < 0.001. Scale bars are shown in the figures.

3.17 GABAergic modulation of low repeat t-LTP induction along the longitudinal axis of the Hippocampus

Since our t-LTP results provided clear differences in magnitude and mechanism of expression of t-LTP along the longitudinal axis of the hippocampus (compare **Fig. 3.19-3.20**), we wanted to investigate how the distinct GABA$_A$ and GABA$_B$ receptor mediated inhibition in DH, IH, and VH might account for these differences in t-LTP. Thus, in the next series of experiments we compared the efficacy to obtain 6x 1:1 and 6x 1:4 t-LTP along the longitudinal axis of the hippocampus under conditions of intact GABAergic inhibition (-PIC/-CGP), with t-LTP when only GABA$_A$Rs were inhibited (+PIC/-CGP), or under complete blockade of GABAergic inhibition (+PIC/+CGP).

Our results indicate that in DH the 6x 1:1 t-LTP paradigm failed to induce potentiation under conditions of intact GABAergic (i.e. GABA$_A$ and GABA$_B$ mediated) inhibition compared to selective GABA$_A$R blockade or complete GABA receptor blockade (intact inhibition: 95.93 ± 7.0%, +PIC/-CGP: 180.40 ± 18.03%, +PIC/+CGP: 190.08 ± 19.02%; ANOVA F$_{(2,22)}$ = 5.799; P = 0.0005, 9/6, 9/5, 6/4, post hoc Tukey-test for intact vs. +PIC/-CGP: P = 0.0014 and for intact inhibition vs. +PIC/+CGP: P = 0.0018; **Fig. 3.35A**). Interestingly, in the IH region 6x 1:1 t-LTP stimulation only induced robust t-LTP when GABA$_A$Rs were blocked selectively, whereas neither complete GABA receptor blockade nor intact GABA inhibition yielded significant t-LTP (intact: 109.49 ± 13.20%, +PIC/-CGP: 171.05 ± 12.86%, and +PIC/+CGP: 122.94 ± 6.10%; ANOVA F$_{(3,30)}$ = 14; P = 0.0009, 10/5, 11/7, 9/5, post hoc Dunnett's Test for +PIC/-CGP vs. intact inhibition: P = 0.0013 and for +PIC/-CGP vs. +PIC/+CGP: P = 0.019; **Fig. 3.35B**). In VH, the 6x 1:1 t-LTP paradigm induced significant potentiation regardless of

GABAergic inhibition in all three conditions (intact: 138.72 ± 12.76%, +PIC/-CGP: 135.93 ± 7.57%, +PIC/+CGP: 143.35 ± 12.40%, 8/5, 12/9, 8/6; **Fig. 3.35C**).
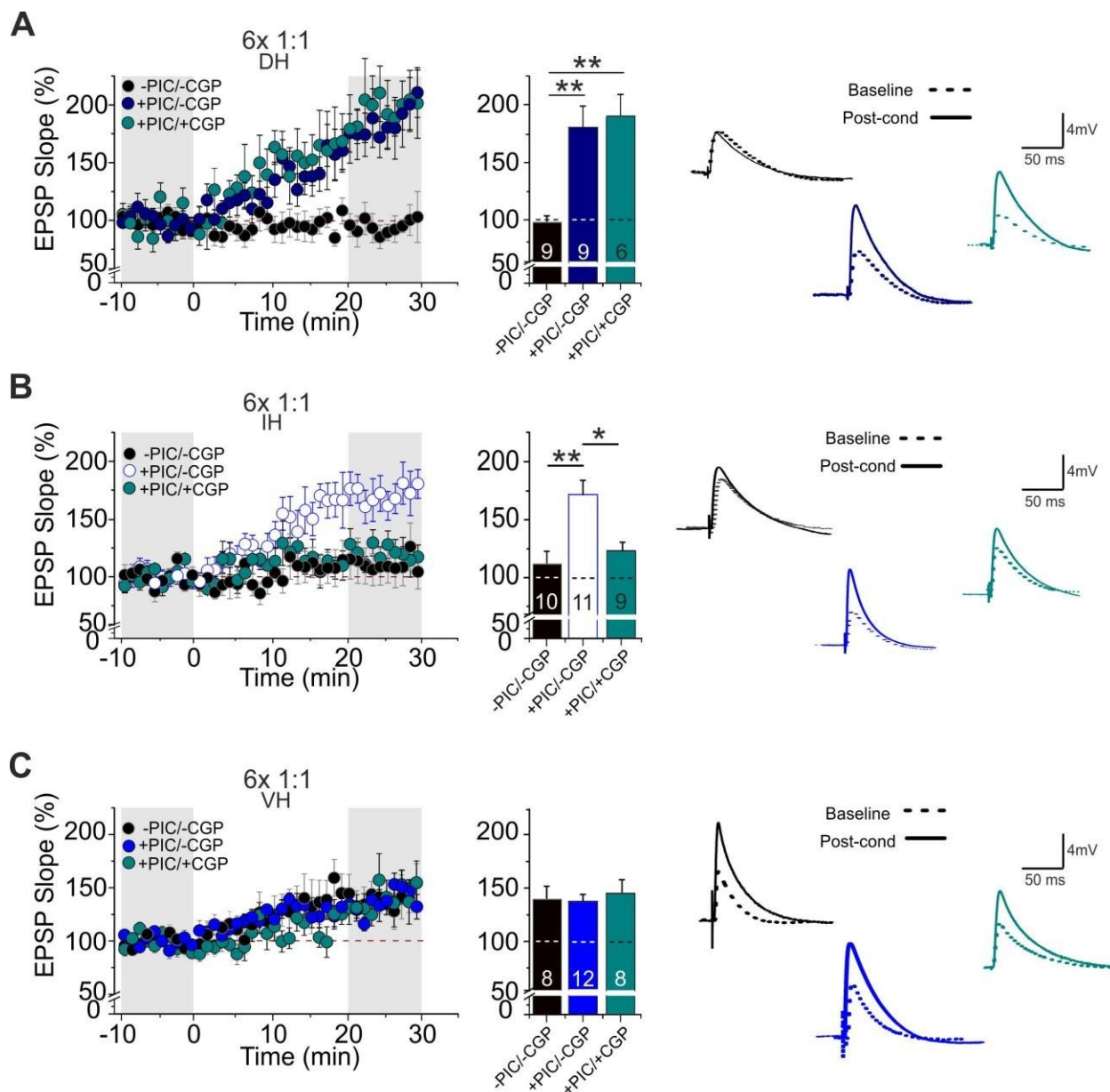
Figure 3.35: GABAergic modulation of low repeat 1:1 t-LTP magnitude along the longitudinal axis of the hippocampus. **A)** 6x 1:1 t-LTP in CA1 PCs of DH under intact GABAergic inhibition (-PIC/-CGP; n=9 / N=6), in response to GABA$_A$R inhibition (+PIC/-CGP; n=9 / N=5), and upon complete blockade of GABAergic inhibition (+PIC/+CGP; n=6 / N=4). 6x 1:1t-LTP was absent under intact GABAergic inhibition. **B)** t-LTP induced by 6x 1:1 protocol in PCs of IH under intact GABAergic inhibition (n=10 / N=5), upon GABA$_A$R inhibition (n=11 / N=7), and upon

complete blockade of GABAergic inhibition (n=9 / N=5), only induced robust t-LTP under sole GABA$_A$ receptor inhibition. **C)** 6x 1:1 t-LTP in CA1 PCs of VH under intact GABAergic inhibition (-PIC/-CGP; n=8 / N=5), in response to GABA$_A$R inhibition (+PIC/-CGP; n=12 / N=9), and upon complete blockade of GABAergic inhibition (+PIC/+CGP; n=8 / N=6). 6x 1:1 t-LTP was independent of GABAergic inhibition all conditions induced robust potentiation independent or GABAergic inhibition. Time course of t-LTP during 30 minutes of recording after t-LTP induction is represented on the left side of each figure. Original traces of EPSP before and after t-LTP induction under diverse GABAergic inhibition are shown on the right. The number of recorded cells is indicated (n) in the bars; N= animal numbers. Data are shown as mean ± SEM. * p < 0.05, and ** p < 0.01. Multiple comparisons were performed with ANOVA using the post hoc Tukey test. Scale bars are shown in the figures.

In the next step, we performed the same set of experiments with GABA receptor inhibitors for the 6x 1:4 (burst) protocol (**Fig. 3.36**). We found that at the DH pole of the hippocampus, the 6x 1:4 t-LTP protocol induced similar magnitudes of potentiation in all three conditions (intact GABAergic inhibition: 139.51 ± 15.74%, +PIC/-CGP: 179.75 ± 15.53%, complete blockade of GABAergic inhibition: 150.20 ± 16.60%, 6/4, 8/4, 6/5; **Fig. 3.36A**). In IH, the 6x 1:4 t-LTP paradigm induced clear and significantly higher potentiation under intact GABAergic inhibition in comparison to t-LTP under complete GABA receptor blockade (intact: 164.38 ± 20.82%, +PIC/+CGP: 107.60 ± 5.31%, ANOVA F $_{(2, 29)}$ = 4.344; 10/5, 11/7, P = 0.022; **Fig. 3.36B**), but the similar t-LTP magnitude in the presence of only the GABA$_A$ receptor inhibitor (+PIC/-CGP: 149.02 ± 13.67%, 11/5; **Fig. 3.36B**), whereas there was no t-LTP under complete GABA receptor blockade compare to 100% baseline (Student's t-test p = 0.18, one-sample t-test).

A similar pattern of t-LTP magnitudes was observed for the 6x 1:4 t-LTP in VH CA1 PCs (intact: 139.60 ± 12.03%, +PIC/-CGP: 137.80 ± 11.01%, complete blockade: 106.45 ± 10.55%; ANOVA F$_{(2, 24)}$ = 2.548, 9/5, 10/7, 8/5, P = 0.099; **Fig. 3.36C**).

Together, these results suggest a complex regulation of 6x 1:1 and 6x 1:4 t-LTP by GABA$_A$ and GABA$_B$ receptor mediated mechanisms that are co-activated in the SC-CA1 circuit by our extracellular SC stimulation. Importantly, these GABAergic mechanisms, which control t-LTP, are differentially recruited along the longitudinal axis of the hippocampus. Blockade of only GABA$_A$ receptor mediated transmission allowed successful induction of 6x 1:1 t-LTP in DH, IH, and VH. Under intact GABAergic conditions, 6x 1:1 t-LTP could be induced only in VH, while intact GABA$_B$R mediated inhibition was beneficial for successful induction of 6x 1:1 t-LTP selectively in IH (**Fig. 3.35**).

In stark contrast, 6x 1:4 t-LTP was successfully induced in all three areas under conditions of intact GABAergic inhibition (-PIC/-CGP) and if only GABA$_A$ receptors were blocked (+PIC/-CGP). However,

complete blockade of GABA$_A$ and GABA$_B$ receptor mediated mechanisms, abolished 6x 1:4 t-LTP (**Fig. 3.36**).
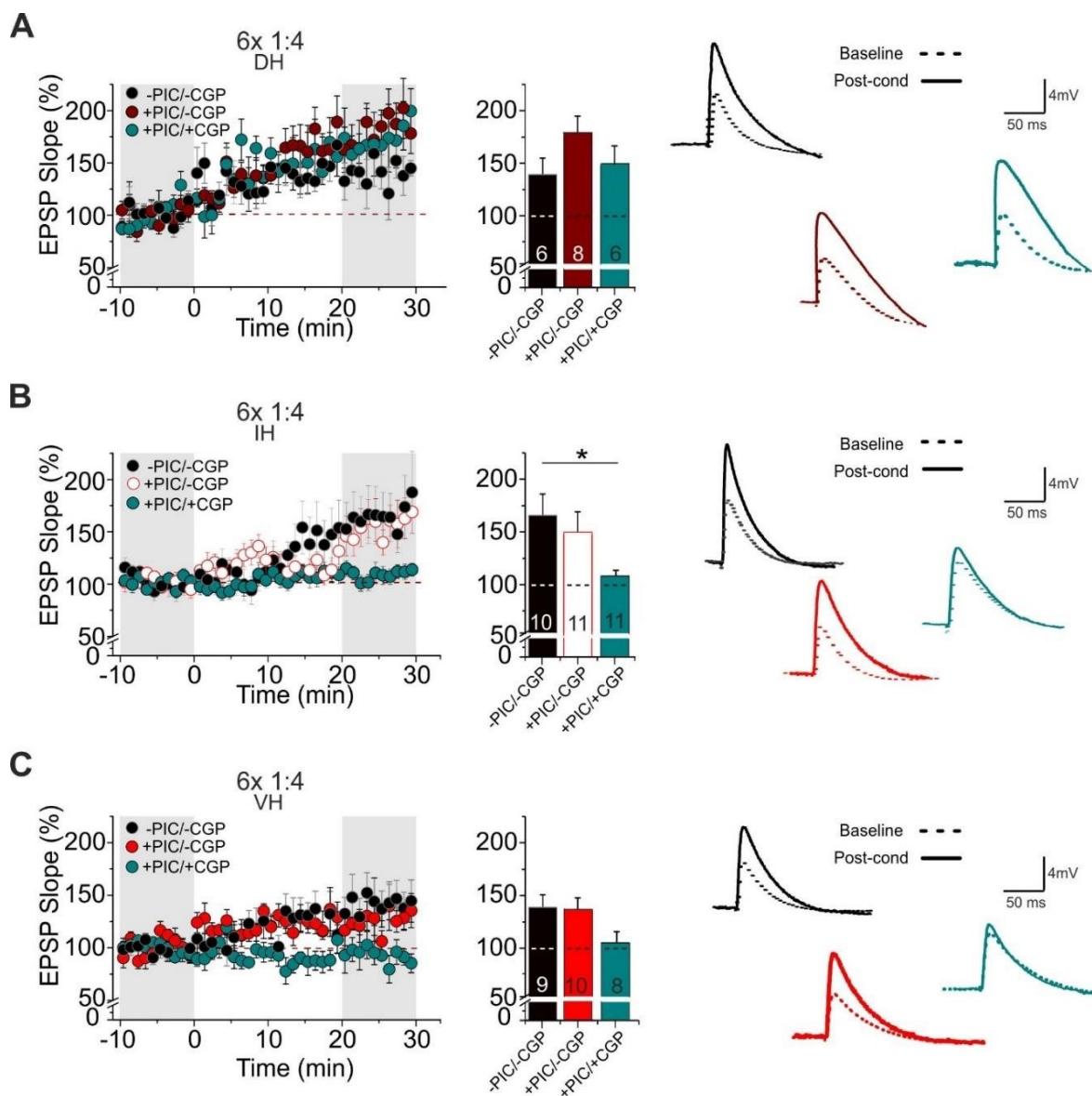
Figure 3.36: GABAergic modulation of low repeat 1:4 t-LTP magnitude at SC-CA1 synapses along the longitudinal axis of the hippocampus. A) In DH, 6x 1:4 t-LTP was not affected by GABAergic inhibition compared to intact GABAergic inhibition (-PIC/-CGP; n=6 / N=4), GABA$_A$R inhibition (+PIC-CGP; n=8 / N=4), and complete GABAergic inhibition blockade (+PIC/+CGP; n=6 / N=5). **B)** In IH PCs, 6x 1:4 t-LTP induced higher potentiation under intact GABAergic inhibition (-PIC/-CGP; n=10 / N=5) and weakest potentiation under complete GABAergic inhibition (+PIC/+CGP; n=11 / N=5). Under sole GABA$_A$R inhibition (+PIC/-CGP; n=11 / N=7) 6x 1:4 t-LTP showed an intermediate potentiation magnitude. **C)** Similar pattern of changes in the magnitude

of potentiation was observed in VH, when 6x 1:4 t-LTP paradigm was applied under con ditions of intact GABAergic inhibition (-PIC/-CGP; n=9 / N=5) upon selective GABA$_A$R inhibition (+PIC/-CGP; n=10 / N=7), and complete blockade of GABAergic inhibition (+PIC/+CGP; n=8 / N=5). Time course of t-LTP during 30 minutes of recording after t-LTP induction is represented on the left side of each figure. Original traces of EPSP before and after t-LTP induction under diverse GABAergic inhibition are shown on the right. The number of recorded cells is indicated (n) in the bars; N= animal numbers. Data are shown as mean ± SEM. * p < 0.05. Multiple comparisons were performed with ANOVA using the post hoc Tukey test. Scale bars are shown in the figures.

3.18 Expression mechanisms of 6x 1:1 and 6x 1:4 t-LTP under diverse conditions of GABAergic inhibition

We previously showed that 6x 1:1 and 6x 1:4 t-LTP rely on distinct pre- and postsynaptic expression mechanisms to induce long lasting synaptic changes under GABA$_A$R blockade (Cepeda-Prado*, Khodaie* et al. 2021). Given the distinct dependence of 6x 1:1 and 6x 1:4 t-LTP on GABAergic inhibition along the longitudinal axis of the hippocampus, we started out to determine how expression loci and mechanisms might be affected by changes in GABAergic modulation. Similar to the experiments described in **Figure 3.35**. Therefore, we assessed PPR before vs. after successful induction of t-LTP, and AMPAR/NMDAR current ratios after successful t-LTP induction by the 6x 1:1 and 6x 1:4 t-LTP paradigms, respectively.

DH: 6x 1:1 t-LTP;

For DH, we already showed in **Figure 3.35** that successful 6x 1:1 t-LTP did not change the PPR under GABA$_A$R blockade (+PIC/-CGP: before t-LTP: 2.08 ± 0.15, after t-LTP: 2.12 ± 0.18). Although there was a trend of 6x 1:1 t-LTP under complete blockade of GABAergic responses (+PIC/+CGP) towards reduced PPR (before: 2.80 ± 0.29, after: 2.16 ± 0.19), this effect did not reach statistical significance (paired Student's t-test, $t_{(5)}$ = 1.926; P = 0.11), whereas intact GABAergic inhibition (-PIC/-CGP) blocked 6x 1:1 t-LTP and therefore revealed also no changes in PPR (**Fig. 3.37A left**). Similar to 6x 1:1 t-LTP in DH under selective GABA$_A$R blockade, we found an increase in AMPAR/NMDAR current ratio also after successful induction of 6x 1:1 t-LTP under complete blockade of GABAergic inhibition (8.93 ± 0.70; **Fig. 3.37A right**), thus indicating a postsynaptic contribution to t-LTP expression. This seems to indicate additional postsynaptic contribution to 6x 1:1 t-LTP expression when GABAergic inhibition is blocked completely.

DH: 6x 1:4 t-LTP;

Also, successful 6x 1:4 t-LTP in DH under selective GABA$_A$R blockade showed an increased AMPAR/NMDAR current ratio (9.15 ± 1.39), speaking in favor of postsynaptic expression. However, under intact GABAergic inhibition (2.66 ± 0.41), or complete blockade of GABAergic inhibition (3.68 ± 0.52) 6x 1:4 t-LTP was most likely not mediated by postsynaptic increase in AMPAR conductance. Accordingly, we found a significantly increased AMPAR/NMDAR current ratio between GABA$_A$R blockade and intact GABAergic inhibition (ANOVA F $_{(2, 26)}$ = 5.45; P = 0.011, **Fig. 3.37B**). These points towards an altered expression mechanism for 6x 1:4 t-LTP when GABAergic inhibition is either fully functional or fully blocked.

IH: 6x 1:1 t-LTP;

In IH under selective GABA$_A$R blockade, 6x 1:1 t-LTP was accompanied by decreased PPR (before: 1.94 ± 0.11, after: 1.32 ± 0.08; paired student's t-test, t $_{(22)}$ = 4.767; p = 0.0017, **Fig. 3.37C left**) and therefore increased glutamate release probability. Since IH showed no 6x 1:1 t-LTP under intact GABAergic conditions (-PIC/-CGP) or under complete blockade of GABAergic inhibition (+PIC/+CGP) the unchanged PPR under both conditions was expected (-PIC/-CGP before: 1.67 ± 0.08, after: 2.04 ± 0.27; (+PIC/+CGP before: 1.81 ± 0.09, after: 1.68 ± 0.13, **Fig. 3.37C left**). Unexpectedly, 6x 1:1 stimulation in IH under complete blockade of GABAergic inhibition enhanced the AMPAR/NMDAR current ratio (+PIC/+CGP: 7.52 ± 1.01, +PIC/-CGP: 3.97 ± 0.91, ANOVA F$_{(2, 20)}$ = 3.791, P= 0.04, post hoc Tukey-test for +PIC/+CGP vs. +PIC/-CGP, P= 0.043, **Fig. 3.37C right**) although t-LTP was not significant under these conditions (compare **Fig. 3.37B**). This might indicate that postsynaptic mechanisms were triggered by this protocol, yet not efficient enough to yield statistically significant 6x 1:1 t-LTP. This interpretation is corroborated by the absence of a similar increase in AMPA/NMDA current ratios (6x 0:0: 4.73 ± 0.94) under the same +PIC/+CGP conditions in negative controls (NC; i.e. 6x 0:0 stimulated) without t-LTP stimulation.

IH: 6x 1:4 t-LTP;

While successful 6x 1:4 t-LTP in IH under conditions of selective GABA$_A$R blockade significantly increased the AMPAR/NMDAR current ratio (+PIC/-CGP: 9.77 ± 1.28), absence of 6x 1:4 t-LTP under complete blockade of GABAergic inhibition (+PIC/+CGP) did – as expected – also not reveal a change in the AMPAR/NMDAR current ratio (5.59 ± 1.14). Unexpectedly, successful 6x 1:4 t-LTP in IH under intact GABAergic conditions (-PIC/-CGP) was also not accompanied by a change in the AMPAR/NMDAR current ratio (5.16 ± 0.63). ANOVA analysis revealed a significant difference between selective GABA$_A$ receptor blockade and the two other conditions (i.e. +PIC/+CGP and -PIC/-CGP, F $_{(3, 28)}$ = 10.01 P= 0.0067; post hoc Tukey-test for +PIC/-CGP vs. PIC/-CGP P: = 0.046, and +PIC/-

CGP vs. complete GABA blockade: P= 0.016; **Fig. 3.37D**). This might indicate that 6x 1:4 t-LTP under -PIC/-CGP conditions does not show the same postsynaptic changes as observed under selective GABA$_A$R blockade.

VH: 6x 1:1 t-LTP;

In VH, successful 6x 1:1 t-LTP did neither affect PPR under intact GABAergic conditions (-PIC/-CGP, before: 1.93 ± 0.29, after: 1.64 ± 0.17), nor under complete GABA receptor blockade (+PIC/+CGP, before: 1.93 ± 0.11, after: 1.92 ± 0.22), but significantly reduced PPR under selective GABA$_A$Rblockade (+PIC/-CGP, before: 1.82 ± 0.2, after: 1.30 ± 0.09; paired Student's t-test, t $_{(20)}$ = 2.308; p = 0.036; **Fig. 3.37E**). This seems to indicate that 6x 1:1 t-LTP expression under intact GABAergic inhibition and under complete blockade of GABAergic inhibition cannot be clearly assigned to presynaptic mechanisms. Regarding postsynaptic expression mechanisms, no significant increase in AMPA/NMDA current ratios after successful 6x 1:1 t-LTP induction in VH was observed either under conditions of selective GABA$_A$R blockade (4.75 ± 0.91), intact GABAergic inhibition (4.87 ± 1.14), or complete blockade of GABAergic inhibition (6.05 ± 1.13; **Fig. 3.37E**). These non-conclusive results for the expression mechanism of 6x 1:1 t-LTP in VH might result from the low magnitude of t-LTP observed under these conditions.

VH: 6x 1:4 t-LTP;

In VH, the AMPAR/NMDAR current ratio after successful 6x 1:4 t-LTP was significantly enhanced under selective GABA$_A$R blockade (+PIC/-CGP: 10.13 ± 0.65) but not after successful t-LTP under conditions of intact GABAergic inhibition (-PIC/-CGP: 5.86 ± 0.33). As expected, the absence of 6x 1:4 t-LTP under complete blockade of GABAergic inhibition was also not accompanied by increased AMPAR/NMDAR current ratios (+PIC/+CGP: 6.45 ± 1.70; ANOVA F$_{(2, 20)}$ = 5.477 P= 0.0127, post hoc Tukey-test for +PIC/-CGP vs. intact P= 0.023, and +PIC/-CGP vs. complete blockade P= 0.043; **Fig. 3.37F**). Thus, while these results for AMPAR/NMDAR current ratios are consistent with the postsynaptic expression of 6x 1:4 t-LTP under selective GABA$_A$R blockade, the same protocol does not reveal postsynaptic expression under conditions of intact GABAergic inhibition.

Overall, these results (summarized in Table 1) indicate a diverse set of expression mechanisms for 6x 1:1 and 6x 1:4 t-LTP along the longitudinal axis of the hippocampus that crucially depends on conditions for GABAergic transmission, stressing the important role of feedforward and feedback inhibition in regulating SC-CA1 synaptic plasticity.
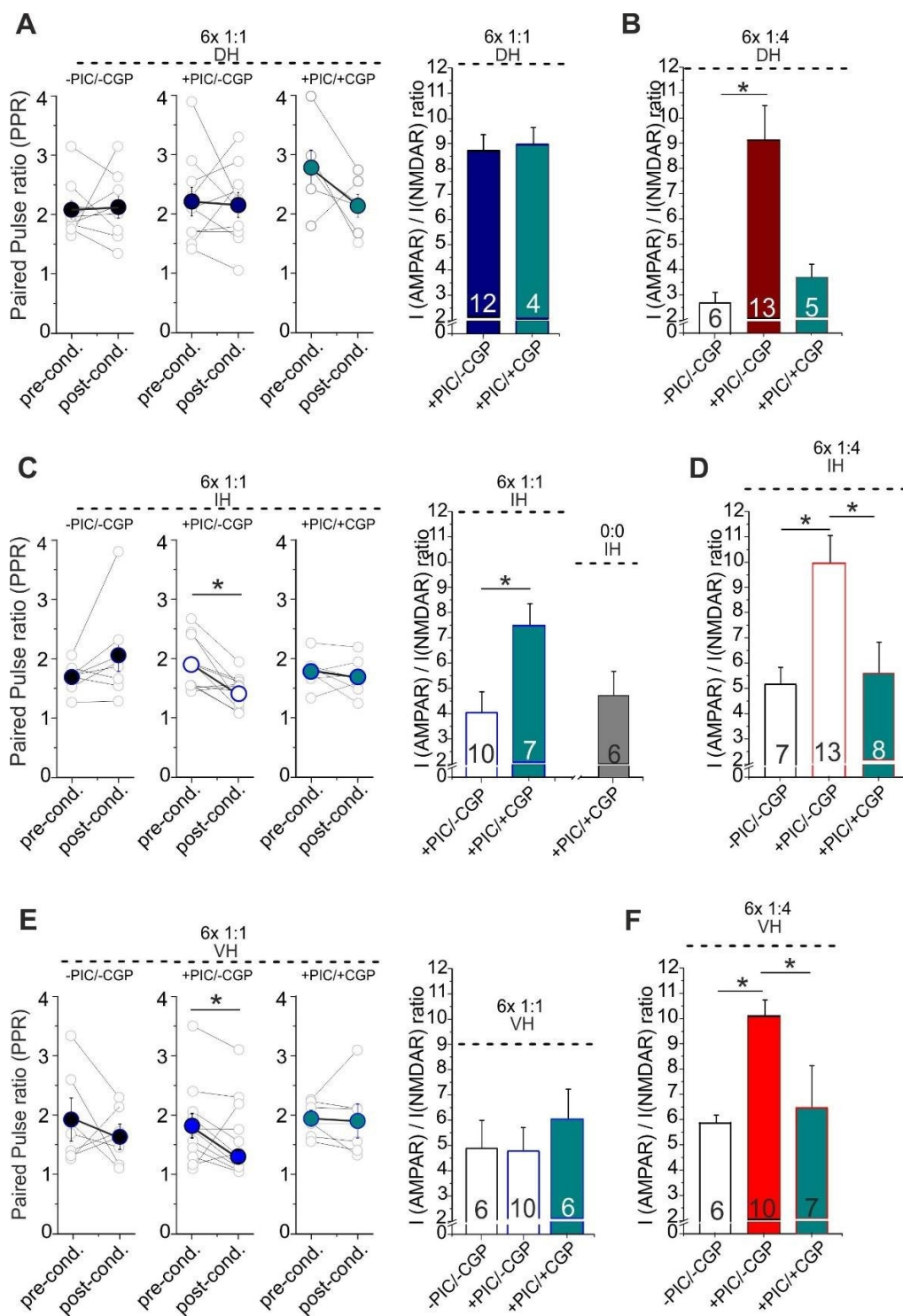
Figure 3.37: Expression mechanisms of low repeat 1:1 and 1:4 t-LTP under diverse GABAergic inhibition. A) Paired pulse ratio (PPR) comparing pre- to post-conditioning in PCs

DH under intact GABAergic inhibition (-PIC/-CGP; n=9 / N=6), GABAAR blockade (+PIC/-CGP; n=10 / N=7), and complete GABAergic inhibition blockade (+PIC/+CGP; n=5/ N=5) shows no significant changes. Although, under full blockade of GABAergic inhibition, there are non-significant changes in release probability (reduction of PPR). Moreover, similar to 6x 1:1 t-LTP expression mechanisms under GABAAR blockade (n=12/ N=7), 6x 1:1 t-LTP showed to be expressed postsynaptically by increasing AMPAR/NMDAR ratio under complete GABAergic inhibition blockade (n=4 / N=4). **B)** Measurement of AMPAR/NMDAR ratio after 6x 1:4 t-LTP paradigm in DH shows postsynaptic changes following successful 6x 1:1 t-LTP only under GABAAR blockade (n=13 / N=8), while AMPAR/NMDAR ratio was unaffected after 6x 1:4 t-LTP under intact GABAergic inhibition (n=6 / N=4) and complete GABAergic inhibition blockade (n=5/ N=4). **C)** 6x 1:1 t-LTP paradigm in IH significantly affects presynaptic glutamate release shown by reduction in PPR for GABAAR blockade (n= 12/ N=8), while PPR was unaffected under intact GABAergic inhibition (n=8 / N=7), and under complete GABAergic inhibition blockade (n=7 / N=6). Whereas AMPAR/NMDAR ratio assessment indicates postsynaptic changes after 6x 1:1 t-LTP paradigms stimulation under complete GABAergic inhibition blockade (n=7 / N=6), unlike to GABAAR blockade (n=10 / N=6), and was unchanged under non-stimulated negative control condition (n=6 / N=3). **D)** 6x 1:4 t-LTP induction in IH protocol enhanced AMPAR/NMDAR ratio under GABAAR blockade (n=13 / N=9) compared to intact (n=7 / N=5), and complete GABAergic blockade (n=8 / N=5). **E)** Despite robust potentiation induced by 6x 1:1 t-LTP paradigm in PCs of the VH region, PPR was only significantly reduced in VH compared pre- to post-conditioning in GABAAR blockade group (n=11 / N=7). It was unaffected in intact GABAergic inhibition (n=7 / N=5) and complete GABAergic inhibition blockade (n=7 / N=5). Although, AMPA/NMDA ratio showed no changes following 6x 1:1 t-LTP paradigms induction under intact (n=6 / N=4), and complete (n=6 / N=5) GABAergic inhibition as well as GABAAR blockade (n=10 / N=5). **F)** AMPAR/NMDAR ratio was also only increased in GABAAR blockade condition (n=10 / N=7) after 6x 1:4 t-LTP induction, while was unaffected in intact (n=6 / N=5) andcomplete blockade condition (n=7 / N=5). The number of recorded cells is indicated (n) in the bars and N= animal number. Data are shown as mean ± SEM. * p < 0.05. Scale bars are shown in the figures. Each dot represents a single cell's response

Our results indicate that 6x 1:1 t-LTP failed to induce robust t-LTP in the IH region under intact GABAergic conditions (**section 3.17, Fig. 3.35**). We performed another set of experiments in IH to test the neuromodulatory signaling effects of DA and NA signaling activation as a possible provider of a gating signal for 6x 1:1 t-LTP induction under intact GABAergic conditions. To do so, we added 20 μM external DA+ Vitamin C 420 μM) to our recording solution. Our results indicate that, while externalDA application could restore 6x 1:1 t-LTP induction under intact GABAergic condition (-PIC/-CGP: 109.49 ± 13.19% vs. -PIC/-CGP +DA: 152.42 ± 14.70%; unpaired Student's t-test, $t_{(15)}$ = 2.144, 10/5, 7/3, p = 0.0488; **Fig. 3.38**), NA signaling by adding Isoproterenol (Iso; 10 μM) as a non-selective β adrenergic agonist to our recording has no effect (-PIC/-CGP; 109.49 ± 13.19% vs. –PIC/-CGP + Isoproterenol: 87.95 ± 4.25%, 10/5, 5/3; **Fig. 3.39**).
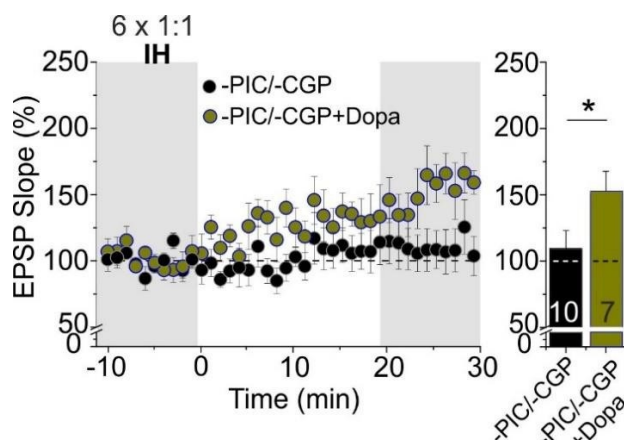
Figure 3.38: Application of exogenous DA rescued 6x 1:1 induced t-LTP under intact GABAergic inhibition. 6x 1:1 t-LTP induction failed to induce robust potentiation under conditions of intact GABAergic inhibition. The number of animals/recordings used for the 6x 1:1 protocol in IH was in –PIC/-CGP: n=10 / N=5 and for –PIC/-CGP with DA (Dopa; 20 μM) added to recording ACSF: n=7 / N=3). Normalized EPSP slope represented over 40 min of the time course. The number of recorded cells is indicated in the bars. N indicates the number of animals used for recordings. Data are represented as mean ± SEM. * p < 0.05.
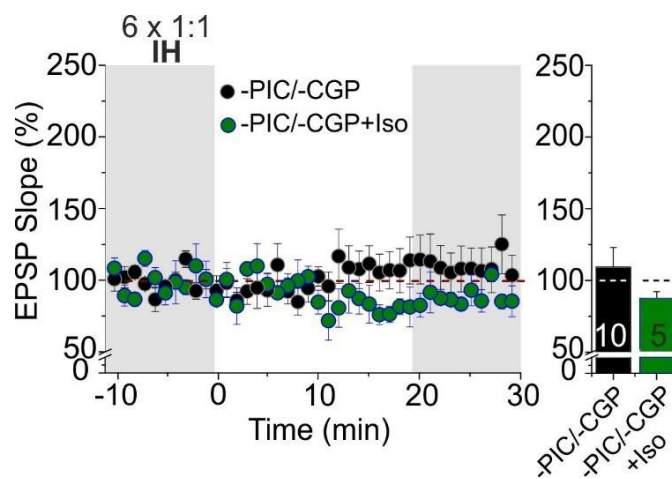
Figure 3.39: Application of exogenous β adrenergic agonist failed to rescue 6x 1:1 induced t-LTP under intact GABAergic inhibition. 6x 1:1 t-LTP induction failed to induce robust potentiation under conditions of intact GABAergic inhibition. The number of animals/recordings used for the 6x 1:1 protocol in IH was in –PIC/-CGP: n=10 / N=5 and for –PIC/-CGP with Isoproterenol (Iso; 10 μM) as a non-selective β adrenergic agonist added to recording ACSF (n=5 / N=3). Normalized EPSP slope represented over 40 min of the time course. The number of recorded cells is indicated in the bars. N indicates the number of animals used for recordings. Data are represented as mean ± SEM.

4 Discussion:

4.1 STDP repeat and time window

The first part of our results revealed that t-LTP at hippocampal SC-CA1 synapses could be induced by only six repeats of presynaptic stimulation paired with either 1 or 4 postsynaptic spikes at low frequency (0.5 Hz). Interestingly, three time repeat of the 6x 1:4 paradigm also led to robust t-LTP synaptic changes at SC-CA1 synapses. However, the underlying mechanisms were not further investigated in this thesis, since 3x 1:1 t-LTP did not yield successful t-LTP. The importance of coincident pairing of presynaptic stimulation with postsynaptic spike was evident from our results that unpaired presynaptic stimulation or postsynaptic spikes had no significant impact on synaptic strength at SC-CA1 synapses (**Fig. 3.4**). This shows that our spike-timing-dependent plasticity (STDP) protocols experimentally mimic the Hebbian learning rule, where precise millisecond timing delays of the presynaptic and postsynaptic firing of action potentials (APs) increases synaptic strength (Markram, Lübke et al. 1997, Yao and Dan 2001, Dan and Poo 2004). Both 6x t-LTP protocols tested in the current project induced robust t-LTP with similar time courses, as shown by previous studies using standard STDP paradigms using a higher number of pairings or higher pairing frequencies (compare, e.g., (Wittenberg and Wang 2006, Couey, Meredith et al. 2007, Yang and Dani 2014, Tigaret, Olivo et al. 2016)). While our lab previously addressed high repeat number of 1:1 and 1:4 paradigms to induce t-LTP at SC-CA1 synapses (Edelmann, Cepeda-Prado et al. 2015), this thesis focused on STDP protocols with low numbers of repeats for t-LTP induction, as discussed by only a few previous studies (Froemke, Tsay et al. 2006, Zhang, Lau et al. 2009, Cui, Prokin et al. 2016, Edelmann, Cepeda-Prado et al. 2017). These Hebbian t-LTP protocols have been described to allow the extension of STDP to behavioral time scales (Drew and Abbott 2006, Gerstner, Lehmann et al. 2018). Interestingly we noticed an expanded t-LTP induction time window to 40 and 100 ms when the 3x 1:4 paradigm was applied (**Fig. 3.5**). While we did not systematically investigate the t-LTP mechanism induced by such a low repeat burst protocol, a similar observation by Bittner and colleagues in mouse hippocampal place cells suggests that low numbers of postsynaptic action potentials induce a long-lasting dendritic depolarization which prolongs the pairing window to roughly 1 s (Bittner, Grienberger et al. 2015, Bittner, Milstein et al. 2017). This time scale of synaptic plasticity most probably follows a

non-Hebbian mechanism. Furthermore, it is assumed that 1:4 t-LTP burst protocols induce longer-lasting and more substantial Ca^{2+} elevations compared to the 1:1 paradigm, which might explain the lower repeat number (3x; **Fig. 3.3**) that is sufficient to induce 3x 1:4 t-LTP in an expanded time window.

4.2 Mechanisms of expression of low repeat t-LTP

Despite the similarities in the number of repeats (6x) and time window (+10 ms), leading to similar magnitudes and time courses of t-LTP at SC-CA1 synapses for both protocols , as shown earlier in the Results section (**Fig. 3.2 and 3.3**), each protocol seems to recruit different expression mechanisms. Synaptic changes induced with the 6x 1:1 paradigm seem to express presynaptically (**Fig. 3.6**), whereas the 6x 1:4 protocol relies predominantly on postsynaptic insertion of AMPA receptors (**Fig. 3.7**). It has been previously well described that depending on experimental conditions or studied brain regions, mechanisms of LTP expression might vary (Costa, Mizusaki, Sjöström, & van Rossum, 2017). A similar diversity in expression loci has also been described by (Edelmann, Cepeda-Prado et al. 2015) for the high repeat paradigms (i.e. 35x 1:4 vs. 100-150x 1:1 t-LTP) , suggesting an important role of pairing patterns for expression loci. This observation leads us to conclude that the pattern of postsynaptic spiking and not the repeat number influences the expression locus for t-LTP (Cepeda-Prado*, Khodaie* et al. 2021). Altered PPR only after induction of 6x 1:1 t-LTP speaks in favor of presynaptic changes in glutamate release (**Fig. 3.6**) in the absence of new AMPA receptor insertion in postsynaptic CA1 cells, as indicated by the constant AMPA/NMDA current ratio after 6x 1:1 t-LTP induction. Such changes in presynaptic glutamate release require the release of a retrograde messenger from postsynaptic cells. To test that, we blocked NO signaling (**Fig. 3.9**) and endocannabinoid signaling (Cepeda-Prado*, Khodaie* et al. 2021), which yielded no blocking effect for 6x 1:1 t-LTP. However, further investigation is required to elucidate presynaptic mechanisms of 6x 1:1 t-LTP, which was beyond the scope of the current thesis.

 The expression mechanism for the 6x 1:4 t-LTP protocol seems to follow the suggested mechanisms for conventional SC-CA1 LTP, with postsynaptic expression via insertion of new AMPARs into the postsynaptic membrane, leading to an increased AMPAR-/NMDAR-mediated current ratio (**Fig. 3.7**). Our group has shown previously that "distinct types of t-LTP" that do not occlude one another can be elicited by high-repeat STDP paradigms (Edelmann, Cepeda-Prado et al. 2015). The results of the

present thesis confirm this observation also for the low repeat 1:1 and 1:4 protocols (Cepeda-Prado*, Khodaie* et al. 2021); **Fig. 3.8A**).

Thus, when applying the 6x 1:4 stimulation protocol after potentiation induced by the 6x 1:1 protocol in the same cell no signs of occlusion were observed. Moreover, both protocols gave rise to similar magnitudes of potentiation. However, the repetition of two consecutive 6x 1:1 stimulations 30 min apart did not result in additional potentiation after the second 6x 1:1 stimulation (**Fig. 3.8B**). This observation indicates that two different protocols can lead to additive potentiation by activating most likely different LTP pathways. In contrast, repetitive stimulation with the 6x 1:1 protocol yields occlusion of LTP, suggesting that repetitive stimulation with identical stimuli leads to saturation of signaling pathways already in response to the first LTP stimulus.

4.3 Dependence of low repeat t-LTP induction on different sources for postsynaptic Ca²⁺ elevation

I tried to investigate the mechanisms involved in t-LTP induction at SC-CA1 synapses using 6x 1:1 and 6x 1:4 t-LTP paradigms. In the first step, the contributions of different sources of Ca^{2+} were tested. Interestingly, showing diverse routes for postsynaptic Ca^{2+} elevation for the low repeat 1:1 and 1:4 protocols to induce t-LTP. LTP at glutamatergic SC-CA1 synapses is known to rely on Ca^{2+} influx via postsynaptic NMDA receptors (Malenka and Bear 2004), also acting as a coincidence detector of timed pre- and postsynaptic activation during STDP (Feldman 2000). Depending on the level of Ca^{2+} influx, it was shown previously to activate separate signaling cascades leading to either LTP or LTD (Lisman 1989, Caporale and Dan 2008). Our results revealed that 6× 1:1 t-LTP depends on Ca^{2+} influx through NMDARs and L-type VGCCs to induce synaptic changes (**Fig. 3.10A and B**). Forthe 6x 1:4 paradigm, a requirement for postsynaptic Ca^{2+} elevation was evident from experiments showing that postsynaptic infusion of the Ca^{2+} chelator BAPTA blocked t-LTP (Cepeda-Prado*, Khodaie* et al. 2021), Still, Ca^{2+} entry via NMDARs or L-type VGCCs was not involved (**Fig. 3.10C andD**). Instead, our data demonstrated that for the 6x 1:4 t-LTP paradigm, the initial postsynaptic Ca^{2+} rise is mediated by group I mGluRs (i.e., mGluR1 and mGluR5) (compare **Fig 3.13B,** and (Kaar and Rae 2015), which played no role in 6x 1:1 t-LTP, that seems to depend exclusively on NMDARs or L- type VGCCs activation for initial postsynaptic Ca^{2+} rise (**Fig 3.13A**). To the best of our knowledge, thisshows for the first time that group I metabotropic GluRs are involved in t-LTP. Moreover, our results

suggest that group I mGluR activation during 6x 1:4 paradigm stimulation triggers activation of IP3Rs (**Fig. 3.14A**) and subsequent RyRs-mediated (**Fig. 3.14B**) calcium-induced Ca^{2+} release from internal stores (compare (Jong, Sergin et al. 2014)). The resulting calcium elevation and additional Ca^{2+} influx via GluA2 subunit-deficient Ca^{2+}-permeable AMPA receptors (cp-AMPARs) might then strengthen additional IP3 and RyR-mediated calcium-induced Ca^{2+} release to successfully boost low-repeat induced burst t-LTP (i.e. 6x 1:4 t-LTP; **Fig. 3.11**). A role of cp-AMPARs in STDP has thus far not been reported and these results represent a crucial new finding that emerges from our study. Our experimental results for 6x 1:1 t-LTP employing inhibitors of cp-AMPARs (**Fig. 3.11 and 3.15**) suggest that also in this case the initial postsynaptic Ca^{2+} rise is strengthened by Ca^{2+} influx through cp-AMPARs into the postsynaptic cell, inducing further Ca^{2+} release via RyRs to amplify and prolong the initial Ca^{2+} signal. Interestingly, the high repeat (70x) 1:1 t-LTP paradigm was not affected by the presence of the cp-AMPAR inhibitor NASPM (**Fig. 3.12A**), whereas the 35x 1:4 protocol failed to induce t-LTP under these conditions (**Fig. 3.12B**). This might indicate that 1:4 t-LTP protocols show an even higher sensitivity to cp-AMPAR activation than the 1:1 t-LTP protocols. Furthermore, it needs to be determined how cp-AMPAR-mediated Ca^{2+} influx is orchestrated with mGluR- and RyR-dependent Ca^{2+} elevation for induction of low repeat 6× 1:4 t-LTP. Likewise, the co-operation of cp-AMPARs with NMDAR- and VGCC dependent Ca^{2+} elevations for inducing 6× 1:1 t-LTP needs to be investigated (Cepeda-Prado*, Khodaie* et al. 2021). In addition to allowing sufficient Ca^{2+} elevation in t-LTP, cp-AMPARs might be involved in DA-dependent priming of synapses for delayed/retroactive reinforcement of LTP or silent eligibility traces (Brzosko, Schultz et al. 2015, He, Huertas et al. 2015, Gerstner, Lehmann et al. 2018). By those eligibility traces or delayed reinforcements, the different time scales between milliseconds and seconds can be bridged, thereby allowing to connect Hebbian synaptic plasticity to behavioral responses and learning. Such mechanisms might also be involved in the signaling mechanisms employed by our low repeat t-LTP protocols (6× 1:1 and 6× 1:4), since both variants of t-LTP show a clear dependence on DA signaling and on cp-AMPARs (**compare Figs. 3.14-15 and 3.24-25**). Additional experiments will be required to determine the time course of activity-dependent cp-AMPAR incorporation during induction of low repeat t-LTP into the postsynaptic membrane (Cepeda-Prado*, Khodaie* et al. 2021).

4.4 Differences in intrinsic excitability and basal synaptic properties of CA1 neurons along the longitudinal axis of the hippocampus

In addition to the meanwhile published results (compare above, results **sections 3.8-3.11 and 3.13-3.15**, and (Cepeda-Prado*, Khodaie* et al. 2021) on the features of the 6x 1:1 and 6x 1:4 t-LTP variants at SC-CA1 synapses of the intermediate hippocampus (IH), starting from **section 3.7** this thesis systematically investigated differences in excitability, basal synaptic transmission, and the mechanisms of 6x 1:1 and 6x 1.4 t-LTP in CA1 pyramidal cells (PCs) along the longitudinal axis of the hippocampus (i.e. DH, IH, VH).

We observed a significantly more depolarized resting membrane potential (RMP) in both VH and IH compared to DH CA1 PCs. Likewise, DH PCs showed a lower firing frequency of APs in response to (increasing intensities) of current injections than both IH and VH PCs. Both properties indicate a stronger intrinsic excitability of CA1 cells closer to the ventral pole of the hippocampus, which is consistent with previous results in the rat hippocampus (Dougherty, Islam et al. 2012). In comparison to the study by Dougherty and colleagues, which recorded only in DH and VH (Dougherty, Islam et al. 2012), we also included recordings in the intermediate region (IH), and found that basal properties of IH and VH are very similar. Consequently, a higher current injection is required to trigger action potentials (APs) in DH (**Fig. 3.16C**). Other previous studies also described electrophysiological distinct subpopulations of CA1 PCs along the transversal and the radial axis of the hippocampus being in line with increasing excitability from dorsal to ventral pole of the hippocampus (Mizuseki, Diba et al. 2011, Marcelin, Liu et al. 2012). Changes in neuronal morphology can affect ionic conductance and changes in somatic R_{in} of neurons, and were used to explain the distinct intrinsic excitability in rat DH CA1 PCs (Dougherty, Islam et al. 2012). A larger dendritic surface in DH CA1 neurons will reduce R_{in}, consequently increasing rheobase, as we noticed in our recordings (**Fig. 3.16D**). Higher excitability of VH PCs might also originate from an increased ratio of excitatory to inhibitory synaptic inputs to VH CA1 neurons, as was suggested previously (Papatheodoropoulos, Asprodini et al. 2002, Derchansky, Shahar et al. 2004). In accordance with these previous data in rats, our synaptic I/O curves clearly indicate a steep increase of excitatory drive at SC inputs from the dorsal to the ventral pole of the mouse hippocampus (compare **Fig. 3.16E**), and this idea is further supported by the known distinct expression patterns of ligand-gated ion channels between VH and DH in rats (Papatheodoropoulos, Moschovos et al. 2005, Pandis, Sotiriou et al. 2006). Specifically, the stronger

expression of M-type (Kv7) potassium channels and higher expression of A-type K^+ channels in DH vs. VH, might contribute to reduced excitability of DH compared to VH CA1 neurons (Hönigsperger, Marosi et al. 2015) and (Marcelin, Liu et al. 2012). Likewise, HCN channel-mediated I_h is also critically important in regulating membrane excitability and is differentially expressed along the dorso-ventral axis (Zemankovics, Káli et al. 2010, Marcelin, Lugo et al. 2012). Together, the complex cooperation of ion channels located in the dendrites, the axons, and the soma seems to account for the higher excitability of postsynaptic CA1 neurons and the steeper slope in excitatory synaptic input-output curves in CA1 neurons at the ventral pole of the hippocampus (compare **Fig. 3.16E** and (Daoudal and Debanne 2003)).

Regarding presynaptic release properties at glutamatergic SC-CA1 synapses, we observed significantly weaker paired-pulse facilitation (PPF) in VH compared to DH. These data speak in favor of a higher initial release probability in VH. Likewise, Papatheodoropoulos and colleagues found in rats that the strength and duration of paired pulse depression (PPD) were much weaker in VH than DH (Papatheodoropoulos, Asprodini et al. 2002), confirming the higher initial release probability at SC-CA1 synapses in VH compared to DH that we describe here for mice. Higher release probability could also be discussed at the network level. In this respect, GABA-mediated recurrent inhibition (RI) was described to control CA1 excitatory output in VH less efficiently than in DH (Petrides, Georgopoulos et al. 2007). Importantly, both GABA and glutamate release are also affected by neuromodulator (i.e., noradrenergic and DAergic inputs) releasing axonal projections to the hippocampus, which are more prominent in VH than DH (Strange, Witter et al. 2014). Neuromodulator and neuropeptide systems have a diverse projection pattern along the hippocampal longitudinal axis. For instance, ventral tegmental area (VTA) neurons prominently project DAergic fibers to VH, but not to DH, and locus coeruleus (LC) noradrenergic terminals show 40% higher density in VH vs. DH (Haring and Davis 1985). Both neuromodulators can therefore enhance cellular excitability through intracellular second-messenger mediated biochemical changes ((Dodt, Pawelzik et al. 1991); discussed in Khodaie et al., in preparation).

On the postsynaptic side of SC-CA1 synapses, previous studies showed distinct NMDAR subunit composition along the dorso-ventral axis. Thus, a lower NR2A/NR2B ratio was detected in VH than in DH, leading to a weaker magnesium block and slower decay of the NMDAR-mediated component of EPSPs in VH (Monyer, Burnashev et al. 1994, Dougherty, Islam et al. 2012). Together, these differences affect excitatory postsynaptic currents (EPSCs) mediated by AMPA and NMDA receptors. EPSP amplitudes and rise-times recorded at the soma critically depend on the local excitability of the

postsynaptic and dendritic membrane, which is regulated by various voltage-gated channels (VGCC). Marcelin and colleagues have shown a heterogeneous expression and distribution of Kv4.2, HCN1, and HCN2 channels between the dorsal and ventral hippocampus, which affects the summation of synaptic inputs (Marcelin, Lugo, et al., 2012). This functional and structural diversity is likely to contribute to the higher EPSC/EPSP amplitudes and longer EPSP rise-times in DH vs. VH (Khodaie et al., in preparation). The EPSC decay time constants are mainly regulated by NMDAR activation and deactivation, and the NR2A/NR2B ratio, and the more prolonged EPSC decay that we observed in VH compared to DH is in line with similar results reported for rat hippocampus (Dougherty, Islam et al. 2012).

4.5 Magnitude of timing-dependent LTP induced by 6x 1:1 and 6x 1:4 paradigms along the longitudinal axis of the hippocampus

We previously introduced two low repeat STDP paradigms, which induced robust LTP in acute hippocampal slices taken from the intermediate hippocampus (IH) (Cepeda-Prado*, Khodaie* et al. 2021). We also showed that distinct types of t-LTP are elicited by the low-repeat 6x 1:1 (presynaptic expression of t-LTP) and 6x 1:4 (postsynaptic expression) paradigms (Cepeda-Prado*, Khodaie* et al. 2021), compared to high-repeat protocols (Edelmann, Cepeda-Prado et al. 2015). In the present study, we now investigated possible differences in the magnitude and mechanisms involved in low repeat t-LTP induction and expression along the longitudinal axis of the hippocampus. Both STDP paradigms revealed significant potentiation in all three hippocampal CA1 regions along the longitudinal axis compared to the negative control (0:0) group (**Fig. 3.18**), still, the magnitude of 6x 1:1 t-LTP in DH PCs was significantly higher compared to the VH (**Fig. 3.19A**). Several mechanisms possibly underlie these differences. First, the described higher release probability and steeper I/O curve for basal SC-CA1 synaptic transmission in VH compared to DH (compare **Fig. 3.17**) might indicate that there is less capacity for further increase in synaptic plasticity in VH. Secondly, Sholl analysis (Sholl 1953) indicated that CA1 PCs at the ventral pole of the hippocampus possess fewer dendritic branches and less dendritic surface area than found at the dorsal pole of the hippocampus (Malik, Dougherty et al. 2016), which could indicate that there is less dendritic space for the activity-dependent formation of new synaptic contacts. Moreover, the differences in dendritic structure, in conjunction with distinct profiles of voltage-dependent dendritic ion channels (Mainen and Sejnowski 1996) between DH and VH could lead to distinct efficacy of back propagating APs to the

postsynaptic sites, thereby affecting postsynaptic Ca^{2+} elevations required for inducing t-LTP. Here, we previously reported that successful induction of 6x 1:1 t-LTP depends on Ca^{2+} influx through NMDARs and VGCCs to induce synaptic changes (Cepeda-Prado*, Khodaie* et al. 2021). However, in rats NMDARs show a gradient of expression along the longitudinal axis in the opposite direction of the hippocampus (DH<IH<VH) (Dubovyk and Manahan-Vaughan 2018), and can therefore not account for more effective t-LTP in DH. Regarding VGCCs, to the best of our knowledge, no previous study determined the expression gradient of VGCCs along the dorso-ventral axis (Khodaie et al., in preparation). Nonetheless, in the rat hippocampus, it was shown that VGCCs appeared to interact more effectively with NMDARs in DH than in the VH (Papatheodoropoulos and Kouvaros 2016), which would be consistent with higher t-LTP in DH vs. VH. Furthermore, metabotropic glutamate receptors (mGlu1R and mGlu2/3R) show higher expression in apical dendrites of VH compared to DH (Dubovyk and Manahan-Vaughan 2018), and mGlu1R predominantly localize on GABAergic interneurons thereby providing distinct network states of the hippocampus in VH via GABAergic fine tuning of dendritic signal processing in CA1 PCs (Ferraguti, Cobden et al. 2004). Consequently, these differences in mGluR-dependent regulation of GABAergic inhibition could explain the lower magnitude of t-LTP in VH compared to DH (Khodaie et al., in preparation).

At the network level, weaker GABAergic inhibition was reported in VH than in DH (Papatheodoropoulos, Asprodini et al. 2002), but since we initially (**Fig. 3.19**) induced 6x 1:1 t-LTP paradigms in the presence of the GABA$_A$R inhibitor picrotoxin, GABAergic effects can most probably not account for stronger 6x 1:1 t-LTP in DH under these recording conditions. Of note, DA levels in the extracellular space were reported to be tenfold higher in DH than in VH (Ishikawa et al., 1982), and could therefore promote more efficient 6x 1:1 t-LTP in DH. However, when trying to compare 6x 1:1 t-LTP magnitudes along the dorso-ventral axis it has to be kept in mind that expression mechanisms differ: the 6x 1:1 paradigm, reduced PPR after successful induction of t-LTP in IH and VH (**Fig. 3.20A**), speaking in favor of increased glutamate release probability as expression mechanisms for t-LTP, whereas in DH PCs we observed enhanced AMPAR mediated current components after induction of 6x 1:1 t-LTP, most likely indicating postsynaptic expression. Thus, more effective 6x 1:1 t-LTP in DH might be explained by switching from pre- to postsynaptic expression between VH and DH (Khodaie et al., in preparation).

Efficacy of 6x 1:4 t-LTP shows a gradient along the dorso-ventral axis (DH>VH), but this effect does not reach statistical significance. In case of 6x 1:4 t-LTP, there is also no change in the t-LTP expression mechanism along the dorso-ventral axis, with DH, IH, and VH all depending on new

AMPAR insertion into the postsynaptic membrane (compare **Fig. 3.20C**). Under baseline conditions, we observed a non-significant slightly lower AMPAR/NMDAR ratio in DH than in IH and VH (**Fig. 3.20C**), which could indicate a stronger contribution of NMDAR or VGCC mediated Ca^{2+} influx during induction of 6x 1:4 t-LTP in DH. Since previous studies indicated either higher or lower expression of AMPARs in VH vs. DH (Pandis, Sotiriou et al. 2006), and (Martens, Capito et al. 1998). It remains unclear whether distinct ratios of AMPAR/NMDAR along the dorso-ventral axis might explain the slight difference in 6x 1:4 t-LTP magnitude. Nevertheless, the changes in AMPAR/NMDAR ratio after 6x 1:4 t-LTP in all hippocampal subfields indicate a similar level of new AMPAR insertion (**Fig. 3.20C**).

4.6 Distinct regulation of STDP by postsynaptic Ca^{2+} elevation along the longitudinal axis of the hippocampus

We previously discussed the importance of Ca^{2+} influx via NMDAR and/or VGCC during 6x 1:1 t-LTP induction in the IH region (**section 4.3, Fig. 3.10**). Then, we tested the NMDAR dependency of both 6x 1:1 and 6x 1:4 t-LTP paradigms. We found that both protocols could induce similarly robust t-LTP in CA1 PCs of both DH (**Fig. 3.21A**) and VH (**Fig. 3.21C**) in the presence of 50 μM APV. This could be explained either by a distinct gradient of expression of NMDAR in S.r. of the hippocampus along its longitudinal axis (DH< IH< VH) reported by (Dubovyk and Manahan-Vaughan 2018) or by heterogeneous expression of NMDAR subunits along the longitudinal axis of the hippocampus (Monyer, Burnashev et al. 1994). There exists also a distinctly different $GABA_B$ receptor mediated response upon SC stimulation along the dorso-ventral axis (**Fig. 3.35**, further discussed in **section 4.8**), which could contribute to different levels of NMDAR control over t-LTP induction in IH compared to DH and VH (Morrisett, Mott et al. 1991). When testing the contribution of VGCC mediated Ca^{2+} influx during 6x 1:4 t-LTP induction, we observed a strong dependence on VGCC in both DH and VH, whereas in IH t-LTP did not depend on VGCCs (**Fig. 3.22**). High intrinsic excitability in VH (**Fig. 3.16C and D**), together with lower GABAergic inhibition in the VH (**Fig. 3.35**), possibly might facilitate activation of VGCC during 6x 1:4 t-LTP paradigms (Khodaie et al., in preparation).

4.7 Catecholaminergic modulation of STDP along the longitudinal axis of the hippocampus

4.7.1 Results with pharmacological tools

We also investigated catecholaminergic modulation of our two low repeat STDP variants. As earlier discussed (**section 1.6**), catecholaminergic terminals can release either NA, DA, or both. When applying the β-adrenergic receptor inhibitor propranolol (PPN; 10 µM) this interfered with 6x 1:4 t-LTP only in the IH region (**Fig. 3.23B**). In comparison, DAergic modulation seems to exert a stronger and much broader modulation on our low repeat STDP paradigms.

In the DH, 6× 1:1 t-LTP remained functional only when either D1-like or D2-like DA receptor signaling was intact (**Fig. 3.24A**). However, 6x 1:4 t-LTP was utterly independent of DAergic signaling. Neither D1-like receptor inhibitors (SCH23390) nor D2-like receptor inhibitors (Sulpiride) or co-application of both blockers interfered with the induction of 6x 1:1 t-LTP in DH (**Fig. 3.25A**). While both paradigms express postsynaptically **(Fig. 3.20C),** burst stimulation of postsynaptic cells by the 6x 1:4 paradigm possibly provided a long-lasting Ca^{2+} elevation activating intracellular signaling cascades triggering Ca^{2+} release from internal sources. Consistent with this observation, extracellular DA levels were shown previously to be tenfold higher in DH compared to VH (Ishikawa, Ott et al. 1982), providing a lasting DA effect known as 'priming' (Christie and Abraham 1992) or 'metaplastic' effects (Abraham and Bear 1996), probably keeping CA1 PCs in DH susceptible for t-LTP induction even in the presence of co-applied D1 and D2-like receptor inhibitors.

In the IH, the 6× 1:4 t-LTP was dependent entirely on intact D2 receptor signaling, shown by the blockade of t-LTP in the presence of a D2-like receptor inhibitor (**Fig. 3.25B**). Little is known about how D2R-mediated signaling controls t-LTP and classical LTP. For the prefrontal cortex, it was suggested that D2 receptor signaling limits feedforward inhibition thereby promoting more effective t-LTP (Xu and Yao 2010). In rats, D2-like receptors are expressed at both pre- and postsynaptic sites and could regulate synaptic plasticity (Dubovyk and Manahan-Vaughan 2019) and control cognitive function (Sokoloff, Diaz et al. 2006). However, the 6× 1:1 t-LTP remained functional when exclusive D1-like or D2-like signaling was intact and only blocked when both antagonists were co-applied (**Fig. 3.24B**).

In the VH, 6x 1:1 showed similar results as observed in IH and required both D1- and D2-like receptor blockade to suppress t-LTP induction (**Fig. 3.24C**). In contrast to the six repeat canonical protocol, the 6× 1:4 t-LTP in VH showed a high dependency on active DAergic signaling of both D1- and D2-

like receptors, with blockade of any DAergic receptor significantly inhibiting t-LTP induction (**Fig. 3.25C)**. This distinctly different dependency of low repeat t-LTP on DAergic signaling along the longitudinal axis might be explained by the heterogeneous expression of D1-like (Dubovyk and Manahan-Vaughan 2018) and D2-like receptors along the longitudinal axis of the hippocampus (Dubovyk and Manahan-Vaughan 2019). It is also known that D2-like receptors generally display a higher affinity for DA compared with D1-like receptors (Beaulieu and Gainetdinov 2011). As discussed earlier, the local DA concentration is much higher in DH than IH and VH, which might contribute to the different DA-dependent effects. It should also be taken into consideration that D1-like and D2-like receptors have different effects on cAMP levels. Thus cAMP increases when D1-like receptors are activated but decreases when D2-like receptors are stimulated (Tritsch and Sabatini 2012). Together with the even more complex D1 and D2 receptor effects that occur independent from cAMP levels ((discussed e.g. in (Beaulieu and Gainetdinov 2011, Edelmann and Lessmann 2018)), a plethora of mechanistic differences between DH, IH, and VH seem to exist that possibly contribute to the above discussed distinct modulation of low repeat t-LTP along the longitudinal axis of the hippocampus. These effects could be described in this thesis but more experiments in the future are needed to more clearly assign them to discrete DA effects. Importantly, in the prefrontal cortex (rats mice??), GABA$_A$ and GABA$_B$ receptors differentially modulate DAergic signaling (Santiago, Machado et al. 1993), Thus DA-dependent regulation of synaptic inhibition might indirectly regulate low repeat t-LTP efficacy at SC-CA1 synapses (discussed further in **section 3.15**, **Fig. 3.33**).

4.7.2 Results employing optogenetic inhibition of catecholamine release

The results of this thesis revealed successful expression of YFP-labeled halorhodopsin in transgenic animals expressing +eNpHR3.0 in the VTA somata and in DAergic inputs projecting to our acute hippocampal slices (**Fig. 3.26**). Optogenetic silencing of these DAergic inputs was ideally suited to address the role of endogenously released DA for low repeat t-LTP. To test the functionality of laser light induced depletion of extracellular DA we investigated the action potential (AP) firing frequency change in CA1 PCs upon laser stimulation (**Fig. 3.27**). In-vitro whole cell recordings from the prefrontal cortex had shown previously an about threefold increase in the spike frequency after bath application of DA (Henze, González-Burgos et al. 2000), which is most likely explained by altered the intrinsic excitability of neurons (Hasselmo 1995). Likewise, our group had shown previously (Edelmann and Lessmann, 2013) that AP frequency of CA1 PCs in IH is reduced in the presence of co-

applied D1 and D2R inhibitors. Consistent with these earlier observations, the spike frequency 5 min after laser stimulation in IH slices of +eNpHR animals revealed the same reduction in AP firing frequency (**Fig. 3.27**), most probably reflecting a reduction in extracellular DA levels in response to light illumination. These effects of DA on AP firing frequency have been attributed to different DA receptors activation and depend on the specific type of neuron investigated (Gerfen and Surmeier 2011). Thus, DA can lead to changes in intrinsic excitability and synaptic integration via PKA-dependent modulation of voltage-gated K^+, Na^+, and Ca^{2+} channels (Tritsch and Sabatini 2012). Studies on pharmacologically isolated currents revealed that D1 receptor signaling enhanced inward rectifier K^+ channels belonging to the Kir2 family (Pacheco-Cano, Bargas et al. 1996) and thereby reduced slowly inactivating A-type K+ currents mediated by K_V4 channels (Kitai and Surmeier 1993). These changes can shift hyperpolarized resting potential known as the 'down state' to depolarize neuronal cells and enhance action potential firing during the 'up state'. These effects might be reversed during laser stimulation induced depletion of DA release in hippocampal slices from +eNpHR3 mice. Changes in RMP of CA1 PCs in hippocampal slices from +eNpHR3 animals induced by laser stimulation (**Fig. 3.28**) are consistent with these observations. DA can be released tonically (volume transmission) and phasically (Zhang, Doyon et al. 2009). The tonic release is likely to occur in our hippocampal slices and might be enhanced by ongoing SC fiber stimulation during t-LTP experiments. Therefore, it is expected that under inhibition of DA release, both 6x 1:1 and 6x 1:4 protocols fail to induce robust t-LTP. In fact, we failed to induce 6x 1:1 t-LTP in response to optogenetic silencing of DA fibers in +eNpHR3 hippocampal slices (**Fig. 3.29A**), which is consistent with inhibition of 6x 1:1 l-LTP when co-applying D1 and D2R blockers, and intact 6x 1:1 t-LTP in hippocampal slices from +eNpHR3 animals in the absence of laser light illumination (**Fig. 3.29B**). The functionality of light illumination via DA release reduction was further shown in +eNpHR3 slices when external DA application in recording ACSF granted a robust t-LTP induction by 6x 1:1 paradigm in +eNpHR3 slices under light illumination (**Fig. 3.30**). We earlier discussed (**section 4.7.1**) how DA regulates mechanisms of t-LTP induction in the IH. However, the importance of DA at different stages of t-LTP induction or expression was an interesting topic of study (**Fig. 3.31**). Changes in synaptic strength during LTP are provided by either enhanced presynaptic release of neurotransmitter (glutamate) or enhanced postsynaptic responsiveness. Induction and expression are two main processes during LTP, initiated by synaptic activation to release glutamate and postsynaptic events leading to Ca^{2+} elevation in postsynaptic cells characterized as an induction process (Abraham and Williams 2003). However, maintenance of LTP over the long-term period depends on

posttranslational modifications such as protein phosphorylation followed by new gene transcription and protein synthesis (Nguyen, Abel et al. 1994). Our results suggest that a high DA level is crucial shortly before and during the induction of 6x 1:1 and 6x 1:4 t-LTP paradigms (**Fig. 3.32**). DA is known to facilitate LTP induction by lowering the threshold to induce LTP (Gao, Sun et al. 2006, Edelmann and Lessmann 2011), increasing glutamate release probability from the presynaptic site via enhancement of axon terminal excitability, facilitating Ca^{2+} influx, or interacting with vesicular release machinery (Tritsch and Sabatini 2012). DAergic signaling modulates internal Ca^{2+} storage and Ca-permeable AMPA receptor expression after t-LTP induction (Cepeda-Prado*, Khodaie* et al. 2021). While these effects might contribute to the inhibitory effects of DA release silencing when DA was depleted before or during t-LTP induction, inhibition of DA release at later time points (i.e. during t-LTP expression) was too late to interfere with 6x 1:1 t-LTP (**Fig. 3.32**).

4.8 GABAergic modulation of 6x 1:1 t-LTP induction along the longitudinal axis of the hippocampus

GABAergic inhibition regulates the activity and balance of neuronal responses during excitation and modulates neuromodulator release (Santiago, Machado et al. 1993, Okun and Lampl 2009). In all previous experiments, we partially blocked GABAergic inhibition by adding 100 µM picrotoxin to our recording ACSF, which blocks $GABA_A$ receptor signaling. In the next step, we recorded 6x 1:1 and 6x 1:4 t-LTP under conditions of intact GABAergic inhibition, allowing to evaluate the role of $GABA_A$R signaling in the induction of both t-LTP paradigms. A previous study suggested opposite gradients of $GABA_A$R (DH>IH>VH) and $GABA_B$R expression (DH<IH<VH) along the longitudinal axis in the rat hippocampus (Dubovyk and Manahan-Vaughan 2018). However, we found a higher $GABA_B$R mediated component response in DH than in IH and VH (**Fig. 3.33A and B**) in our mouse hippocampal slices. These seemingly discordant results could indicate a species difference or might reflect that receptor activation is not only a function of receptor expression but also of GABA release, which might differ between DH and VH CA1 circuits. Yet, to the best of our knowledge, no previous study reported differences in extracellular GABA levels along the dorso-ventral axis. Regarding its role in t-LTP, GABA is known to act as a Hebbian/anti-Hebbian switch, which mainly acts on postsynaptic $GABA_A$ receptor sites (Paille, Fino et al. 2013). At the same time, GABAergic modulation on the presynaptic site of glutamatergic synapses is even more complex. Thus, at hippocampal MF synapses it was reported that $GABA_A$R activation can depolarize presynaptic terminals (Ruiz, Fabian-

Fine et al. 2003, Pugh and Jahr 2011). However, controversial results exist on whether this depolarization reduces (Jackson and Zhang 1995, Wang, Kloc et al. 2019) or rather enhances glutamate release (Stell, Rostaing et al. 2007, Zorrilla de San Martin, Trigo et al. 2017). While all these previous results were obtained by exogenous application of the GABA$_A$R agonist muscimol to measure changes in glutamate release, we here addressed physiological activation of GABA$_A$Rs. Muscimol application in acute hippocampal slices reduced axonal excitability (Ruiz, Fabian-Fine et al. 2003). This is consistent with lower glutamate release under intact GABAergic inhibition (-PIC/-CGP) compared to selective GABA$_A$R blockade (+PIC/-CGP). In these experiments, our mEPSC recordings (**Fig. 3.34**), revealed significantly increased glutamate release probability only in IH, when GABA$_A$ receptors were inhibited (+picrotoxin). The intermediate location of IH along the dorso-ventral axis, where both glutamate release probability (DH<IH<VH, **Fig. 3.17B**), and GABAergic inhibition as well as GABA$_A$R expression (DH>IH>VH) are in balance might provide a specific control over glutamate release (Dubovyk and Manahan-Vaughan 2018). Moreover, GABAergic signaling is also known to control DA release from DAergic fibers (Santiago et al., 1993b), thereby modulating the excitability of pre- and postsynaptic cells of glutamatergic synapses through regulation of voltage-gated ion channels (Edelmann and Lessmann 2011). This complex interaction of GABAergic and DAergic regulation could account for our observation that glutamate release probability at SC-CA1 synapses in IH is increased (i.e. PPR is decreased) under conditions of intact GABAergic inhibition (**Fig. 3.34D)**.

6x 1:1 t-LTP in VH was unaffected under intact GABAergic inhibition, possibly due to naturally higher presynaptic glutamate release probability compared to IH region (**Fig. 3.17B**) as was suggested previously in rat hippocampus (Papatheodoropoulos and Kostopoulos 2000, Zucker and Regehr 2002), together with weaker GABAergic inhibition in the VH (Papatheodoropoulos, Asprodini et al. 2002) making 6x 1:1 t-LTP less sensitive for GABAergic modulation. This idea was confirmed by our observation that in VH 6x 1:1 t-LTP was merely insensitive to both GABA$_A$ and GABA$_B$ receptor mediated inhibition (**Fig. 3.35C).** On the same vein, the glutamate release profile in VH remained unaffected by GABA$_A$R (**Fig. 3.34E and F**). These results suggest that 6x 1:1 t-LTP in the VH is largely independent from GABAergic inhibition.

In DH, our results suggest that 6x 1:1 t-LTP is expressed postsynaptically (compare **Fig. 3.20**) and glutamate release is not affected by GABAergic inhibition (compare **Fig. 3.34A and B**). At the postsynaptic site, intact GABAergic inhibition (-PIC/-CGP) might reduce CA1 PC excitability, thereby suppressing activation of L-type-VGCC and NMDARs, which are critical for successful induction of 6x

1:1 t-LTP (Cepeda-Prado*, Khodaie* et al. 2021). This might explain the absence of 6x 1:1 t-LTP in DH when GABAergic inhibition is intact (**Fig. 3.34A**).

Several studies have focused on $GABA_AR$ signaling during high frequency and low-frequency synaptic stimulation (Seabrook, Easter et al. 1997, Gaiarsa, Caillard et al. 2002, Shen, Wang et al. 2013), and concluded that modulation and expression of different types of synaptic plasticity crucially depend on $GABA_ARs$ trafficking (Collingridge, Isaac et al. 2004). Yet, the role of $GABA_BRs$ – especially in regulating t-LTP largely unknown. At the presynaptic site, $GABA_BR$ blockade seems to enhance glutamate release probability (Kantamneni 2015), which would be expected to facilitate 6x 1:1 t-LTP in IH and VH. However, 6x 1:1 t-LTP was unaffected by complete blockade of GABAergic inhibition in VH (+PIC/+CGP, **Fig. 3.35C**), and even blocked 6x 1:1 t-LTP in IH (**Fig. 3.35B**). Several in vivo and in vitro studies revealed a complex modulation of LTP by $GABA_BR$ signaling, and the region of the hippocampus and type of stimulation appeared to influence the effect of $GABA_BR$ mediated inhibition for LTP outcome (Olpe, Wörner et al. 1993, Brucato, Levin et al. 1996). While, Olpe and Karlsson found that the blockade of $GABA_BR$ facilitates LTP induction in CA1 (Olpe and Karlsson 1990), opposing results were reported by others (Davies, Starkey et al. 1991). Importantly, NMDAR-dependent LTP is critically dependent on the reduction of inhibition (disinhibition) provided by $GABA_BRs$ activation (Mott and Lewis 1991). This disinhibition is mainly provided by GABA mediated reduction of GABA release via $GABA_B$ autoreceptors on GABAergic terminals (Davies, Starkey et al. 1991). As we previously reported that 6x 1:1 t-LTP in the IH is NMDAR- dependent (Cepeda-Prado*, Khodaie* et al. 2021), a similar mechanism of $GABA_BR$ mediated disinhibition of presynaptic glutamate release could account for our observation of blocked 6x 1:1 t-LTP under complete blockade of GABAergic inhibition in IH (**Fig. 3.35B**).

In DH, 6x 1:1 t-LTP induction occurs independently from NMDAR activation (**Fig. 3.21A**). Thus $GABA_BR$ mediated disinhibition of CA1 PCs might not be required for LTP, explaining the robust 6x 1:1 t- t-LTP observed under conditions of complete blockade of GABAergic inhibition (**Fig. 3.35A**). The known NMDAR expression gradient (DH< IH<VH) also speaks in favor of a reduced role of NMDAR activation and therefore $GABA_BR$ mediated disinhibition for 6x 1:1 t-LTP in DH (Dubovyk and Manahan-Vaughan 2018).

4.9 GABAergic modulation of 6x 1:4 t-LTP induction along the longitudinal axis of the hippocampus

While our 6x 1:4 t-LTP paradigm induced robust t-LTP in DH independent of GABAergic inhibition, the magnitude of t-LTP in IH and VH was not affected by $GABA_A$ receptor blockade but highly sensitive to additional $GABA_B$ receptor antagonism. Two types of glutamatergic inputs control GABA release from interneurons: either SC stimulation leads to feed-forward inhibition, or feed-back inhibition is triggered by postsynaptic spiking of CA1 PCs (Blasco-Ibanez and Freund 1995, Maccaferri and McBain 1995). Burst stimulation of postsynaptic CA1 neurons, similar as we induce with our 6x 1:4 paradigm, could activate feedback-inhibition, increasing GABA release, and followed by activation of $GABA_B$ autoreceptors on interneuron presynaptic terminals, potently suppressing further GABA release, discussed earlier as disinhibition (Davies, Starkey et al. 1991, Liang, Carlson et al. 2006). Thus, burst stimulation with our 6x 1:4 protocol under intact GABAergic inhibition could lower GABA release at inhibitory synapses onto CA1 neurons and onto DA fibers whose release is essential for successful induction of 6x 1:4 t-LTP (Cepeda-Prado et al., 2021). Despite intact GABAergic receptor activation of DAergic fibers, sufficient amounts of DA will probably be released, since the low repeat protocols we use should not yield GABAR stimulation sufficient to abrogate DA release. Lower levels of GABAergic inhibition onto CA1 PCs through $GABA_B$ autoreceptors on GABAergic terminals will thus facilitate its depolarization, allowing to induce robust t-LTP in all studied hippocampal regions (**Fig. 3.36**). Minor differences in magnitudes of 6x 1:4 t-LTP seen with intact GABAergic inhibition (IH>DH=VH) might result from differences in the efficacy of $GABA_A$ receptor mediated inhibition (DH>IH>VH), distinct efficiency of neuromodulatory inputs (lower level of catecholaminergic fibers in IH vs. DH and VH; data not shown), or other differences at the SC-CA1 circuit level along the dorso-ventral axis.

The lower magnitude of 6x 1:4 t-LTP under complete blockade of GABAergic inhibition in IH and VH (**Fig. 3.36 B and C**) could be explained by two separate mechanisms.

In the first scenario (at the network level), complete blockade of GABAergic inhibition will suppress $GABA_B$ autoreceptor regulation of interneurons, such that the level of released GABA will increase thereby effectively counteracting CA1 neuron and dopamine fiber depolarization. This would negatively affect dopamine release (Santiago, Machado et al. 1993), and reduce glutamate release from SC axons, thereby counteracting the depolarization of postsynaptic CA1 cells. In a previous study we provided evidence that insertion of new AMPARs (including cp-AMPARs) into the

postsynaptic cell membrane is actively promoted by D1 and D2 dopamine receptor signaling, thereby supporting 6x 1:4 t-LTP expression (Cepeda-Prado*, Khodaie* et al. 2021). Therefore, reduction of dopamine release could significantly affect the magnitude of 6x 1:4 t-LTP.

In DH of male rats, the extracellular dopamine concentration was shown to be tenfold higher compared to VH and IH (Ishikawa, Ott et al. 1982). This could compensate the reduction of dopamine release imposed by the high level of extracellular GABA in the absence of GABA$_B$ autoreceptor regulation, and stimulate D2-like receptors that exist on GABAergic terminals, thereby down-regulating GABA release (Momiyama and Koga 2001). This would allow efficient induction of 6x 1:4 t-LTP under the complete block of GABAergic inhibition only in DH. These two explanations described above are just a part of the complex interactions of dopaminergic and GABAergic transmission in the SC-CA1 circuit that might account for the observed differences in 6x 1:4 t-LTP between DH, IH, and VH. The level of dopamine release was also shown to be extensively controlled by GABA release and GABAergic receptor activity (Santiago, Machado et al. 1993).

In the second scenario (at the cellular level), three possible mechanisms could be considered. First, GABA$_B$R activity was shown to determine excitatory neuronal architecture via the ability to regulate Arc/Arg3.1 (Terunuma, Revilla-Sanchez et al. 2014), and blockade of GABA$_B$Rs could therefore affect postsynaptic excitability through regulation of glutamate receptor or VGCC activity. Secondly, GABA$_B$R activation could enhance mGluR activity (Hirono, Yoshioka et al. 2001), which plays an essential role for 6x 1:4 t-LTP (Cepeda-Prado*, Khodaie* et al. 2021). Third and, most importantly, GABA$_B$R activation promotes through cross talk with mGluRs insertion of new AMPARs (including cp-AMPARs) into the postsynaptic cell membrane (Kelly, Farrant et al. 2009). Since we previously proved insertion of cp-AMPARs and the insertion of GluA2 containing new AMPARs to be instrumental for postsynaptic expression of low repeat t-LTP (Cepeda-Prado*, Khodaie* et al. 2021), this GABA$_B$R effect might be essential for expression of 6x 1:4 t-LTP.

4.10 DAergic signaling modulates GABAergic control over STDP

Our results in **Figure 3.35** revealed that under intact GABAergic inhibition, our 6x 1:1 SDTP paradigm failed to induce robust t-LTP in both DH and IH. So far, we have discussed the interaction of excitatory and inhibitory systems (**section 4.8 and 4.9 and Fig. 3.34**) and DAergic modulation of t-LTP, which indirectly works via the excitatory systems (**section 3.13.2**). However, previous studies described how DA release from DAergic fibers depends on and interacts with GABAergic modulation

(Santiago, Machado et al. 1993), suggesting a higher DA release in the presence of a GABA$_A$R blocker. While D1 receptor mRNA exists in about 30%–60% of all GABA-containing cortical interneurons (Santana, Mengod et al. 2009), D2- like receptors are less likely to distribute widely over GABAergic interneurons (Khan, Gutiérrez et al. 1998). Still, GABA releases probability onto PFC pyramidal neurons was shown to be reduced by D2-like receptor activation (Xu and Yao 2010). Explaining of complex interaction of these two network required further investigation, which was beyond the scope of the current thesis.

4.11 General conclusion

In summary, we used two different low repeat STDP protocols at SC-CA1 synapses to record synaptic plasticity of SC-CA1 synapses at the single cell level in postsynaptic CA1 neurons. At the first point, the current thesis suggests that cellular and molecular mechanisms underlying low repeat t-LTP induction and expression mechanisms critically depend on the hippocampus's stimulation pattern and the longitudinal axis. These experiments prove that complex hippocampal micro-networks provided by distinct expression patterns of excitatory, inhibitory, and modulatory responses diversely affect and regulate t-LTP induction along the longitudinal axis of the hippocampus. This plethora of coexisting plasticity mechanisms along the longitudinal axis of the hippocampus is ideally suited to enable each hippocampal pole (dorsal vs ventral) to fulfil its multiplexed functions in memory storage.

5 References

Abbott, L. F. and S. B. Nelson (2000). "Synaptic plasticity: taming the beast." <u>Nature neuroscience</u> **3**(11): 1178-1183.

Abraham, W. C. and M. F. Bear (1996). "Metaplasticity: the plasticity of synaptic plasticity." <u>Trends in neurosciences</u> **19**(4): 126-130.

Abraham, W. C. and J. M. Williams (2003). "Properties and mechanisms of LTP maintenance." <u>The Neuroscientist</u> **9**(6): 463-474.

Adcock, R. A., A. Thangavel, S. Whitfield-Gabrieli, B. Knutson and J. D. Gabrieli (2006). "Reward-motivated learning: mesolimbic activation precedes memory formation." <u>Neuron</u> **50**(3): 507-517.

Ali, A. B. and A. M. Thomson (1998). "Facilitating pyramid to horizontal oriens-alveus interneurone inputs: dual intracellular recordings in slices of rat hippocampus." <u>The Journal of physiology</u> **507**(1): 185-199.

Amaral, D., P. Andersen, J. O'Keefe and R. Morris (2007). <u>The hippocampus book</u>, Oxford University Press.

Amaral, D. G. and M. P. Witter (1989). "The three-dimensional organization of the hippocampal formation: a review of anatomical data." <u>Neuroscience</u> **31**(3): 571-591.

Andersen, P., T. Blackstad and T. Lömo (1966). "Location and identification of excitatory synapses on hippoeampal pyramidal cells." <u>Experimental brain research</u> **1**(3): 236-248.

Arnsten, A. F., M. J. Wang and C. D. Paspalas (2012). "Neuromodulation of thought: flexibilities and vulnerabilities in prefrontal cortical network synapses." <u>Neuron</u> **76**(1): 223-239.

Aston-Jones, G. and F. Bloom (1981). "Activity of norepinephrine-containing locus coeruleus neurons in behaving rats anticipates fluctuations in the sleep-waking cycle." <u>Journal of Neuroscience</u> **1**(8): 876-886.

Aston-Jones, G., J. Rajkowski, P. Kubiak and T. Alexinsky (1994). "Locus coeruleus neurons in monkey are selectively activated by attended cues in a vigilance task." <u>Journal of Neuroscience</u> **14**(7): 4467-4480.

Balschun, D. and W. Wetzel (2002). "Inhibition of mGluR5 blocks hippocampal LTP in vivo and spatial learning in rats." <u>Pharmacology Biochemistry and Behavior</u> **73**(2): 375-380.

Barria, A., V. Derkach and T. Soderling (1997). "Identification of the Ca2+/calmodulin-dependent protein kinase II regulatory phosphorylation site in the α-amino-3-hydroxyl-5-methyl4-isoxazole-propionate-type glutamate receptor." <u>Journal of Biological Chemistry</u> **272**(52): 32727-32730.

Baude, A., C. Bleasdale, Y. Dalezios, P. Somogyi and T. Klausberger (2007). "Immunoreactivity for the GABAA receptor α1 subunit, somatostatin and connexin36 distinguishes axoaxonic, basket, and bistratified interneurons of the rat hippocampus." <u>Cerebral cortex</u> **17**(9): 2094-2107.

Baulac, M., C. Verney and B. Berger (1986). "Dopaminergic innervation of the parahippocampal and hippocampal regions in the rat." <u>Revue neurologique</u> **142**(12): 895-905.

Bear, M. F. and R. C. Malenka (1994). "Synaptic plasticity: LTP and LTD." <u>Current opinion in neurobiology</u> **4**(3): 389-399.

Beaulieu, J.-M. and R. R. Gainetdinov (2011). "The physiology, signaling, and pharmacology of dopamine receptors." Pharmacological reviews **63**(1): 182-217.

Bender, V. A., K. J. Bender, D. J. Brasier and D. E. Feldman (2006). "Two coincidence detectors for spike timing-dependent plasticity in somatosensory cortex." Journal of Neuroscience **26**(16): 4166-4177.

Bergles, D. E., V. A. Doze, D. V. Madison and S. J. Smith (1996). "Excitatory actions of norepinephrine on multiple classes of hippocampal CA1 interneurons." Journal of Neuroscience **16**(2): 572-585.

Bergson, C., L. Mrzljak, J. F. Smiley, M. Pappy, R. Levenson and P. S. Goldman-Rakic (1995). "Regional, cellular, and subcellular variations in the distribution of D1 and D5 dopamine receptors in primate brain." Journal of Neuroscience **15**(12): 7821-7836.

Berridge, C. W. and B. D. Waterhouse (2003). "The locus coeruleus–noradrenergic system: modulation of behavioral state and state-dependent cognitive processes." Brain research reviews **42**(1): 33-84.

Berridge, M. J. (2005). "Unlocking the secrets of cell signaling." Annu. Rev. Physiol. **67**: 1-21.

Berridge, M. J. and R. F. Irvine (1984). "Inositol trisphosphate, a novel second messenger in cellular signal transduction." Nature **312**(5992): 315-321.

Beyeler, A., P. Namburi, G. F. Glober, C. Simonnet, G. G. Calhoon, G. F. Conyers, R. Luck, C. P. Wildes and K. M. Tye (2016). "Divergent routing of positive and negative information from the amygdala during memory retrieval." Neuron **90**(2): 348-361.

Bezaire, M. J. and I. Soltesz (2013). "Quantitative assessment of CA1 local circuits: knowledge base for interneuron-pyramidal cell connectivity." Hippocampus **23**(9): 751-785.

Bittner, K. C., C. Grienberger, S. P. Vaidya, A. D. Milstein, J. J. Macklin, J. Suh, S. Tonegawa and J. C. Magee (2015). "Conjunctive input processing drives feature selectivity in hippocampal CA1 neurons." Nature neuroscience **18**(8): 1133-1142.

Bittner, K. C., A. D. Milstein, C. Grienberger, S. Romani and J. C. Magee (2017). "Behavioral time scale synaptic plasticity underlies CA1 place fields." Science **357**(6355): 1033-1036.

Blasco-Ibanez, J. and T. Freund (1995). "Synaptic input of horizontal interneurons in stratum oriens of the hippocampal CA1 subfield: structural basis of feed-back activation." European Journal of Neuroscience **7**(10): 2170-2180.

Bliss, T. V. and G. L. Collingridge (1993). "A synaptic model of memory: long-term potentiation in the hippocampus." Nature **361**(6407): 31.

Blitzer, R. D., J. H. Connor, G. P. Brown, T. Wong, S. Shenolikar, R. Iyengar and E. M. Landau (1998). "Gating of CaMKII by cAMP-regulated protein phosphatase activity during LTP." Science **280**(5371): 1940-1943.

Blundon, J. A. and S. S. Zakharenko (2008). "Dissecting the components of long-term potentiation." The Neuroscientist **14**(6): 598-608.

Bolshakov, V. Y., H. Golan, E. R. Kandel and S. A. Siegelbaum (1997). "Recruitment of new sites of synaptic transmission during the cAMP-dependent late phase of LTP at CA3–CA1 synapses in the hippocampus." Neuron **19**(3): 635-651.

Booker, S. A., A. Gross, D. Althof, R. Shigemoto, B. Bettler, M. Frotscher, M. Hearing, K. Wickman, M. Watanabe and Á. Kulik (2013). "Differential GABAB-receptor-mediated effects in perisomatic- and dendrite-targeting parvalbumin interneurons." Journal of Neuroscience **33**(18): 7961-7974.

Brager, D. H., M. Capogna and S. M. Thompson (2002). "Short-term synaptic plasticity, simulation of nerve terminal dynamics, and the effects of protein kinase C activation in rat hippocampus." The Journal of physiology **541**(2): 545-559.

Brennan, P., H. Kaba and E. B. Keverne (1990). "Olfactory recognition: a simple memory system." Science **250**(4985): 1223-1226.

Brodal, A. (1947). "The hypocampus and the sense of smell; a review." Brain: a journal of neurology.

Brucato, F., E. Levin, D. Mott, D. Lewis, W. Wilson and H. Swartzelder (1996). "Hippocampal long-term potentiation and spatial learning in the rat: effects of GABAB receptor blockade." Neuroscience **74**(2): 331-339.

Brzosko, Z., S. B. Mierau and O. Paulsen (2019). "Neuromodulation of spike-timing-dependent plasticity: past, present, and future." Neuron **103**(4): 563-581.

Brzosko, Z., W. Schultz and O. Paulsen (2015). "Retroactive modulation of spike timing-dependent plasticity by dopamine." elife **4**: e09685.

Buhl, E. H., K. Halasy and P. Somogyi (1994). "Diverse sources of hippocampal unitary inhibitory postsynaptic potentials and the number of synaptic release sites." Nature **368**(6474): 823-828.

Bui, A. D., T. M. Nguyen, C. Limouse, H. K. Kim, G. G. Szabo, S. Felong, M. Maroso and I. Soltesz (2018). "Dentate gyrus mossy cells control spontaneous convulsive seizures and spatial memory." Science **359**(6377): 787-790.

Burman, M. A., M. J. Starr and J. C. Gewirtz (2006). "Dissociable effects of hippocampus lesions on expression of fear and trace fear conditioning memories in rats." Hippocampus **16**(2): 103-113.

Burton, B. G., V. Hok, E. Save and B. Poucet (2009). "Lesion of the ventral and intermediate hippocampus abolishes anticipatory activity in the medial prefrontal cortex of the rat." Behavioural brain research **199**(2): 222-234.

Burwell, R. D. and D. G. Amaral (1998). "Perirhinal and postrhinal cortices of the rat: interconnectivity and connections with the entorhinal cortex." Journal of Comparative Neurology **391**(3): 293-321.

Buzsáki, G. (1989). "Two-stage model of memory trace formation: a role for "noisy" brain states." Neuroscience **31**(3): 551-570.

Caballero, A., K. C. Diah and K. Y. Tseng (2013). "Region-specific upregulation of parvalbumin-, but not calretinin-positive cells in the ventral hippocampus during adolescence." Hippocampus **23**(12): 1331-1336.

Cahill, L. and J. McGaugh (1996). The neurobiology of memory for emotional events: adrenergic activation and the amygdala. Proceedings of the Western Pharmacology Society.

Cahill, L. and J. L. McGaugh (1998). "Mechanisms of emotional arousal and lasting declarative memory." Trends in neurosciences **21**(7): 294-299.

Cajal, S. (1911). "Ramon y: Histologie du Systeme nerveux." Vol. II: 197.

Caporale, N. and Y. Dan (2008). "Spike timing-dependent plasticity: a Hebbian learning rule." Annual review of neuroscience **31**(1): 25-46.

Caporale, N. and Y. Dan (2008). "Spike timing–dependent plasticity: a Hebbian learning rule." Annu. Rev. Neurosci. **31**: 25-46.

Cenquizca, L. A. and L. W. Swanson (2007). "Spatial organization of direct hippocampal field CA1 axonal projections to the rest of the cerebral cortex." Brain research reviews **56**(1): 1-26.

Cepeda-Prado, E. A., B. Khodaie, G. D. Quiceno, S. Beythien, E. Edelmann and V. Lessmann (2021). "Calcium-Permeable AMPA Receptors Mediate Timing-Dependent LTP Elicited by Low Repeat Coincident Pre-and Postsynaptic Activity at Schaffer Collateral-CA1 Synapses." Cerebral Cortex.

Cepeda-Prado, E. A., B. Khodaie, G. D. Quiceno, S. Beythien, V. Leßmann and E. Edelmann (2019). "Calcium-permeable AMPA receptors mediate timing-dependent LTP elicited by six coincident action potentials at Schaffer collateral-CA1 synapses." bioRxiv: 719633.

Cepeda, C. and M. S. Levine (2006). "Where do you think you are going? The NMDA-D1 receptor trap." Science Signaling 2006(333): pe20-pe20.

Chamberland, S., C. Salesse, D. Topolnik and L. Topolnik (2010). "Synapse-specific inhibitory control of hippocampal feedback inhibitory circuit." Frontiers in cellular neuroscience 4: 130.

Chamberland, S. and L. Topolnik (2012). "Inhibitory control of hippocampal inhibitory neurons." Frontiers in neuroscience 6: 165.

Chebib, M. and G. A. Johnston (1999). "The 'ABC' of GABA receptors: a brief review." Clinical and experimental pharmacology and physiology 26(11): 937-940.

Christie, B. R. and W. C. Abraham (1992). "Priming of associative long-term depression in the dentate gyrus by θ frequency synaptic activity." Neuron 9(1): 79-84.

Collingridge, G. (1987). "The role of NMDA receptors in learning and memory." Nature 330(6149): 604-605.

Collingridge, G. L., J. T. Isaac and Y. T. Wang (2004). "Receptor trafficking and synaptic plasticity." Nature Reviews Neuroscience 5(12): 952-962.

Couey, J. J., R. M. Meredith, S. Spijker, R. B. Poorthuis, A. B. Smit, A. B. Brussaard and H. D. Mansvelder (2007). "Distributed network actions by nicotine increase the threshold for spike-timing-dependent plasticity in prefrontal cortex." Neuron 54(1): 73-87.

Cui, Y., I. Prokin, H. Xu, B. Delord, S. Genet, L. Venance and H. Berry (2016). "Endocannabinoid dynamics gate spike-timing dependent depression and potentiation." Elife 5: e13185.

Czéh, B., Z. K. K. Varga, K. Henningsen, G. L. Kovács, A. Miseta and O. Wiborg (2015). "Chronic stress reduces the number of GABAergic interneurons in the adult rat hippocampus, dorsal-ventral and region-specific differences." Hippocampus 25(3): 393-405.

Dan, Y. and M.-m. Poo (2004). "Spike timing-dependent plasticity of neural circuits." Neuron 44(1): 23-30.

Dan, Y. and M.-M. Poo (2006). "Spike timing-dependent plasticity: from synapse to perception." Physiological reviews 86(3): 1033-1048.

Daoudal, G. and D. Debanne (2003). "Long-term plasticity of intrinsic excitability: learning rules and mechanisms." Learning & memory 10(6): 456-465.

Daubner, S. C., T. Le and S. Wang (2011). "Tyrosine hydroxylase and regulation of dopamine synthesis." Archives of biochemistry and biophysics 508(1): 1-12.

Davies, C. H., S. J. Starkey, M. F. Pozza and G. L. Collingridge (1991). "GABA B autoreceptors regulate the induction of LTP." Nature 349(6310): 609-611.

Davies, C. H., S. J. Starkey, M. F. Pozza and G. L. Collingridge (1991). "GABAB autoreceptors regulate the induction of LTP." Nature 349(6310): 609-611.

de Hoz, L., J. Knox and R. G. Morris (2003). "Longitudinal axis of the hippocampus: both septal and temporal poles of the hippocampus support water maze spatial learning depending on the training protocol." Hippocampus 13(5): 587-603.

Derchansky, M., E. Shahar, R. Wennberg, M. Samoilova, S. Jahromi, P. Abdelmalik, L. Zhang and P. Carlen (2004). "Model of frequent, recurrent, and spontaneous seizures in the intact mouse hippocampus." Hippocampus **14**(8): 935-947.

Dobrunz, L. E. and C. F. Stevens (1997). "Heterogeneity of release probability, facilitation, and depletion at central synapses." Neuron **18**(6): 995-1008.

Dodt, H.-U., H. Pawelzik and W. Zieglga (1991). "Actions of noradrenaline on neocortical neurons in vitro." Brain research **545**(1-2): 307-311.

Dohlman, H. G., J. Thorner, M. G. Caron and R. J. Lefkowitz (1991). "Model systems for the study of seven-transmembrane-segment receptors." Annual review of biochemistry **60**(1): 653-688.

Dolorfo, C. L. and D. G. Amaral (1998). "Entorhinal cortex of the rat: topographic organization of the cells of origin of the perforant path projection to the dentate gyrus." Journal of Comparative Neurology **398**(1): 25-48.

Dougherty, K. A., T. Islam and D. Johnston (2012). "Intrinsic excitability of CA1 pyramidal neurones from the rat dorsal and ventral hippocampus." The Journal of physiology **590**(22): 5707-5722.

Dougherty, K. A., D. A. Nicholson, L. Diaz, E. W. Buss, K. M. Neuman, D. M. Chetkovich and D. Johnston (2013). "Differential expression of HCN subunits alters voltage-dependent gating of h-channels in CA1 pyramidal neurons from dorsal and ventral hippocampus." Journal of neurophysiology **109**(7): 1940-1953.

Douglas, R. J. and R. L. Isaacson (1964). "Hippocampal lesions and activity." Psychonomic Science **1**(1): 187-188.

Drew, P. J. and L. Abbott (2006). "Extending the effects of spike-timing-dependent plasticity to behavioral timescales." Proceedings of the National Academy of Sciences **103**(23): 8876-8881.

Drinkwater, N., C. L. Gee, M. Puri, K. R. Criscione, M. J. McLeish, G. L. Grunewald and J. L. Martin (2009). "Molecular recognition of physiological substrate noradrenaline by the adrenaline-synthesizing enzyme PNMT and factors influencing its methyltransferase activity." Biochemical journal **422**(3): 463-471.

Drolet, P., L. Bilodeau, A. Chorvatova, L. Laflamme, N. Gallo-Payet and M. D. Payet (1997). "Inhibition of the T-type Ca2+ current by the dopamine D1 receptor in rat adrenal glomerulosa cells: requirement of the combined action of the Gβγ protein subunit and cyclic adenosine 3′, 5′-monophosphate." Molecular Endocrinology **11**(4): 503-514.

Dubovyk, V. and D. Manahan-Vaughan (2019). "Gradient of expression of dopamine D2 receptors along the dorso-ventral axis of the hippocampus." Frontiers in synaptic neuroscience **11**: 28.

Dubovyk, V. and D. Manahan-Vaughan (2018). "Less means more: The magnitude of synaptic plasticity along the hippocampal dorso-ventral axis is inversely related to the expression levels of plasticity-related neurotransmitter receptors." Hippocampus **28**(2): 136-150.

Dudman, J. T., D. Tsay and S. A. Siegelbaum (2007). "A role for synaptic inputs at distal dendrites: instructive signals for hippocampal long-term plasticity." Neuron **56**(5): 866-879.

Edelmann, E., E. Cepeda-Prado, M. Franck, P. Lichtenecker, T. Brigadski and V. Leßmann (2015). "Theta burst firing recruits BDNF release and signaling in postsynaptic CA1 neurons in spike-timing-dependent LTP." Neuron **86**(4): 1041-1054.

Edelmann, E., E. Cepeda-Prado and V. Leßmann (2017). "Coexistence of multiple types of synaptic plasticity in individual hippocampal CA1 pyramidal neurons." Frontiers in synaptic neuroscience **9**: 7.

Edelmann, E. and V. Lessmann (2011). "Dopamine modulates spike timing-dependent plasticity and action potential properties in CA1 pyramidal neurons of acute rat hippocampal slices." Frontiers in synaptic neuroscience **3**: 6.

Edelmann, E. and V. Lessmann (2013). "Dopamine regulates intrinsic excitability thereby gating successful induction of spike timing-dependent plasticity in CA1 of the hippocampus." Frontiers in neuroscience **7**: 25.

Edelmann, E. and V. Lessmann (2018). "Dopaminergic innervation and modulation of hippocampal networks." Cell and tissue research **373**(3): 711-727.

Eghbali, M., J. Curmi, B. Birnir and P. Gage (1997). "Hippocampal GABA A channel conductance increased by diazepam." Nature **388**(6637): 71-75.

Elfant, D., B. Z. Pál, N. Emptage and M. Capogna (2008). "Specific inhibitory synapses shift the balance from feedforward to feedback inhibition of hippocampal CA1 pyramidal cells." European Journal of Neuroscience **27**(1): 104-113.

Elias, G. M. and R. A. Nicoll (2007). "Synaptic trafficking of glutamate receptors by MAGUK scaffolding proteins." Trends in cell biology **17**(7): 343-352.

Fanselow, M. S. and H.-W. Dong (2010). "Are the dorsal and ventral hippocampus functionally distinct structures?" Neuron **65**(1): 7-19.

Farrant, M. and Z. Nusser (2005). "Variations on an inhibitory theme: phasic and tonic activation of GABA A receptors." Nature Reviews Neuroscience **6**(3): 215-229.

Feldman, D. E. (2000). "Timing-based LTP and LTD at vertical inputs to layer II/III pyramidal cells in rat barrel cortex." Neuron **27**(1): 45-56.

Ferraguti, F., P. Cobden, M. Pollard, D. Cope, R. Shigemoto, M. Watanabe and P. Somogyi (2004). "Immunolocalization of metabotropic glutamate receptor 1α (mGluR1α) in distinct classes of interneuron in the CA1 region of the rat hippocampus." Hippocampus **14**(2): 193-215.

Ferry, B., P. J. Magistretti and E. Pralong (1997). "Noradrenaline Modulates GIutamate-mediated Neurotransmission in the Rat Basolateral Amygdala In Vitro." European Journal of Neuroscience **9**(7): 1356-1364.

Fink, A. E. and T. J. O'Dell (2009). "Short trains of theta frequency stimulation enhance CA1 pyramidal neuron excitability in the absence of synaptic potentiation." Journal of Neuroscience **29**(36): 11203-11214.

Fink, A. E., J. Sarinana, E. E. Gray and T. J. O'dell (2007). "Activity-dependent depression of local excitatory connections in the CA1 region of mouse hippocampus." Journal of neurophysiology **97**(6): 3926-3936.

FISONE, G. (2010). "3.3 Intracellular Dopamine Signaling." Dopamine handbook: 100.

Fitzsimonds, R. M. and M.-m. Poo (1998). "Retrograde signaling in the development and modification of synapses." Physiological reviews **78**(1): 143-170.

Foote, S., G. Aston-Jones and F. Bloom (1980). "Impulse activity of locus coeruleus neurons in awake rats and monkeys is a function of sensory stimulation and arousal." Proceedings of the National Academy of Sciences **77**(5): 3033-3037.

Fox, C. J., K. I. Russell, Y. T. Wang and B. R. Christie (2006). "Contribution of NR2A and NR2B NMDA subunits to bidirectional synaptic plasticity in the hippocampus in vivo." Hippocampus **16**(11): 907-915.

Freund, T. F. and G. Buzsaki (1996). "Interneurons of the hippocampus." Hippocampus **6**(4): 347-470.

Freund, T. F. and A. I. Gulyás (1997). "Inhibitory control of GABAergic interneurons in the hippocampus." Canadian journal of physiology and pharmacology **75**(5): 479-487.

Frey, U., Y.-Y. Huang and E. R. Kandel (1993). "Effects of cAMP simulate a late stage of LTP in hippocampal CA1 neurons." Science **260**(5114): 1661-1664.

Froemke, R. C., I. A. Tsay, M. Raad, J. D. Long and Y. Dan (2006). "Contribution of individual spikes in burst-induced long-term synaptic modification." Journal of neurophysiology.

Fuentealba, P., R. Begum, M. Capogna, S. Jinno, L. F. Marton, J. Csicsvari, A. Thomson, P. Somogyi and T. Klausberger (2008). "Ivy cells: a population of nitric-oxide-producing, slow-spiking GABAergic neurons and their involvement in hippocampal network activity." Neuron **57**(6): 917-929.

Furtak, S. C., S. M. Wei, K. L. Agster and R. D. Burwell (2007). "Functional neuroanatomy of the parahippocampal region in the rat: the perirhinal and postrhinal cortices." Hippocampus **17**(9): 709-722.

Gaiarsa, J.-L., O. Caillard and Y. Ben-Ari (2002). "Long-term plasticity at GABAergic and glycinergic synapses: mechanisms and functional significance." Trends in neurosciences **25**(11): 564-570.

Gangarossa, G., S. Longueville, D. De Bundel, J. Perroy, D. Hervé, J. A. Girault and E. Valjent (2012). "Characterization of dopamine D1 and D2 receptor-expressing neurons in the mouse hippocampus." Hippocampus **22**(12): 2199-2207.

Gao, C., X. Sun and M. E. Wolf (2006). "Activation of D1 dopamine receptors increases surface expression of AMPA receptors and facilitates their synaptic incorporation in cultured hippocampal neurons." Journal of neurochemistry **98**(5): 1664-1677.

Gao, J., A. A. Voss, I. N. Pessah, F. T. Lauer, T. M. Penning and S. W. Burchiel (2005). "Ryanodine receptor-mediated rapid increase in intracellular calcium induced by 7, 8-benzo (a) pyrene quinone in human and murine leukocytes." Toxicological Sciences **87**(2): 419-426.

Gasbarri, A., M. G. Packard, E. Campana and C. Pacitti (1994). "Anterograde and retrograde tracing of projections from the ventral tegmental area to the hippocampal formation in the rat." Brain research bulletin **33**(4): 445-452.

Gerfen, C. R. and D. J. Surmeier (2011). "Modulation of striatal projection systems by dopamine." Annual review of neuroscience **34**: 441.

Gerstner, W., M. Lehmann, V. Liakoni, D. Corneil and J. Brea (2018). "Eligibility traces and plasticity on behavioral time scales: experimental support of neohebbian three-factor learning rules." Frontiers in neural circuits **12**: 53.

Ghanbarian, E. and F. Motamedi (2013). "Ventral tegmental area inactivation suppresses the expression of CA1 long term potentiation in anesthetized rat." PLoS One **8**(3): e58844.

Glykys, J. and I. Mody (2007). "The main source of ambient GABA responsible for tonic inhibition in the mouse hippocampus." The Journal of physiology **582**(3): 1163-1178.

Golding, N. L., T. J. Mickus, Y. Katz, W. L. Kath and N. Spruston (2005). "Factors mediating powerful voltage attenuation along CA1 pyramidal neuron dendrites." The Journal of physiology **568**(1): 69-82.

Granado, N., O. Ortiz, L. M. Suárez, E. D. Martín, V. Ceña, J. M. Solís and R. Moratalla (2008). "D1 but not D5 dopamine receptors are critical for LTP, spatial learning, and LTP-Induced arc and zif268 expression in the hippocampus." Cerebral cortex **18**(1): 1-12.

Greengard, P. (2001). "The neurobiology of slow synaptic transmission." Science 294(5544): 1024-1030.

Gribkoff, V. K. and J. H. Ashe (1984). "Modulation by dopamine of population responses and cell membrane properties of hippocampal CA1 neurons in vitro." Brain research 292(2): 327-338.

Hájos, N., I. Katona, S. Naiem, K. Mackie, C. Ledent, I. Mody and T. F. Freund (2000). "Cannabinoids inhibit hippocampal GABAergic transmission and network oscillations." European Journal of Neuroscience 12(9): 3239-3249.

Hansen, N. and D. Manahan-Vaughan (2014). "Dopamine D1/D5 receptors mediate informational saliency that promotes persistent hippocampal long-term plasticity." Cerebral Cortex 24(4): 845-858.

Hargreaves, E. L., G. Rao, I. Lee and J. J. Knierim (2005). "Major dissociation between medial and lateral entorhinal input to dorsal hippocampus." science 308(5729): 1792-1794.

Haring, J. H. and J. N. Davis (1985). "Differential distribution of locus coeruleus projections to the hippocampal formation: anatomical and biochemical evidence." Brain research 325(1-2): 366-369.

Hasselmo, M. E. (1995). "Neuromodulation and cortical function: modeling the physiological basis of behavior." Behavioural brain research 67(1): 1-27.

He, K., M. Huertas, S. Z. Hong, X. Tie, J. W. Hell, H. Shouval and A. Kirkwood (2015). "Distinct eligibility traces for LTP and LTD in cortical synapses." Neuron 88(3): 528-538.

Hebb, D. O. (1949). "The first stage of perception: growth of the assembly." The Organization of Behavior 4: 60-78.

Hebb, D. O. (2005). The organization of behavior: A neuropsychological theory, Psychology Press.

Hefft, S., U. Kraushaar, J. RP Geiger and P. Jonas (2002). "Presynaptic short-term depression is maintained during regulation of transmitter release at a GABAergic synapse in rat hippocampus." The Journal of physiology 539(1): 201-208.

Henze, D. A., G. R. González-Burgos, N. N. Urban, D. A. Lewis and G. Barrionuevo (2000). "Dopamine increases excitability of pyramidal neurons in primate prefrontal cortex." Journal of neurophysiology 84(6): 2799-2809.

Henze, D. A., N. N. Urban and G. Barrionuevo (2000). "The multifarious hippocampal mossy fiber pathway: a review." Neuroscience 98(3): 407-427.

Hirono, M., T. Yoshioka and S. Konishi (2001). "GABAB receptor activation enhances mGluR-mediated responses at cerebellar excitatory synapses." Nature neuroscience 4(12): 1207-1216.

Hoge, J. and R. P. Kesner (2007). "Role of CA3 and CA1 subregions of the dorsal hippocampus on temporal processing of objects." Neurobiology of learning and memory 88(2): 225-231.

Hönigsperger, C., M. Marosi, R. Murphy and J. F. Storm (2015). "Dorsoventral differences in Kv7/M-current and its impact on resonance, temporal summation and excitability in rat hippocampal pyramidal cells." The Journal of physiology 593(7): 1551-1580.

Hsu, K.-S. (1996). "Characterization of dopamine receptors mediating inhibition of excitatory synaptic transmission in the rat hippocampal slice." Journal of neurophysiology 76(3): 1887-1895.

Hu, H., E. Real, K. Takamiya, M.-G. Kang, J. Ledoux, R. L. Huganir and R. Malinow (2007). "Emotion enhances learning via norepinephrine regulation of AMPA-receptor trafficking." Cell 131(1): 160-173.

Huang, E. P. (1998). "Synaptic plasticity: going through phases with LTP." Current Biology 8(10): R350-R352.

Huang, Y.-Y. and E. R. Kandel (1995). "D1/D5 receptor agonists induce a protein synthesis-dependent late potentiation in the CA1 region of the hippocampus." Proceedings of the National Academy of Sciences **92**(7): 2446-2450.

Hunsaker, M. R. and R. P. Kesner (2008). "Dissociations across the dorsal–ventral axis of CA3 and CA1 for encoding and retrieval of contextual and auditory-cued fear." Neurobiology of learning and memory **89**(1): 61-69.

Isaacson, J., J. Solis and R. Nicoll (1993). "Local and diffuse synaptic actions of GABA in the hippocampus." Neuron **10**(2): 165-175.

Ishikawa, K., T. Ott and J. L. McGaugh (1982). "Evidence for dopamine as a transmitter in dorsal hippocampus." Brain Research **232**(1): 222-226.

Ishizuka, N., J. Weber and D. G. Amaral (1990). "Organization of intrahippocampal projections originating from CA3 pyramidal cells in the rat." Journal of comparative neurology **295**(4): 580-623.

Ito, H. T. and E. M. Schuman (2007). "Frequency-dependent gating of synaptic transmission and plasticity by dopamine." Frontiers in neural circuits **1**: 1.

Izquierdo, I. and J. H. Medina (1997). "Memory formation: the sequence of biochemical events in the hippocampus and its connection to activity in other brain structures." Neurobiology of learning and memory **68**(3): 285-316.

Jackson, M. B. and S. J. Zhang (1995). "Action potential propagation and propagation block by GABA in rat posterior pituitary nerve terminals." The Journal of Physiology **483**(3): 597-611.

Jang, H. J., H. Chung, J. M. Rowland, B. A. Richards, M. M. Kohl and J. Kwag (2020). "Distinct roles of parvalbumin and somatostatin interneurons in gating the synchronization of spike times in the neocortex." Science advances **6**(17): eaay5333.

Jay, T. M. (2003). "Dopamine: a potential substrate for synaptic plasticity and memory mechanisms." Progress in neurobiology **69**(6): 375-390.

Jonas, P., G. Major and B. Sakmann (1993). "Quantal components of unitary EPSCs at the mossy fibre synapse on CA3 pyramidal cells of rat hippocampus." The Journal of physiology **472**(1): 615-663.

Jong, Y.-J. I., I. Sergin, C. A. Purgert and K. L. O'Malley (2014). "Location-dependent signaling of the group 1 metabotropic glutamate receptor mGlu5." Molecular pharmacology **86**(6): 774-785.

Kaada, B., E. W. Rasmussen and O. Kveim (1961). "Effects of hippocampal lesions on maze learning and retention in rats." Experimental Neurology **3**(4): 333-355.

Kaar, A. and M. G. Rae (2015). Metabotropic glutamate receptor-mediated cyclic ADP ribose signalling, Portland Press Ltd.

Kampa, B. M., J. J. Letzkus and G. J. Stuart (2007). "Dendritic mechanisms controlling spike-timing-dependent synaptic plasticity." Trends in neurosciences **30**(9): 456-463.

Kantamneni, S. (2015). "Cross-talk and regulation between glutamate and GABAB receptors." Frontiers in Cellular Neuroscience **9**: 135.

Karagas, N. E. and K. Venkatachalam (2019). "Roles for the endoplasmic reticulum in regulation of neuronal calcium homeostasis." Cells **8**(10): 1232.

Katsuki, H., Y. Izumi and C. F. Zorumski (1997). "Noradrenergic regulation of synaptic plasticity in the hippocampal CA1 region." Journal of neurophysiology **77**(6): 3013-3020.

Kauer, J. A. and R. C. Malenka (2006). "LTP: AMPA receptors trading places." Nature neuroscience **9**(5): 593-594.

Kelly, L., M. Farrant and S. G. Cull-Candy (2009). "Synaptic mGluR activation drives plasticity of calcium-permeable AMPA receptors." Nature neuroscience 12(5): 593-601.

Kempadoo, K. A., E. V. Mosharov, S. J. Choi, D. Sulzer and E. R. Kandel (2016). "Dopamine release from the locus coeruleus to the dorsal hippocampus promotes spatial learning and memory." Proceedings of the National Academy of Sciences 113(51): 14835-14840.

Kepecs, A. and G. Fishell (2014). "Interneuron cell types are fit to function." Nature 505(7483): 318-326.

Kesner, R. P., M. R. Hunsaker and W. Ziegler (2011). "The role of the dorsal and ventral hippocampus in olfactory working memory." Neurobiology of learning and memory 96(2): 361-366.

Khan, Z. U., A. Gutiérrez, R. Martín, A. Peñafiel, A. Rivera and A. De La Calle (1998). "Differential regional and cellular distribution of dopamine D2-like receptors: an immunocytochemical study of subtype-specific antibodies in rat and human brain." Journal of Comparative Neurology 402(3): 353-371.

Kim, C. S. and D. Johnston (2015). "A1 adenosine receptor-mediated GIRK channels contribute to the resting conductance of CA1 neurons in the dorsal hippocampus." Journal of neurophysiology 113(7): 2511-2523.

Kimble, D. P. (1963). "The effects of bilateral hippocampal lesions in rats." journal of Comparative and Physiological Psychology 56(2): 273.

Kishi, T., T. Tsumori, S. Yokota and Y. Yasui (2006). "Topographical projection from the hippocampal formation to the amygdala: a combined anterograde and retrograde tracing study in the rat." Journal of Comparative Neurology 496(3): 349-368.

Kitai, S. and D. Surmeier (1993). "Cholinergic and dopaminergic modulation of potassium conductances in neostriatal neurons." Advances in neurology 60: 40-52.

Kjelstrup, K. G., F. A. Tuvnes, H.-A. Steffenach, R. Murison, E. I. Moser and M.-B. Moser (2002). "Reduced fear expression after lesions of the ventral hippocampus." Proceedings of the National Academy of Sciences 99(16): 10825-10830.

Klausberger, T. (2009). "GABAergic interneurons targeting dendrites of pyramidal cells in the CA1 area of the hippocampus." European Journal of Neuroscience 30(6): 947-957.

Klausberger, T., P. J. Magill, L. F. Márton, J. D. B. Roberts, P. M. Cobden, G. Buzsáki and P. Somogyi (2003). "Brain-state-and cell-type-specific firing of hippocampal interneurons in vivo." Nature 421(6925): 844-848.

Kohara, K., M. Pignatelli, A. J. Rivest, H.-Y. Jung, T. Kitamura, J. Suh, D. Frank, K. Kajikawa, N. Mise and Y. Obata (2014). "Cell type–specific genetic and optogenetic tools reveal hippocampal CA2 circuits." Nature neuroscience 17(2): 269.

Korsakoff, S. S. (1889). "Etude médico-psychologique sur une forme des maladies de la mémoire." Revue Philosophique 28(501): e530.

Kullmann, D., F. Asztely and M. Walker (2000). "The role of mammalian ionotropic receptors in synaptic plasticity: LTP, LTD and epilepsy." Cellular and Molecular Life Sciences CMLS 57(11): 1551-1561.

Kullmann, D. M. (2011). "Interneuron networks in the hippocampus." Current opinion in neurobiology 21(5): 709-716.

Kveim, O., J. Setekleiv and B. Kaada (1964). "Differential effects of hippocampal lesions on maze and passive avoidance learning in rats." Experimental Neurology 9(1): 59-72.

Laurberg, S. (1979). "Commissural and intrinsic connections of the rat hippocampus." Journal of Comparative Neurology **184**(4): 685-708.

Leão, R. N., S. Mikulovic, K. E. Leão, H. Munguba, H. Gezelius, A. Enjin, K. Patra, A. Eriksson, L. M. Loew and A. B. Tort (2012). "OLM interneurons differentially modulate CA3 and entorhinal inputs to hippocampal CA1 neurons." Nature neuroscience **15**(11): 1524-1530.

Lee, I. and R. P. Kesner (2003). "Time-dependent relationship between the dorsal hippocampus and the prefrontal cortex in spatial memory." Journal of Neuroscience **23**(4): 1517-1523.

Lee, S. P., C. H. So, A. J. Rashid, G. Varghese, R. Cheng, A. J. Lança, B. F. O'Dowd and S. R. George (2004). "Dopamine D1 and D2 receptor Co-activation generates a novel phospholipase C-mediated calcium signal." Journal of Biological Chemistry **279**(34): 35671-35678.

Lee, V. and J. Maguire (2014). "The impact of tonic GABAA receptor-mediated inhibition on neuronal excitability varies across brain region and cell type." Frontiers in neural circuits **8**: 3.

Legault, M., P.-P. Rompré and R. A. Wise (2000). "Chemical stimulation of the ventral hippocampus elevates nucleus accumbens dopamine by activating dopaminergic neurons of the ventral tegmental area." Journal of Neuroscience **20**(4): 1635-1642.

Lemon, N. and D. Manahan-Vaughan (2006). "Dopamine D1/D5 receptors gate the acquisition of novel information through hippocampal long-term potentiation and long-term depression." Journal of Neuroscience **26**(29): 7723-7729.

Lenz, R. A., T. A. Pitler and B. E. Alger (1997). "High intracellular Cl− concentrations depress G-protein-modulated ionic conductances." Journal of Neuroscience **17**(16): 6133-6141.

Lesburguères, E., O. L. Gobbo, S. Alaux-Cantin, A. Hambucken, P. Trifilieff and B. Bontempi (2011). "Early tagging of cortical networks is required for the formation of enduring associative memory." Science **331**(6019): 924-928.

Lester, R. A., J. D. Clements, G. L. Westbrook and C. E. Jahr (1990). "Channel kinetics determine the time course of NMDA receptor-mediated synaptic currents." Nature **346**(6284): 565-567.

Levone, B. R., M. G. Codagnone, G. M. Moloney, Y. M. Nolan, J. F. Cryan and O. F. O'Leary (2021). "Adult-born neurons from the dorsal, intermediate, and ventral regions of the longitudinal axis of the hippocampus exhibit differential sensitivity to glucocorticoids." Molecular psychiatry **26**(7): 3240-3252.

Liang, S.-L., G. C. Carlson and D. A. Coulter (2006). "Dynamic regulation of synaptic GABA release by the glutamate-glutamine cycle in hippocampal area CA1." Journal of Neuroscience **26**(33): 8537-8548.

Lisman, J. (1989). "A mechanism for the Hebb and the anti-Hebb processes underlying learning and memory." Proceedings of the National Academy of Sciences **86**(23): 9574-9578.

Lisman, J. (2017). "Glutamatergic synapses are structurally and biochemically complex because of multiple plasticity processes: long-term potentiation, long-term depression, short-term potentiation and scaling." Phil. Trans. R. Soc. B **372**(1715): 20160260.

Lisman, J., A. A. Grace and E. Duzel (2011). "A neoHebbian framework for episodic memory; role of dopamine-dependent late LTP." Trends in neurosciences **34**(10): 536-547.

Liu, L., T. P. Wong, M. F. Pozza, K. Lingenhoehl, Y. Wang, M. Sheng, Y. P. Auberson and Y. T. Wang (2004). "Role of NMDA receptor subtypes in governing the direction of hippocampal synaptic plasticity." Science **304**(5673): 1021-1024.

Loy, R., D. A. Koziell, J. D. Lindsey and R. Y. Moore (1980). "Noradrenergic innervation of the adult rat hippocampal formation." Journal of Comparative Neurology **189**(4): 699-710.

Lüscher, C. and R. C. Malenka (2012). "NMDA receptor-dependent long-term potentiation and long-term depression (LTP/LTD)." Cold Spring Harbor perspectives in biology **4**(6): a005710.

Maccaferri, G., J. David, B. Roberts, P. Szucs, C. A. Cottingham and P. Somogyi (2000). "Cell surface domain specific postsynaptic currents evoked by identified GABAergic neurones in rat hippocampus in vitro." The Journal of physiology **524**(1): 91-116.

Maccaferri, G. and C. J. McBain (1995). "Passive propagation of LTD to stratum oriens-alveus inhibitory neurons modulates the temporoammonic input to the hippocampal CA1 region." Neuron **15**(1): 137-145.

Madison, D. V. and R. A. Nicoll (1988). "Norepinephrine decreases synaptic inhibition in the rat hippocampus." Brain research **442**(1): 131-138.

Magee, J. C. and E. P. Cook (2000). "Somatic EPSP amplitude is independent of synapse location in hippocampal pyramidal neurons." Nature neuroscience **3**(9): 895-903.

Mainen, Z. F. and T. J. Sejnowski (1996). "Influence of dendritic structure on firing pattern in model neocortical neurons." Nature **382**(6589): 363-366.

Makhinson, M., J. K. Chotiner, J. B. Watson and T. J. O'Dell (1999). "Adenylyl cyclase activation modulates activity-dependent changes in synaptic strength and Ca2+/calmodulin-dependent kinase II autophosphorylation." Journal of Neuroscience **19**(7): 2500-2510.

Malenka, R. C. (2001). "Synaptic plasticity."

Malenka, R. C. (2003). "The long-term potential of LTP." Nature Reviews Neuroscience **4**(11): 923-926.

Malenka, R. C. and M. F. Bear (2004). "LTP and LTD: an embarrassment of riches." Neuron **44**(1): 5-21.

Malik, R., K. A. Dougherty, K. Parikh, C. Byrne and D. Johnston (2016). "Mapping the electrophysiological and morphological properties of CA 1 pyramidal neurons along the longitudinal hippocampal axis." Hippocampus **26**(3): 341-361.

Manahan-Vaughan, D. and A. Kulla (2003). "Regulation of depotentiation and long-term potentiation in the dentate gyrus of freely moving rats by dopamine D2-like receptors." Cerebral Cortex **13**(2): 123-135.

Manita, S., T. Suzuki, M. Inoue, Y. Kudo and H. Miyakawa (2007). "Paired-pulse ratio of synaptically induced transporter currents at hippocampal CA1 synapses is not related to release probability." Brain research **1154**: 71-79.

Marcelin, B., Z. Liu, Y. Chen, A. S. Lewis, A. Becker, S. McClelland, D. M. Chetkovich, M. Migliore, T. Z. Baram and M. Esclapez (2012). "Dorsoventral differences in intrinsic properties in developing CA1 pyramidal cells." Journal of Neuroscience **32**(11): 3736-3747.

Marcelin, B., J. N. Lugo, A. L. Brewster, Z. Liu, A. S. Lewis, S. McClelland, D. M. Chetkovich, T. Z. Baram, A. E. Anderson and A. Becker (2012). "Differential dorso-ventral distributions of Kv4. 2 and HCN proteins confer distinct integrative properties to hippocampal CA1 pyramidal cell distal dendrites." Journal of Biological Chemistry **287**(21): 17656-17661.

Markram, H., W. Gerstner and P. J. Sjöström (2012). "Spike-timing-dependent plasticity: a comprehensive overview." Frontiers in synaptic neuroscience **4**: 2.

Markram, H., J. Lübke, M. Frotscher and B. Sakmann (1997). "Regulation of synaptic efficacy by coincidence of postsynaptic APs and EPSPs." Science **275**(5297): 213-215.

Martens, U., B. Capito and A. Wree (1998). "Septotemporal distribution of [3 H] MK-801,[3 H] AMPA and [3 H] kainate binding sites in the rat hippocampus." Anatomy and embryology **198**(3): 195-204.

Martens, U., B. Capito and A. Wree (1998). "Septotemporal distribution of [3H] MK-801,[3H] AMPA and [3H] Kainate binding sites in the rat hippocampus." Anatomy and embryology **198**(3): 195-204.

Masquelier, T., R. Guyonneau and S. J. Thorpe (2009). "Competitive STDP-based spike pattern learning." Neural computation **21**(5): 1259-1276.

Massey, P. V., B. E. Johnson, P. R. Moult, Y. P. Auberson, M. W. Brown, E. Molnar, G. L. Collingridge and Z. I. Bashir (2004). "Differential roles of NR2A and NR2B-containing NMDA receptors in cortical long-term potentiation and long-term depression." Journal of Neuroscience **24**(36): 7821-7828.

McDonald, R. J., J. Jones, B. Richards and N. S. Hong (2006). "A double dissociation of dorsal and ventral hippocampal function on a learning and memory task mediated by the dorso-lateral striatum." European Journal of Neuroscience **24**(6): 1789-1801.

McGaugh, J. L. (2000). "Memory--a century of consolidation." Science **287**(5451): 248-251.

McGaugh, J. L. (2004). "The amygdala modulates the consolidation of memories of emotionally arousing experiences." Annu. Rev. Neurosci. **27**: 1-28.

McGaugh, J. L., L. Cahill and B. Roozendaal (1996). "Involvement of the amygdala in memory storage: interaction with other brain systems." Proceedings of the National Academy of Sciences **93**(24): 13508-13514.

McGaugh, J. L., I. B. Introini-Collison, L. F. Cahill, C. Castellano, C. Dalmaz, M. B. Parent and C. L. Williams (1993). "Neuromodulatory systems and memory storage: role of the amygdala." Behavioural brain research **58**(1-2): 81-90.

McIntyre, C. K., T. Miyashita, B. Setlow, K. D. Marjon, O. Steward, J. F. Guzowski and J. L. McGaugh (2005). "Memory-influencing intra-basolateral amygdala drug infusions modulate expression of Arc protein in the hippocampus." Proceedings of the National Academy of Sciences **102**(30): 10718-10723.

Megıas, M., Z. Emri, T. Freund and A. Gulyas (2001). "Total number and distribution of inhibitory and excitatory synapses on hippocampal CA1 pyramidal cells." Neuroscience **102**(3): 527-540.

Metz, A. E., T. Jarsky, M. Martina and N. Spruston (2005). "R-type calcium channels contribute to afterdepolarization and bursting in hippocampal CA1 pyramidal neurons." Journal of Neuroscience **25**(24): 5763-5773.

Milior, G., M. A. Di Castro, L. Pepe'Sciarria, S. Garofalo, I. Branchi, D. Ragozzino, C. Limatola and L. Maggi (2016). "Electrophysiological properties of CA1 pyramidal neurons along the longitudinal axis of the mouse hippocampus." Scientific reports **6**(1): 1-9.

Mizuseki, K., K. Diba, E. Pastalkova and G. Buzsáki (2011). "Hippocampal CA1 pyramidal cells form functionally distinct sublayers." Nature neuroscience **14**(9): 1174-1181.

Molinoff, P. B. and J. Axelrod (1971). "Biochemistry of catecholamines." Annual review of biochemistry **40**(1): 465-500.

Momiyama, T. and E. Koga (2001). "Dopamine D2-like receptors selectively block N-type Ca2+ channels to reduce GABA release onto rat striatal cholinergic interneurones." The Journal of physiology **533**(2): 479-492.

Monyer, H., N. Burnashev, D. J. Laurie, B. Sakmann and P. H. Seeburg (1994). "Developmental and regional expression in the rat brain and functional properties of four NMDA receptors." Neuron **12**(3): 529-540.

Morrisett, R., D. Mott, D. Lewis, H. S. Swartzwelder and W. Wilson (1991). "GABAB-receptor-mediated inhibition of the N-methyl-D-aspartate component of synaptic transmission in the rat hippocampus." Journal of Neuroscience **11**(1): 203-209.

Moser, E., M.-B. Moser and P. Andersen (1993). "Spatial learning impairment parallels the magnitude of dorsal hippocampal lesions, but is hardly present following ventral lesions." Journal of neuroscience **13**(9): 3916-3925.

Moser, M.-B., E. I. Moser, E. Forrest, P. Andersen and R. Morris (1995). "Spatial learning with a minislab in the dorsal hippocampus." Proceedings of the National Academy of Sciences **92**(21): 9697-9701.

Moser, M. B. and E. I. Moser (1998). "Functional differentiation in the hippocampus." Hippocampus **8**(6): 608-619.

Mott, D. D. and D. V. Lewis (1991). "Facilitation of the induction of long-term potentiation by GABAB receptors." Science **252**(5013): 1718-1720.

Mukherjee, S. and D. Manahan-Vaughan (2013). "Role of metabotropic glutamate receptors in persistent forms of hippocampal plasticity and learning." Neuropharmacology **66**: 65-81.

Naie, K. and D. Manahan-Vaughan (2005). "Pharmacological antagonism of metabotropic glutamate receptor 1 regulates long-term potentiation and spatial reference memory in the dentate gyrus of freely moving rats via N-methyl-D-aspartate and metabotropic glutamate receptor-dependent mechanisms." European Journal of Neuroscience **21**(2): 411-421.

Nasse, J. S. and J. B. Travers (2014). "Adrenoreceptor modulation of oromotor pathways in the rat medulla." Journal of neurophysiology **112**(3): 580-593.

Neve, K. A., J. K. Seamans and H. Trantham-Davidson (2004). "Dopamine receptor signaling." Journal of receptors and signal transduction **24**(3): 165-205.

Neves, G., S. F. Cooke and T. V. Bliss (2008). "Synaptic plasticity, memory and the hippocampus: a neural network approach to causality." Nature Reviews Neuroscience **9**(1): 65.

Nguyen, P. V., T. Abel and E. R. Kandel (1994). "Requirement of a critical period of transcription for induction of a late phase of LTP." Science **265**(5175): 1104-1107.

Nicoll, R. A. (2017). "A brief history of long-term potentiation." Neuron **93**(2): 281-290.

Nicoll, R. A. and D. Schmitz (2005). "Synaptic plasticity at hippocampal mossy fibre synapses." Nature Reviews Neuroscience **6**(11): 863.

Nullmeier, S., P. Panther, M. Frotscher, S. Zhao and H. Schwegler (2014). "Alterations in the hippocampal and striatal catecholaminergic fiber densities of heterozygous reeler mice." Neuroscience **275**: 404-419.

Okun, M. and I. Lampl (2009). "Balance of excitation and inhibition." Scholarpedia **4**(8): 7467.

Olpe and G. Karlsson (1990). "The effects of baclofen and two GABAB-receptor antagonists on long-term potentiation." Naunyn-Schmiedeberg's archives of pharmacology **342**(2): 194-197.

Olpe, H., W. Wörner and T. Ferrat (1993). "Stimulation parameters determine role of GABAB receptors in long-term potentiation." Experientia **49**(6): 542-546.

Otmakhova, N. A. and J. E. Lisman (1996). "D1/D5 dopamine receptor activation increases the magnitude of early long-term potentiation at CA1 hippocampal synapses." Journal of Neuroscience **16**(23): 7478-7486.

Otto, T., H. Eichenbaum, C. G. Wible and S. I. Wiener (1991). "Learning-related patterns of CA1 spike trains parallel stimulation parameters optimal for inducing hippocampal long-term potentiation." Hippocampus **1**(2): 181-192.

Pacheco-Cano, M., J. Bargas, S. Hernandez-Lopez, D. Tapia and E. Galarraga (1996). "Inhibitory action of dopamine involves a subthreshold Cs+-sensitive conductance in neostriatal neurons." Experimental brain research **110**(2): 205-211.

Paille, V., E. Fino, K. Du, T. Morera-Herreras, S. Perez, J. H. Kotaleski and L. Venance (2013). "GABAergic circuits control spike-timing-dependent plasticity." Journal of Neuroscience **33**(22): 9353-9363.

Pandis, C., E. Sotiriou, E. Kouvaras, E. Asprodini, C. Papatheodoropoulos and F. Angelatou (2006). "Differential expression of NMDA and AMPA receptor subunits in rat dorsal and ventral hippocampus." Neuroscience **140**(1): 163-175.

Papatheodoropoulos, C. (2015). "Higher intrinsic network excitability in ventral compared with the dorsal hippocampus is controlled less effectively by GABA B receptors." BMC neuroscience **16**(1): 1-11.

Papatheodoropoulos, C., E. Asprodini, I. Nikita, C. Koutsona and G. Kostopoulos (2002). "Weaker synaptic inhibition in CA1 region of ventral compared to dorsal rat hippocampal slices." Brain research **948**(1-2): 117-121.

Papatheodoropoulos, C. and G. Kostopoulos (2000). "Dorsal-ventral differentiation of short-term synaptic plasticity in rat CA1 hippocampal region." Neuroscience letters **286**(1): 57-60.

Papatheodoropoulos, C. and S. Kouvaros (2016). "High-frequency stimulation-induced synaptic potentiation in dorsal and ventral CA1 hippocampal synapses: the involvement of NMDA receptors, mGluR5, and (L-type) voltage-gated calcium channels." Learning & Memory **23**(9): 460-464.

Papatheodoropoulos, C., C. Moschovos and G. Kostopoulos (2005). "Greater contribution of N-methyl-D-aspartic acid receptors in ventral compared to dorsal hippocampal slices in the expression and long-term maintenance of epileptiform activity." Neuroscience **135**(3): 765-779.

Papez, J. W. (1937). "A proposed mechanism of emotion." Archives of Neurology & Psychiatry **38**(4): 725-743.

Paulsen, O. and E. Moser (1998). "A model of hippocampal memory encoding and retrieval: GABAergic control of synaptic plasticity." Trends in neurosciences **21**(7): 273-278.

Peng, Z., B. Hauer, R. M. Mihalek, G. E. Homanics, W. Sieghart, R. W. Olsen and C. R. Houser (2002). "GABAA receptor changes in δ subunit-deficient mice: Altered expression of α4 and γ2 subunits in the forebrain." Journal of Comparative Neurology **446**(2): 179-197.

Petrides, T., P. Georgopoulos, G. Kostopoulos and C. Papatheodoropoulos (2007). "The GABA A receptor-mediated recurrent inhibition in ventral compared with dorsal CA1 hippocampal region is weaker, decays faster and lasts less." Experimental brain research **177**(3): 370-383.

Plant, K., K. A. Pelkey, Z. A. Bortolotto, D. Morita, A. Terashima, C. J. McBain, G. L. Collingridge and J. T. Isaac (2006). "Transient incorporation of native GluR2-lacking AMPA receptors during hippocampal long-term potentiation." Nature neuroscience **9**(5): 602-604.

Pouille, F. and M. Scanziani (2001). "Enforcement of temporal fidelity in pyramidal cells by somatic feed-forward inhibition." Science **293**(5532): 1159-1163.

Pouille, F. and M. Scanziani (2004). "Routing of spike series by dynamic circuits in the hippocampus." Nature **429**(6993): 717-723.

Price, C. J., R. Scott, D. A. Rusakov and M. Capogna (2008). "GABAB receptor modulation of feedforward inhibition through hippocampal neurogliaform cells." Journal of Neuroscience **28**(27): 6974-6982.

Pugh, J. R. and C. E. Jahr (2011). "Axonal GABAA receptors increase cerebellar granule cell excitability and synaptic activity." Journal of Neuroscience **31**(2): 565-574.

Rall, W. (1959). "Branching dendritic trees and motoneuron membrane resistivity." Experimental neurology **1**(5): 491-527.

Rall, W. (1964). "Theoretical significance of dendritic trees for neuronal input-output relations." Neural theory and modeling: 73-97.

RANKIN, M. L., L. A. Hazelwood, R. B. Free, E. Rex, R. Roof and D. Sibley (2010). "3.1 Molecular Pharmacology of the Dopamine Receptors." Dopamine handbook **63**.

Rebola, N., M. Carta and C. Mulle (2017). "Operation and plasticity of hippocampal CA3 circuits: implications for memory encoding." Nature Reviews Neuroscience **18**(4): 208-220.

Remondes, M. and E. M. Schuman (2003). "Molecular mechanisms contributing to long-lasting synaptic plasticity at the temporoammonic–CA1 synapse." Learning & Memory **10**(4): 247-252.

Risold, P. and L. Swanson (1996). "Structural evidence for functional domains in the rat hippocampus." Science **272**(5267): 1484-1486.

Rogers, J. L., M. R. Hunsaker and R. P. Kesner (2006). "Effects of ventral and dorsal CA1 subregional lesions on trace fear conditioning." Neurobiology of learning and memory **86**(1): 72-81.

Roggenhofer, E., P. Fidzinski, J. Bartsch, F. Kurz, O. Shor and J. Behr (2010). "Activation of dopamine D1/D5 receptors facilitates the induction of presynaptic long-term potentiation at hippocampal output synapses." European Journal of Neuroscience **32**(4): 598-605.

Rolls, E. T. (1996). "A theory of hippocampal function in memory." Hippocampus **6**(6): 601-620.

Rose, M. (1935). "Cytoarchitektonik und Myeloarchitektonik der Großhirnrinde." Handbuch der Neurologie **1**: 588-778.

Rosen, Z. B., S. Cheung and S. A. Siegelbaum (2015). "Midbrain dopamine neurons bidirectionally regulate CA3-CA1 synaptic drive." Nature neuroscience **18**(12): 1763-1771.

Rossato, J. I., L. R. Bevilaqua, I. Izquierdo, J. H. Medina and M. Cammarota (2009). "Dopamine controls persistence of long-term memory storage." Science **325**(5943): 1017-1020.

Roth, F. C. and A. Draguhn (2012). "GABA metabolism and transport: effects on synaptic efficacy." Neural plasticity **2012**.

Ruiz, A., R. Fabian-Fine, R. Scott, M. C. Walker, D. A. Rusakov and D. M. Kullmann (2003). "GABAA receptors at hippocampal mossy fibers." Neuron **39**(6): 961-973.

Russo, S. J. and E. J. Nestler (2013). "The brain reward circuitry in mood disorders." Nature Reviews Neuroscience **14**(9): 609-625.

Sacktor, T. C. (2008). "PKMζ, LTP maintenance, and the dynamic molecular biology of memory storage." Progress in brain research **169**: 27-40.

Sah, P. and J. M. Bekkers (1996). "Apical dendritic location of slow afterhyperpolarization current in hippocampal pyramidal neurons: implications for the integration of long-term potentiation." Journal of Neuroscience **16**(15): 4537-4542.

Sah, P. and J. D. Clements (1999). "Photolytic Manipulation of [Ca2+] iReveals Slow Kinetics of Potassium Channels Underlying the Afterhyperpolarization in Hipppocampal Pyramidal Neurons." Journal of Neuroscience **19**(10): 3657-3664.

Sallard, E., D. Letourneur and P. Legendre (2021). "Electrophysiology of ionotropic GABA receptors." Cellular and Molecular Life Sciences **78**(13): 5341-5370.

Sanes, J. R. and J. W. Lichtman (1999). "Can molecules explain long-term potentiation?" Nature neuroscience **2**(7): 597-604.

Sannino, S., F. Russo, G. Torromino, V. Pendolino, P. Calabresi and E. De Leonibus (2012). "Role of the dorsal hippocampus in object memory load." Learning & Memory **19**(5): 211-218.

Santana, N., G. Mengod and F. Artigas (2009). "Quantitative analysis of the expression of dopamine D1 and D2 receptors in pyramidal and GABAergic neurons of the rat prefrontal cortex." Cerebral Cortex **19**(4): 849-860.

Santiago, M., A. Machado and J. Cano (1993). "Regulation of prefrontal cortical dopamine release by dopamine receptor agonists and antagonists." European journal of pharmacology **239**(1-3): 83-91.

Santiago, M., A. Machado and J. Cano (1993). "Regulation of the prefrontal cortical dopamine release by GABAA and GABAB receptor agonists and antagonists." Brain research **630**(1-2): 28-31.Schaffer, K. (1892). "Beitrag zur histologie der ammonshornformation." Archiv für mikroskopischeAnatomie **39**(1): 611-632.

Scharfman, H. E. and M. V. Chao (2013). "The entorhinal cortex and neurotrophin signaling in Alzheimer's disease and other disorders." Cognitive neuroscience **4**(3-4): 123-135.

Schousboe, A. (2000). "Pharmacological and functional characterization of astrocytic GABA transport: a short review." Neurochemical research **25**(9): 1241-1244.

Schumacher, A., E. Vlassov and R. Ito (2016). "The ventral hippocampus, but not the dorsal hippocampus is critical for learned approach-avoidance decision making." Hippocampus **26**(4): 530-542.

Scoville, W. B. and B. Milner (1957). "Loss of recent memory after bilateral hippocampal lesions." Journal of neurology, neurosurgery, and psychiatry **20**(1): 11.

Seabrook, G., A. Easter, G. Dawson and B. Bowery (1997). "Modulation of long-term potentiation in CA1 region of mouse hippocampal brain slices by GABAA receptor benzodiazepine site ligands." Neuropharmacology **36**(6): 823-830.

Segev, I., J. Rinzel and G. M. Shepherd (2003). The Theoretical Foundation of Dendritic Function: The Collected Papers of Wilfrid Rall with Commentaries, The MIT Press.

Semyanov, A., M. C. Walker and D. M. Kullmann (2003). "GABA uptake regulates cortical excitability via cell type–specific tonic inhibition." Nature neuroscience **6**(5): 484-490.

Shen, F., F. Wang, G. Yang, L. Miao, E. Wang, J. Xu, Y. Xu and T. Sun (2013). "The effects of low-frequency electric stimulus on hippocampal of Effects of low-frequency electric stimulus on hippocampal of α5 subunit of extra synapse GABAA receptor in kainic acid-induced epilepsy rats." Zhonghua yi xue za zhi **93**(7): 550-553.

Shi, S.-H., Y. Hayashi, J. A. Esteban and R. Malinow (2001). "Subunit-specific rules governing AMPA receptor trafficking to synapses in hippocampal pyramidal neurons." Cell **105**(3): 331-343.

Sholl, D. A. (1953). "Dendritic organization in the neurons of the visual and motor cortices of the cat." Journal of anatomy **87**(Pt 4): 387.

Sik, A., M. Penttonen, A. Ylinen and G. Buzsáki (1995). "Hippocampal CA1 interneurons: an in vivo intracellular labeling study." Journal of Neuroscience **15**(10): 6651-6665.

Small, S. A., A. S. Nava, G. M. Perera, R. DeLaPaz, R. Mayeux and Y. Stern (2001). "Circuit mechanisms underlying memory encoding and retrieval in the long axis of the hippocampal formation." Nature neuroscience **4**(4): 442-449.

Smith, C. C. and R. W. Greene (2012). "CNS dopamine transmission mediated by noradrenergic innervation." Journal of Neuroscience **32**(18): 6072-6080.

Soghomonian, J.-J. and D. L. Martin (1998). "Two isoforms of glutamate decarboxylase: why?" Trends in pharmacological sciences **19**(12): 500-505.

Sokoloff, P., J. Diaz, B. L. Foll, O. Guillin, L. Leriche, E. Bezard and C. Gross (2006). "The dopamine D3 receptor: a therapeutic target for the treatment of neuropsychiatric disorders." CNS & Neurological Disorders-Drug Targets (Formerly Current Drug Targets-CNS & Neurological Disorders) **5**(1): 25-43.

Somayaji, M. and D. Sulzer "Investigating pre-clinical dopamine physiology in Parkinson."

Somogyi, J., A. Szabo, P. Somogyi and K. P. Lamsa (2012). "Molecular analysis of ivy cells of the hippocampal CA1 stratum radiatum using spectral identification of immunofluorophores." Frontiers in neural circuits **6**: 35.

Somogyi, P. and T. Klausberger (2005). "Defined types of cortical interneurone structure space and spike timing in the hippocampus." The Journal of physiology **562**(1): 9-26.

Soriano, E., R. Nitsch and M. Frotscher (1990). "Axo-axonic chandelier cells in the rat fascia dentata: Golgi-electron microscopy and immunocytochemical studies." Journal of Comparative Neurology **293**(1): 1-25.

Staff, N. P., H.-Y. Jung, T. Thiagarajan, M. Yao and N. Spruston (2000). "Resting and active properties of pyramidal neurons in subiculum and CA1 of rat hippocampus." Journal of neurophysiology **84**(5): 2398-2408.

Stell, B. M., P. Rostaing, A. Triller and A. Marty (2007). "Activation of presynaptic GABAA receptors induces glutamate release from parallel fiber synapses." Journal of Neuroscience **27**(34): 9022-9031.

Strange, B. A., M. P. Witter, E. S. Lein and E. I. Moser (2014). "Functional organization of the hippocampal longitudinal axis." Nature Reviews Neuroscience **15**(10): 655.

Stuber, G. D., A. M. Stamatakis and P. A. Kantak (2015). "Considerations when using cre-driver rodent lines for studying ventral tegmental area circuitry." Neuron **85**(2): 439-445.

Study, R. and J. Barker (1981). "Diazepam and (--)-pentobarbital: fluctuation analysis reveals different mechanisms for potentiation of gamma-aminobutyric acid responses in cultured central neurons." Proceedings of the National Academy of Sciences of the United States of America **78**(11): 7180.

Swanson, L., J. Wyss and W. Cowan (1978). "An autoradiographic study of the organization of intrahippocampal association pathways in the rat." Journal of comparative neurology **181**(4): 681-715.

Takechi, H., J. Eilers and A. Konnerth (1998). "A new class of synaptic response involving calcium release in dendritic spines." Nature **396**(6713): 757-760.

Taylor, C. W. and S. C. Tovey (2010). "IP3 receptors: toward understanding their activation." Cold Spring Harbor perspectives in biology **2**(12): a004010.

Terunuma, M., R. Revilla-Sanchez, I. M. Quadros, Q. Deng, T. Z. Deeb, M. Lumb, P. Sicinski, P. G. Haydon, M. N. Pangalos and S. J. Moss (2014). "Postsynaptic GABAB receptor activity regulates excitatory neuronal architecture and spatial memory." Journal of Neuroscience **34**(3): 804-816.

Tidball, P., H. V. Burn, K. L. Teh, A. Volianskis, G. L. Collingridge and S. M. Fitzjohn (2017). "Differential ability of the dorsal and ventral rat hippocampus to exhibit group I metabotropic

glutamate receptor–dependent synaptic and intrinsic plasticity." <u>Brain and neuroscience advances</u> **1**: 2398212816689792.

Tigaret, C. M., V. Olivo, J. H. Sadowski, M. C. Ashby and J. R. Mellor (2016). "Coordinated activation of distinct Ca2+ sources and metabotropic glutamate receptors encodes Hebbian synaptic plasticity." <u>Nature communications</u> **7**(1): 1-14.

Tigaret, C. M., V. Olivo, J. H. Sadowski, M. C. Ashby and J. R. Mellor (2016). "Coordinated activation of distinct Ca 2+ sources and metabotropic glutamate receptors encodes Hebbian synaptic plasticity." <u>Nature communications</u> **7**(1): 1-14.

Treves, A. and E. T. Rolls (1992). "Computational constraints suggest the need for two distinct input systems to the hippocampal CA3 network." <u>Hippocampus</u> **2**(2): 189-199.

Tritsch, N. X. and B. L. Sabatini (2012). "Dopaminergic modulation of synaptic transmission in cortex and striatum." <u>Neuron</u> **76**(1): 33-50.

Tse, D., R. F. Langston, M. Kakeyama, I. Bethus, P. A. Spooner, E. R. Wood, M. P. Witter and R. G. Morris (2007). "Schemas and memory consolidation." <u>Science</u> **316**(5821): 76-82.

Tully, K. and V. Y. Bolshakov (2010). "Emotional enhancement of memory: how norepinephrine enables synaptic plasticity." <u>Molecular brain</u> **3**(1): 1-9.

Undieh, A. S. (2010). "Pharmacology of signaling induced by dopamine D1-like receptor activation." <u>Pharmacology & therapeutics</u> **128**(1): 37-60.

Valley, G. E. and H. Wallman (1948). "Vacuum tube amplifiers."

Van Stegeren, A. H. (2008). "The role of the noradrenergic system in emotional memory." <u>Acta psychologica</u> **127**(3): 532-541.

Voglis, G. and N. Tavernarakis (2006). "The role of synaptic ion channels in synaptic plasticity." <u>EMBO reports</u> **7**(11): 1104-1110.

Wagner, J. and B. Alger (1995). "GABAergic and developmental influences on homosynaptic LTD and depotentiation in rat hippocampus." <u>Journal of Neuroscience</u> **15**(2): 1577-1586.

Wang, H., A. O. Ardiles, S. Yang, T. Tran, R. Posada-Duque, G. Valdivia, M. Baek, Y.-A. Chuang, A. G. Palacios and M. Gallagher (2016). "Metabotropic glutamate receptors induce a form of LTP controlled by translation and arc signaling in the hippocampus." <u>Journal of Neuroscience</u> **36**(5): 1723-1729.

Wang, L., M. Kloc, E. Maher, A. Erisir and A. Maffei (2019). "Presynaptic GABAA receptors modulate thalamocortical inputs in layer 4 of rat V1." <u>Cerebral Cortex</u> **29**(3): 921-936.

Wang, X., P. Zhong, Z. Gu and Z. Yan (2003). "Regulation of NMDA receptors by dopamine D4 signaling in prefrontal cortex." <u>Journal of Neuroscience</u> **23**(30): 9852-9861.

Waterhouse, B. D. and R. L. Navarra (2019). "The locus coeruleus-norepinephrine system and sensory signal processing: A historical review and current perspectives." <u>Brain research</u> **1709**: 1-15.

Wei, C.-l., Y.-h. Liu, M.-h. Yang, Z.-q. Liu and W. Ren (2013). "Dopamine inhibits high-frequency stimulation-induced long-term potentiation of intrinsic excitability in CA1 hippocampal pyramidal neurons." <u>Neurosignals</u> **21**(3-4): 150-159.

Wernicke, C. (1881). "Lehrbuch der gehirnkrankheiten (Vol. 2.)." <u>Berlin, Germany: Theodore Fischer</u>.

Wiera, G., D. Nowak, I. Van Hove, P. Dziegiel, L. Moons and J. W. Mozrzymas (2017). "Mechanisms of NMDA receptor-and voltage-gated L-type calcium channel-dependent hippocampal LTP critically rely on proteolysis that is mediated by distinct metalloproteinases." <u>Journal of Neuroscience</u> **37**(5): 1240-1256.

Winder, D. G., K. C. Martin, I. A. Muzzio, D. Rohrer, A. Chruscinski, B. Kobilka and E. R. Kandel (1999). "ERK plays a regulatory role in induction of LTP by theta frequency stimulation and its modulation by β-adrenergic receptors." Neuron **24**(3): 715-726.

Wittenberg, G. M. and S. S.-H. Wang (2006). "Malleability of spike-timing-dependent plasticity at the CA3–CA1 synapse." Journal of Neuroscience **26**(24): 6610-6617.

Witter, M. P., H. Groenewegen, F. L. Da Silva and A. Lohman (1989). "Functional organization of the extrinsic and intrinsic circuitry of the parahippocampal region." Progress in neurobiology **33**(3): 161-253.

Wyllie, D., M. Livesey and G. Hardingham (2013). "Influence of GluN2 subunit identity on NMDA receptor function." Neuropharmacology **74**: 4-17.

Xu, T.-X. and W.-D. Yao (2010). "D1 and D2 dopamine receptors in separate circuits cooperate to drive associative long-term potentiation in the prefrontal cortex." Proceedings of the National Academy of Sciences **107**(37): 16366-16371.

Yang, H. W., Y. W. Lin, C. D. Yen and M. Y. Min (2002). "Change in bi-directional plasticity at CA1 synapses in hippocampal slices taken from 6-hydroxydopamine-treated rats: the role of endogenous norepinephrine." European Journal of Neuroscience **16**(6): 1117-1128.

Yang, K. and J. A. Dani (2014). "Dopamine D1 and D5 receptors modulate spike timing-dependent plasticity at medial perforant path to dentate granule cell synapses." Journal of Neuroscience **34**(48): 15888-15897.

Yao, H. and Y. Dan (2001). "Stimulus timing-dependent plasticity in cortical processing of orientation." Neuron **32**(2): 315-323.

Yavich, L., R. Lappalainen, J. Sirviö, A. Haapalinna and E. MacDonald (1997). "α2-Adrenergic control of dopamine overflow and metabolism in mouse striatum." European journal of pharmacology **339**(2-3): 113-119.

Zemankovics, R., S. Káli, O. Paulsen, T. F. Freund and N. Hájos (2010). "Differences in subthreshold resonance of hippocampal pyramidal cells and interneurons: the role of h-current and passive membrane characteristics." The Journal of physiology **588**(12): 2109-2132.

Zhang, J.-C., P.-M. Lau and G.-Q. Bi (2009). "Gain in sensitivity and loss in temporal contrast of STDP by dopaminergic modulation at hippocampal synapses." Proceedings of the National Academy of Sciences **106**(31): 13028-13033.

Zhang, L., W. M. Doyon, J. J. Clark, P. E. Phillips and J. A. Dani (2009). "Controls of tonic and phasic dopamine transmission in the dorsal and ventral striatum." Molecular pharmacology **76**(2): 396-404.

Zola-Morgan, S. and L. R. Squire (1993). "Neuroanatomy of memory." Annual review of neuroscience **16**(1): 547-563.

Zorrilla de San Martin, J., F. F. Trigo and S. y. Kawaguchi (2017). "Axonal GABAA receptors depolarize presynaptic terminals and facilitate transmitter release in cerebellar Purkinje cells." The Journal of physiology **595**(24): 7477-7493.

Zucker, R. S. and W. G. Regehr (2002). "Short-term synaptic plasticity." Annual review of physiology **64**(1): 355-405

Declaration of honour

I hereby declare that I have prepared this thesis without the impermissible help of third parties and that none other that the aids indicated have been used; all sources of information are clearly marked, indicating my own publications.

In particular I have not consciously:

- fabricated data or rejected undesirable results,
- misused statistical methods with the aim of drawing other conclusions than those warranted by the available data,
- plagiarized external data or publications,
- presented the results of other researchers in distorted way.

I am aware that violations of copyright may lead to injection and damage claims by the author and also to prosecution by law enforcement authorities. I hereby agree that the thesis may be electronically reviewed with aim of identifying plagiarism. This work has not been submitted as a doctoral thesis in the same or similar form in Germany, nor in any other country. It has not yet been published as a whole."

Magdeburg, 30.11.2022

Babak Khodaie